Annual Technical Progress Report
Report Number 15323R07
(October 1, 2003 – September 30, 2004)

DEVELOPMENT AND OPTIMIZATION OF GAS-ASSISTED GRAVITY DRAINAGE (GAGD) PROCESS FOR IMPROVED LIGHT OIL RECOVERY

Work Performed Under Cooperative Agreement
DE-FC26-02NT15323

By

Dandina N. Rao, Ph. D., P. Eng.
(Principal Investigator)

Subhash C. Ayirala, M. S.
Madhav M. Kulkarni, M. S.
Amit P. Sharma, M. S.
(Graduate Research Assistants)

The Craft & Hawkins Department of Petroleum Engineering
Louisiana State University and Agricultural & Mechanical College
Baton Rouge, LA 70803

October 2004

Prepared for
U. S. Department of Energy
National Petroleum Technology Office

DISCLAIMER

ABSTRACT

This report describes the progress of the project "Development and Optimization of Gas-Assisted Gravity Drainage (GAGD) Process for Improved Light Oil Recovery" for the duration of the second project year (October 1, 2003 – September 30, 2004). There are three main tasks in this research project. Task 1 is scaled physical model study of GAGD process. Task 2 is further development of vanishing interfacial tension (VIT) technique for miscibility determination. Task 3 is determination of multiphase displacement characteristics in reservoir rocks.

In Section I, preliminary design of the scaled physical model using the dimensional similarity approach has been presented. Scaled experiments on the current physical model have been designed to investigate the effect of Bond and capillary numbers on GAGD oil recovery. Experimental plan to study the effect of spreading coefficient and reservoir heterogeneity has been presented. Results from the GAGD experiments to study the effect of operating mode, Bond number and capillary number on GAGD oil recovery have been reported. These experiments suggest that the type of the gas does not affect the performance of GAGD in immiscible mode. The cumulative oil recovery has been observed to vary exponentially with Bond and capillary numbers, for the experiments presented in this report. A predictive model using the bundle of capillary tube approach has been developed to predict the performance of free gravity drainage process.

In Section II, a mechanistic Parachor model has been proposed for improved prediction of IFT as well as to characterize the mass transfer effects for miscibility development in reservoir crude oil-solvent systems. Sensitivity studies on model results indicate that provision of a single IFT measurement in the proposed model is sufficient for reasonable IFT predictions. An attempt has been made to correlate the exponent (n) in the mechanistic model with normalized solute compositions present in both fluid phases. IFT measurements were carried out in a standard ternary liquid system of benzene, ethanol and water using drop shape analysis and capillary rise techniques. The experimental results indicate strong correlation among the three thermodynamic properties solubility, miscibility and IFT. The miscibility determined from IFT measurements for this ternary liquid system is in good agreement with phase diagram and solubility data, which clearly indicates the sound conceptual basis of VIT technique to determine fluid-fluid miscibility. Model fluid systems have been identified for VIT experimentation at elevated pressures and temperatures.

Section III comprises of the experimental study aimed at evaluating the multiphase displacement characteristics of the various gas injection EOR process performances using Berea sandstone cores. During this reporting period, extensive literature review was completed to: (i) study the gravity drainage concepts, (ii) identify the various factors influencing gravity stable gas injection processes, (iii) identify various multiphase mechanisms and fluid dynamics operative during the GAGD process, and (iv) identify important dimensionless groups governing the GAGD process performance. Furthermore, the dimensional analysis of the GAGD process, using Buckingham-Pi theorem to isolate the various dimensionless groups, as well as experimental design based on these dimensionless quantities have been completed in this reporting period. On the experimental front, recommendations from previous WAG and CGI have been used to modify the experimental protocol. This report also includes results from scaled preliminary GAGD displacements as well as the details of the planned GAGD corefloods for the next quarter.

The technology transfer activities have mainly consisted of preparing technical papers, progress reports and discussions with industry personnel for possible GAGD field tests.

Table of Contents

I. DESIGN AND DEVELOPMENT OF A SCALED PHYSICAL EXPERIMENTAL GAGD MODEL 8

***1.1 Introduction*........ 8**

***1.2 Literature Review*........ 8**
1.2.1 Horizontal wells 9
1.2.2 Scaled Model Studies 9
1.2.3 Factors Affecting Gravity Drainage 10
1.2.4 Summary of Literature Review 12

***1.3 Dimensional Analysis approach for scaling gravity drainage experiments* 13**
1.3.1 Development of the Scaled Physical Model using dimensional analysis 14

***1.4 Experimental Design and scaling of the current physical model* 17**
1.4.1 Effect of Bond Number 17
1.4.2 Effect of Capillary Number 17
1.4.3 Effect of Operating Mode 18
1.4.4 Effect of Heterogeneity 18
1.4.5 Experimental Setup 18
1.4.6 Experimental Plan 20

***1.5 Experimental Results* 21**
1.5.1 Constant Pressure GAGD Experiments 21
1.5.2 Constant Rate GAGD experiments to study the effect of Bond number 23
1.5.3 Effect of Capillary Number on GAGD oil recovery 26

***1.6 A Predictive model for the Free Gravity Drainage Process using a Bundle-of-Capillary-Tube Method* 28**
1.6.1 Results from Free-Gravity Drainage Experiments 29
1.6.2 Bundle-of-Capillary-Tube Model Development 31
1.6.3 Capillary Tube Radius Size Distribution 31
1.6.4 Model results 37
1.6.5 Discussion 37

***1.7 Preliminary conclusions and status* 40**

***1.8 Future Work* 41**

***References* 42**

II. FURTHER DEVELOPMENT OF THE VANISHING INTERFACIAL TENSION (VIT) TECHNIQUE 44

2.1 The Proposed Mass Transfer Enhanced Mechanistic Parachor Model................. 44
2.1.1 Introduction.. 44
2.1.2 Parachor Model 45
2.1.3 The Proposed Modification for Mass Transfer.. 46
2.1.4 Results and Discussion 49
2.1.5 Application of the Proposed Mechanistic Model to More Reservoir Fluids 53
2.1.6 Sensitivity Studies on Proposed Mechanistic Model 53
2.1.7 Generalized Correlations for Prediction of Exponent (n) in Mechanistic Model 54
2.1.8 Prediction of Dynamic Gas-Oil Miscibility 57

2.2 IFT Measurements in a Standard Ternary Liquid System 58
2.2.1 Introduction.. 58
2.2.2 Experimental System and Procedure 59
2.2.3 Solubility and Miscibility 60
2.2.4 Solvent-Oil Ratio Effects on IFT.. 60
2.2.5 Capillary Rise Technique... 62
2.2.6 Correlation of Miscibility and Solubility with IFT 64

2.3 High Pressure High temperature VIT Experimental System.................................. 65
2.3.1 Design and Assembly of VIT Experimental System 65
2.3.2 Identification of Model Fluid Systems for VIT Experimentation......................... 65

2.4 Conclusions 65
2.4.1 The Proposed Mass Transfer Enhanced Mechanistic Parachor Model.............. 65
2.4.2 IFT Measurements in a Standard Ternary Liquid System.................................. 67
2.4.3 High Pressure High Temperature VIT Experimental System............................. 67

2.5 Future Plans... 68

References 68

III. DETERMINATION OF MULTIPHASE DISPLACEMENT CHARACTERISTICS IN RESERVOIR ROCKS 96

3.1 Literature Review on EOR by Gas Injection... 96
3.1.1 Gas Injection EOR 97
3.1.2 Gas Gravity Drainage... 98
3.1.3 Displacement Instabilities for Gravity Stable Gas Flow through Porous Media 99
3.1.4 Critical Rates for Gravity Drainage 102
3.1.5 Laboratory Studies for Gravity Drainage... 104
3.1.6 Field Studies of Gravity Drainage 106
3.1.7 Literature Review Summary.. 115
- Gravity Drainage Laboratory Studies 115
- Gravity Drainage Field Studies.. 115

3.2 Operating Multiphase Mechanisms during Gas Gravity Drainage....................... 116
3.2.1 Gravity Segregation 117

3.2.2 Effect of Wettability ... 117
3.2.3 Effect of Spreading Coefficient ... 117
3.2.4 Effect of Miscibility ... 118
3.2.5 Effect of Mobile Water Saturation ... 119
3.2.6 Effect of Connate Water Saturation ... 119
3.2.7 Effect of Reservoir Heterogeneity ... 120

3.3 Operating Fluid Dynamics during Gas Gravity Drainage ... **120**
3.3.1 Effect of Injection Mode ... 121
- Secondary Mode Gas Gravity Drainage ... 121
- Tertiary Mode Gas Gravity Drainage ... 121

3.3.2 Gravity versus Capillary versus Viscous Force Effects ... 122
3.3.3 Effect of Dispersion and Flow Regime Characterization ... 123
- Dispersion ... 123
- Flow Regime Characterization ... 123

3.3.4 Relative Permeability ... 127
3.3.5 Oil Recovery Characteristics ... 127

3.4 Dimensionless Reservoir Characterization ... **127**
3.4.1 Scalability of Physical Effects / Boundary Conditions ... 128
3.4.2 Dimensional Analysis of the Gravity Stable Gas Injection Process ... 129
3.4.3 Dimensionless Number(s) Governing Gravity Stable Gas Injection ... 131

3.5 Dimensional Similarity Approach for Experimental Design ... **132**
3.5.1 Calculation of Dimensionless Numbers for Field Projects ... 132
- Calculation of Dimensionless Numbers for Field Projects – A Case Study ... 133
- Important Conclusions from these Calculations – Example Case Study ... 134

3.5.2 Calculation of Dimensionless Numbers for Laboratory Core Displacements ... 135
3.5.3 Flow Regime Characterization of Gas Assisted Gravity Drainage Applications ... 137
3.5.4 Experimental Design Strategy ... 140
- Experimental Design Considerations ... 140
- Experimental Flow Chart ... 142

3.5.5 Experimental Apparatus, Protocol, and Scope ... 142
- Experimental Apparatus ... 142
- Research Scope ... 143

3.6 Continued CGI / WAG Experimentation ... **143**
3.6.1 WAG and CGI Experimentation on 6-ft Berea Core ... 144
3.6.2 Secondary WAG and CGI Corefloods ... 146
- Secondary Miscible CGI Flood ... 146
- Secondary Miscible WAG Flood ... 147
- Comparison between Secondary and Tertiary CGI / WAG Corefloods ... 148

3.6.3 Use of CO_2 Saturated Brine for WAG and CGI Corefloods ... 152
3.6.4 ‘Happy-Medium’ between WAG and CGI: Hybrid-WAG Coreflood ... 154
3.6.5 Preliminary Conclusions from Horizontal Mode Corefloods ... 155

3.7 Gravity Stable GAGD Experimentation **.. 156**
3.7.1 Immiscible Gravity Stable (GS) GAGD Floods 156
3.7.2 Miscible Gravity Stable (GS) GAGD Floods 160
3.7.3 Comparison of Immiscible and Miscible Gravity Stable GAGD Floods 160
- Effect of Injection Rate on Secondary Immiscible GAGD Floods..................... 160
- Effect of Injection Mode on Immiscible GAGD Floods 164
- Effect of Injection Mode on Miscible GAGD Floods 166
- Effect of Miscibility Development on GAGD Floods.. 166
- Itemized Preliminary Conclusions from Gravity Stable GAGD Corefloods...... 168

3.8 Preliminary Conclusions **.. 168**

3.9 Project GAGD: Task III – Status and Future Work **.. 169**
- Task III – 3 Status 169
- Task III – Future Work 170

References **.. 170**

IV. TECHNOLOGY TRANSFER EFFORTS 176

4.1 Technical Papers Prepared during this Reporting Period **..................................... 176**

Appendix A: Calculation of Dimensionless Numbers for Field Projects – A Case Study (West Hackberry Field – Louisiana) **.. 178**

I. Design and Development of a Scaled Physical Experimental GAGD Model

1.1 Introduction

This section of the annual report will discuss the progress made on Task I during the second year of this project. Progress made in this Task during the first year has been reported in the previous annual technical report and the first two quarterly reports (15323R03, 15323R01 and 1532R02). In those reports, a thorough survey of literature in the related area has been reported. The design and setup of the current bead-pack visual model, liquid injection system, and the setup of the image acquisition and data gathering system have been discussed. Free gravity drainage experiments were conducted and the observations and inferences from those experiments were discussed.

This section contains the detailed literature review conducted during the second year of the project. The design of the scaled model using the dimensional similarity approach will be discussed. Scaled experiments on the Hele-Shaw type physical model were carried out during this quarter are reported. The effect of Bond number and capillary number on GAGD performance during forced gravity drainage experiments will be discussed. A Bundle of capillary tube model has been developed for the free gravity drainage process to predict performance and will be discussed in this report.

1.2 Literature Review

Field review conducted on nine gravity drainage field projects by Kulkarni (2004), indicates that all the nine field projects in various parts of the world were successfully implemented. The oil recovery from these projects has been as high as 90% of Initial oil in place (IOIP) in tertiary mode after secondary waterfloods. Although, two of the nine projects were deemed economically unsuccessful, the others were all lucrative. These projects were implemented on a large variety of geological settings, ranging from formations that were sandstone (mostly water wet) to carbonates and dolomites (mostly oil wet. This clearly indicates that gravity drainage can be implemented to wide variety of geological setting.

However, these projects were implemented on pinnacle reefs type reservoirs. Gravity drainage using vertical wells might not yield similar recoveries if these were horizontal type reservoirs. As mentioned earlier, gravity override becomes a problem in conventional horizontal gas injection EOR processes, unfavorable mobility ratio in such processes results in early gas breakthrough, lower gas utilization factor and poor oil recoveries. The inclusion of horizontal wells in horizontal type reservoirs to facilitate the gravity stable oil drainage appears to be a solution to this problem.

1.2.1 Horizontal wells

Horizontal wells have long been used in several field applications. The key parameters that controls the success of horizontal wells are: (i) fracture intensity, (ii) hydrocarbon pay zone thickness, (iii) well spacing, (iv) vertical communication, (v) formation damage and post drilling cleanup ability, (vi) geological control, (vii) multi-well prospect and (viii) cooperation in geological, reservoir, drilling and completion departments (Lacy et al., 1992). Horizontal wells allow increased reservoir contact area, increased productivity over vertical wells and reduce coning tendencies in reservoir with bottom water drive and top gas cap drive because of a low pressure drawdown around the well bore. The application of horizontal well in GAGD will account for stable displacement of oil from the top of the reservoir to the well, reduce early gas breakthrough and reduce the residual oil saturation (Joshi, 2003). However, the applicability of horizontal well will depend on the parameters discussed above.

1.2.2 Scaled Model Studies

Displacement experiments in the laboratory have been extensively used to investigate the production behavior of petroleum reservoirs. Stahl et al. (1943) conducted the first scaled gravity drainage experiments. Air was used to displace various fluids from a column containing Wilcox sand. They reported results showing the dependence of liquid saturation on column height at both equilibrium and dynamic conditions. Scaled experiments investigating gravity segregation has been studied by Craig at al. (1957) and Templeton et al. (1961) in glass bead systems. Meszaros at al. (1990) used a series of partially scaled 2-dimensional models to study the effect of inert gas injection on heavy oil recovery, 70% oil in place was recovered in their study. Such experiments are representative of the reservoir if they are carried out in models that are properly scaled. The performance of oil reservoirs is governed by the value of a number of variables, which includes (i) fluid-fluid interfacial tension, (ii) fluid viscosities, (iii) wettability, (iv) spreading coefficient, (iv) fluid-fluid density difference, (v) rock porosity, (vii) absolute and relative permeability and (vii) initial water saturation. These variables can be combined to form dimensionless groups. The derivation of these groups is done using two general methods.

1) Dimensional Analysis (Geertsma et al., 1955)
2) Inspectional Analysis (Ruark,1935)

Dimensional analysis is the process of combining two or more variables into a group that would be dimensionless. The effect on certain variable is then studied in terms of the group instead of individual variables in the group. Rappaport (1955) suggests that if the ratio of dimensionless groups at a larger geometric scale to dimensionless groups at a smaller geometric scale is kept equal to one, then the mechanisms occurring on both the scale would be similar. However, the above statement is true only if both of the scales are geometrically similar.

Inspectional analysis is a similar method for obtaining dimensionless groups to study the mechanistic behavior of a process. However, inspectional analysis is based on the underlying physical laws, usually expresses in the form of partial differential equations and boundary conditions. Inspectional analysis can be done even with an incomplete set of equations and through the analysis; at least some of the dimensionless groups can be obtained (Shook, 1992). Inspectional analysis is stronger than dimensional analysis in the sense that it take into account the underlying physical laws involved in the flow behavior. However, dimensional analysis has been found sufficiently useful for processes involving similar flow behavior (Hagoort, 1990).

1.2.3 Factors Affecting Gravity Drainage

Along with edge water drive and solution gas drive, gravity drainage has long been recognized as one of the three important natural drive mechanism for expelling oil from the reservoir rock. However, the quantification of oil recovery due to drainage has long been a concern. It has long been a concern to identify the contribution of oil recovery due to gravity drainage alone. Calhoun (1953) suggests that if drainage was occurring, those wells lowest in the structure should recover the highest amount of cumulative oil. During the early life of the reservoir, the reservoir tends to produce by solution gas drive, depending upon how much pressure drawdown is available. Although, the primary mechanism is solution gas drive, some drainage is still evident in the reservoir during production period at the lower part of the reservoir. However, when the reservoir pressure depletes, gravity drainage seems to be taking place at greater portions of the reservoir (Lewis, 1943).

Lewis (1943) suggests that the force of gravity provides sufficient amount of mechanical energy that can drain a large percentage of oil from the sand, but the important concern is not how much potential mechanical energy is there in the reservoir but how effective it will be in displacing oil. The distribution of oil within the pore space of the porous media plays an important role in the viability of the oil being recovered efficiently.

Oren et al., (1994), suggest that the static pore-scale distribution of three fluids in a porous media is determined by a complex interaction involving physical phenomena such as Wettability (rock-fluid interactions), spreading phenomena, Capillary pressure, mobility, viscosity and buoyancy.

Grattoni et al., (2002), reports that wettability in conjunction with the spreading characteristics of the oil plays an important role in displacing residual oil from the pores. Grattoni et al., (2002) conducted experiments using large sintered packs, with different matrix wettability and with oils having different spreading coefficients for evaluating the performance of a depressurization process. Results from these experiment indicates that in a water-wet medium, for spreading oils, the physical form of the oil becomes transformed from immobile ganglia into mobile oil films, which can be transported by the gas. For non-spreading oils, oil has to be pushed out by the gas as discontinuous ganglia, so less oil is produced. In contrast, in an oil-wet system, the oil phase already exists as continuous film on the solid surface so that the generation of gas effectively expands the oil phase, enabling the oil to be produced in larger quantities even at lower gas saturations. It can be concluded from this work that rock wettability and oil spreading behavior have an influence on the performance of gas drives.

Moreover, most of the reservoirs have been reported as being mixed wet, in which continuous and distinct oil and water-wetting surfaces coexist in the porous media. Laboratory and network model studies conducted by Rao et al., (1992), Salatheil, (1973), Morrow (1991) and network model studies of Kovscek (1993), indicate that lower residual oil saturation can be obtained for a mixed wet porous media as compared to water wet medium.

The preferential spreading of one fluid over the other in a porous media has been quantified using the spreading coefficient (S). Studies conducted by Blunt et al(1995), Oren et al.,(1995); Mani et al.,(1996) and Grattoni et al.,(2000) emphasizes the importance of film flow behavior in a drainage dominated environment. Mani et al., (1996) reports that for spreading oil system where, S>0, the residual oil saturation is far less than in a non-spreading oil system. If S>0, the interfacial energy of a three phase fluid system is decreased by having a film of oil between the gas phase and the water phase, and thus, oil spreads spontaneously between gas and water. The stability of the oil film becomes a crucial factor in facilitating the drainage of the film owing to gravity. Blunt et al., (1995) report that the thickness and stability of the oil film can be determined using a parameter α. This parameter governs the distribution of oil, water and gas in vertical equilibrium for a spreading system. Where, $\alpha = \sigma_{ow}(\rho_o - \rho_g) / \sigma_{go}(\rho_w - \rho_o)$, and ρ_o, ρ_g and ρ_w are the density of oil, gas and water respectively. Experiments conducted by the Blunt (1995) indicate that if α>1, there is a height above the oil/water contact, beyond which oil only exists as molecular film, with negligible saturation. When α<1, large quantities of oil remain in the pore space and gravity drainage is not efficient. The author also indicates that a negative spreading coefficient leaves behind large quantities of trapped oil in the reservoir, resulting in poor recoveries. Literature on spreading coefficient makes drives us on studying its effect on the gravity drainage of oil assisted by invasion of gas into the model. More literature on spreading coefficient is discussed in Section 3 of this report.

The distribution of oil, gas and water in the reservoir pores is controlled by their capillary interaction and the wetting characteristics of the reservoir rock. Whenever immiscible phases coexist in the porous media as in essentially all processes of interests, surface energy related to the fluid interfaces influences the distribution, saturations, and the displacement of the phases. Most of the EOR processes tend to reduce the interfacial forces existing across the interface of two phases. However, in immiscible processes capillary force exists and forces the denser fluid to retain in the pore spaces. Lewis et al., (1942) suggest that the self propulsion of oil downward through sand under the impulse of its own weight occurs in two zones. At the top where the liquid is in contact with free gas, the sand is only partially oil saturated and capillarity controls the flow. Below the base of this capillary zone, which corresponds to a free surface, the sand is saturated or nearly saturated with liquid and flow follows hydraulic laws. Therefore the complete knowledge of the capillary action in the porous media is necessary to predict the saturations and displacement of the displaced phase. Kantzas et al. (1988) presented equations to predict the saturations of each phase inside the capillaries of arbitrary pore sizes. Capillary pressure versus saturation plots for the three phase systems in capillaries of regular pore geometries were also developed. Li and Horne (2003) developed an analytical model based on capillary pressure curves to match and predict the oil production by free-fall gravity drainage. The model was able to match the experimental and numerical simulation data of oil recovery as well as the oil production data from Lakeview pool and Midway sunset field. These analytical model may find application in prediction of oil recovery for the propose GAGD process.

1.2.4 Summary of Literature Review

The effect of gravity tends to segregate fluids in the reservoir in order to maintain the density equilibrium (Muskat, 1949). Gravity segregation of fluids in horizontal reservoirs often leads to gas override and gas coning problems during a gas injection process. However, Field reviews indicate that gravity stable gas injection are technically successful in dipping reservoirs and are applicable to large variety of geological settings. Recent advances in horizontal well technology have demonstrated that the use of horizontal wells could minimize problems such as gas override and gas coning. Moreover, the use of horizontal wells in naturally fractured reservoirs often results in higher productivity. Horizontal wells could find favorable prospects in gravity stable gas injection processes in horizontal reservoirs. This study aims on investigating the success of a gravity drainage process using horizontal wells.

Film flow characteristics of reservoir fluids are crucial for the implementation of gravity drainage processes. Rock wettability in conjunction with spreading coefficient determines the residual oil saturation for a drainage process. Capillarity plays an important role in the fluid distribution, fluid saturations and the displacement process. Viscosity ratio along with capillary number could determine the flow regime during a gas injection scheme. This work aims on the determination of the effect of all these parameters on GAGD performance.

1.3 Dimensional Analysis approach for scaling gravity drainage experiments

In designing an experiment for the GAGD process it is necessary to be able to quantify the governing forces, in order to show their individual effects on oil recovery. Viscosity, capillary and gravity forces have been identified as the crucial forces that govern a gravity drainage process (Leverett, 1940; Craig, 1957; Hagoort, 1980 and Meszaros, 1990). Blunt et al. (1995) reports that film flow plays an important role in gravity drainage of oil. It is necessary to be able to scale the laboratory results to field scale, in order to investigate their effect on real production scenario. Scaling is a process for extrapolating results obtained in the laboratory scale to the field scale (Shook et al., 1992). Scaling of the GAGD process will involve use of dimensionless numbers that relate the effect of the various variables and forces involved in the drainage process. The basic use of scaling in petroleum literature was outlined by Rapoport (1955). Usage of dimensionless numbers will reduce the number of parameters in the problem statement. The performance of GAGD will hence be a function of the dimensionless groups as opposed to each individual parameter. This reduction is particularly useful in the designing of experimental work where the minimization reduces the number of experiments (Shook et al., 1992). The various dimensionless numbers obtained from literature for gravity stable displacements are listed in Table 1.1.

Table 1.1: Dimensionless groups used for GAGD experimental design

S. No:	Similarity Groups	Formulation	References
1.	Geometric Aspect Ratio (R_L)	$R_L = \frac{L}{H}\sqrt{\frac{K_V}{K_H}}$	Shook et al, 1992
2.	Capillary Number (N_c) Ratio of viscous forces to capillary forces	$\frac{v\mu}{\sigma}$	Grattoni et al, 2000
3.	Bond Number (N_B) Ratio of Gravity forces to capillary forces	$\frac{\Delta\rho g\left(\frac{K}{\phi}\right)}{\sigma}$	Grattoni et al, 2000
4.	Fluid property group (α)	$\frac{\sigma_{ow}(\rho_o-\rho_g)}{\sigma_{go}(\rho_w-\rho_o)}$	Kantzas et al, 1988 and Blunt et al, 1995.

5.	Gravity Number (N_G) Ratio of gravity forces to viscous forces	$\frac{\Delta\rho_{og} g K}{\mu_o v_d}$	Shook et al, 1992.
6.	Fluid property ratio (α)	$\alpha = \frac{\sigma_{ow}(\rho_o - \rho_g)}{\sigma_{go}(\rho_w - \rho_o)}$	Blunt et al, 1995.

The following relationship has to be satisfied in the process of designing an experiment to reflect similar performance at field scale.

$$\gamma\left(\frac{L}{H}\sqrt{\frac{K_V}{K_H}}\right) = \gamma\left(\frac{v\mu}{\sigma}\right) = \gamma\left(\frac{\Delta\rho g\left(\sqrt{\frac{K}{\phi}}\right)}{\sigma}\right) = \gamma\left(\frac{\Delta\rho_{og} gK}{\mu_o v_d}\right) = \gamma\left(\frac{\sigma_{ow}(\rho_0 - \rho_g)}{\sigma_{go}(\rho_w - \rho_o)}\right) = 1 \quad \text{.........(1.1)}$$

Where γ refers to the ratio of dimensionless numbers at field scale to that of the physical model.

1.3.1 Development of the Scaled Physical Model using dimensional analysis

According to Stegemeier et al. (1980), a scaled physical model is developed through various steps. The governing equations for the process have to be identified in order to adequately scale the process. The similarity groups have to be determined through dimensional or inspectional analysis. A prototype field has to be selected, in order to match the similarity parameters between the desired model and the selected field. Model properties are then determined through calculations, engineering judgment and resource availability. We have attempted to follow this approach for developing a scaled physical model of the GAGD process.

After the selection of similarity parameters for the GAGD process, a prototype field was selected. In this study, Weeks Island ‘S’ Sand reservoir was chosen. Weeks Island ‘S’ sand reservoir was a technically successful gravity drainage project.

The relationship presented in Equation 1.1, is the governing criterion for scaling the process, which is in agreement with the scaling laws presented by Rapoport (1955). A model is said to be completely scaled if the above relationship is obeyed. Limitations of physical model arise because of the unavailability of materials and fluids having physical properties that will satisfy all scaling requirements (Stegemeier et al., 1980).

In order to have a better visual insight into the fluid flow behavior of a GAGD process, a two-dimensional model was chosen. Blunt et al, report that taller columns are required to study the film flow behavior of oil in a gravity drainage process for a water-wet media. In order to study the effect of α and model height on the gravity drainage performance, varying the height of packing will be necessary. However, in order to scale the prototype field length a model height of 2 ft has been used in the following calculations.

$$R_{L_P} = R_{L_M} = \frac{L_P}{H_P}\sqrt{\frac{K_V}{K_H}} = \frac{L_M}{H_M}\sqrt{\frac{K_V}{K_H}} = \frac{500}{186}\sqrt{1.0} = 2.69 \text{ ....(1.2)}$$

Where $L_M = \frac{2.69 \times H_M}{\sqrt{\frac{K_V}{K_H}}} = \frac{2.69 \times 2}{1} = 5.38\,ft$. The model permeability was determined using the Bond Number. The porosity of the model was chosen to be the same (26%) as in the field. The desired porosity effect can be obtained by selecting the grain diameter, using the Carman-Kozeny relationship. The following equations demonstrate the methodology behind the absolute permeability scaling of the model.

$$N_{B_P} = N_{B_M} = \left[\frac{\Delta\rho g\left(\frac{K}{\phi}\right)}{\sigma}\right]_M = \left[\frac{\Delta\rho g\left(\frac{K}{\phi}\right)}{\sigma}\right]_P = 1.6 \times 10^{-5} \text{ ....(1.3)}$$

Where $K_M = 1.6 \times 10^{-5} \times \frac{\sigma_M \times \phi_M}{(\rho_o - \rho_g)_M \times g} = 10.48D$. The grain diameter for the model is then selected using the Carman-Kozeny relationship.

$$D_P = \sqrt{\frac{72\tau(1-\phi)^2 K}{\phi^3}} \text{ ....(1.4)}$$

Where D_P=0.152 mm. Glass beads of this diameter are available; hence it is reasonable to choose the porosity as 26%, which is similar to that of the prototype field.

The capillary number relationship is used to scale the gas injection rates for the model. The gas injection rates plays a very crucial role in a stable gravity drainage process, therefore an error in the gas injection rate prediction could affect the model performance to a large extent. The following calculations are done for scaling gas injection rates for the model.

$$N_{C_M} = N_{C_P} = \left[\frac{v\mu}{\sigma}\right]_M = \left[\frac{v\mu}{\sigma}\right]_P = 2.85 \times 10^{-8} \text{ ....(1.5)}$$

$$v_M = 2.85 \times \frac{\sigma_M}{\mu_M} = 1.0591 \times 10^{-8}\, m/s$$

$$Q_M = v_M \times A_M = 1.266 SCF/D$$

The gravity number was not used in the calculation of the model parameters but the similarity relationships were still satisfied for the scaled model. Table 1.2 shows the model parameters identified through this analysis.

Table 1.2: Similarity parameters for the scaled Physical model

Parameters	Weeks Island		Model	
Thickness (H)	186	ft	2-8	ft
Length (L)	500	ft	5.38	ft
Width (W)	N/A	ft	0.08	ft
Absolute Permeability (K)	1200	mD	10480	mD
Project Area (A)	348480	ft^2	0.448	ft^2
Oil Viscosity (μ_o)	0.45	cP	64.5	cP
Gas Viscosity (μ_g)	0.0192	cP	0.0182	cP
Gas-Oil Interfacial Tension (σ_{og})	2.4	dynes/cm	24	dynes/cm
Oil Density (ρ_o)	54.0	lb/ft^3	53.9	lb/ft^3
Gas Density (ρ_g)	0.4	lb/ft^3	0.1	lb/ft^3
Water Density (ρ_w)	58.7	lb/ft^3	62.3	lb/ft^3
Porosity (ϕ)	0.26		0.26	
Average Pressure (P_{avg})	4714.7	psia	14.7	psia
K_v/K_h	1		1	
Gas injection rate (Q_g)	1411592	SCF/D	1.266	SCF/D
Gas formation volume factor (B_g)	0.00358		1	
Geometric aspect ratio (R_L)	2.69		2.69	
Bond Number (N_B)	1.6E-05		1.6E-05	
Capillary Number (N_c)	2.85E-08		2.85E-08	
Alpha (α)	4.276		10.56	
Gravity Number (N_g)	192.48		192.48	

All the above-mentioned parameters can be satisfied in the scaled model. The flood pair of paraffin oil and air satisfies the fluid properties and the fluid-fluid interaction parameters listed in Table 1.2.

The preliminary design of the scaled physical model is subjected to changes that could take into account other factors such as spreading coefficient, heterogeneity (grain size distribution) and miscibility.

Scaled experiments on the current physical model are underway. Various experiments have been carried out on the physical model to simulate the dimensionless numbers calculated from field production data in order to capture the operating mechanism in those fields. Detailed dimensional analysis of the current gravity drainage projects will be discussed in section 3 of this report.

1.4 Experimental Design and scaling of the current physical model

Literature reveals that the important forces that control the performance of a gravity drainage process are capillary, viscous and buoyant forces. This study will aim on investigating the effect of all these forces in addition to the spreading coefficient and wettability on GAGD performance. All the experiments conducted in this study will attempt to study the effect of Capillary number, Bond number, Spreading coefficient, α, mode of injection (secondary/tertiary), rock wettability and mode of gas injection (constant pressure/ constant rate) on the performance of GAGD.

1.4.1 Effect of Bond Number

The effect of Bond number on GAGD oil recovery will be studied by using glass beads of varying grain sizes and the same fluid-fluid system (Decane-N_2) in our case. Bond number (N_B) is defined as the ratio of gravitational forces over that of the capillary forces (Table 1.1). Bond number is directly proportional to the absolute permeability of the sand pack, and the density difference of the reservoir. Absolute permeability of a consolidated porous media is a strong function of the grain diameter and is given by the Carman-Kozeny equation (Equation 1.4). Where D_P is the grain diameter, τ is the tortuosity and ϕ is the porosity of the bead pack.

However, it is out of the scope of this study to measure the tortuosity of the sand pack, therefore the typical value of 1.5, for sand packs is used as the tortuosity in the above equation. Moreover, permeability decreases weakly with tortuosity, and tortuosity does not vary vastly (White, 2004). In order to obtain favorable and realistic Bond numbers, fluid-fluid interaction parameters (interfacial tension) are also important The Bond number ranges obtained from the field is the basis of the experimental design for studying their effect on GAGD recovery.

Experiments will be conducted by selecting proper grain sizes and fluids to simulate the Bond numbers obtained from field production data.

1.4.2 Effect of Capillary Number

The capillary number plays a very important role in deciding the stability of the gas displacement process. The importance of capillary number and the viscosity ratio of the displacing and displaced fluid have been mentioned in the literature review section. Viscous forces have an effect on the drainage process.

In this study we intend to quantify the viscous forces with respect to the capillary forces by using the capillary number. To obtain different capillary numbers, two different fluid-fluid systems have been selected, namely (Decane-CO_2 and Paraffin-CO_2). However, the ranges of capillary number obtained through selection of different fluid-fluid system are not large in magnitude as compared to the ranges obtained through selection of different gas flow rates. Different gas flow rates were obtained through the constant mass flow controller. Capillary numbers of various orders of magnitude were obtained for each experiment.

1.4.3 Effect of Operating Mode

Literature reveals that the spreading phenomenon of oil during drainage is an important factor that determines the residual oil saturations. Hence it is important to study the effect of spreading coefficient on GAGD oil recovery. For this purpose two fluid-fluid pairs that will yield a positive and a negative spreading coefficient will be chosen. The displacement, drainage and/or film flow behavior in the physical model will be captured using digital cameras, to gain an understanding of the predominating flow mechanism in the gas-assisted gravity drainage process.

Lewis (1943) suggests the following modes of operating a gravity-stable gas injection process:

A. Gas injection at a constant pressure.
B. Restore and maintain or partially restore gas pressure after depletion of pressure
C. Reduce pressure gradually, so that gas and oil can segregate continuously by counter flow.
D. Produce field in two stages, first under solution gas-drive conditions until the gas has been practically eliminated from the oil, then by gravity drainage.

A and C method, mentioned by Lewis (1943) are useful for commercial production from primary reservoirs. A thorough comparison between these two modes of gravity drainage process seems to be useful for a GAGD process. Experiments will be conducted to identifying the most favorable operating mode for GAGD. Gas injection at constant pressure mode and gas injection at constant rate mode will be studied.

Besides the two operating modes of gas injection we will also investigate the effect of mobile and immobile or connate water saturation on GAGD, this will be achieved by conducting GAGD in primary recovery mode and secondary recovery mode (after waterflooding).

1.4.4 Effect of Heterogeneity

The effect of heterogeneity on GAGD will be studied using glass beads with specific grain size distribution. Glass beads having a grain size distribution of more than one will provide permeability contrast at different portions of the bead pack. Artificial fractures will also be induced in the model in order to study the effect of fractures on GAGD oil recovery.

1.4.5 Experimental Setup

- **Apparatus**

A Hele-Shaw type physical model is being used for studying the feasibility of GAGD as a potential EOR technique. The Hele-Shaw model is a 2-D visual model, having an Aluminum frame and two 16”×24” ×1” Pyrex glass windows, separated by a plastic spacer. The Pyrex glass is held together by bolts, which are fastened to the aluminum frame. The physical model is packed with glass beads. A schematic of the complete experimental setup is shown in Figure 1.1.

This 2-D Physical model will be used to investigate the performance of GAGD and the effect of the variables on its performance. Visual experiments will be carried out using different fluids and packing, in order to obtain dimensionless numbers that fall in the same ranges as that of the field

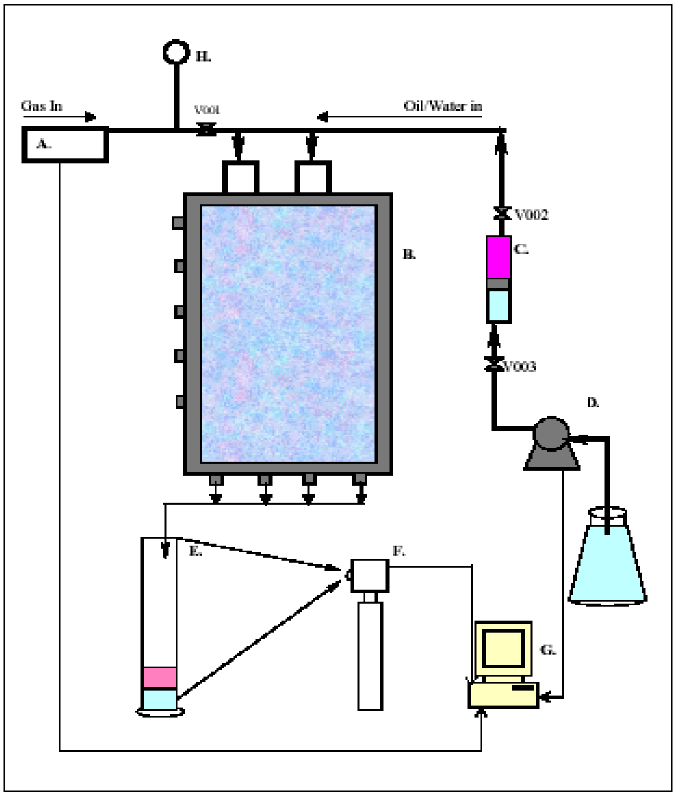

Figure 1.1: Schematic diagram of the Physical Model

A. Mass flow controller/ Pressure regulator.
B. Physical model.
C. Transfer vessels.
D. Pump.
E. Separator.
F. Camera.
G. Data acquisition system and imaging computer.
H. Pressure Gauge.

- **Experimental Protocol**

  The following experimental protocol will be used for all the experiments:

  1. Dismantle the physical model.
  2. Fill model with glass beads
  3. Apply vacuum to the model and check for leaks.
  4. Imbibe distilled water in the model from the bottom.
  5. Drain water by pumping oil at the top from the transfer vessel through (V002) into the model.
  6. Calibrate and Caliper the Vision system and the data acquisition software.
  7. Set Mass flow controller or the pressure regulator to the desired gas flow rate or injection pressure respectively.
  8. Open the gas injection valve (V001) and Start Data Acquisition system.
  9. Repeat step 1 to 9 for consecutive runs.

  Ranges of dimensionless numbers from field review have been obtained by Kulkarni, (2004). These ranges of dimensionless numbers will be duplicated in the series of experiments conducted under this study. Different fluid-fluid combination and grain sizes will be used in order to provide ranges of numbers typically obtained in the field. The field ranges of numbers are listed in Table 1.3 (Kulkarni, 2004).

Table 1.3: Field ranges of dimensionless groups

Field Ranges	**Capillary Number (N_C)**	**Bond Number (N_B)**	**Gravity Number (N_G)**
Minimum	1.12E-09	1.21E-05	875
Maximum	4.18E-08	2.84E-07	0.39

Various fluid-fluid triplets have been investigated for the experiments on the physical model. Considerations have been given to the toxicity and other hazard they may pose. Paraffin and Decane have finally been chosen as the fluids for most of the experiments, except the one for investigating the effect of spreading coefficient on GAGD oil recovery.

1.4.6 Experimental Plan

The variables to be investigated for a detailed study to determine the feasibility of GAGD as a potential EOR process has been discussed in the previous section. Experiments will be conducted to investigate the effect of Bond number, Capillary number, Spreading coefficient, operating parameter/mode and heterogeneity. The following fluids shown in Table 1.4 have been chosen as potential candidates for investigating the effects of spreading coefficient. In order to cover the ranges of dimensionless numbers that were obtained from field data, a detailed plan for this study has been laid out in Table 1.5.

Table 1.4: Plan for studying the effect of spreading coefficient on GAGD

Fluids	σ	Density	Viscosity	Spreading coefficient (S)
Hexane	18.4	659	0.336	3.4
Isoamyl alcohol	23.7	854	N/A	44
TCE	30	1460	1.206	7.2
CCl4	27	1594	0.97	0.6
n-pentane+paraffin+n-butyl alcohol	23.6	779	64.5	-1.2
n-pentane+paraffin	22.8	777	0.84	2.7

Table 1.5: Plan for studying the effect of Bond number and Capillary number on GAGD

Type Of Experiment	Fluid-Fluid System	Grain Size	Gas Flow Rates cc/min	NB	NC	Field Ranges	
						Max	Min
Capillary Number Variation	Decane-N_2	0.5 mm	2	4.0E-04	5.3E-09	4.2E-08	1.2E-09
	Decane-N_2	0.5 mm	20	3.5E-04	5.3E-08		
	Decane-N_2	0.5 mm	200	3.5E-04	5.3E-07		
Bond Number Variation	Decane-N_2	0.1 mm	20	3.6E-05	1.7E-07	1.2E-05	2.8E-07
	Decane-N_2	0.05	20	1.2E-06	1.7E-07		
	Decane-N_2	0.02	20	1.0E-07	1.7E-07		

To study the effect of reservoir heterogeneity, artificial heterogeneity, such as vertical faults, horizontal faults and permeability contrasts will be simulated in the model by placing thin mesh, between grains and filling the model in layers by using different types of grain sizes.

1.5 Experimental Results

Experimental results obtained to study the effect of operating conditions, type of gas injectant and the effect of Bond number and capillary numbers have been completed and are reported under this section. The protocol mentioned in the above section was strictly followed to conduct all these experiments.

1.5.1 Constant Pressure GAGD Experiments

Experiments were conducted to identifying the various mechanisms that are dominant and the critical parameters that affect the gravity drainage performance during the GAGD experiments. Bond number and capillary numbers are being used to characterize performance of all the GAGD experiments.

The first sets of experiments were conducted at constant pressure gas injection into the model. These experiments are listed as Run CP1 and Run CP2 in Table 1.6.

The constant pressure experiments were conducted using two different gases to verify and demonstrate that the type of gas does not affect the GAGD performance under immiscible conditions. As can be seen from Table 1.6, except the type of gas Injectant, all the other parameters were the same for both runs. This provides us with a common ground for comparison based on capillary numbers.

Table 1.6: Model Parameters for Constant Pressure Runs (4 psig)

Run Number	**Run CP1**	**Run CP2**
Fluid-Fluid System	Paraffin-CO_2	Paraffin-N_2
Oil Viscosity (cP)	65	65
Gas Viscosity (cP)	0.01462	0.01755
Oil Density (Kg/m^3)	864	864
Gas Density (Kg/m^3)	1.808	1.1651
Grain Diameter (mm)	0.5	0.5
Absolute Permeability (D)	152 D	152 D
Total Water Imbibed (cc)	520	522
Total Water Drained (cc)	480	480
Total oil in the cell (cc)	480	480
Porosity of the Bead Pack	0.413	0.414
Connate Water Saturation (%)	8	8
Initial Oil Saturation (%)	92	92
Bond number	4.0E-04	4.1E-04
Capillary Number	1.62E-08	1.95E-08

Similar values of connate water saturation and porosity were obtained for both these runs, indicating similar packing during both the runs, and providing fair performance evaluations based on injectant types.

Figure 1.2 shows the results obtained from the runs at constant pressure. The oil production rates in both the cases were almost identical. This symbolizes that the type of Injectant has minimal influence on GAGD performance at constant pressure and immiscible conditions. The gravity drainage rates tend to increase after gas breakthrough if the mode of gas injection is constant pressure. Muskat (1949) explains that maintaining reservoir pressure is the ideal mode for gas injection. Since the inlet pressure was maintained at 4 psi using a pressure regulator, the gas injection rates were varied to provide that much pressure in the model and hence accounted for higher oil recoveries as opposed to constant rate injection mode, wherein gas injection rates were constant and pressure in the model decreased due to oil depletion.

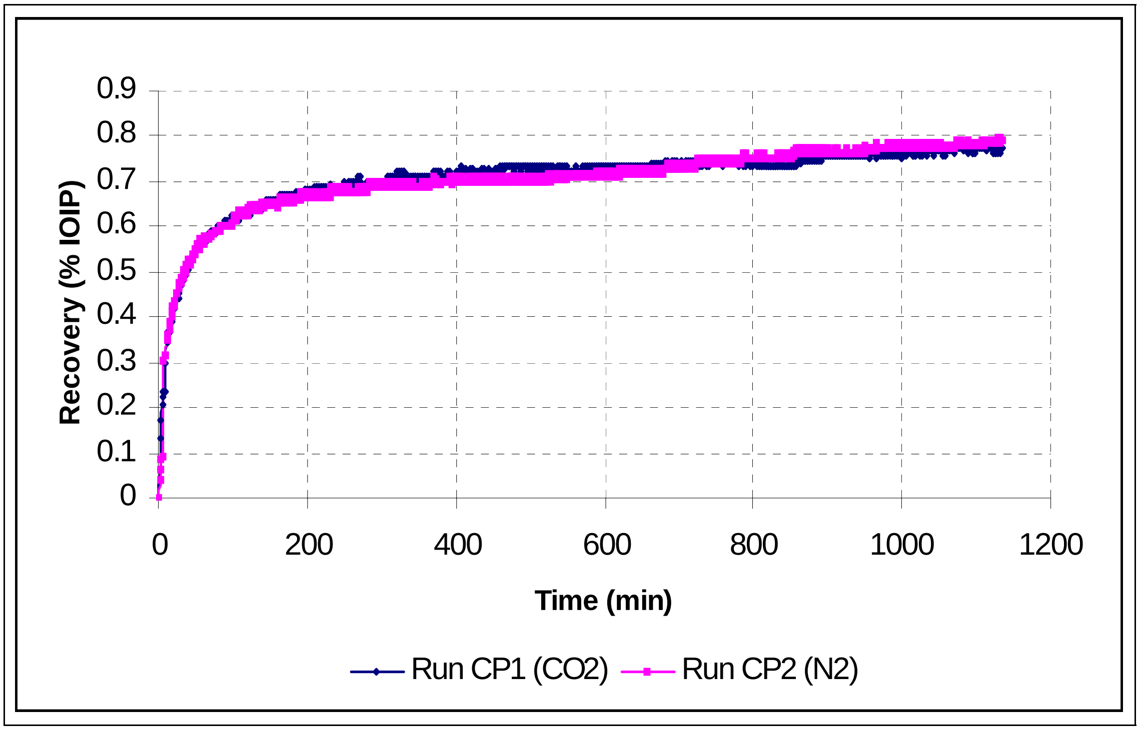

Figure 1.2: Recovery plots for Constant Pressure Runs CP1 and CP2.

1.5.2 Constant Rate GAGD experiments to study the effect of Bond number

Constant rate GAGD experiments were performed using a mass flow controller. The mass flow controller was calibrated and assembled with the model for allowing gas to be injected at constant volumetric rates. Three experiments were conducted to determine the effect of Bond number and capillary number on the GAGD performance. These experiments are listed as Run # CR1, Run # CR2, Run # CR3 and Run # CR4 in Table 1.7.

Run CR1 was conducted using glass beads of 0.5mm diameter whereas Run CR2 and Run CR3 were carried out using glass beads of 0.15mm diameter and Run CR4 with 0.065mm. The purpose was to study the effect of Bond numbers on GAGD performance. Absolute permeability is a function of grain diameter. Increase in grain diameter tends to increase the absolute permeability, which increases the Bond number.

From Figure 1.3 it can be seen that a much higher ultimate recovery is obtained using larger grain size, which can be attributed to the fact that, larger grain size provides for a higher value of absolute permeability and Bond number. Recoveries from Run CR2 and Run CR3 are similar, which again confirms the fact that type of gas injected has less effect on oil recoveries for an immiscible process,. A comparison between oil recoveries at constant pressure (Run # CP1) and recoveries at constant rates (Run # CR1) are shown in Figure 1.4.

Table 1.7: Constant Rate 2D Experiments to study the effect of Bond number on oil recovery.

Run Number	Run CR1	Run CR2	Run CR3	Run CR4
Fluid-Fluid System	Decane-CO_2	Decane-CO_2	Decane-N_2	Decane-N_2
Oil Viscosity (cP)	0.84	0.84	0.84	0.84
Gas Viscosity (cP)	0.01462	0.01462	0.01755	0.01755
Oil Density (Kg/m^3)	734	734	734	734
Gas Density (Kg/m^3)	1.808	1.808	1.1651	1.1651
Grain Diameter (mm)	0.5	0.15	0.15	0.065
Absolute Permeability (D)	152	43	43	10.2
Total Water Imbibed (cc)	523	546	538	548
Total Water Drained (cc)	460	430	430	412
Total oil in the cell (cc)	460	430	430	412
Porosity of the Bead Pack (ϕ)	0.415	0.433	0.426	0.43
Water Saturation (%)	12	22	20	24
Oil Saturation (%)	88	78	80	76
Bond Number	3.5E-04	3.6E-05	3.5E-05	7.07E-06
Capillary Number	5.35E-08	5.35E-08	6.43E-08	6.43E-08

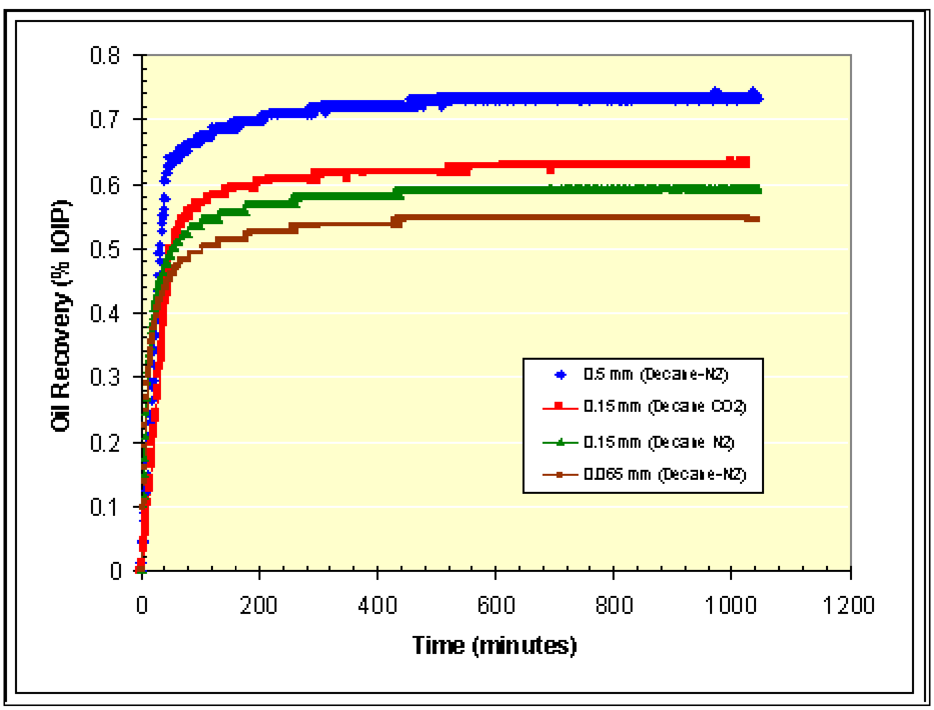

Figure 1.3: Recovery Plots for Run CR1, CR2, CR3 and CR4.

Figure 1.4 shows a steady increase in the recovery performance after gas breakthrough for the constant pressure run, whereas very little additional oil is recovered after gas breakthrough during the constant rate runs. This appears to indicate that the reservoir pressure maintenance could be a critical factor for the GAGD process.

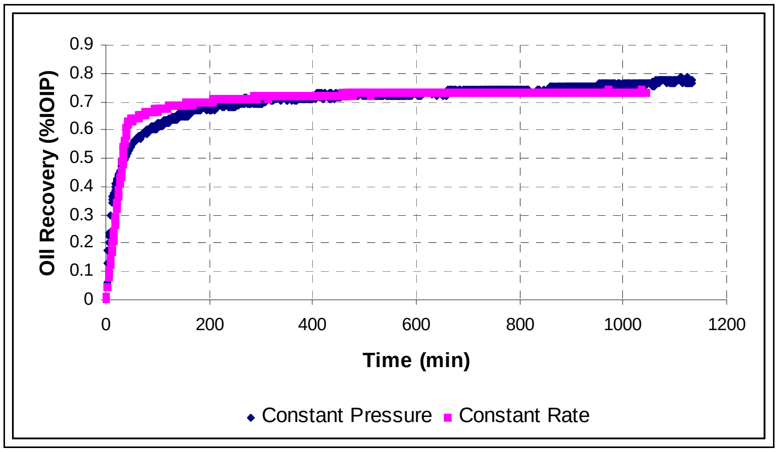

Figure 1.4: Recovery comparison for constant rate and constant pressure runs.

A wide range of capillary and Bond numbers were chosen to study the recovery performance of the GAGD process. Table 1.8 demonstrates that the effect of Bond number on GAGD oil recovery. Comparing Run CR1 and CR2, it can be seen that there is an 11% increase in recovery for a 10 times higher Bond number process. However, between Run CR2 and CR3, the incremental oil recovery with glass beads of similar grain size is not that large for a slight variation in the capillary numbers. Figure 1.5 shows that there is an increase in oil recovery with an increase in the bond number for all the cases and the trend is almost linear.

Table 1.8: Dependence of Oil recovery on Bond and Capillary Numbers

Runs at low N_C Variation	Bond Number (N_B)	Capillary Number (N_C)	Recovery (%IOIP)
Run CP1	4.0E-04	1.620E-08	79.36
Run CP2	4.1E-04	1.953E-08	78.3
Run CR1	3.5E-04	5.357E-08	73
Run CR2	3.6E-05	5.357E-08	62
Run CR3	3.5E-05	6.431E-08	59
Run CR4	7.1E-06	6.430E-08	54.38

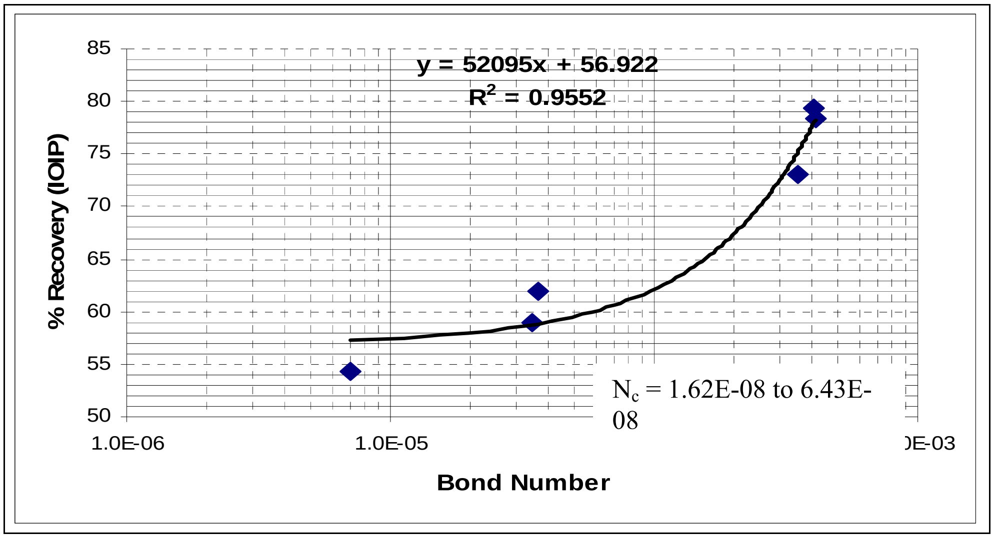

Figure 1.5: Effect of Bond Number on Oil recovery by GAGD

1.5.3 Effect of Capillary Number on GAGD oil recovery

To investigate the effect of capillary numbers on GAGD oil recovery, three runs were carried out at different flow rates to obtain significant variation in the capillary numbers. The details of these runs are presented in Table 1.9. The recoveries oil recoveries obtained from these runs are presented in Figure 1.6.

Table 1.9: Constant Rate 2D Experiments to study the effect of the variation of capillary Numbers on oil recovery

Run Number	Run CR3	Run CR5	Run CR6
Fluid-Fluid System	Decane-N2	Decane-N_2	Decane-N_2
Gas Flow rate (cc/min)	50	20	5
Oil Viscosity (cP)	0.84	0.84	0.84
Gas Viscosity (cP)	0.01755	0.01755	0.01755
Oil Density (Kg/m^3)	734	734	734
Gas Density (Kg/m^3)	1.1651	1.1651	1.1651
Grain Diameter (mm)	0.15	0.15	0.15
Absolute Permeability (D)	41.2	43	43
Total Water Imbibed (cc)	514.8	538	522
Total Water Drained (cc)	410	430	404
Total oil in the cell (cc)	410	430	404
Porosity of the Bead Pack	0.408	0.426	0.414
Water Saturation (%)	20.3	20	22.6
Oil Saturation (%)	79.0	80	77.4
Bond Number	3.0E-05	3.5E-05	3.1E-05
Capillary Number	1.33E-07	6.43E-08	1.60E-08

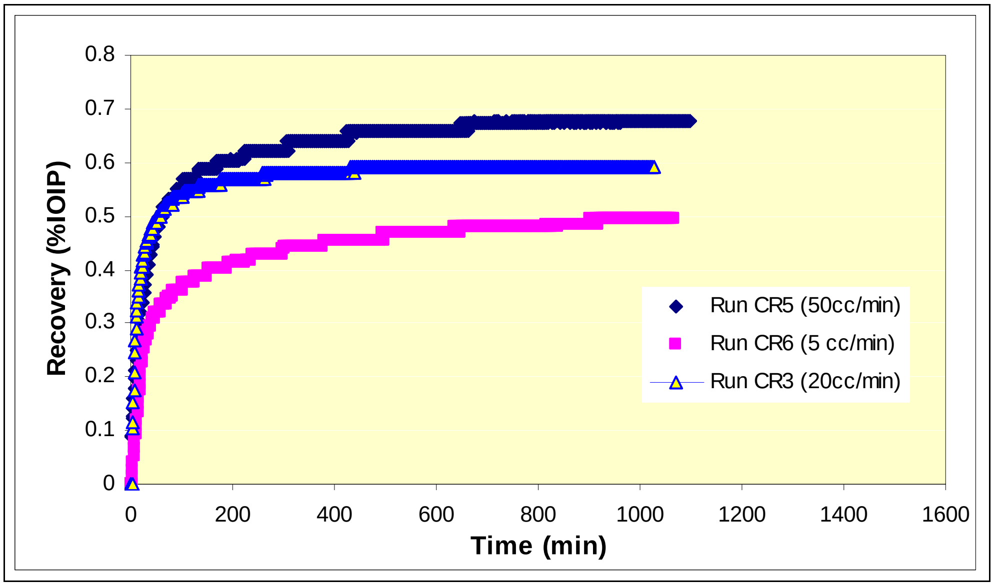

Figure 1.6: Oil recoveries obtained from different gas injection rates

Figure 1.6 demonstrates that an increase in capillary numbers results in a significant increase in the oil recovery. However, the capillary number can only be increased to a certain critical value. If the gas flow rates are too high that the flow regime is no longer stable, then gravity stable flood cannot be achieved. This study also intends to investigate the critical value of gas flow rates so as to obtain the most optimum operating conditions. Table 1.10 shows that a significant increase in oil recovery can be obtained with the increase in capillary number by tens of magnitude. Figure 1.7 demonstrates a linear trend in oil recovery with the increase in gas flow rates. The dimensionless numbers obtained from field production data, coreflood experiments and the physical model has been plotted against their corresponding recoveries and is presented in Section 3 of this report. From the plot presented in Task III, a typical behavior in recovery variation with respect to dimensionless numbers can be observed.

Table 1.10: Oil recovery variation with capillary numbers

Runs at low N_C Variation	**Bond Number (N_B)**	**Capillary Number (N_C)**	**Recovery (%IOIP)**
Run CR5 (50 cc/min)	3.0E-05	1.331E-07	67
Run CR3 (20 cc/min)	3.5E-05	6.431E-08	59
Run CR6 (5cc/min)	3.1E-05	1.602E-08	49

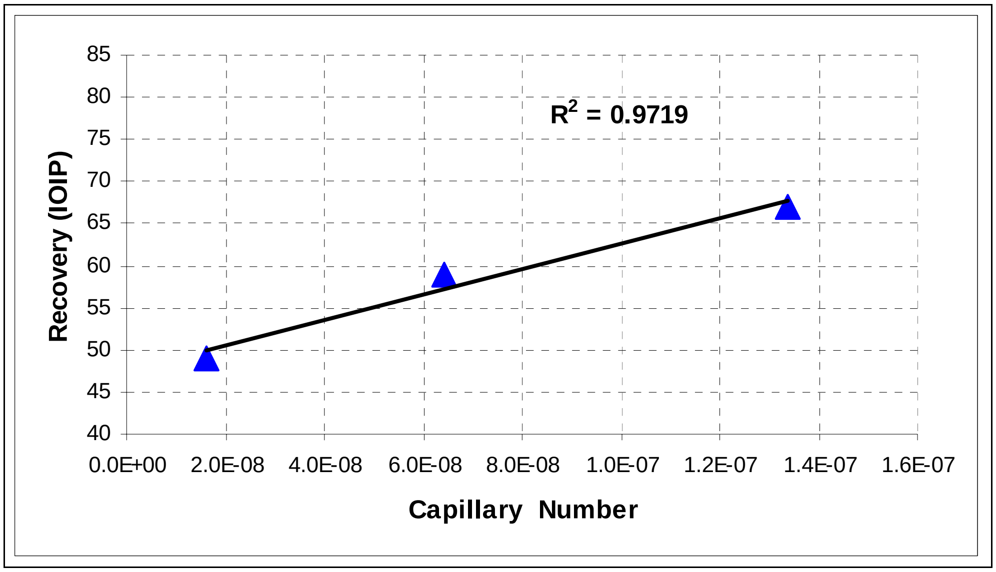

Figure 1.7: Effect of Capillary Number on Oil recovery by GAGD

1.6 A Predictive model for the Free Gravity Drainage Process using a Bundle-of-Capillary-Tube Method

Porous media have abilities to transmit and retain fluid by their interconnected pore structure and capillary forces. The transport properties of a porous medium depend on properties of the fluids, porous media, and their interactions. When three phases, namely, oil, water and gas, are present in a porous medium, the fluid distribution and flow capacity depends on the thermodynamic properties of the fluids and wettability of the porous media. Multiphase flow in porous media can be modeled with appropriate modifications in the Darcy's law, which was originally derived for single-phase flow. The concept of relative permeability that lumps the effects of fluid-fluid and rock-fluid interactions has been used in the Darcy's law application for characterization to flow in porous media. However, the lumping of the rock-fluid interactions may mask the effects of the physical forces. Hence one of the objectives of the scaled physical model study of gravity drainage process is to investigate the effects of individual forces and their interplays. In a typical water-wet reservoir operating under gas gravity drainage, water coats all the grain surfaces and occupies the smallest pores and may remain immobile during some part of the process. Mobile oil occupies relatively larger pores and drains down by gravity; gas occupies the pore space left by oil. In such a process, even in a 3D reservoir condition, the flow is primarily in one dimension downwards, which is especially true in the upper portion of the reservoir. These features make it possible to model the process with a simple bundle-of-capillary-tube model, which has been applied to study flow in porous media in the field of petroleum engineering (Nutt, 1982).

This section reports the detailed development of the bundle-of-capillary-tube model. A spreadsheet program has been development and the results from the model are compared with the free gravity drainage experimental results on the 2D Hele-Shaw type physical model. Some of the model parameters are determined based on the match with the experimental results. Physical basis and justification for the model are discussed.

1.6.1 Results from Free-Gravity Drainage Experiments

To help better understand the gravity drainage process and model development, preliminary free gravity drainage experiments were conducted with a bead pack at the connate water saturation. The oil, Decane or paraffin (dyed red, referred as oil or oleic phase), drains under gravitational force only (free gravity drainage); no external pressure was applied.

- **Free Gravity Drainage with Decane**

In this run, the bead pack was fully saturated with water first, recorded a volume of 492 cc. Then Decane was injected at an injection rate of 6 cc/min to displace water and create a pre-gravity-drainage condition. Decane broke through after 68 minutes (0.83 pore volume (PV)), with an ultimate recovery of 115 cc (Figure 1.8). Therefore the initial oil in place (IOIP) was 425 cc, which is the total injected volume of 540 cc (90 min x 6 cc/min) minus the produced volume of Decane. The displacement results in an average Decane saturation of 0.86 in the pack.

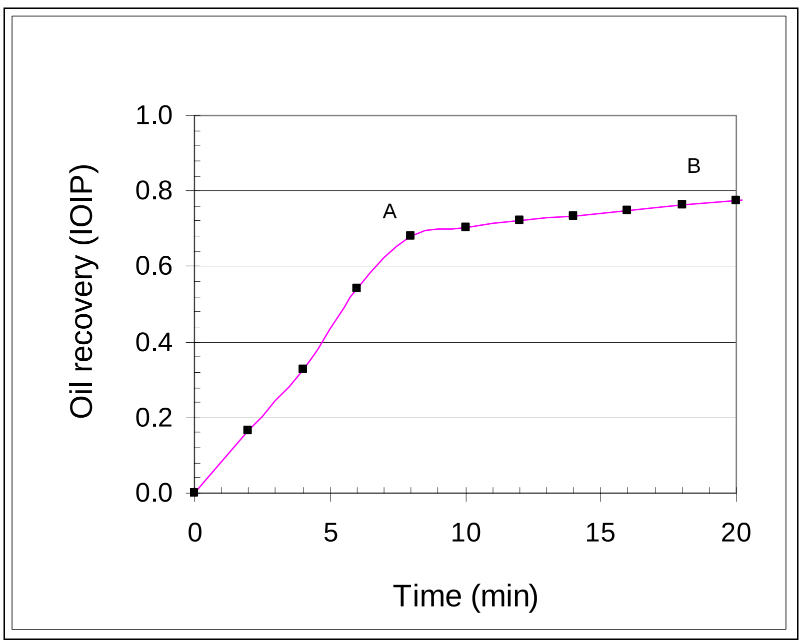

Figure 1.8: Oil recovery as a fraction of the IOIP versus time for Decane (Experiment Run 1).

Figure 1.8 plots the oil recovery (as a fraction of initial oil in place (IOIP)) versus time during the gravity drainage process. In the first ten minutes before the point "A"

(0.68 IOIP), production rate was high and almost constant. After point “A”, the oil production was much slower to reach point “B”. The ultimate production, after 24 hours, was 0.96 IOIP (not shown in the figure).

- **Free Gravity Drainage with Paraffin**

This run was conducted in a similar manner to Run 1. The cumulative oil recovery versus time is plotted in Figure 1.9. Due to the higher viscosity of paraffin compared to Decane, it was possible to observe the air-oil interface and its movement within the model. The air/oil interface between the gas zone and oil bank are shown as Figure 1.10. Residual oil in gas zone was evident as indicated by the dark dots whose saturation can be inferred from material balance. Oil drainage ceased at the time in Figure 1.10(b) likely due to the capillary end effect. During the process, no water was produced, supporting the assumption that water (at its initial saturation of 0.082) was immobile during gravity drainage.

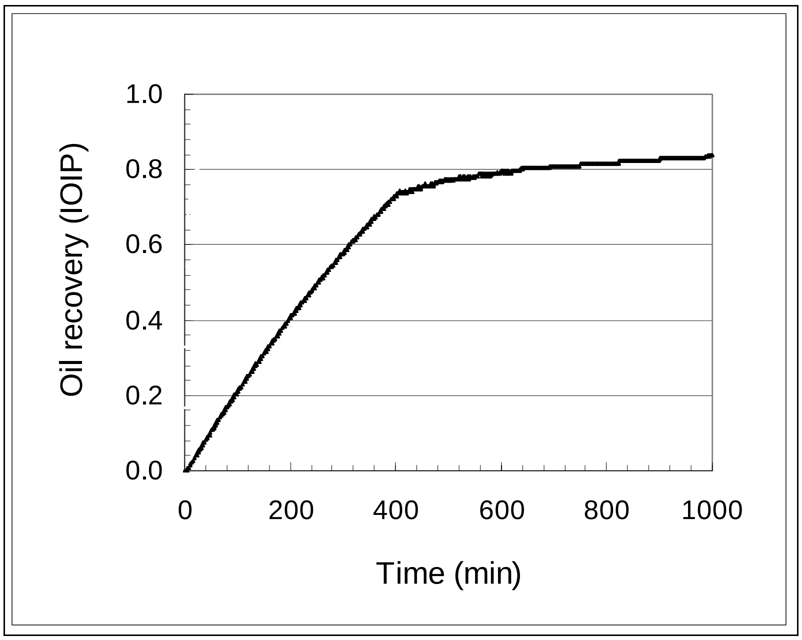

Figure 1.9: Oil recovery as a fraction of the IOIP versus time for paraffin (Experiment Run 2).

The gravity drainage process can be characterized by two stages; the first stage corresponds to an oleic single-phase drainage at a higher rate where in the oil bank rapidly shrinks while producing oil at nearly constant rate, whereas the second stage corresponds to the time after air break through at the outlet, and is characterized by multiphase flow at a lower oil drainage rates. Oil flows in oil-depleted bead pack during this stage, and this flow is often referred as film flow, which is characterized by hydraulic continuity of the oil phase, and is also characterized by relative permeability being at the order of squared oil saturation (DiCarlo, et al., 2000).

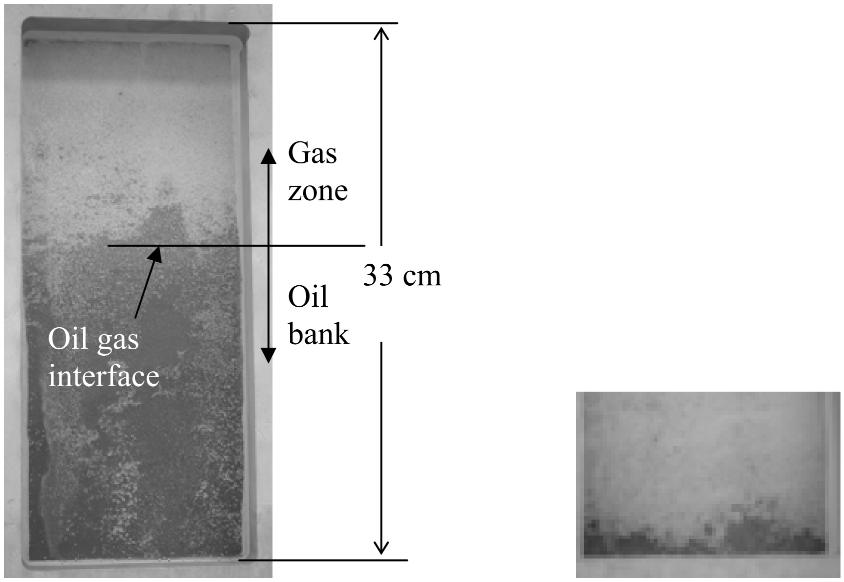

(a)
(b)

Figure 1.10: (a). imagine of the oil/gas interface in the visual model. (b). Illustration of the capillary end-effect. (Experiment Run 2).

1.6.2 Bundle-of-Capillary-Tube Model Development

In the bundle-of-capillary-tube model, a vertical capillary tube with radius, $r_{i,}$ is the basic building block and the porous medium is assumed to consist of a series of such tubes in the same length but with different radii. The radii of tubes correspond to the pore-throat radius of porous media, which depends on particle size and packing and can be described by using of a size distribution function. The following model development uses the experimental cases as the target i.e., parameters are taken from experimental Run 1 and 2.

1.6.3 Capillary Tube Radius Size Distribution

The glass bead pack in experiments has particle sizes from 0.4 to 0.6 mm. Range of pore throat sizes can be obtained from the following pore throat and particle size relations (Saputelli et al., 1998),

$r_{min} = 0.1547\ r_{p(min)}$……………………………………………………………………(1.6)

$r_{max} = 0.404\ r_{p(max)}$……………………………………………………………………..(1.7)

Where r_{min} and r_{max} are the minimum and maximum pore throat sizes; $r_{p(min)}$ and $r_{p(max)}$ are the minimum and maximum particle sizes. The pore throat sizes that correspond to the radius of the capillary tubes are assumed to obey the distribution function as described by eq. 1.8.

$$\gamma(r_i) = (1.0/r_i + 100\, r_i) / \int_{r_{min}}^{r_{max}} (1.0/r_i + 100.0 r_i) dr_i \quad (1.8)$$

Where $\gamma(r_i)$ is a hypothetical probability-density function, but the trend (Figure 1.5) that smaller pores dominating is reasonable and have some indirect support from the pore throat size distribution of measured real porous media (Manwart, et al., 2000).

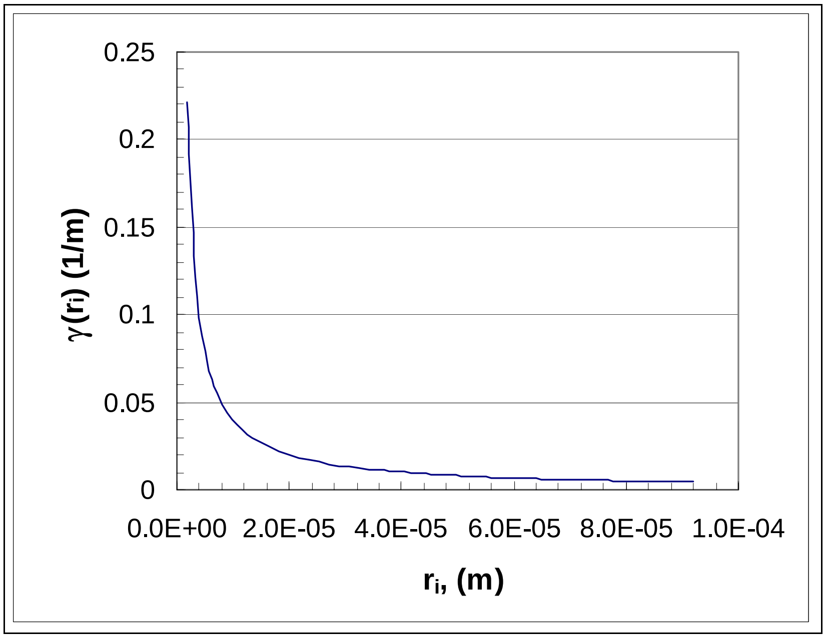

Figure 1.11: Probability density function of pore throat radius

- **Flow in a Capillary Tube**

Consider a representative capillary as shown in Figure 1.12(a) for analysis. It is assumed that fluid (oil) originally in place flows in three modes: bulk flow, film flow, and residual (no flow). As indicated in Figure 1.12(a), bulk flow takes place in the center of portion of the tube representing 80% of the fluid in volume; film flow takes place as film along the wall representing 20% of the fluid in volume with 5% as residual. Some rationale of these assumptions is discussed later.

The bulk flow is driven by gravitational force, and limited by capillary pressure that acts at the oil/gas interface (Figure 1.12(a)). The average velocity of the bulk flow across a cross-sectional area perpendicular to z direction is given by Hagen-Poiseuille law (Bird et al., 1960).

$$u_b = \nabla \mathscr{P} r_i^2/(8\mu) \quad (1.9)$$

Where u_b is the average velocity in z direction in the bulk flow, μ is fluid viscosity, and

$$\nabla\mathscr{P} = \nabla(\rho g\,(L\text{-}z) - p_c) \quad \ldots\ldots\ldots\ldots\ldots\ldots\ldots\ldots\ldots\ldots\ldots\ldots\ldots\ldots\ldots\ldots\ldots (1.10)$$

Is the potential gradient along the vertical direction within the oil bank (length, L-z), ρ is the fluid density, and g is the gravitational acceleration, capillary pressure, pc, at the gas-oil interface can be represented by,

$$p_c = 2\sigma \cos\theta / r_i \quad \ldots\ldots\ldots\ldots\ldots\ldots\ldots\ldots\ldots\ldots\ldots\ldots\ldots\ldots\ldots\ldots\ldots\ldots (1.11)$$

σ is the interfacial tension between the oil and air, θ is the contact angle that can be assumed to be zero here because of the spreading condition assumption. Thus, we have,

$$\begin{aligned}\nabla\mathscr{P} &= \nabla(\rho g\,(L\text{-}z) - p_c)\\ &= (\rho g\,(L\text{-}z) - p_c)/((L\text{-}z))\\ &= (\rho g - p_c/(L\text{-}z)) \quad \ldots\ldots\ldots\ldots\ldots\ldots\ldots\ldots\ldots\ldots\ldots\ldots\ldots\ldots (1.12)\end{aligned}$$

and finally,

$$\begin{aligned}u_b &= \nabla\mathscr{P}\, r_i^2/(8\mu)\\ &= r_i^2(\rho g - (2\sigma/r_i)/(L\text{-}z))/(8\mu) \quad \ldots\ldots\ldots\ldots\ldots\ldots\ldots\ldots\ldots\ldots\ldots\ldots (1.13)\end{aligned}$$

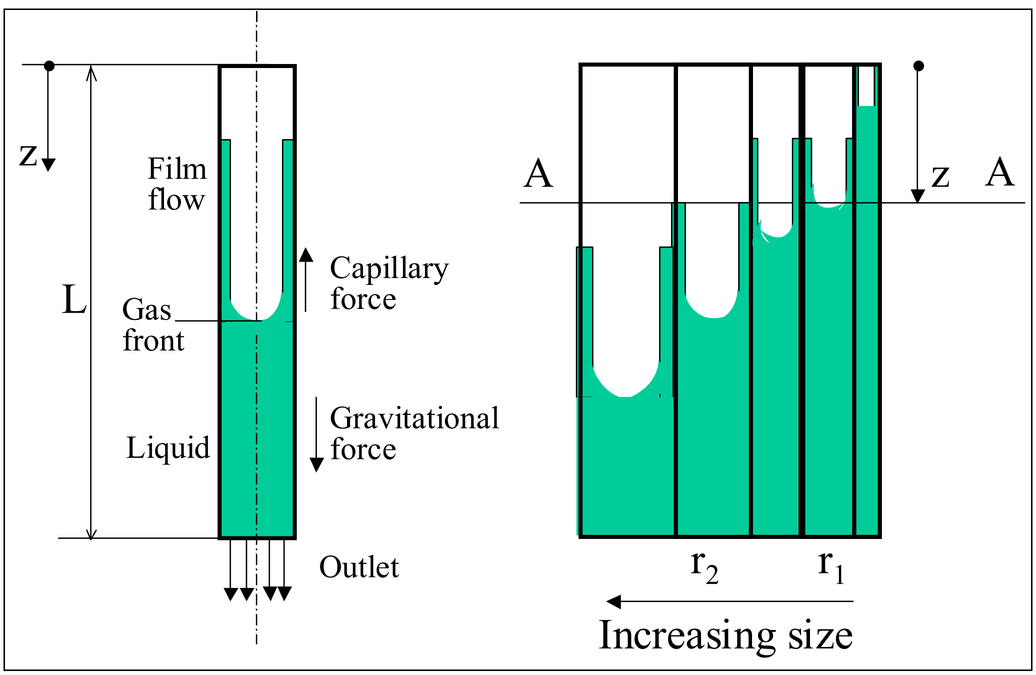

(a) (b)

Figure 1.12: (a). Schematic of fluid flow in a capillary tube. (b). Illustration of fluid flow in multiple capillary tubes.

- **Film Flow**

Film flow velocity is giving by eq. 1.14 (Bird, et al., 1960),

$u_f = \delta^2 \rho g/(3\mu)$ ……………….....……………………………………………………..(1.14)

Where δ is the thickness of the film. The film thickness can be determined by the assumption that the liquid in film flow mode represents 20% of the total volume,

$\delta = r_i/18.94$ ….………………………………………………………………….(1.15)

Notice we assumed 5% of the total volume as the residual and thus the film flow portion is only 15% of the total volume.

- **Determine Average Liquid Saturation at a Cross Section**

With eqs. 1.14 and 1.15, we can calculate oil saturation, S_o at a specific time t at a position z (e. g., A-A cross section in Figure 1.12(b)). At this cross section, there is a tube where the bulk flow interface just arrives, the radii of this particular tube, r_1, can be determined by using of eq. 1.16,

$u_b = r_1^2(\rho g - (2\sigma/r_1)/(L\text{-}z))/(8\mu) = z/t$ ………………………………...…….……..(1.16)

Solving eq. 1.16 for r_1, we get:

$r_1 = \sigma/((L\text{-}z)\rho g)+0.5((2\sigma/((L\text{-}z)\rho g)^2 + 32z\mu/(\rho g t))^{1/2}$ ………………………………..(1.17)

Similarly, at the same time and position (z), there is a tube where the top of the film just arrives, the radii of this particular tube, r_2, can be determined with,

$u_f = \delta^2 \rho g/(3\mu) = z/t$…………………………………...………………………….(1.18)

Using eq. 10 to substitute for δ and solve eq. 13 for r_2, we get:

$r_2 = 18.94\ (3\mu z/(\rho g t))^{1/2}$………………………………………………………….(1.19)

With r_1 and r_2 determined, we can calculate fluid distribution across the whole range of the capillary tubes, representing the porous media. Tubes with radius from r_{min} to r_1 are still liquid filled; tubes with radius from r_1 to r_2 are partially liquid filled with the liquid film on the wall (20%); tubes with radius from r_2 to r_{max} are only filled with the residual liquid (5%).

The cross-sectional area of tubes that have radius between size r_1 and r_2 can be determined by integrating the following term over the range of the tube sizes,

$\int_{r_1}^{r_2} \pi r_i^2 \gamma(r_i) dr_i$,

in the case of tubes with a distribution function of eq. 3, integration can be made theoretically and numerically. The average liquid saturation at the time at position z, is then,

$$S_o(z, t) = \left(\int_{r_{min}}^{r_1} \pi r_i^2 \gamma(r_i) dr_i + 0.2\int_{r_1}^{r_2} \pi r_i^2 \gamma(r_i) dr_i + 0.05\int_{r_2}^{r_{max}} \pi r_i^2 \gamma(r_i) dr_i\right) / \int_{r_{min}}^{r_{max}} \pi r_i^2 \gamma(r_i) dr_i \quad \text{......(1.20)}$$

Where the first term on the numerator represents fully saturated tubes; second term represents tubes with film flow; and the third term for tubes with residual oil only. The denominator gives the total cross-sectional area. With known oil saturation as a function of height and time, the oil produced at the outlet can be easily calculated from material balance of the oil phase.

- **Numerical Schemes and Model Modification**

A spreadsheet package with VBA macro has been developed to calculate saturation profile at any given time and position for any combination of parameters and tube size distribution functions. Numerical tests were conducted using the above approaches.

Table 1.11 shows parameters of the porous media used in the model. These parameter values are taken from experiment Run 2. Where L is the length of the bead pack used; g is the gravity acceleration, ρ, μ and σ are the liquid density, viscosity, and interfacial tension with air, respectively. These parameter values are the preliminary estimations for the case of experimental Run 2. Three phase interfacial tensions between the oleic phase and air in the presence of water have not been measured; values in Table 1.11 are estimations. However, these values for interfacial tension will be changed in sensitivity studies. r_{min} and r_{max} are calculated from eqs. 1.6 and 1.7 with the size of the glass beads used (ranging from 0.4 – 0.6 mm in diameter).

Table 1.11: Input parameters in the bundle-of-capillary-tube model for the paraffin case (experiment Run 2)

L =	0.33	m
r_{min} =	0.00006188	m
r_{max} =	0.00009282	m
g =	9.81	m s^{-2}
ρ =	700	kg/m^3
μ =	0.06	Pa s
σ =	0.01	N/m

Equally distributed positions along the vertical direction (z values) are assigned in the first column from 0 to 0.33 m. At given time(s) eqs. 1.17 and 1.19 are used to determine r_1 and r_2 at all the different z values, the terms in eq. 1.20 are then evaluated and So (z, t) calculated at this time step, t. Instantaneous oil saturation distribution along the pack or saturation profile is obtained from which the instantaneous cumulative oil recovery can be calculated using material balance. Repetition of this procedure the saturation profile was obtained and plotted to generate the oil recovery versus time curve.

Figure 1.13 shows the comparison of model results and the experimental data in the cumulative oil recovery curves. Although, the model results have a tendency of rapid flow followed by a much slower flow, are off the target considerably. Till this point, we have no adjustable parameter in the calculations. This discrepancy is attributable to the tortuosity effect, which is higher in a real bead pack rather than a straight capillary. Tortuosity decreases the flow potential for the bulk flow. Shape of the capillary tubes is also a likely factor responsible for this observed discrepancy. Noncircular cross section shaped tubes may be more representative of the irregular shaped void space in a bead pack and the increased flow resistance. To take the tortuosity and shape factor into account, we used a value of 6.0 as a tortuosity-shape factor in equations for the bulk flow in all the calculations follows.

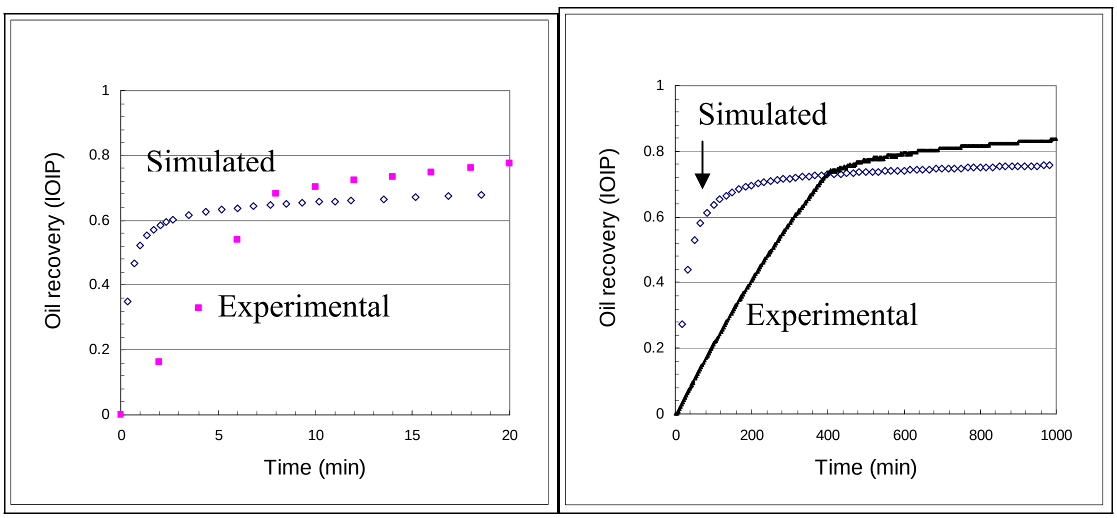

(a)

(b)

Figure 1.13: (a). Comparison of results of the model and the experimental Run 1. (b) Comparison of results of the model and the experimental Run 2.

Another discrepancy is the inability of the model to match the later flow stages in the experiment (Figure 1.13). Since the later stage is controlled by film flow in smaller tubes, it is reasonable to assume that the slower film flow in the model is responsible for the discrepancy. In bundle-of-capillary-tube model, no cross-flow is allowed; tubes are isolated from each other. In real porous media, cross-flow likely occurs. More discussion on cross-flow is included later. In the calculations reported here, a cross-flow factor of 0.1 was used to multiply the viscosity term in film flow equations (eq. 1.15) to increase the rate of this film flow to obtain better match with the experimental recovery data.

1.6.4 Model results

Due the introduction of the tortuosity-shape factor and cross-flow factor, improved match of experimental data were obtained and are shown in Figures 1.14 and 1.15 for experimental Runs 1 and 2. As shown, the cumulative oil recovery is matched well in both the initial fast flowing stage and the later slow production stage. The saturation profiles in Figure 1.14(a) and 1.15(a) are given for the five time steps. There are two striking features of these saturation profiles. The capillary end-effect is shown with the higher outlet residual oil saturation. Another interesting feature is the lack of a shock front or an abrupt change of oil saturation as normally observed in a displacement process. These are only preliminary results and the model is being evaluated for sensitivity.

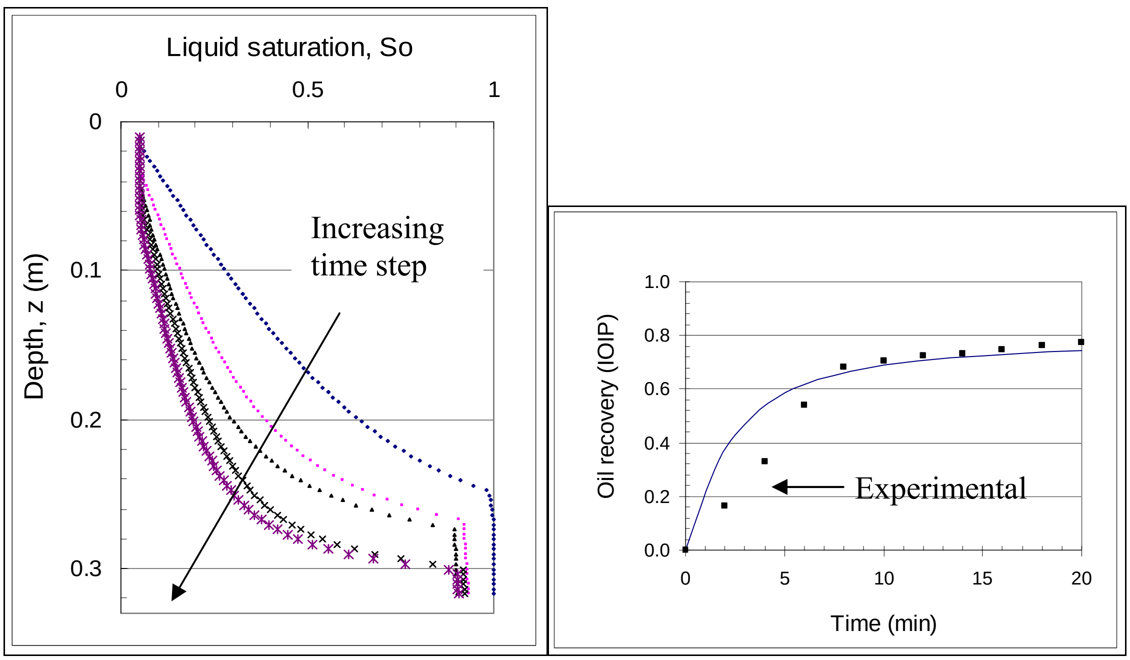

(a) (b)

Figure 1.14: (a). Simulated oil saturation profile along the pack at five time steps. (b) Comparison of results of the model and the experimental Run 1.

1.6.5 Discussion

- **Justification of the Model Parameters**

There are few parameters in this model that are arbitrary. However, these parameters are not totally without physical basis. It is widely accepted that a free gravity drainage process consists of two stages, the single-phase bulk flow and a film flow stage (Saidi and Sakthikumar, 1993, Grattoni, et al., 2001). Bulk flow is single-phase flow of oil, resulting in linear response in oil recovery with time, as indicated in the early stage in the experiments. The film flow is characterized by the oil flow with air/gas having already invaded in the porous media, the oil flows as continuous film along the walls in the presence of gas. The 80%/20% split in bulk/film flow is based on the high break through oil recovery in most free gravity drainage experiments. Although arbitrarily determined, this split does not appear to alter the trend of the model results and is kept the same value throughout all calculations. The film flow is a slow process but leads to very high ultimate oil recovery. Ultimate recovery can be as high as 90-99% IOIP in laboratory, the 5% residual oil saturation assumption is based on the results of experimental data reported in the literature (Dumore and Schols, 1974; Vizika, 1993; Blunt, et al., 1994).

The tortuosity-shape coefficient, (τ) that takes account of the fact that the fluid flow in a porous media takes a longer path than a straight line. The tortuosity-shape factor (τ) is used in the calculations as a multiplier to increase the term (L-z) for the bulk flow. This effectively reduces the potential gradient and slows down the bulk flow. A value of 6 for τ is reasonable in the range of 2-3 is generally considered reasonable for tortuosity and the same is true for the shape factor.

η is a cross-flow factor that accelerates the film flow to take into account the effect of cross-flow of fluid from smaller tubes to larger tubes that is not considered directly in the model. In porous media, narrower channels are connected to the wider channels, and it is conceivable that liquid in the narrower channels prefers to flow in the wider channels should the wider channels become air occupied due to the density contrast. However, the capillary pressure works in the reverse direction, and limits this kind of cross flow. The balance of gravity and capillary forces determines the cross-flow effects. A cross-flow factor of 0.1 is introduced in the model to accelerate the film flow. Further testing of the model for its sensitivity to these adjustable parameters and comparison with additional experiments would enable a more mechanistic model with prediction capabilities.

- **Capillary-Force Effects**

Capillary force has three effects in this process. Firstly, it causes the well-known capillary end-effect, the accumulation of wetting phase at the outlet. This accumulation of wetting phase occurs both in laboratory and in the reservoir. However, the length of the wetting phase accumulation due to this effect depends on capillary threshold pressure, which is the same if interfacial tension and the porous media are the same in the lab as in the field. Thus, the range of length affected is the same. Hence, this phenomenon would have a more severe effect in the laboratory than in the reservoir scale. Efforts to limit or eliminate this effect have been reported in the literature (Dullien, et al., 1991) with limited success.

Secondly, capillary pressure contributes to the pressure gradient in the bulk flow of oil, although this maybe quite insignificant, especially in the early stage when hydraulic head is overwhelmingly large (2-3 orders of magnitude, unless $z \approx L$) compared to the capillary pressure contribution, as indicated in Eq. 1.21.

$$\nabla \mathscr{P} = (\rho g\,(L-z) - p_c)/(L-z) \qquad (1.21)$$

The pressure gradient contributed from the gravity force is a constant ρg, while the pressure gradient contributed from the capillary pressure increases with z. The capillary end-effect is a result of the forces being equal to each other (analogous to a capillary rise experiment).

Thirdly, capillary pressure dictates the saturation profile in the gas-invaded zone. In the extreme case of no capillary pressure, miscible displacement occurs and ideally there is no oil left behind. Due to the unfavorable mobility ratio, gas has the tendency to finger and leave oil behind its front. This tendency is suppressed by the density difference, or buoyancy force. The buoyancy force has a tendency to squeeze the gas out of the still partially oil saturated zone (oil is in hydraulic continuity if it spreads on water). However, capillary force traps the gas and prevents a complete segregation to occur, thus some kind of balance is reached with gradual increasing oil saturation downward in the gas invaded zone. The oil saturation profile is determined by a balance of capillary, viscous and gravity forces.

- **Saturation Profiles**

It appears that shock fronts do not form in a free gravity drainage process as indicated in the oil saturation profiles in the model results (Figure 1.8(a) and 1.9(a)).

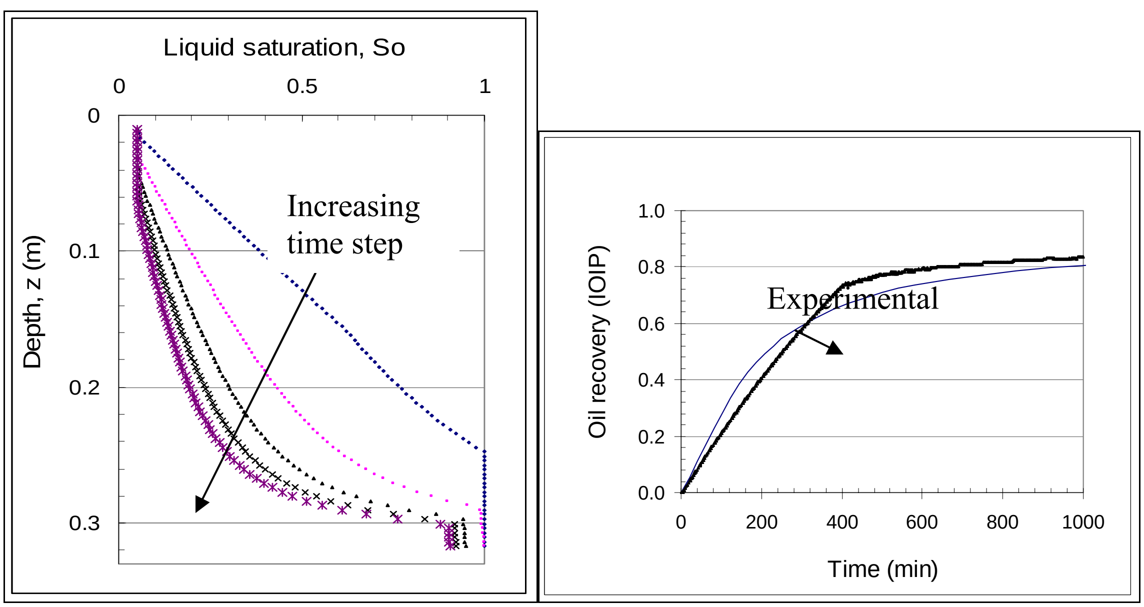

(a) (b)

Figure 1.15: (a). Simulated oil saturation profile along the pack at five time steps. (b) Comparison of results of the model and the experimental Run 2.

Saturation profile measured with CT-scan (Sahni, et al., 1998) and radioactive tracer technique (Naylor and Frorup, 1989) indicate a lack of saturation shock in free gravity drainage experiments. Buckley-Leverett shock (Lake, 1989) is formed by a mechanism of self-sharpening of the displacing fluid. It is easy to understand from the traditional relative permeability function and Darcy's law, higher saturation propagates at a higher velocity over a range of saturation, therefore, any saturation that is lower than a certain value cannot be present in a displacement and a shock is formed. However, the formation of shock front is a theoretical solution without capillary pressure effects; and the formation of a shock front in laboratory is a result of negligible capillary pressure. In addition, in a free gravity drainage process, the displacing gas phase, does not really push the liquid, rather, it merely fills up the voids left by liquid phase, making it a different process from a forced displacement process. The bundle-of-capillary-tube model appears to demonstrate the individual effects of the gravity, viscous and capillary forces, and their interplay.

1.7 Preliminary conclusions and status

The preliminary design of the scaled physical model has been presented. An analytical model to predict free gravity drainage performance has been developed and several forced gravity drainage experiments on the current physical model has been completed to study the effect of the following variables on GAGD performance:

- The effect of Bond and capillary numbers on GAGD performance
- The GAGD performance at constant pressure and constant rate conditions.
- GAGD performance with different injectants.
- Development of a free gravity drainage model.

The following preliminary conclusions can be made based on the physical model experiments:

- The type of gas injectant does not affect the oil recovery by GAGD in immiscible mode, in-fact the rate of recovery is totally identical (Figure 1.2). This can be attributed to the fact that the capillary numbers for both the gases are close
- Slightly higher cumulative oil recovery (7-8% greater) may be obtained at constant pressure gas floods as opposed to constant rate gas floods (Figure 1.4)
- A straight line relationship between the total recovery and Bond number is obtained from the six drainage experiment reported (Figure 1.5), with an R^2 of 0.95.
- A linear relationship of total oil recovery and the capillary number is observed as well (Figure 1.7). Although, it can not be stated for sure until more experiments are carried out to ascertain this fact.
- A bundle-of-capillary-tube model has been initiated for free gravity drainage process in porous media.

- Several adjustable parameters in the model have enabled the predictions to match the experimental results reasonably well.
- Further testing of the model for its sensitivity to these adjustable parameters and comparison with additional experiments would enable a more mechanistic model with prediction capabilities.

Experiments conducted during this period suggest that the GAGD performance is sensitive to Bond numbers as well as capillary numbers. Pressure maintenance by injecting gas at constant pressure seems to be more promising than constant rate gas injection. There is a minimal effect on oil production rates using different types of gas injectant.

1.8 Future Work

Planned Activities

The future work will involve obtaining of required fluids and glass beads, modification in the physical model, and mathematical modeling of the GAGD process.

The anticipated time frame for the various tasks is summarized below:

- Investigation of the effect of mobile water saturation:1 week
- Investigation of the effect of spreading coefficient on GAGD: 2 weeks
- Investigation of the effect of wettability on GAGD: 2 weeks
- Investigation of the effect of Heterogeneity on GAGD: 2 weeks

Nomenclature:

α = fluid property relationship

D_p = Grain diameter, [L]

ϕ = Porosity

g = gravity constant, $[LT^{-2}]$

H = Reservoir/sand pack thickness, [L]

K = Absolute permeability, $[L^2]$

μ = gas viscosity, $[ML^{-1}T^{-1}]$

μ_o = oil viscosity, $[ML^{-1}T^{-1}]$

N_B = Bond number, $[ML^{-1}T^{-1}]$

N_C = Capillary number

N_G = Gravity number

R_L = Geometric aspect ratio

ρ_o = oil density, $[ML^{-3}]$

ρ_g = gas density, $[ML^{-3}]$

ρ_w = water density, $[ML^{-3}]$

σ_{ow} = oil-water interfacial tension, $[MT^{-2}]$

σ_{go} = gas-oil interfacial tension, $[MT^{-2}]$

σ = gas-oil interfacial tension, $[MT^{-2}]$

For the Bundle-of capillary tube model

L = core length, m

p =pressure in phase i, Pa

p_c = capillary pressure, Pa

$\mathscr{P}$ =potential gradient, Pa/m

r =radius of capillary tube, m

S =saturation

t = time, s

u =velocity, m/s

z =vertical coordinate, m

δ =film thickness, m

μ =viscosity, Pa.s

σ = oil gas interfacial tension, N/m

ρ =density, kg/m^3

η =cross-flow factor

τ = tortuosity factor

Δ =differential of that quantity

∇ = gradient of that quantity

Subscripts

P = Prototype

M = Model

b = bulk

f = film

o = oil phase

i =variable representing any discrete value

Δ = differential of that quantity

∇ = gradient of that quantity

References

1. Bird, B. R., Stewart, W., E., and Lightfoot, E. N., 1960. *Transport Phenomena,* John Wiley & Sons., 1960.
2. Blunt, M. J., Fenwick, D. H., and Zhou, D. 1994. "What Determines Residual Oil saturation in Three-Phase Flow," SPE 27816, paper presented at the SPE/DOE 9th Symposium on Improved Oil Recovery, Tulsa, OK, April 17 – April 20, 1994.
3. Blunt, M., Zhou, D and Fenwick, D.: "Three-Phase Flow and Gravity Drainage in Porous Media," Transport in porous media, 20, 77-103, 1995.
4. Carman, P. C. 1937. "Fluid Flow through Granular Beds," *Trans. inst. Chem. Engrs* (London) (1937) 150-166.

5. Craig, F.F., Sanderlin, J.L., Moore, D.W and Geffen, T.M.: "A Laboratory Study of Gravity Segregation in Frontal Drives," *Trans*., AIME (1957) 210, 275-281.
6. DiCarlo, D. A., Sahni, A., and Blunt, M., 2000. "Three-Phase Relative Permeability of Water-Wet, Oil-Wet, and Mixed-Wet Sandpacks," *SPE J.* (March 2000) 82-91.
7. Dulien, F. A. L., Catalan, L., Chatzis, I., and Collins, A., 1991. "Recovery of Waterflood Residual Oil with Low Pressure Inert Gas Injection, Assisted by Gravity Drainage from Water-Wet and Oil-Wet Cores," Petroleum Society of CIM/AOSTRA 1991 Technical Conference, April 21-24, 1991, BANFF.
8. Dumore, J. M. and Schols, R. S. 1974. "Drainage Capillary-Pressure Functions and the Influence of Connate Water," *SPE J* (October 1974), 437-444.
9. Grattoni, C.A., Jing, X.D and Dawe, R.A.: "Dimensionless Groups for three-phase gravity drainage flow in porous media," *J. Pet. Sci & Engg.,* 29 (2001), 53-65.
10. Hagoort, J.: "Oil Recovery by Gravity Drainage," SPE 7424, SPEJ, June 1980, 139-150.
11. Kantzas, A., Chatzis, I and Dullien, F.A.L.: "Mechanism of Capillary Displacement of Residual oil by Gravity-Assisted Inert Gas Injection," SPE 17506, *SPE Rocky Mountain Regional Meeting*, Casper, WY.
12. Lake, L. W., 1989. *Enhanced Oil Recovery*, Prentice Hall, Englewood Cliffs, NJ (1989).
13. Leverett, M.C.: "Capillary Behavior in Porous Solids," *Trans*. AIME (Oct. 1940), 153-169.
14. Lewis, O.J.: "Gravity drainage in Oil Fields," Trans. A.I.M.E., volume 155, pp. 133, 1944.
15. Manwart, C., Torquato, S., and Hilfer, R., 2000. "Stochastic Reconstruction of Sandstones," *Physical Review E. Statistical Physics, Plasmas, Fluids, and Related Interdisciplinary Topics*, **v 62**, n 1 B, Jul, 2000, p 893-899.
16. Meszaros, G., Chakma, A and Islam, M.R.: "Scaled Model Studies and Numerical Simulation of Inert Gas Injection with Horizontal Wells", SPE 2059, Presented at the annual technical conference and exhibition of the SPE, New Orleans, LA, September 23-26, 1990.
17. Muskat, M.: *Physical Principles of Oil Production,* McGraw-Hill Book Company, New York, 1949, pp. 484-512.
18. Naylor, P., and Frorup, M., 1989. "Gravity-Stable Nitrogen Displacement of Oil," SPE 19641, paper presented at the 64th Annual Technical Conference and Exhibition of the Society of Petroleum Engineers held in San Antonio, TX, October 8-11, 1989.
19. Nutt, C. W., "The Physical Basis of the Displacement of Oil from Porous Media by other Fluids: a Capillary Bundle Model," *Proc. Roy. Soc. Lond*., **A382**, 155-178, 1982.
20. Rapoport, L.A.: " Scaling Laws for Use in Design and Operation of Water-Oil flow models," *trans.* AIME (1954) 204, 143-150.
21. Sahni, A., Burger, J., and Blunt, M., 1998. "Measurement of Three phase Relative Permeability during Gravity Drainage using CT Scanning," SPE 39655, paper presented at the SPE/DOE Improved Oil Recovery Symposium held in Tulsa, Oklahoma, April 19-22, 1998.
22. Saidi, M. A., and Sakthikumar, S., 1993. "Gas Gravity Drainage under Secondary and Tertiary Conditions in Fractured Reservoirs," SPE 25614, paper presented at the SPE program Committee. 1993.
23. Saputelli, A. L., Dawe, A. R., and Grattoni, C., 1998. "Pore Scale Gravity Drainage under Different Wettabilities and Multiphase Coexistence," SPE 39621, presented at the 1998 SPE/DOE Improved Oil Recovery Symposium held in Tulsa, Oklahoma, 19-22 April 1998.
24. Shook. M., Li, Dachang and Lake, L.: "Scaling immiscible Flow Through Permeable Porous Media by Inspectional Analysis," In Situ, 16 (4), 311-349, 1992.
25. Stegemeier, G.L., Laumbach, D.D and Volek, C.W.: "representing Steam Process with Vacuum Models," SPE 6787, *SPEJ*, 151-174, June 1980.
26. Vizika, O. 1993. "Effect of the Spreading Coefficient on the Efficiency of Oil Recovery with Gravity Drainage," Proceedings of the Symposium on Enhanced Oil Recovery, 205 th National Meeting, American Chemical Society, Denver, CO, March 28- April 2, 1993, 154-158.

II. Further Development of the Vanishing Interfacial Tension (VIT) Technique

The research work done under this task during the first year reporting period of this project (Report # 15323R01, April 2003; Report # 15323R02, July 2003 and Report # 15323R03, October 2003) focused mainly on three subtasks. Under subtask I, the VIT measurements of gas-oil miscibility for Rainbow Keg River (RKR) and Terra Nova reservoir fluids have been compared with EOS and Parachor computational models. Gas-oil miscibility over-predictions were obtained with both the computational models when compared to VIT measurements. The inability of these models to account for counter-directional mass transfer effects that can occur in reality between the fluids has been identified as the cause for these over-predictions. Under subtask II, IFT measurements were carried out for a standard ternary liquid system of benzene, ethanol and water. Conceptually different regions of solubility characteristics were shown to correlate solubility, miscibility and interfacial tension. Under subtask 3, a high pressure high temperature VIT experimental system for IFT measurements at reservoir conditions has been designed and fabricated. All the necessary accessories and instruments for the complete assembly of experimental setup have been procured. The schematic flow diagram to facilitate the assembly of the VIT experimental system has been prepared. The further progress made in these three subtasks during the second year reporting period is briefly discussed in the following sections.

2.1 The Proposed Mass Transfer Enhanced Mechanistic Parachor Model

2.1.1 Introduction

Interfacial tension is an important property for many processes and phenomena, such as enhanced oil recovery by gas injection, flow through porous media, and mass and heat transfer. However, the experimental data on interfacial tension for complex fluid systems involving multicomponent phases are scarce. Therefore, there has long been a need for a simple and accurate computational model for prediction of interfacial tension in multicomponent hydrocarbon systems. Several models have been proposed for the calculation of interfacial tension of simple fluids and mixtures in the past few decades. The most important among these models are the Parachor model (Macleod, 1923; Sudgen, 1924), the corresponding states theory (Brock and Bird, 1955), thermodynamic correlations (Clever and Chase, 1963) and the gradient theory (Carey, 1979).

While most of the thermodynamic properties refer to individual fluid phases, interfacial tension (IFT) is unique in the sense that it is a property of the interface between the phases. The IFT, being a property of interface, is strongly dependent on the compositions of fluid phases in contact, which in turn depend on the mass transfer interactions between the phases. The commonly occurring mass transfer mechanisms between the fluid phases to attain equilibrium are vaporization, condensation or a combination of the two. In the vaporizing drive mechanism, the vaporization of lighter components (C_1 to C_3) from the liquid (crude oil) to hydrocarbon vapor phase promotes the attainment of miscibility of the two phases. In condensing drive mechanism, the condensation of intermediate and heavy components (C_4 to C_8) from hydrocarbon gas to the crude oil is responsible for attaining miscibility between fluid phases. In combined condensation and vaporization drive mechanism, the simultaneous counter-directional mass transfer mechanisms, that is, vaporization of lighter components from crude oil to gas and condensation of intermediate and heavy components from gas to crude oil, are responsible for attaining miscibility of the phases. These mass transfer interactions affect the compositions of both phases and hence their interfacial tension can be used to infer information on mass transfer interactions taking place prior to the attainment of fluid phase equilibrium and miscibility.

Almost all currently available IFT models have been extensively tested for either pure compounds or binary mixtures. The use of these models to predict interfacial tension in complex hydrocarbon systems involving multicomponents in both the phases is only limited and not well documented. Furthermore, none of these models provides information on mass transfer interactions occurring prior to attaining fluid phase equilibria. Hence, a mass transfer enhanced mechanistic model, based on the Parachor method, has been proposed in this section for prediction of interfacial tension as well as for the identification of governing mass transfer mechanism for fluid phase equilibria in complex multicomponent hydrocarbon systems.

2.1.2 Parachor Model

This model is the oldest among all the IFT prediction models and because of simplicity is still most widely used in petroleum industry to estimate the interfacial tension between fluids. Empirical density correlations are used in this model to predict the interfacial tension.

Macleod-Sudgen (Macleod, 1923; Sudgen, 1924) related surface tension of a pure compound to the density difference between the phases, as:

$$\sigma^{1/4} = P(\rho_M^L - \rho_M^V) \quad \text{...} \quad (2.1)$$

Where σ is the surface tension in dynes/cm, ρ_M^L and ρ_M^V are the molar density of the liquid and vapor phases, respectively, in gmole/cm^3 and the proportionality constant, P is known as the Parachor. The Parachor values of various pure compounds have been determined from measured surface tension data using Eq. 2.1. The Parachor values of different pure compounds are reported in the literature by several investigators (Quale, 1953; Fanchi, 1990; Ali, 1994; Schechter and Guo, 1998).

The equation proposed by Macleod-Sudgen (Macleod, 1923; Sudgen, 1924) was later extended to multicomponent hydrocarbon mixtures using the simple molar averaging technique of Weinaug and Katz's (Weinaug and Katz, 1943) for the mixture Parachor,

$$\sigma^{1/4} = \rho_M^L \sum x_i P_i - \rho_M^V \sum y_i P_i \quad \text{...} \quad (2.2)$$

Where x_i and y_i are the mole fractions of component i in the liquid and vapor phases, respectively, and P_i is the Parachor of the component i. Parachor values of pure compounds are used in Eq. 2.2 to calculate the interfacial tension of the mixtures, considering the Parachor value of a component in a mixture is the same as that when pure (Danesh, 1998).

This model has been extensively used for prediction of surface tension of pure compounds. However, the model gives poor IFT predictions for complex multicomponent hydrocarbon mixtures (Danesh et al., 1991). Several attempts have been already made in the past to improve the Parachor model predictions for multicomponent systems. Fawcett (1994) has reviewed these reported studies. These attempts are mostly directed at improving the Weinaug and Katz's (Weinaug and Katz, 1943) molar averaging technique for the mixture Parachor determination. The Hough-Stegemeier (Hough and Stegemeier, 1961) correlation has the same form as the Weinaug-Katz correlation, but with a different set of empirical parameters. Other investigators have modified the Weinaug-Katz correlation with more complex mixing rules for multicomponent mixtures (Hugill and Van Welsenes, 1986), or with a parameter, which varies with the density difference between the fluid phases (Danesh et al., 1991). The Lee-Chien's modification (Lee and Chien, 1984) is based on critical scaling theory and still retains the same functional form of W-K correlation. All these modifications are intended to match the experimental data based on empirical correlations and there is no strong theoretical background associated with them.

2.1.3 The Proposed Modification for Mass Transfer

In the application of the conventional Parachor model to multicomponent mixtures, Parachor values of pure components are used in IFT predictions, considering each component of the mixture as if all the others were absent. Therefore, the lack of mass transfer effects on Parachor values to account for interactions with other components in a mixture appears to be the main reason for poor IFT predictions from the original Parachor model in complex multicomponent hydrocarbon systems.

Therefore, a mechanistic Parachor model has been proposed, in which, the ratio of diffusivity coefficients between the fluid phases raised to an exponent is introduced into the Parachor model to account for mass transfer effects. The mass transfer interactions for phase equilibria between any two fluid phases take place by diffusion due to concentration gradient and by dispersion. Hence diffusivities are used in the mechanistic model to account for mass transfer interactions. Furthermore, only diffusivities can reasonably represent mass transfer interactions in complex multicomponent systems like crude oil-hydrocarbon gas mixtures involving multicomponents in both the phases. The ratio of diffusivities in both directions (vaporizing and condensing) between the fluid phases raised to an exponent used in the mechanistic model, enables the retention of the same dimensions of the original Parachor model. The proposed mechanistic model is given by:

$$\sigma^{1/4} = \left(\frac{D_{os}}{D_{so}}\right)^n (\rho_M^L \sum x_i P_i - \rho_M^V \sum y_i P_i) \quad \text{(2.3)}$$

Where, D_{os} is the diffusivity of oil in gas (solvent), D_{so} is the diffusivity of gas (solvent) in oil and n is the exponent, whose sign and value characterize the type and extent of governing mass transfer mechanism for fluid phase equilibria. If n > 0, the governing mass transfer mechanism for fluid phase equilibria is vaporization of lighter components from the oil to the gas phase. If n < 0, the governing mass transfer mechanism for fluid phase equilibria is condensation of intermediate to heavy components from the gas to the crude oil. The value of n equal to zero indicates the absence of mass transfer mechanisms and hence the mechanistic model reverts back to the original Parachor model. The higher the numerical value of n (irrespective of its sign), the greater is the extent of the governing mass transfer mechanism.

Sigmund (1976) used Wilke equation (Wilke, 1950) for comparison with the experimental data of diffusivities between two nine-component gas mixtures and found that Wilke equation is capable of giving good estimates of diffusivities even for the cases where one mixture diffuses into another mixture. Fayers (1992) has compared the diffusivity data of multicomponent systems at reservoir conditions obtained from various correlations with experiments and concluded that Wilke-Chang equation (Wilke and Chang, 1955) is the best available empirical correlation to compute the diffusivities in multicomponent hydrocarbon systems. Hence, the diffusivities between the fluid phases are computed, using the empirical correlation of Wilke and Chang (Wilke and Chang, 1955; Wilke, 1949), given by:

$$D_{AB} = \frac{(117.3 \times 10^{-18})(\varphi M_B)^{0.5} T}{\mu v_A^{0.6}} \quad \text{(2.4)}$$

Where D_{AB} = diffusivity of solute A in very dilute solution in solvent B, m^2/sec

M_B = molecular weight of the solvent, kg/kmol

T = temperature, K

μ = solution viscosity, kg/m.sec

ν_A = solute molal volume at normal boiling point, m^3/kmol

φ = association factor for solvent, set equal to unity since the solvents used in this study are unassociated.

Eq. 2.4 is extended to multicomponent hydrocarbon mixtures, using:

$$M_B = \sum x_{Bi} M_{Bi} \quad \text{......} \quad (2.5)$$

$$\nu_A = \sum x_{Ai} \nu_{Ai} \quad \text{......} \quad (2.6)$$

Where, x_i is the mole fraction of the component i in the mixture, M_{Bi} is the molecular weight of the component i and ν_{Ai} is the molal volume of the component i at normal boiling point.

An objective function (Δ) is defined as the sum of weighted squared deviations between the original Parachor model predictions and experimental IFT values and is given by:

$$\Delta = \sum_{j=1}^{N} \left[w_j \left(\frac{\sigma_j^{pred}(X) - \sigma_j^{\exp}}{\sigma_j^{\exp}} \right) \right]^2 \quad \text{......} \quad (2.7)$$

Where, each element of the objective function expresses the weighted difference between the predicted and experimental interfacial tension values, σ^{pred} and σ^{exp}, respectively; w is the weighting factor and N represents the number of measured data points to be fitted; X designates the correction factor to the original Parachor model prediction.

The mass transfer enhancement parameter (k), a correction to the original Parachor model to account for mass transfer effects, is then defined as the correction factor (X) at which the objective function (Δ) becomes the minimum. The mechanistic Parachor model is now given by:

$$\sigma^{1/4} = (k)(\rho_M^L \sum x_i P_i - \rho_M^V \sum y_i P_i) \quad \text{......} \quad (2.8)$$

From Eqs. 2.3 and 2.8, the exponent n, characterizing the governing mass transfer mechanism for fluid phase equilibria, can be computed using:

$$k = \left(\frac{D_{os}}{D_{so}} \right)^n \quad \text{......} \quad (2.9)$$

Therefore, the objectives of this study are to utilize the proposed mechanistic Parachor model to (1) calculate interfacial tension in complex vapor-liquid systems involving multicomponents in both phases; (2) evaluate the model effectiveness by comparing the interfacial tensions determined from the model with experimental measurements; and (3) identify the governing mass transfer mechanism for fluid phase equilibria. For this purpose, three reservoir crude oil-gas systems of Rainbow Keg River, Terra Nova and Schrader Bluff have been used, since the fluids compositions and the phase behavior data needed for IFT calculations and the experimental IFT measurements are readily available (Rao, 1997; Rao and Lee, 2002; Sharma et al., 1995). Flash calculations are carried out using QNSS/Newton algorithm (Nghiem and Heidemann, 1982) and Peng-Robinson equation of state (Peng and Robinson, 1976), within a commercial simulator (Computer Modeling Group Ltd., 2001).

2.1.4 Results and Discussion

- **Rainbow Keg River Reservoir**

The crude oil and hydrocarbon gas compositions and the temperature from Rao (1997) are used in IFT computations for this reservoir. The IFT measurements at various C_{2+} enrichments in hydrocarbon gas phase and at various pressures reported by Rao (1997) are used for comparison with model predictions. A mixture consisting of 10 mole% of crude oil and 90 mole% of hydrocarbon gas is used as the feed composition in the computations to match the composition used in the reported experiments.

The comparison of IFT predictions by the original Parachor model with experiments at various C_{2+} enrichments in gas phase is given in Tables 2.1 and 2.2, for pressures 14.8 MPa and 14.0 MPa, respectively. These results are also shown in Figures 2.1 and 2.2. As can be seen, similar trends in IFT are observed for both the pressures. The match between the experiments and the model predictions is not good and IFT under-predictions are obtained with the Parachor model. This is in agreement with Cornelisse et al. (1993), who made similar observations for n-Decane and carbon dioxide systems.

The disagreement between the experiments and the model predictions, as seen in Figures 2.1 and 2.2, are attributed mainly to the absence of mass transfer effects in the original Parachor model. Hence correction factors are used for original Parachor model predictions to minimize the objective function (Δ), which is the sum of weighted squared deviations between the model predictions and experimental values. The correction factors and the resulting objective functions for this crude oil-gas system are shown in Figure 2.3. The mass transfer enhancement parameters (k), the correction factors at which objective function becomes the minimum, are estimated to be 1.30 and 1.26, respectively for pressures of 14.8 MPa and 14.0 MPa.

The computed diffusivities between the fluid phases at various C_{2+} enrichments in hydrocarbon gas phase for RKR fluids at pressures of 14.8 MPa and 14.0 MPa are given in Table 2.3. The mass transfer interactions between the fluid phases declined slightly as the C_{2+} enrichment in hydrocarbon gas phase is increased for both the pressures. However, the ratio of diffusivities in both directions (oil to gas and gas to oil) remains almost the same at all C_{2+} enrichments in gas phase. The average ratios of diffusivities between the fluids at all C_{2+} enrichments are 3.70 and 3.92, respectively for pressures 14.8 MPa and 14.0 MPa. From the mass transfer enhancement parameters and the average ratios of diffusivities between the fluid phases, the exponent (n) characterizing the governing mass transfer mechanism is found to be +0.20 and +0.17, respectively for pressures 14.8 MPa and 14.0 MPa. These values of n being greater than zero indicate that the vaporization of components from the crude oil into the gas phase is the mass transfer mechanism that governs the fluid phase equilibria of these reservoir fluids. This can be attributed to the presence of significant amounts of lighter components (52 mole% C_1 to C_3) in the crude oil of this reservoir (Rao, 1997).

The comparison between the IFT predictions of mass transfer enhanced mechanistic Parachor model with experiments at various C_{2+} enrichments in gas phase is given in Tables 2.4 and 2.5, respectively, for pressures 14.8 MPa and 14.0 MPa. These results are shown in Figures 2.4 and 2.5, respectively, at these pressures. Since the optimization of the mass transfer enhancement parameter (k) is based on minimizing the sum of squared deviations between the experimental and calculated values, the mechanistic model predictions matched well with the experiments for both the pressures.

- **Terra Nova Reservoir**

The crude oil and gas compositions and the temperature from Rao and Lee (2002) are used in IFT computations for this case. IFT measurements, at various C_{2+} enrichments in hydrocarbon gas, from Rao and Lee (2002), are used for comparison with model predictions. A mixture consisting of 8 mole% of crude oil and 92 mole% of gas is used as the feed composition in the calculations in order to match the composition used in experiments.

The comparison of experimental IFT's with original Parachor model predictions at different C_{2+} enrichments in gas phase and at a pressure of 30 MPa is given in Table 2.6 and shown in Figure 2.6. As can be seen, the match between the experiments and the model predictions is very poor and large IFT under-predictions are obtained with the Parachor model. This appears to be mainly due to the absence of mass transfer effects in the Parachor model. Therefore, as before, correction factors are used for Parachor model predictions to minimize the objective function (Δ), the sum of weighted squared deviations between the model predictions and experimental values. The correction factors and the resulting objective functions for this crude oil-gas system are shown in Figure 2.7. The mass transfer enhancement parameter (k), the correction factor at which objective function becomes the minimum, is found to be 4.58.

The calculated diffusivities between the fluid phases at different C_{2+} enrichments in gas phase for Terra Nova fluids at a pressure of 30 MPa are given in Table 2.7. The mass transfer interactions between the fluids decreased slightly as the C_{2+} enrichment in gas is increased. However, the ratio of diffusivities between the fluids remains nearly constant irrespective of C_{2+} enrichment in gas phase. These findings are similar to those observed with RKR fluids. The average ratio of diffusivities between the fluids at various C_{2+} enrichments is computed to be 3.28. From the mass transfer enhancement parameter and the average ratio of diffusivities between the fluid phases, the exponent (n) characterizing the governing mass transfer mechanism is found to be +1.28. The positive sign of n indicates that even for these reservoir fluids, vaporization of components from the crude oil into the gas phase is the controlling mass transfer mechanism for attaining the fluid phase equilibria. Furthermore, relatively higher value of n obtained for this crude oil-gas system compared to RKR fluids imply more pronounced vaporization mass transfer effects in the Terra Nova reservoir fluids. This can be attributed to the presence of relatively larger amounts of lighter components (56 mole% C_1 to C_3) in the Terra Nova crude oil compared to 52 mole% C_1 to C_3 in RKR crude oil (Rao, 1997; Rao and Lee, 2002).

The comparison between the mass transfer enhanced mechanistic Parachor model IFT predictions and the experiments at various C_{2+} enrichments in gas phase is given in Table 2.8 and shown in Figure 2.8 for a pressure of 30 MPa. As expected, an excellent match is obtained between the experiments and the mechanistic model predictions.

- **Schrader Bluff Reservoir**

The crude oil and gas compositions and the temperature and pressures from Sharma et al. (1995) are used in IFT calculations of this reservoir. Experimental data on IFT is not available for these reservoir fluids to compare with model predictions. However, the crude oil of this reservoir is experimentally shown to be miscible with the gas mixtures at a minimum miscibility enrichment (MME) of 15 mole% natural gas (NGL) in CO_2/NGL mixture and 50 mole% NGL in Prudhoe Bay gas (PBG)/NGL mixture at reservoir conditions (Sharma et al., 1995). Review of literature shows that the zero IFT is a necessary and sufficient condition to attain miscibility (Benham et al., 1965; Holm, 1987; Lake, 1989). But, the gas-oil interfacial tension can be measured to a very low value only up to 0.001 mN/m with the available experimental methods (Danesh et al., 1991). Hence, the interfacial tensions between oil and the gas are presumed to be 0.001 mN/m at the minimum miscibility enrichments of the two gas mixtures for comparison with model predictions. A mixture consisting of 5 mole% of crude oil and 95 mole% of solvent is used as the feed composition in IFT calculations.

The Parachor model IFT predictions for Schrader Bluff crude oil at different NGL enrichments in PBG/NGL solvent is given in Table 2.9 and shown in Figure 2.9. The predicted IFT at the MME of 50 mole% NGL in the PBG/NGL solvent is 4.73 mN/m, much higher than the presumed experimental value of 0.001 mN/m at this enrichment. Hence, correction factor (X) is used for Parachor model prediction to determine the mass transfer enhancement parameter (k) and is computed to be 0.00023. The computed diffusivities between the fluids at different NGL enrichments in PBG/NGL solvent at reservoir conditions are given in Table 2.10. The average ratio of diffusivities for all NGL enrichments in PBG/NGL solvent is 120.91 (Table 2.10). From the average ratio of diffusivities and the mass transfer enhancement parameter, the exponent (n) characterizing the governing mass transfer mechanism is determined as –1.747. The value of n less than zero indicates that the condensation of heavier components from solvent to oil phase is the controlling mass transfer mechanism for fluid phase equilibria of these reservoir fluids. The proposed mass transfer enhanced mechanistic model IFT predictions for this crude oil-solvent system at different NGL enrichments in solvent are shown in Table 2.9 and Figure 2.9.

The Parachor model IFT predictions for Schrader Bluff crude oil at different NGL enrichments in CO_2/NGL solvent is given in Table 2.9 and shown in Figure 2.10. As can be seen in Figure 2.10 and Table 2.9, the predicted IFT at the MME of 15 mole% NGL in CO_2/NGL solvent is 0.044 mN/m, higher than the experimental value of 0.001 mN/m at this enrichment. Hence, as done before, correction factor (X) is used for Parachor model prediction to compute the mass transfer enhancement parameter (k) and is determined to be 0.023. The calculated diffusivities between the fluid phases at different NGL enrichments in CO_2/NGL solvent at reservoir conditions are given in Table 2.10. The average ratio of diffusivities for all NGL enrichments in CO_2/NGL solvent is 71.75 (Table 2.10). From the average ratio of diffusivities and the mass transfer enhancement parameter, the exponent (n) characterizing the mass transfer mechanism is computed as –0.883. The negative sign of n indicates that the condensation of heavier components from solvent to oil phase is the governing mass transfer mechanism for the attainment of fluid phase equilibria of these fluids. The proposed mass transfer enhanced mechanistic model IFT predictions for this crude oil-solvent system at different NGL enrichments in solvent are given in Table 2.9 and shown in Figure 2.10.

The governing mass transfer mechanism of condensation as identified by the proposed mechanistic model for fluid phase equilibria of Schrader Bluff fluids is substantiated by the presence of only limited amount of lighter components i.e. 26.64 mole% C_1 to C_2 in the crude oil of this reservoir (Sharma et al., 1995). Furthermore, relatively higher value of exponent (n) in the proposed mechanistic model for crude oil-solvent system with PBG/NGL solvents, when compared to that with CO_2/NGL solvents indicate more pronounced condensation mass transfer effects in the crude oil-solvent system containing PBG/NGL solvents. This can be attributed to the presence of relatively larger amounts of heavier components in PBG/NGL solvents when compared to CO_2/NGL solvents.

2.1.5 Application of the Proposed Mechanistic Model to More Reservoir Fluids

The proposed mechanistic model has been further extended to three more reservoir crude oils namely crude oil A, crude oil C and crude oil D. The crude oil compositions and the experimentally measured interfacial tensions between the equilibrium vapor and liquid phases of these crude oils at different pressures and at reservoir temperature from Firoozabadi et al. (1988) are used for comparison with the proposed model predictions.

These three crude oils were from different reservoirs with gravities ranging from 31 to 35^o API (0.87 to 0.85 gm/cc). The key physical characteristics of the crude oils used are described in Table 2.11. From the Table 2.11, it can be seen that the crude oil C is the lightest when compared to the other two crude oils A and D, as it has higher C_1-C_3 molar composition and lower C_{7+} molecular weight.

The comparison of the experimental IFT measurements with the original Parachor model and the proposed mechanistic model IFT predictions are shown in Figures 2.11-2.13 and Tables 2.12-2.14 respectively, for crude oil A, crude oil C and crude oil D. From these tables and figures, it can be seen that the match between the experiments and the original parachor model is poor and significant IFT under-predictions are obtained with Parachor model for all the three crude oil systems studied. The average absolute deviations between the Parachor model and the experimental data for the three crude oils ranged from 36.8% to 57.2%. Contrarily, excellent match between the proposed mechanistic model and the experimental data can be seen for the three crude oil systems considered. The average absolute deviations ranging from 6.8% to 10.6% are obtained between the proposed mechanistic model and the experiments for all the three systems.

The exponents of +0.61, +1.78, and +0.928 are obtained in the proposed mechanistic model for crude oils A, C and D, respectively to best fit the experimental data. The positive exponents in the mechanistic model indicate that vaporization of lighter components (C_1-C_3) from crude oil is the governing mass transfer mechanism for the attainment of fluid phase equilibria between the equilibrium liquid and vapor phases of these crude oils. This is substantiated by the fact that these three crude oil systems contain only crude oil in the feed and hence the vaporization of lighter components from the crude oil is responsible for forming the equilibrium vapor phase.

2.1.6 Sensitivity Studies on Proposed Mechanistic Model

Sensitivity studies were carried out for RKR and Terra Nova reservoir fluids to determine the effect of number of experimental IFT measurement data points on the proposed mechanistic model results. The exponents obtained by using different single experimental IFT measurements in the mechanistic model are shown in Table 2.15 and Table 2.16 for

RKR and Terra Nova reservoir fluids, respectively. The comparision of IFT predictions from the mechanistic model obtained by using three different single IFT measurements namely high IFT, medium IFT and low IFT with the original Parachor model and the mechanistic model with all the available experimental data are shown in Figures 2.14 and 2.15 for RKR and Terra Nova fluids, respectively. From Figure 2.14 for RKR fluids, it can be seen that there is no significant differences among the mechanistic model IFT predictions using single high and medium IFT measurement points and all the experimental data in the mechanistic model. However, the use of low single IFT measurement point in the mechanistic model resulted in significantly deviating IFT values when compared to the mechanistic model with all the experimental points. It can be further observed that even the provision of single low IFT measurement point as input to the mechanistic model yielded better IFT predictions compared to original Parachor model. Similar results can be seen even for Terra Nova fluids. From Figure 2.15 for Terra Nova fluids, it can be seen that the provisions of single high, medium and low IFT measurement points as well as all the experimental data in the mechanistic model resulted in almost similar IFT predictions. The IFT predictions from all these combinations matched extremely well with experiments when compared to original Parachor model. Based on these observations, it can be concluded that the provision of a single high or medium experimental IFT measurement in the proposed mechanistic model is sufficient for reasonable IFT predictions from the model. Thus, the mechanistic model IFT predictions with a single experimental IFT measurement of medium or high IFT range can be used to infer miscibility conditions without the need for low IFT measurements, which are considered somewhat difficult to make.

2.1.7 Generalized Correlations for Prediction of Exponent (n) in Mechanistic Model

- **Parachor Physics and Thermodynamics**

Parachor is defined as the molar volume at such a temperature at which surface tension has the unit value as long as this temperature does not approach the critical temperature (Exner, 1967), as described by the following Eqs. 2.10 and 2.11.

$$P = \frac{M}{\rho_l - \rho_v}\sigma^{1/4} \quad \text{...} \quad (2.10)$$

Where, P is the Parachor, ρ_l and ρ_v denote densities in liquid and vapor phase, respectively, σ is the surface tension and M is the molecular weight.

At temperatures lower than critical temperature, ρ_v can be neglected when compared to ρ_l and hence Eq. 2.10 simplifies to

$$P = M\rho_l^{-1}\sigma^{1/4} \quad \text{...} \quad (2.11)$$

Parachor is compound specific. Parachor is temperature independent at temperatures below critical temperature for all non-polar and little polar compounds (Exner, 1967), as described below. Eq. 2.11 can be written in more general form as,

$$P = M\rho_l^{-1}\sigma^{\alpha} \qquad (2.12)$$

Differentiation of Eq. 2.12 with respect to temperature yields,

$$\frac{\partial P}{\partial T}P^{-1} = \alpha\sigma^{-1}\frac{\partial \sigma}{\partial T} - \rho_l^{-1}\frac{\partial \rho_l}{\partial T} \qquad (2.13)$$

With the assumption of temperature independence of Parachor, Eq. 2.13 reduces to

$$\frac{\partial \sigma}{\partial T}\left(\frac{\partial \rho_l}{\partial T}\right)^{-1} = \alpha^{-1}\sigma\rho_l^{-1} \qquad (2.14)$$

Exner (1967) tested the temperature dependence of Parachor for polar and non-polar compounds by plotting the left hand $\left(\frac{\partial \sigma}{\partial T}\left(\frac{\partial \rho_l}{\partial T}\right)^{-1}\right)$ and the right hand sides $\left(\sigma\rho_l^{-1}\right)$ of Eq. 2.14. This plot is included as Figure 2.16 for reference. From this plot, it can be seen that, the straight-line slope for all non-polar or little polar compounds such as hydrocarbons is almost 4.0, which satisfies the exponent of α = ¼ in the Eq. 2.11. Therefore, for these compounds a temperature independent Parachor can be assumed. However, for polar compounds, the slope of straight-line lower than 4.0 obtained indicates a higher value of exponent in Eq. 2.11 suggesting moderate increase of Parachor with temperature. Hence, temperature independence cannot be assumed for the Parachors of strongly associated compounds.

Parachor value of a compound is related to its molecular weight. Firoozibadi et al. (1988) used the data from Katz et al. (1943) and Rossini (1953) to show a linear straight-line relationship between Parachor and molecular weight for n-alkanes. They also computed the Parachors of crude cuts of various crude oils from surface tension measurements and showed a quadratic relationship between Parachor and molecular weight for all the crude cuts, except for the residues. They attributed this discontinuity for the last heavy residue fractions largely to the presence of asphaltene materials. The plot of Firoozabadi et al. (1988) showing the effect of molecular weight on Parachor for crude cuts and n-paraffins is included as Figure 2.17.

Parachor value of a compound does not depend on pressure (Firoozabadi et al., 1988). Firoozabadi et al. (1988) determined the Parachors of different crude cuts of various crude oils at different pressures and reported similar Parachor values for individual crude cuts at all the pressures tested. The data showing the Parachor independence with pressure from the study of Firoozabadi et al. (1988) is summarized in Table 2.17.

Parachor value of a mixture is related to solute concentration (Hammick and Andrew, 1929; Bowden and Butler, 1939). Hammick and Andrew (1929) computed Parachor values of mixtures of benzene (non-associated solvent) with various non-associated solutes such as carbon tetrachloride, m-xylene, cyclohexane and chloroform, using surface tension measurements. They found that the Parachor values of the solution are linearly related to solute concentration and are either increased or decreased as the solute concentration in the solution is increased. The data from the study of Hammick and Andrew (1929) is plotted in Figure 2.18.

- **Relationship Between Exponent (n) and Parachor**

Interestingly, the exponent (n) in the proposed mechanistic model exhibits similar characteristics as the Parachor. The exponent is specific for a crude oil (equilibrium liquid and vapor phases) or crude oil-solvent system. It is independent of pressure (as can be seen in Figures 2.11-2.13). Based on our work so far, the exponent appears to be independent of temperature, although this needs to be still verified with experiments. Based on these observations, like for the Parachor, a linear relationship between the exponent and solute composition is hypothesized. For testing this hypothesis, crude oil-solvent (Terra Nova and RKR fluids) and crude oil (crude oils A, C and D) systems of this study have been used.

In crude oil-solvent systems such as RKR and Terra Nova fluids, simultaneous counter-directional mass transfer interactions occur from both the oil and solvent (gas) phases. These include vaporization of lighter components (C_1-C_3) from crude oil phase to solvent (gas) phase and condensation of intermediate to heavier components (C_4-C_{7+}) from the solvent (gas) phase to crude oil phase. Therefore, the compositions of (C_1-C_3) in crude oil and (C_4-C_{7+}) in gas constitute the solute composition. These compositions are normalized as a molar ratio: (C_1-C_3)/(C_4-C_{7+}) in crude oil to represent vaporizing drive mechanism from the oil and (C_4-C_{7+})/(C_1-C_3) in gas phase to represent condensing drive mechanism from the gas. The mechanistic model exponents for the two crude oil-solvent systems of RKR and Terra Nova are now related to the normalized solute compositions using multiple regression analysis. The results are summarized in Figure 2.19. From Figure 2.19, it can be seen that a good linear relationship between the exponent and the normalized solute compositions is obtained for the two crude oil-solvent systems with a correlation coefficient of 0.984. The regression equation used for predicting the exponent (n) values is also shown in Figure 2.19. Higher absolute value of the slope for vaporizing drive mechanism (8.129) when compared to condensing drive mechanism (1.045) in the regression equation indicates that the vaporization of lighter components from crude oil to gas phase is the governing mass transfer mechanism for the attainment of fluid phase equilibria between the vapor and liquid phases of these two crude oil-solvent systems. The regression equation needs to be extended to more crude oil-solvent systems so as to develop a generalized correlation for *a- priori* estimation of exponent (n) in the mechanistic model for crude oil-solvent systems. Then the exponent (n) in the mechanistic model can be simply determined by using the compositions of crude oil and solvent and thereby completely eliminating the need for experimental data in the proposed mechanistic model.

In crude oil systems such as crude oils A, C and D, the equilibrium vapor phase is formed primarily due to vaporization of lighter components (C_1-C_3) from crude oil. Therefore, the composition of lighter ends (C_1-C_3) in the crude oil constitutes the solute composition. Hence the mechanistic model exponents for these three crude oil systems are related to the normalized solute composition (C_1-C_3)/(C_4-C_{7+}) in the crude oil, using regression analysis. The results are shown in Figure 2.20. As before for the crude oil-solvent systems, a good linear relationship between the exponent and the normalized solute composition can be seen even in this case with a correlation coefficient of 0.988. The regression equation obtained is shown in Figure 2.20. This regression equation if generalized using more crude oil systems, can be used for *a-priori* prediction of exponent (n) in the mechanistic model for crude oil systems simply by knowing the composition of crude oil, without fitting any experimental data.

Thus the Parachor and the exponent (n) in the mechanistic model have similar characteristics. The summary of similarities observed in the characteristics between the exponent (n) and the Parachor are shown in Table 2.18.

2.1.8 Prediction of Dynamic Gas-Oil Miscibility

The use of diffusion coefficients in the proposed mechanistic model and the ability of model to provide information on mass transfer mechanisms indicate that the IFT measurements used for the development of the proposed model are dynamic in nature. This is further supported with the fact that several investigators (Rosen and Gao, 1995; Taylor and Nasr-EI-Din, 1996; Campanelli and Wang, 1999; Diamant et al., 2001) used diffusion coefficients in their models to predict dynamic interfacial tension in brine-crude oil-surfactant systems. Therefore, the dynamic interfacial tension predictions from the proposed mechanistic model can be plotted against solvent enrichment or pressure and the extrapolation of the plot to zero interfacial tension can be used to infer dynamic miscibility. Hence the IFT's from the proposed model can be used to predict dynamic miscibility of the most popular gas injection EOR projects. The ongoing IFT measurements with live reservoir crude oil and brine systems at elevated pressures and temperatures in our laboratory support this dynamic nature of IFT. However, the IFT experiments being planned with reservoir crude oil-gas systems at reservoir conditions are anticipated to reveal more information in future.

2.2 IFT Measurements in a Standard Ternary Liquid System

2.2.1 Introduction

The primarily available experimental methods to evaluate fluid-fluid miscibility under reservoir conditions are the slim-tube displacement, the rising bubble apparatus and the pressure composition diagrams. However, recently the new Vanishing Interfacial Tension (VIT) technique has been reported for experimental determination of miscibility conditions in gas-oil systems (Rao, 1997; Rao et al., 1999; Rao and Lee, 2002). This technique relies on the concept that at miscibility, the interfacial tension between the fluids must become zero due to the absence of an interface. In this method, the interfacial tension between the fluids is measured at reservoir temperature at varying pressures or enrichment levels of gas phase. The minimum miscibility pressure (MMP) or minimum miscibility enrichment (MME) is then determined by extrapolating the plot of interfacial tension, against pressure or enrichment, to zero interfacial tension. None of the other previously mentioned experimental techniques provides such direct and quantitative information on interfacial tension. In addition to being quantitative in nature, this new VIT technique is quite rapid as well as cost effective. The VIT technique has been applied successfully to evaluate gas-oil miscibility in two field gas injection projects (Rao, 1997; Rao et al., 1999; Rao and Lee, 2002).

The terms, miscibility, solubility and interfacial tension, are commonly used in phase behavior studies of ternary fluid systems. Review of literature shows that zero interfacial tension is a necessary and sufficient condition to attain miscibility (Benham et al., 1965; Holm, 1987; lake, 1989). Blanco et al. (1996) measured vapor-liquid equilibrium data at 141.3 kPa for the mixtures of methanol with n-pentane and n-hexane and then determined upper critical solubility for methanol, n-hexane mixtures from the measured miscibility data. This intuitively suggests the relationship of miscibility with upper critical solubility of a solute in solvent for ternary fluid systems. Lee (1999) modified the adsorption model proposed by van Oss, Chaudhury and Good (1987) by the inclusion of equilibrium spreading pressure to calculate the liquid-liquid interfacial tension. This study related equilibrium interfacial film pressure and the interfacial tension for prediction of miscibility of liquids and pointed out that the theory of miscibility of liquids can be applicable to the solubility of a solute in a solvent. Thus the distinction between the terms miscibility and solubility still appears to be unclear, leading to their synonymous use in some quarters.

Interfacial tension being a property of the interface between two fluids is assumed to be dependent on molar ratio of the two fluids (solvent-oil ratio) in the feed mixture. Simon et al. (1978) measured the IFT of a reservoir crude oil at various solvent-oil ratios in the feed using high-pressure interfacial tensiometer. The results from this experimental study indicated strong dependence of IFT on solvent-oil ratio in the feed, in which an increase of IFT was observed with an increase in concentration of CO_2 gas in the feed.

Such a dependence of IFT on solvent-oil ratio in the feed indicates the role of mass transfer effects on IFT. This necessitates the need to explore solvent-oil ratio effects on IFT between pre-equilibrated and non-equilibrated fluids.

Therefore, the objectives of the study under this section are to correlate miscibility and solubility with interfacial tension, to study the solvent-oil ratio effects on IFT as well as to investigate the applicability of the new VIT technique to determine the miscibility in ternary fluid systems. For this purpose, the standard ternary liquid system of ethanol, water and benzene is chosen since their phase behavior and solubility data are readily available (Chang and Moulton, 1953; Sidgwick and Spurrel, 1920). The IFT measurements were carried out in pendent drop mode, using the drop shape analysis (Kruss Manual, 2000) and the capillary rise technique.

2.2.2 Experimental System and Procedure

The schematic of the experimental setup used to measure the IFT using drop shape analysis technique is shown in Figure 2.21. It consists of an optical cell, solvent reservoir, injection system to inject oil, light source and a camera system connected to a computer for image capture and analysis. Different molar solutions of ethanol and water were prepared using the desired volumetric percentages. These solutions were used as the solvents non-equilibrated with benzene in the experiments. For preparation of solvent solutions pre-equilibrated with benzene, 1000 ml of the non-equilibrated solvent was taken in a glass flask and measured volume of benzene, slightly above the solubility limit corresponding to that solvent composition, was poured into the flask. The flak was tightly closed and rigorously mixed for 12 hours. After mixing, the solution is filtered, using hardened ashless Whatman filter paper. Now, the filtered solution is allowed to settle for another 12 hours. Afterwards, the equilibrated benzene and solvent phases of the solution were carefully collected and stored. The optical cell is first cleaned with deionized water and then with acetone. The solvent (pre-equilibrated or non-equilibrated) is taken in a container (solvent reservoir), which was kept at a sufficient height to allow flow by gravity. The cell was gradually filled up and some solvent was allowed to drain from the top to ensure that there were no trapped air bubbles in the cell. The benzene is now injected into the cell, using the injection system, drop by drop. A few benzene drops were allowed to rise through the solvent and rest at the top of the cell to allow for fluid equilibration. Now, a benzene drop was allowed to hang from the capillary tip and the drop image is captured on the computer using the camera system. The captured drop image was then analyzed for IFT using the drop shape analysis technique (Kruss Manual, 2000).

2.2.3 Solubility and Miscibility

The solubility diagram, solubility data and different regions of solubility characteristics for this standard system have been already reported (Report # 15323R02, July 2003). From this diagram, the complete solubility (miscibility) of benzene in aqueous ethanol can be seen at 78% ethanol enrichment. The ternary phase diagram of this standard system reported by Chang and Moulton (1953) is shown in Figure 2.22. From the ternary phase diagram, it can be seen that the limiting tie line passing through the oil (benzene) intersects the solvent (aqueous ethanol) at an ethanol enrichment of 83%. Hence, this becomes the minimum miscibility ethanol enrichment for the system to attain miscibility. Thus the minimum miscibility ethanol enrichments for this standard ternary fluid system by both the phase diagram (83%) and the solubility data (78%) appear to be in good agreement.

2.2.4 Solvent-Oil Ratio Effects on IFT

At first, a calibration IFT experiment was conducted for a known standard fluid pair of n-Decane and water. An IFT value of 49.0 ± 0.15 mN/m was obtained, which is in good agreement with the published value of 50.5 mN/m reported by Jennings (1967). Then, different molar feed compositions corresponding to 0, 10 and 40 volume % oil in the solvent were used to study the solvent-oil ratio effects on IFT measurements. The IFT's between the non-equilibrated fluids could not be measured above 40% ethanol enrichment, using the drop shape analysis technique. At these higher ethanol enrichments, pendent drops could not be formed as the oil quickly escaped in streaks through the solvent. All the measured IFT experimental values for non-equilibrated fluids at different ethanol enrichments in aqueous phase and at different solvent-oil ratios in the feed mixtures of aqueous ethanol and benzene are summarized in Table 2.19 and Figure 2.23. The standard deviations in the range of 0.03 to 0.11 obtained in measured IFT values indicate extremely low variation in the measurements. The important observations from Table 2.19 and Figure 2.23 are the following.

The IFT gradually decreases as the ethanol enrichment increases in aqueous phase. At ethanol enrichments of up to 20% in aqueous phase, IFT is found to be independent of solvent-oil ratio in the feed. However, for the ethanol enrichments of 30% and above, an increase in IFT is observed as the solvent-oil ratio in feed is decreased. The increase of IFT with decrease in solvent-oil ratio is low at 30% ethanol enrichment and then becomes noticeable at higher ethanol enrichments in aqueous phase. The possible reasons for the observed solvent-oil ratio effects on IFT are discussed below.

As can be seen from the solubility data of this standard ternary system (Report #15323R02, July 2003), benzene solubility in aqueous ethanol starts at an ethanol enrichment of 35% and then gradually increases to become completely soluble at an ethanol enrichment of 78%. Hence solubility of benzene in aqueous ethanol does not come into picture during the IFT measurements in insoluble regions of ethanol enrichments below 35%. Hence, absence of solvent-oil ratio effects on IFT is observed at ethanol enrichments below 30%. At ethanol enrichments above 35% in aqueous phase, the dissolution of benzene in aqueous ethanol interferes with IFT measurements due to varying amounts of benzene at different solvent-oil ratios in the feed. This results in the dependence of IFT on feed solvent-oil ratio in partially soluble regions at ethanol enrichments of 30% and greater. Above 35% ethanol enrichment, benzene solubility effects become more pronounced as the ethanol enrichment in aqueous phase increases further. As a result, noticeable solvent-oil ratio effects on IFT can be seen in Figure 2.23 as the ethanol enrichment in aqueous phase is increased.

The solubility effects of benzene observed in aqueous ethanol in partially soluble regions at ethanol enrichments of 30% and above can be eliminated by using aqueous ethanol pre-equilibrated with benzene as solvent in IFT measurements. Figures 2.24 and 2.25 demonstrate the effects of benzene solubility on benzene drop size in non-equilibrated and pre-equilibrated 30% aqueous ethanol solvent, respectively. As can be seen in Figure 2.24, benzene drop gradually reduces in size with time and completely vanishes within 4 hours in non-equilibrated aqueous ethanol solvent. This can be attributed to solubility of benzene in non-equilibrated aqueous ethanol. However, contrarily, absence of benzene solubility effects in aqueous ethanol pre-equilibrated with benzene can be seen in Figure 2.25. The benzene drop is able to retain its original size and shape in the solvent even after 4.5 hours. These observations clearly suggest that compositional effects on IFT in partially soluble regions can be removed by the use of pre-equilibrated solutions during the experiments.

Thus IFT dependence on feed solvent-oil ratio for non-equilibrated fluids in partially soluble regions appears to be due to benzene dissolution in aqueous ethanol. Therefore, all the changes in IFT observed with non-equilibrated solutions in partially soluble regions at ethanol enrichments of 30% and above at different feed compositions can be attributed mainly to benzene solubility effects and not to solvent-oil ratio in the feed mixture (Table 2.19 and Figure 2.23). To further substantiate this conclusion, IFT measurements were repeated using pre-equilibrated fluids at 30% and 40% ethanol enrichments in aqueous phase for various solvent-oil ratios in the feed. The results are summarized in Table 2.20 and shown in Figure 2.26. From Table 2.20 and Figure 2.26, it can be clearly seen that no noticeable changes in IFT were observed for various solvent-oil ratios in the feed at these ethanol enrichments of pre-equilibrated fluids. Therefore, it can be concluded that the use of pre-equilibrated solutions in the partially soluble regions for IFT measurements eliminates the compositional effects on IFT and that the IFT is independent of solvent-oil ratio in the feed.

2.2.5 Capillary Rise Technique

This technique was adapted to measure the low IFT's that could not be measured using drop shape analysis technique at ethanol enrichments above 40%. The schematic of this technique is illustrated in Figure 2.27. The force balance in the capillary is given by,

$$2\pi r\sigma\cos\theta = \pi r^2 h\Delta\rho\frac{g}{g_c} \qquad (2.15)$$

Solving for interfacial tension, σ, gives

$$\sigma = \frac{rh\Delta\rho g}{2\cos\theta g_c} \qquad (2.16)$$

Where, σ = interfacial tension in $dynes/cm$

r = pore throat radius in cm

h = capillary rise in cm

Δρ = density difference between the fluids in gms/cc

θ = equilibrium contact angle in degrees

g = acceleration due to gravity (980 $cm/\sec^2$)

g_c = conversion (1 $\frac{gm.cm/\sec^2}{dyne}$)

At first, this technique was calibrated for a known low IFT standard fluid pair of n-Butanol and water, using two different capillary sizes. IFT values of 1.72 and 1.79 mN/m were obtained for capillary diameters of 0.09 and 0.025 cm, respectively. These values were in good agreement with the value of 1.8 mN/m reported by Mannhardt (1987) for this standard system. Now, certain volume of aqueous ethanol at a particular ethanol enrichment is taken in a glass beaker. Measured volume of benzene slightly about one and half times above the solubility limit is added to the aqueous ethanol. The two fluid phases are thoroughly mixed by shaking and allowed to settle for about one hour. Now, the solution separates into two phases with less denser fluid phase at the top and more denser fluid phase residing at the bottom. A glass capillary tube (radius r = 0.09 cm) is then carefully inserted into the beaker using an adjustable stand so that it is completely immersed in the two fluid phases. Care is taken to avoid the contact of bottom end of the capillary tube with glass beaker bottom. The interface between the fluid phases slowly rises through the capillary and stabilizes at a definite height (initial rise) within a time of about 10 minutes. The rise is then measured using a cathetometer that reads in units of one-tenth of a millimeter. The rise is continuously monitored and recorded as a function of time for about one hour. However, no changes in rise were observed from the initial rise for the entire one-hour time period at all ethanol enrichments used in this study. This demonstrates the capability of this technique to provide equilibrium IFT measurements quickly. This observation indicates the superior nature of this technique over spinning drop apparatus, another IFT measurement technique most widely preferred for low IFT measurements. Other researchers have reported or shown that longer time periods of few hours is needed to obtain equilibrium IFT for low IFT systems in a spinning drop apparatus (Mannhardt, 1987; Taylor and Nasr-EI-Din, 1996). At 75% ethanol enrichment in aqueous phase, near miscible conditions are visually observed as both the fluid phases of aqueous ethanol and benzene resulted in a single phase with immediate contact during equilibration. However, excess amounts of benzene were then added to separate the single phase into two fluid phases for IFT measurements.

The densities of the pre-equilibrated fluid phases are measured using a PAAR DMA512 density meter. All the measured capillary heights and the densities of the fluid phases at ethanol enrichments above 40% are summarized in Table 2.21. From Table 2.21, it can be seen that as the ethanol enrichment in aqueous phase increases from 50 to 75%, the density difference between the fluid phases decreases from 0.0128 gm/cc to 0.0003 gm/cc. Contrarily, an increase in capillary rise from 0.53 cm to 0.98 cm can be seen as the ethanol enrichment in aqueous phase is increased. This observation suggests that the density difference and the capillary rise are inversely related and hence a good precision of IFT measurement can be made even in low IFT regions using this technique due to decent measurable heights in capillary. This is identified as the other advantage associated with this technique.

The equilibrium contact angles to be used in the capillary rise equation (Eq. 2.16) for IFT calculations are measured using an ambient optical cell, pre-equilibrated fluid phases and glass substrates with which the capillary tubes are made. The photograph of the equipment used for contact angle measurements is shown in Figure 2.28. The glass substrate is first aged in pre-equilibrated aqueous ethanol solvent for about 24 hours. The aged glass substrate is then placed in a crystal holder and assembled carefully into the thoroughly cleaned optical cell. The pre-equilibrated aqueous ethanol solvent is taken in a large container kept at sufficient height and allowed to flow into the cell by gravity. After the cell is filled, some solvent is allowed to drain from the top to ensure the removal of trapped air bubbles in the cell. Now, the pre-equilibrated benzene drop is placed on the glass crystal using an injection syringe from the bottom of the cell. The cell is then set-aside with all the valves closed to age for 24 hours for the solvent-oil-crystal interactions to reach equibrium. After 24 hours of aging, the equilibrium contact angle is measured using an eye-piece goniometer and light source. The measured equilibrium benzene contact angles at different ethanol enrichments in aqueous phase are given in Table 2.22 and shown in Figure 2.29. From Table 2.22 and Figure 2.29, it can be seen that, the benzene equilibrium contact angles gradually decrease from 48^{o} at 0 % ethanol enrichment to 26^o at 20 % ethanol enrichment in aqueous phase and then remains unchanged (25^o) for ethanol enrichments of 30% and 40%. Therefore, it is reasonable to presume that there will be no change in benzene equilibrium contact angles from 25^o with ethanol enrichment at ethanol enrichments above 30%. Hence, an equilibrium contact angle of 25^o was used in capillary rise IFT calculations at all ethanol enrichments above 40%, as indicated by the extrapolated line in Figure 2.29. The summary of all IFT calculations for obtaining low IFT's above 40% ethanol enrichments using the capillary rise technique is shown in Table 2.21. As can be seen in Table 2.21, an IFT value of as low as 0.014 mN/m is measured at 75% ethanol enrichment in aqueous phase with this technique.

2.2.6 Correlation of Miscibility and Solubility with IFT

The measured IFT's of benzene in aqueous ethanol obtained using pendent drop technique at ethanol enrichments below 40% and the capillary rise technique at ethanol enrichments above 40% are plotted against ethanol enrichment in aqueous phase in Figure 2.30 to correlate IFT and miscibility. From Figure 2.30, it can be seen that IFT decreases exponentially as the ethanol enrichment in aqueous phase is increased and reduces to a low value of 0.014 mN/m at 75% enrichment. The regression equation obtained is IFT = 32.58 e $^{(-0.0928 \text{ * Mole\% of Ethanol})}$ with a correlation coefficient (R^2) = 0.9811. Log (IFT) is plotted against ethanol enrichment in Figure 2.31 to clearly observe the trend in the low IFT region. The extrapolation of this semi-log plot indicates a possible very low IFT value of 0.001 mN/m at 81 % ethanol enrichment. Since, the gas-oil interfacial tension can be measured to a very low value of only up to 0.001 mN/m with the available experimental methods (Danesh et al., 1991), it is reasonable to assume this IFT value at miscibility. The miscibility conditions determined from phase diagram (83 %) and solubility data (78 %) for this ternary liquid system are also shown in Figure 2.31 for better comparison. From this comparison, it can be seen that the miscibility condition obtained from the VIT technique (81 %) is in good agreement with phase diagram (83 %) and the solubility data (78 %). Therefore, it can be concluded that the new VIT technique so far applied to determine miscibility in gas-oil systems can be used for miscibility evaluation even in ternary liquid systems. This clearly exposes the sound conceptual basis of the new VIT technique to determine the fluid-fluid miscibility.

In order to determine the existence of a direct correlation between solubility and IFT, solubility is plotted against 1/IFT in Figure 2.32. The IFT values from the regression equation of Figure 2.30, are used at ethanol enrichments corresponding to the solubility values in the plot. As can be seen in Figure 2.32, solubility is linearly related to (1/IFT), indicating a strong mutual relationship between these two thermodynamic properties. The relationship obtained is solubility = 168.53/IFT with a correlation coefficient (R^2) = 0.9931. Therefore, the relationship between solubility and IFT in ternary liquid systems can be generalized as solubility= c/IFT where c is a system dependent constant. Thus solubility has a strong correlation with IFT and hence can be used for IFT predictions in soluble regions.

2.3 High Pressure High temperature VIT Experimental System

2.3.1 Design and Assembly of VIT Experimental System

The assembly of high pressure and high temperature VIT experimental system is completed and the system is now operational. This system has a unique capability to facilitate reservoir condition testing at 400 ^oF and 20,000 psi. The frontal view of the assembled VIT experimental system installed at the Rock Fluids Interactions Laboratory of Petroleum Engineering Department at LSU is shown in Figure 2.33. The design of the system allows measuring both interfacial tension and dynamic (water advancing and receding) contact angles at reservoir conditions. Currently the system is being used for reservoir condition dynamic contact angle and oil-water interfacial tension measurements. However, slight design modifications and procurement of a gas chromatograph for the analysis of gas samples are still need to be made to facilitate the planned VIT experimentation with gas-oil systems. The VIT experimentation with the model fluid systems of known phase behavior characteristics will be conducted upon the availability of the system.

2.3.2 Identification of Model Fluid Systems for VIT Experimentation

The model fluid systems consisting of single, binary and tertiary components of n-C_1, C_4, C_{10} and C_{16} (different molar compositions) in oil phase with known CO_2 minimum miscibility pressures at reservoir temperatures are identified for laboratory VIT experimentation at elevated pressures and temperatures. Care is taken to include the fluid systems with known miscibility conditions of all the currently available experimental techniques (slim-tube, rising bubble and pressure-composition). The model fluid systems identified, their miscibility conditions and the experimental techniques used are summarized in Table 2.23.

2.4 Conclusions

2.4.1 The Proposed Mass Transfer Enhanced Mechanistic Parachor Model

- A mechanistic Parachor model has been developed to include mass transfer effects for prediction of gas-oil interfacial tension as well as to indicate the governing mass transfer mechanism prior to the attainment of fluid phase equilibria and miscibility in reservoir crude oil and reservoir crude oil-solvent systems.
- The ratio of diffusivities between the fluid phases raised to an exponent is introduced into the Parachor model to incorporate mass transfer effects. The sign and value of the exponent in the mechanistic model characterize the type and the extent of

governing mass transfer mechanism prior to attaining fluid phase equilibria and miscibility.

- The performance of the proposed mechanistic model has been tested for several reservoir crude oil-gas and reservoir crude oil systems to evaluate its effectiveness.
- For Rainbow Keg River reservoir fluids, the positive exponents (+0.20, +0.17) in the mechanistic model indicate that the governing mass transfer mechanism is the vaporization of lighter components from crude oil into the gas phase for attaining the fluid phase equilibria and dynamic miscibility.
- For Terra Nova reservoir fluids, the positive exponent (+1.28) in the mechanistic model indicates the vaporization of light hydrocarbon components from crude oil into the gas phase to be the governing mass transfer mechanism for achieving fluid phase equilibria and dynamic miscibility.
- The relatively higher value of positive exponent in the mechanistic model for Terra Nova fluids compared to RKR fluids indicates more pronounced vaporization mass transfer effects in Terra Nova fluids. This is substantiated by the presence of relatively higher content of light hydrocarbon components (C_1 to C_3) in Terra Nova crude oil.
- The negative exponents (-0.883, -1.747) in the mechanistic Parachor model for Schrader Bluff reservoir fluids indicate that the condensation of heavier components from solvent to oil phase is the governing mass transfer mechanism for fluid phase equilibria of these fluids.
- The relatively higher absolute value of negative exponent in the proposed mechanistic model for Schrader Bluff fluids with PBG/NGL solvents compared to CO_2/NGL solvents indicate more pronounced condensation mass transfer effects in these reservoir fluids containing PBG/NGL solvents.
- The positive exponents of +0.61, +1.78 and +0.928 obtained in the mechanistic model for the three crude oil systems of A, C and D, respectively, indicate that vaporization of lighter components from the crude oil is the governing mass transfer mechanism for the attainment of fluid phase equilibria between the equilibrium liquid and vapor phases of these crude oils.
- The sensitivity studies on model results for RKR and Terra Nova reservoir fluids indicate that the provision of a single high or medium range IFT measurement in the proposed mechanistic model is sufficient for reasonable IFT predictions from the proposed model.
- An attempt has been made to correlate the exponent (n) in the mechanistic model with normalized solute compositions present in both the fluid phases for both the reservoir crude oil-gas and reservoir crude oil systems. These correlations, if generalized using

more crude oil-solvent and crude oil systems, can be used for *a-priori* estimation of exponent (n) in the mechanistic model.

- Use of diffusion coefficients in the mechanistic model indicates dynamic nature of IFT. Hence, IFT predictions from the model can be used to determine dynamic gas-oil miscibility in gas injection EOR projects.
- Based on our ongoing study, it appears that in most cases of gas-oil interactions, mass transfer occurs in both directions and hence combined vaporizing/condensing mode is the cause of miscibility development.
- The proposed mechanistic model can be utilized to identify the predominating mechanism in the combined vaporizing/condensing mode and to determine the dynamic gas-oil miscibility.

2.4.2 IFT Measurements in a Standard Ternary Liquid System

- IFT measurements were carried out in a standard ternary liquid system of ethanol, water and benzene.
- In insoluble regions, absence of solvent-oil ratio effects on interfacial tension is observed.
- IFT dependence on solvent-oil ratio in the feed is noticeable in soluble regions.
- This study has identified the need to use pre-equilibrated solutions in soluble regions to remove compositional effects on interfacial tension.
- Capillary rise technique has been used to measure the low IFT's occurring above 40% ethanol enrichment.
- IFT is strongly correlated to solubility and miscibility.
- IFT gradually decreases as ethanol enrichment in aqueous phase is increased and vanishing nature of IFT is clearly evident as miscibility is approached.
- IFT is related to solubility with a generalized relationship, solubility=c/IFT, where c is a system dependent constant.
- This study has demonstrated the strong conceptual basis of the new VIT technique and its applicability to determine miscibility in ternary liquid systems as well.
- The conceptual extension of all these experimental findings to gas-oil systems at reservoir conditions would be useful in quick, accurate and cost-effective determination of miscibility conditions for gas injection EOR projects.

2.4.3 High Pressure High Temperature VIT Experimental System

- The high pressure high temperature VIT experimental system has been designed, fabricated, assembled and is currently operational.
- Model fluid systems with known miscibility conditions have been identified for VIT experimentation at elevated pressures and temperatures.

2.5 Future Plans

- To extend the application of the proposed mechanistic model to more crude oil and crude oil-solvent systems to generalize the developed regression models
- To conduct VIT experiments with the identified model fluid systems at elevated pressures and temperatures
- To conduct IFT experiments with reservoir crude oil-gas systems at reservoir conditions to validate the dynamic nature of the proposed mechanistic model

References

1. Ali, J.K.: "Predictions of Parachors and Petroleum Cuts and Pseudo Components," *Fluid Phase Equilibria*, **95** (1994) 383-398.
2. Benham, A.L., Dowden, W.E. and Kunzman, W.J.: "Miscible Fluid Displacement - Prediction of Miscibility," Petroleum Transactions Reprint Series No. 8, Society of Petroleum Engineers of AIME (1965) 123.
3. Blanco, A.M. and Ortega, J.: "Experimental Study of Miscibility, Density and Isobaric Vapor-Liquid Equilibrium Values for Mixtures of Methanol in Hydrocarbons (C_5, C_6)," *Fluid Phase Equilibria*, **122** (1996) 207-222.
4. Bowden, S.T. and Butler, E.T.: "Intermolecular Forces in Liquid Systems. Part II. Viscosity, Surface Tension, and Parachor Relationships in Binary Systems," *J. Chem. Soc.*, **140** (1939) 79- 83.
5. Brock, H.L. and Bird, R.B.: "Surface Tension and Principle of Corresponding States," *AIChE J.*, **1** (1955) 174-177.
6. Campanelli, J.R. and Wang, X.: "Dynamic Interfacial Tension of Surfactant Mixtures at Liquid - Liquid Interfaces," *J. Colloid and Interface Sci.*, **213** (1999) 340-351.
7. Carey, B.S.: "The Gradient Theory of Fluid Interfaces," *PhD Dissertation* (1979), University of Minnesota, Minneapolis.
8. Chang, Y.C. and Moulton, R.W.: "Quaternary Liquid Systems with Two Immiscible Liquid Pairs," *Industrial Engineering Chemistry*, **45** (1953) 2350-2361.
9. Clever, H.L. and Chase, W.E., Jr.: "Thermodynamics of Liquid Surfaces, Surface Tension of n-hexane-cyclohexane mixtures at 25, 30 and 35^o C," *J. Chem. Eng. Data*, **8** (1963) 291-292.
10. Computer Modeling Group Ltd., Winprop Phase Property Program, Calgary, Canada, 2001.
11. Cornelisse, P.M.W., Peters, C.J. and de Swaan Arons, J.: "Application of the Peng-Robinson Equation of State to Calculate Interfacial Tensions and Profiles at Vapor-Liquid Interfaces," Fluid *Phase Equilibria*, **82** (1993) 119-129.
12. Danesh, A.: *PVT and Phase Behavior of Petroleum Reservoir Fluids*, Elsevier Science B.V., Amsterdam (1998) 281-299.
13. Danesh, A.S., Dandekar, A.Y., Todd, A.C. and Sarkar, R.: "A Modified Scaling Law and Parachor Method Approach for Improved Prediction of Interfacial Tension of Gas-

Condensate Systems," paper SPE 22710 presented at the 66th SPE Annual Technical Conference and Exhibition, Dallas, TX, October 6-9, 1991.

14. Diamant, H., Ariel, G. and Andelman, D.: "Kinetics of Surfactant Adsorption: the Free Energy Approach," *Colloids and Surfaces A: Physicochemical and Eng. Aspects*, **183-185** (2001) 259-276.
15. Elsharkawy, A.M., Poettmann, F.H. and Christiansen, R.L.: "Measuring CO_2 Minimum Miscibility Pressure: Slim-Tube or Rising-Bubble Method?," *Energy & Fuels*, **10** (1996) 443-449.
16. Exner, O.: "Additive Physical Properties. III. Re-Examination of the Additive Character of Parachor," *Collect. Czech. Chem. Commun.*, **32** (1967) 24-54.
17. Fanchi, J.R.: "Calculation of Parachors for Compositional Simulation: An Update," *SPE Reservoir Engineering*, **5** (1990) 433-436.
18. Fawcett, M.J.: "Evaluation of Correlations and Parachors to Predict Low Interfacial Tension in Condensate Systems," paper SPE 28611 presented at the 69th SPE Annual Technical Conference and Exhibition, New Orleans, LA, September 25-28, 1994.
19. Fayers, F.J: "Crossflow Mechanisms by Gas Drive in Heterogeneous Reservoirs," paper SPE 24934 presented at the 67th SPE Annual Technical Conference and Exhibition, Washington, DC, October 4-7, 1992.
20. Firoozabadi, A., Katz, D.L., Saroosh, H. and Sajjadian, V.A.: "Surface Tension of Reservoir Crude Oil/Gas Systems Recognizing the Asphalt in the Heavy Fraction," *SPE Reservoir Engineering* (Feb. 1988) 265-272.
21. Hammick, D.L. and Andrew, L.W.: "The Determination of the Parachors of Substances in Solution," *J. Chem. Soc.*, **130** (1929) 754-759.
22. Holm, L.W.: "Miscible Displacement," in H.B. Bradley (Ed.), *Petroleum Engineering Hand Book*, Society of Petroleum Engineers, Richardson, TX (1987) 1-45.
23. Hough, E.W. and Stegemeier, G.L.: "Correlation of Surface and Interfacial Tension of Light Hydrocarbons in the Critical Region," *SPEJ*, **1** (1961) 259-263.
24. Hugill, J.A. and Van Welsenes, A.J.: "Surface Tension: A Simple Correlation for Natural Gas and Condensate Systems," *Fluid Phase Equilibria*, **29** (1986) 383.
25. Jennings, Jr., H.Y.: The Effect of Temperature and Pressure on the Interfacial Tension of Benzene-Water and Normal Decane-Water," *Journal of Colloid and Interface Science*, **24** (1967) 323-329.
26. Katz, D.L., Monroe, R.R. and Trainer, R.P.: "Surface Tension of Crude Oils Containing Dissolved Gases," *JPT* (Sept. 1943) 1-10.
27. Kruss User's Manual, *Drop Shape analysis*, Kruss GmbH, Hamburg 2000.
28. Lake, L.W.: *Enhanced Oil Recovery*, Prentice-Hall Englewood Cliffs, NJ (1989) 234.

29. Lee, L.H.: "Relevance of Film Pressures to Interfacial Tension, Miscibility of Liquids, and Lewis Acid - Base Approach," *Journal of Colloid and Interface Science*, **214** (1999) 64-78.
30. Lee, S.T. and Chien, M.C.H.: "A New Multicomponent Surface Tension Correlation Based on Scaling Theory," paper SPE 12643 presented at the SPE/DOE Fourth Symposium on Enhanced Oil Recovery, Tulsa, OK, April 15-18, 1984.
31. Mannhardt, K: "The Measurement of Interfacial Tension by the Spinning Drop Apparatus," Technical Report Submitted to Petroleum Recovery Institute, Calgary, Canada, Mar. 13 (1987).
32. Macleod, D.B.: "On a Relation Between Surface Tension and Density," *Trans. Faraday Soc*., **19** (1923) 38-42.
33. Metcalfe, R.S. and Yarborough, L.: "The Effect of Phase Equilibria on the CO_2 Displacement Mechanism," Paper SPE 7061 presented at the SPE-AIME 5th Symposium on Improved Methods for Oil Recovery, Tulsa, OK, April 16-18, 1978.
34. Mihcakan, M. and Poettmann, F.H.: "Minimum Miscibility Pressure, Rising Bubble Apparatus and Phase Behavior," Paper SPE 27815 presented at the SPE/DOE 9th Symposium on Improved Oil Recovery, Tulsa, OK, April 17-20, 1994.
35. Nghiem, L.X. and Heidemann, R.A.: "General Acceleration Procedure for Multiphase Flash Calculations with Application to Oil-Gas-Water Systems," paper presented at the 2nd European Symposium on Enhanced Oil Recovery, Paris, France, November 8-10, 1982.
36. Peng, D.Y. and Robinson, D.B.: "A New Two-Constant Equation of State," *Ind. Eng. Chem. Fundam*., **15** (1976) 59-64.
37. Quale, O.R.: "The Parachors of Organic Compounds," *Chem. Review,* **53** (1953) 439-586.
38. Rao, D.N.: "A New Technique of Vanishing interfacial Tension for Miscibility Determination," *Fluid Phase Equilibria*, **139** (1997) 311-324.
39. Rao, D.N. and Lee, J.I.: "Application of the New Vanishing Interfacial Tension Technique to Evaluate Miscibility Conditions for the Terra Nova Offshore Project," *Journal of Petroleum Science and Engineering*, **35** (2002) 247-262.
40. Rao, D.N., Mcintyre, F.J. and Fong, D.K.: "Application of a New Technique to Optimize Injection Gas Composition for the Rainbow Keg River F Pool Miscible Flood," *JCPT* (Dec. 1999) 38.
41. Rao, D.N., Xu, Q., Ayirala, S.C., Kulkarni, M.M. and Sharma, A.P.: "Development and Optimization of Gas-Assisted Gravity Drainage (GAGD) Process for Improved Light Oil Recovery," Quarterly Technical Progress Report to DOE, Report #15323R01, April 2003.
42. Rao, D.N., Xu, Q., Ayirala, S.C., Kulkarni, M.M. and Sharma, A.P.: "Development and Optimization of Gas-Assisted Gravity Drainage (GAGD) Process for Improved Light Oil Recovery," Quarterly Technical Progress Report to DOE, Report #15323R02, July 2003.

43. Rao, D.N., Xu, Q., Ayirala, S.C., Kulkarni, M.M. and Sharma, A.P.: "Development and Optimization of Gas-Assisted Gravity Drainage (GAGD) Process for Improved Light Oil Recovery," Quarterly Technical Progress Report to DOE, Report #15323R03, October 2003.
44. Rosen, M.J. and Gao, T.: "Dynamic Surface Tension of Aqueous Surfactant Solutions 5. Mixtures of Different Charge Type Surfactants," *J. Colloid and Interface Sci*., **173** (1995) 42-48.
45. Rossini, F.D., *Selected Values of Physical and Thermodynamic Properties of Hydrocarbons and Related Compounds*, Carnegie Press, Pittsburgh (1953).
46. Schechter, D.S. and Guo, B.: "Parachors Based on Modern Physics and Their Uses in IFT Prediction of Reservoir Fluids," *SPE Reservoir Evaluation & Engineering*, **1** (1998) 207-217.
47. Sharma, G.D., Kamath, V.A., Khataniar, S. and Patil, S.L.: "Study of Hydrocarbon Miscible Solvent Slug Injection Process for Improved Recovery of Heavy oil from Schrader Bluff Pool, Milne Point Unit, Alaska," Final Report under Contract No. DE-FG22-93BC14864, USDOE (November 1995).
48. Sidgwick, N.V. and Spurrel, W.J.: "The System Benzene-Ethyl Alcohol-Water between +25^o and –5^o," *Journal of Chemical Society*, **117** (1920) 1397-1404.
49. Sigmund, P.M.: "Prediction of Molecular Diffusion at Reservoir Conditions. Part II – Estimating the Effects of Molecular Diffusion and Convective Mixing in Multicomponent Systems," *JCPT* (July-September 1976) 53-62.
50. Simon, R., Rosman, A. and Zana, E.: "Phase-Behavior Properties of CO_2-Reservoir Oil Systems," *SPEJ* (Feb. 1978) 20-26.
51. Sudgen, S.: "The Variation of Surface Tension with Temperature and Some Related Functions," *Journal of Chemical Society*, **125** (1924) 32-41.
52. Taylor, K.C. and Nasr-EI-Din, H.A.: "The Effect of Synthetic Surfactants on the Interfacial Behavior of Crude Oil/Alkali/Polymer Systems," *Colloids and Surfaces A: Physicochemical and Eng. Aspects*, **108** (1996) 49-72.
53. Van Oss, C.J., Chaudhury, M.K. and Good, R.J.: "Monopolar Surfaces," *Adv. Colloid Interface Sci*., **28** (1987) 35.
54. Weinaug, C.F. and Katz, D.L.: "Surface Tensions of Methane-Propane Mixtures," *Industrial Engineering Chemistry*, **35** (1943) 239-246.
55. Wilke, C.R.: "Diffusional Properties of Multicomponent Gases," *Chem. Eng. Progress*, **46** (1950) 95-104.
56. Wilke, C.R. and Chang, P.: "Correlation of Diffusion Coefficients in Dilute Solutions," *AIChE J*., **1** (1955) 264-270.
57. Wilke, C.R.: "Estimation of Liquid Diffusion Coefficients," *Chem. Eng. Progress*, **45** (1949) 218-224.

Table 2.1: Comparison of IFT Measurements with Parachor Model for RKR Fluids at 87 °C and 14.8 MPa

Enrichment (Mole% C_{2+}+CO_2)	IFT (mN/m)		Weighted Squared Deviation
	Experimental (Rao, 1997)	Parachor Model	
17.79	4.26	2.91	0.1000
21.64	3.89	2.59	0.1124
25.85	3.27	2.21	0.1043
30.57	2.69	1.81	0.1065
33.86	2.13	1.54	0.0762
37.70	1.52	1.24	0.0347
43.07	0.97	0.85	0.0166
48.39	0.53	0.50	0.0028
49.28	0.27	0.48	0.0061
		Objective Function (Δ) =	0.5595

Table 2.2: Comparison of IFT Measurements with Parachor Model for RKR Fluids at 87 °C and 14.0 MPa

Enrichment (Mole% C_{2+}+CO_2)	IFT (mN/m)		Weighted Squared Deviation
	Experimental (Rao, 1997)	Parachor Model	
32.68	2.86	1.88	0.1167
37.55	1.89	1.46	0.0518
41.45	1.51	1.14	0.0610
42.61	1.39	1.04	0.0620
47.48	0.70	0.68	0.0007
		Objective Function (Δ) =	0.2921

Table 2.3: Diffusivities between Oil and Gas at Various C_{2+} Enrichments for RKR Fluids (87 °C)

14.8 MPa				14.0 MPa			
(Mole% C_{2+}+ CO_2)	D_{os} (m^2/s)	D_{so} (m^2/s)	D_{os}/D_{so}	(Mole% C_{2+}+CO_2)	D_{os} (m^2/s)	D_{so} (m^2/s)	D_{os}/D_{so}
17.79	3.45E-08	9.69E-09	3.56	32.68	3.44E-08	8.67E-09	3.97
21.64	3.45E-08	9.40E-09	3.68	37.55	3.34E-08	8.39E-09	3.98
25.85	3.42E-08	9.11E-09	3.75	41.45	3.21E-08	8.18E-09	3.93
30.57	3.36E-08	8.81E-09	3.81	42.61	3.17E-08	8.12E-09	3.91
33.86	3.29E-08	8.62E-09	3.82	47.48	2.99E-08	7.89E-09	3.79
37.70	3.19E-08	8.41E-09	3.80				
43.07	3.03E-08	8.14E-09	3.73				
48.39	2.85E-08	7.89E-09	3.61				
49.28	2.83E-08	7.88E-09	3.59				
		Average =	3.70			Average =	3.92

Table 2.4: Comparison of IFT Measurements with Mechanistic Parachor Model for RKR Fluids at 87 ^{o}C and 14.8 MPa

Enrichment (Mole% C_{2+}+CO_2)	IFT (mN/m)		Weighted Squared Deviation
	Experimental (Rao, 1997)	Mechanistic Parachor Model	
17.79	4.26	3.79	0.0123
21.64	3.89	3.36	0.0184
25.85	3.27	2.88	0.0144
30.57	2.69	2.36	0.0155
33.86	2.13	2.00	0.0035
37.70	1.52	1.61	0.0034
43.07	0.97	1.10	0.0175
48.39	0.53	0.65	0.0535
49.28	0.27	0.63	0.0173
		Objective Function (Δ) =	0.1558

Table 2.5: Comparison of IFT Measurements with Mechanistic Parachor Model for RKR Fluids at 87 ^{o}C and 14.0 MPa

Enrichment (Mole% C_{2+}+CO_2)	IFT (mN/m)		Weighted Squared Deviation
	Experimental (Rao, 1997)	Mechanistic Parachor Model	
32.68	2.86	2.37	0.0290
37.55	1.89	1.84	0.0007
41.45	1.51	1.43	0.0026
42.61	1.39	1.32	0.0029
47.48	0.70	0.86	0.0518
		Objective Function (Δ) =	0.0871

Table 2.6: Comparison of IFT Measurements with Parachor Model for Terra Nova Fluids at 96 ^{o}C and 30.0 MPa

Enrichment (Mole% C_{2+}+CO_2)	IFT (mN/m)		Weighted Squared Deviation
	Experimental (Rao and Lee, 2002)	Parachor Model	
9.49	3.19	0.78	0.5694
11.79	3.09	0.66	0.6204
14.22	2.60	0.58	0.6052
18.57	2.02	0.41	0.6376
24.64	1.07	0.23	0.6147
27.77	0.73	0.15	0.6265
		Objective Function (Δ) =	3.6738

Table 2.7: Diffusivities between Oil and Gas at Various C_{2+} Enrichments for Terra Nova Fluids (96 ^oC and 30.0 MPa)

(Mole% C_{2+}+ CO_2)	D_{os} (m^2/s)	D_{so} (m^2/s)	D_{os}/D_{so}
9.49	2.39E-08	7.39E-09	3.23
11.79	2.34E-08	7.14E-09	3.28
14.22	2.32E-08	7.05E-09	3.29
18.57	2.24E-08	6.77E-09	3.31
24.64	2.12E-08	6.44E-09	3.29
27.77	2.04E-08	6.25E-09	3.27
		Average =	3.28

Table 2.8: Comparison of IFT Measurements with Mechanistic Parachor Model for Terra Nova Fluids at 96 ^oC and 30.0 MPa

Enrichment (Mole% C_{2+}+CO_2)	IFT (mN/m)		Weighted Squared Deviation
	Experimental (Rao and Lee, 2002)	Mechanistic Parachor Model	
9.49	3.19	3.59	0.0154
11.79	3.09	3.00	0.0008
14.22	2.60	2.64	0.0003
18.57	2.02	1.86	0.0060
24.64	1.07	1.06	0.0001
27.77	0.73	0.70	0.0020
		Objective Function (Δ) =	0.0245

Table 2.9: Parachor and Mechanistic Parachor Model IFT Predictions for Schrader Bluff Fluids (1300 psi and 82^{o}F)

(PBG + NGL) Solvents			(CO_2 + NGL) Solvents		
NGL (Mole%)	IFT (mN/m)			IFT (mN/m)	
	Parachor	Mechanistic Parachor	NGL (Mole%)	Parachor	Mechanistic Parachor
0	5.40	0.00124	0	0.197	0.0045
30	4.77	0.00109	10	0.078	0.0018
40	4.72	0.00108	15	0.044	0.0010
50	4.73	0.00108			

Table 2.10: Diffusivities between Oil and Solvent at Various NGL Enrichments in Solvent for Schrader Bluff Fluids (1300 psi and 82^oF)

(PBG + NGL) Solvents				(CO_2 + NGL) Solvents			
NGL (Mole%)	D_{os} (m^2/s)	D_{so} (m^2/s)	D_{os}/D_{so}	NGL (Mole%)	D_{os} (m^2/s)	D_{so} (m^2/s)	D_{os}/D_{so}
0	2.05E-08	9.38E-11	218.38	0	7.57E-09	1.05E-10	72.42
30	8.75E-09	8.25E-11	106.09	10	6.47E-09	8.97E-11	72.15
40	5.51E-09	6.37E-11	86.47	15	5.94E-09	8.41E-11	70.67
50	5.19E-09	7.15E-11	72.69				
		Average	120.91			Average	71.75

Table 2.11: Physical Properties of Crude Oils Used in further Application of the Mechanistic Parachor Model (Firoozabadi et al., 1988)

Crude Oil	Saturation Pressure (psi)	Temperature (^oF)	(C_1-C_3) Mole%	C_{7+} M.wt	C_{7+} Sp.gravity
A	2155	130	46.52	227.4	0.870
C	4589	180	64.64	217.0	0.838
D	2573	170	51.18	234.3	0.868

Table 2.12: Comparison of IFT Measurements with Parachor and Mechanistic Parachor Model Predictions for Crude Oil A

Pressure (psia)	Exp. IFT (mN/m)	Parachor Model		Mechanistic Model	
		IFT (mN/m)	Abs. Dev. (%)	IFT (mN/m)	Abs. Dev. (%)
2150	5.5	3.03	44.91	4.76	13.50
1650	6.7	4.61	31.19	7.24	8.02
1150	10.1	6.73	33.37	10.57	4.61
185	19.5	12.16	37.64	19.09	2.09
Average			36.78		7.06

Table 2.13: Comparison of IFT Measurements with Parachor and Mechanistic Parachor Model Predictions for Crude Oil C

Pressure (psia)	Exp. IFT (mN/m)	Parachor Model		Mechanistic Model	
		IFT (mN/m)	Abs. Dev. (%)	IFT (mN/m)	Abs. Dev. (%)
3815	1.3	0.54	58.62	1.25	3.98
3315	2.3	0.89	61.48	2.06	10.62
2815	3.3	1.42	56.97	3.29	0.16
2315	4.6	2.23	51.52	5.17	12.46
Average			57.15		6.81

Table 2.14: Comparison of IFT Measurements with Parachor and Mechanistic Parachor Model Predictions for Crude Oil D

Pressure (psia)	Exp. IFT (mN/m)	Parachor Model		Mechanistic Model	
		IFT (mN/m)	Abs. Dev. (%)	IFT (mN/m)	Abs. Dev. (%)
2010	6.0	2.73	54.50	5.26	12.33
1610	8.5	4.16	51.06	8.01	5.76
1110	10.3	6.08	40.97	11.70	13.63
Average			48.84		10.57

Table 2.15: Model Exponents for different Single Experimental IFT Measurement Points in the Mechanistic Parachor Model for RKR Reservoir at 14.8 MPa and 87^{o} C

Enrichment (C_{2+} %)	IFT (mN/m)			C.F (k)	D_{os}/D_{so}	n
	Experimental	Parachor	Mechanistic Parachor			
17.79	4.26	2.910	4.26	1.46	3.56	0.30
21.64	3.89	2.590	3.89	1.50	3.68	0.31
25.85	3.27	2.210	3.27	1.47	3.75	0.29
30.57	2.69	1.810	2.69	1.48	3.81	0.29
33.86	2.13	1.540	2.13	1.39	3.82	0.25
37.70	1.52	1.240	1.52	1.23	3.80	0.16
43.07	0.97	0.850	0.97	1.15	3.73	0.11
48.39	0.53	0.500	0.53	1.10	3.61	0.07

Table 2.16: Model Exponents for different Single Experimental IFT Measurement Points in the Mechanistic Parachor Model for Terra Nova Reservoir at 30.0 MPa and 96^{o} C

Enrichment (C_{2+} %)	IFT (mN/m)			C.F (k)	D_{os}/D_{so}	n
	Experimental	Parachor	Mechanistic Parachor			
9.49	3.19	0.783	3.19	4.08	3.23	1.20
11.79	3.09	0.656	3.09	4.71	3.28	1.30
14.22	2.60	0.577	2.60	4.51	3.29	1.27
18.57	2.02	0.407	2.02	4.97	3.31	1.34
24.64	1.07	0.231	1.07	4.63	3.29	1.29
27.77	0.73	0.152	0.73	4.80	3.27	1.33

Table 2.17: Effect of Pressure on Parachors of Crude Cuts (Firoozabadi et al., 1988)

Crude	Cut M.wt	Pressure (psia)	Surface Tension (mN/m)	Parachor
A	303.0	2013	13.9 ± 0.3	772
		1013	15.7 ± 0.6	777
		13	27.6	780
B	338.5	1013	16.2 ± 0.5	826
		513	19.2 ± 0.4	828
C	285.0	1013	19.1 ± 0.4	738
		513	20.4 ± 0.4	729
		13	30.2	750

Table 2.18: Summary of Similarities Observed Between the Exponent (n) in the Mechanistic Model and the Parachor Properties

S.No	Parachor	Exponent (n)
1	Compound specific	Specific for a crude oil (equilibrium liquid and vapor phases) or crude oil-solvent system
2	Independent of temperature	Appears to be temperature independent and still needs to be examined
3	Independent of pressure	Independent of pressure
4	Linearly related to solute concentration	Linearly related to solute composition present in either of the two fluid phases in equilibrium

Table 2.19: Measured Interfacial Tension Data of Benzene in Non-equilibrated Aqueous Ethanol at Various Ethanol Enrichments and Feed Compositions Using Pendent Drop Technique

Solvent (Mole%)		Feed Composition (Mole%)		Benzene IFT (mN/m)
Ethanol	Water	Solvent	Benzene	
0	100	100.0	0.0	32.58 ± 0.110
		97.8	2.2	32.59 ± 0.030
		88.0	12.0	32.62 ± 0.030
10	90	100.0	0.0	12.11 ± 0.110
		97.4	2.6	12.11 ± 0.060
		86.2	13.8	12.16 ± 0.045
20	80	100.0	0.0	4.85 ± 0.064
		97.0	3.0	4.84 ± 0.080
		84.4	15.6	5.00 ± 0.050
30	70	100.0	0.0	2.30 ± 0.035
		96.6	3.4	2.31 ± 0.040
		82.5	17.5	2.62 ± 0.030
40	60	100.0	0.0	1.23 ± 0.052
		96.2	3.8	1.41 ± 0.050
		80.7	19.3	1.99 ± 0.048

Table 2.20: Measured Interfacial Tension Data of Benzene in Pre-equilibrated Aqueous Ethanol at 30% and 40% Ethanol Enrichments and Various Feed Compositions Using Pendent Drop Technique

Solvent (Mole%)		Feed Composition (Mole%)		Benzene IFT
Ethanol	Water	Solvent	Benzene	(mN/m)
30	70	100.0	0.0	2.94 ± 0.048
		96.6	3.4	2.94 ± 0.055
		82.5	17.5	3.12 ± 0.023
40	60	100.0	0.0	0.09 ± 0.004
		96.2	3.8	0.09 ± 0.004
		80.7	19.3	0.09 ± 0.004

Table 2.21: Measured Interfacial Tension Data of Benzene in Pre-equilibrated Aqueous Ethanol at Ethanol Enrichments above 40% Using Capillary Rise Technique

Ethanol Enrichment (Mole%)	Phase Densities (gm/cc)		Contact Angle (degrees)	Capillary Rise (cm)	IFT (mN/m)
	Solvent	Oil			
50	0.8725	0.8597	25	0.53	0.3301
60	0.8641	0.8579	25	0.59	0.1780
70	0.8612	0.8594	25	0.68	0.0596
75	0.8579	0.8576	25	0.98	0.0143

Table 2.22: Measured Equilibrium Benzene Contact Angles at Various Ethanol Enrichments

Ethanol Enrichment (Mole%)	Equilibrium Time (hrs)	Benzene Contact Angle (^{o})
0	24	48
10	24	33
20	24	26
30	24	25
40	24	25

Table 2.23: Summary of Identified Model Fluid Systems with Known Phase Behavior Characteristics for VIT Experimentation

Reference	Oil Composition (Mole%)	Temperature (^{o} F)	Minimum Miscibility Pressure (psia)		
			Slim-tube	RBA	PXD
Elsharkawy et al. (1996)	100 % n-C_{10}	100	1250	1280	-
Elsharkawy et al. (1996) Mihcakan & Yarborough (1994)	43% n-C_5 + 57% n-C_{16}	122	1550	1550	1500
Metcalfe & Yarborough (1978)	25% n-C_1 + 30% n-C_4 + 45% n-C_{10}	160	1700	-	1700

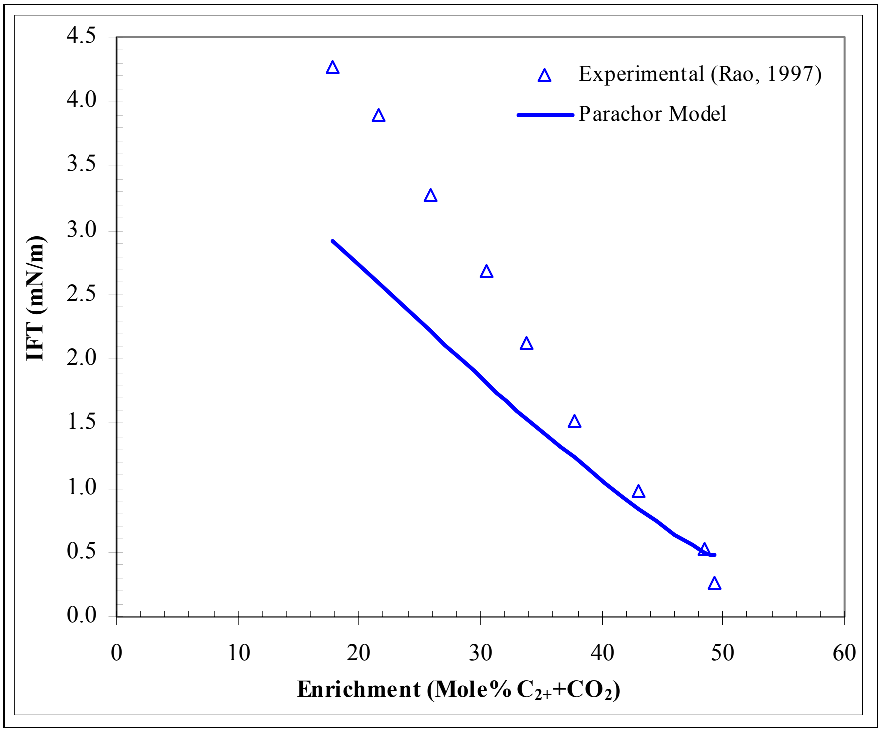

Figure 2.1: Comparison between IFT Measurements and Parachor Model for RKR Fluids at 87 ^oC and 14.8 MPa

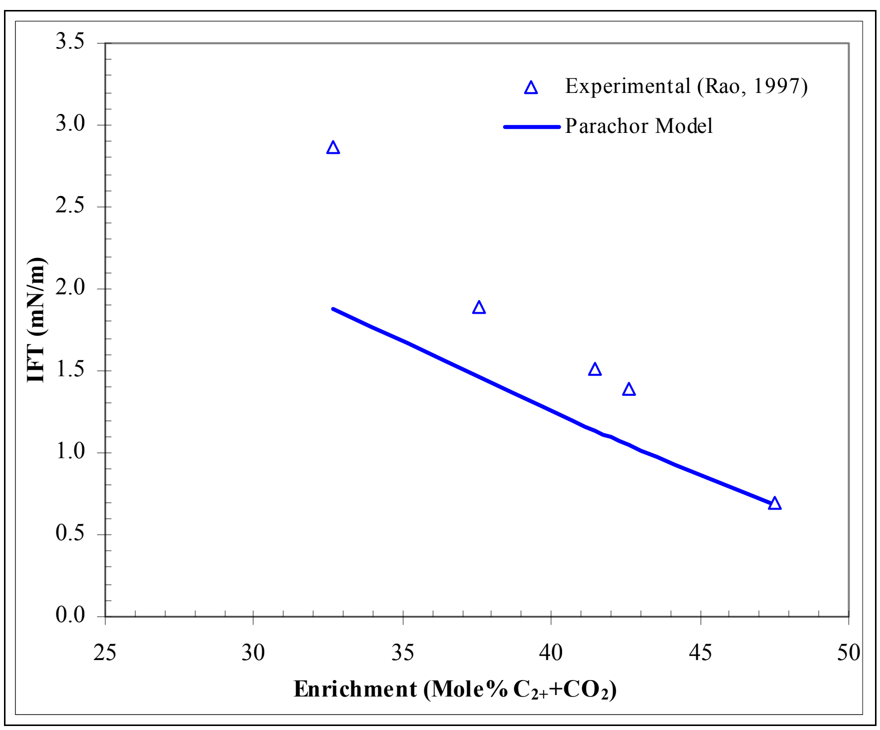

Figure 2.2: Comparison between IFT Measurements and Parachor Model for RKR Fluids at 87 ^oC and 14.0 MPa

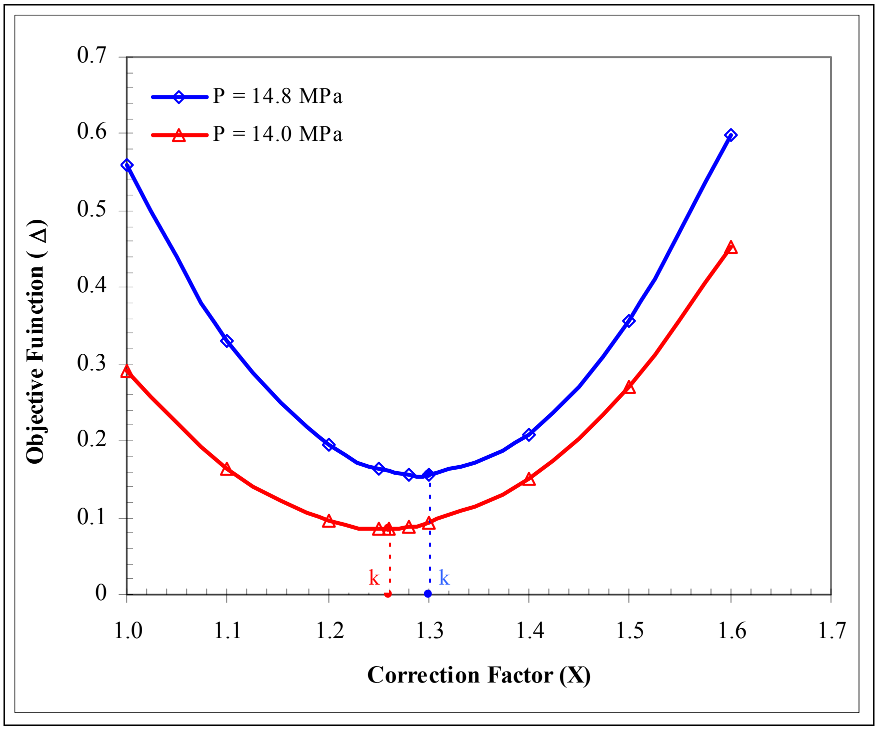

Figure 2.3: Determination of Mass Transfer Enhancement Parameters for RKR Fluids

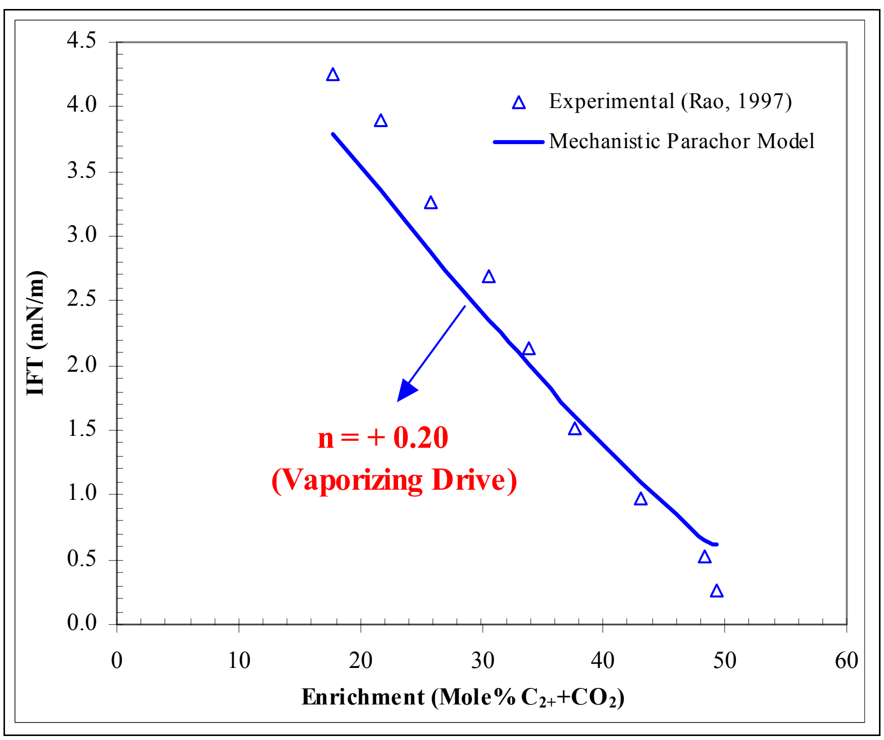

Figure 2.4: Comparison between IFT Measurements and Mechanistic Parachor Model for RKR Fluids at 87 °C and 14.8 MPa

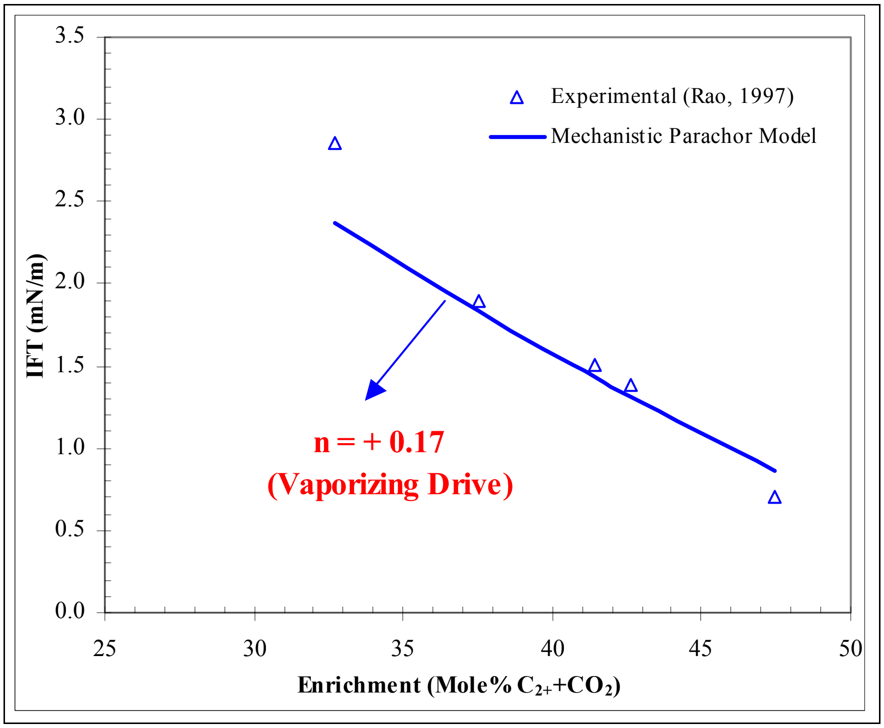

Figure 2.5: Comparison between IFT Measurements and Mechanistic Parachor Model for RKR Fluids at 87 ^{o}C and 14.0 MPa

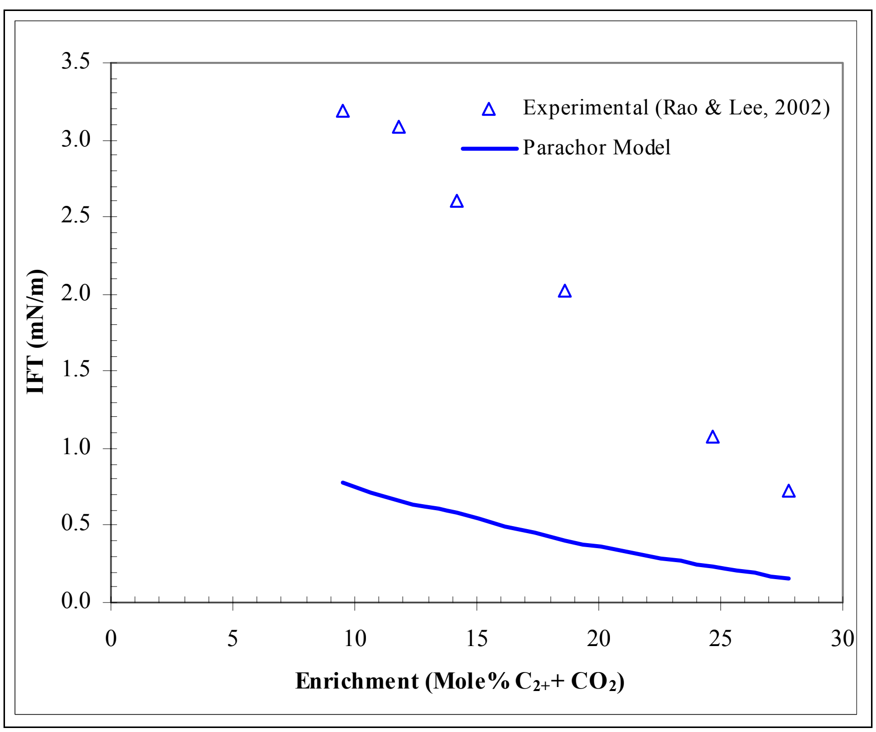

Figure 2.6: Comparison between IFT Measurements and Parachor Model for Terra Nova Fluids at 96 ^{o}C and 30.0 MPa

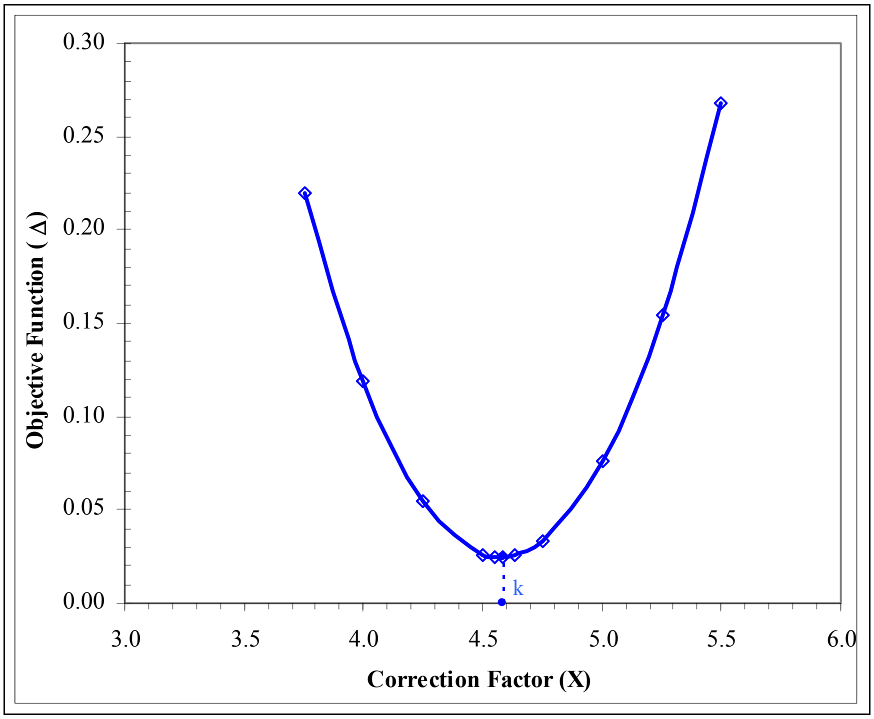

Figure 2.7: Determination of Mass Transfer Enhancement Parameter for Terra Nova Fluids

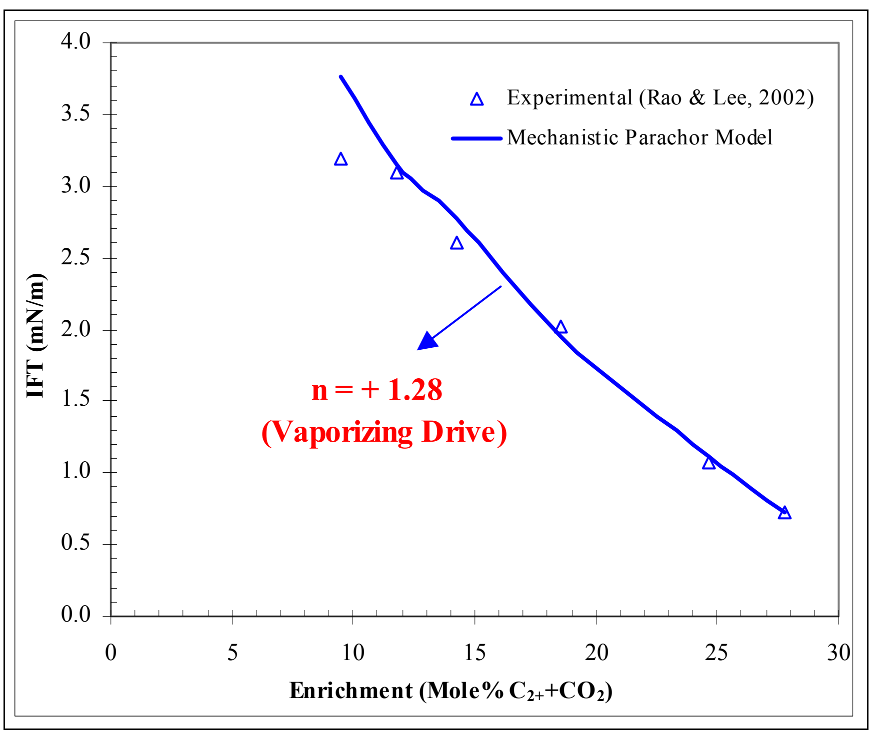

Figure 2.8: Comparison between IFT Measurements and Mechanistic Parachor Model for Terra Nova Fluids at 96 °C and 30.0 MPa

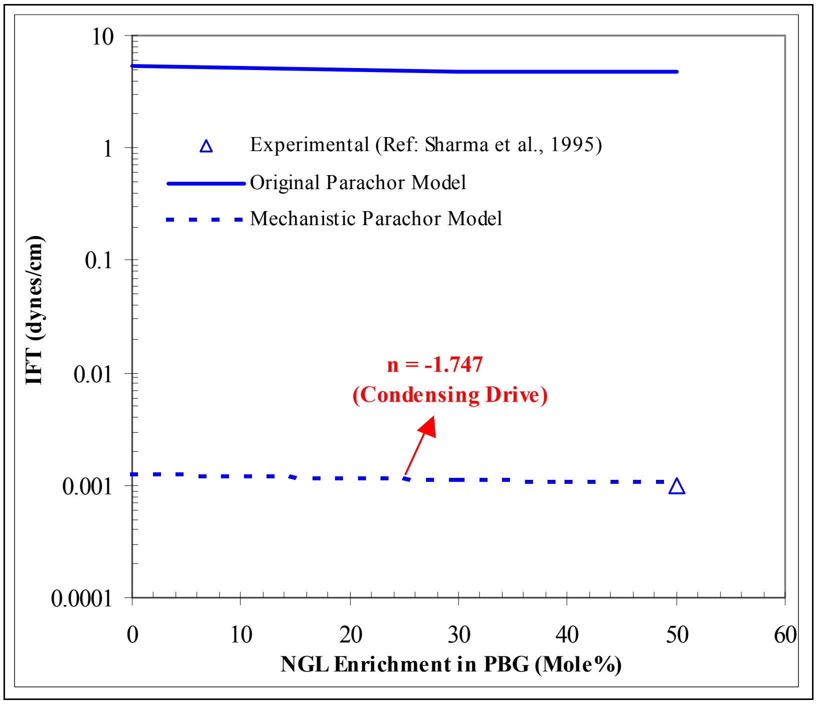

Figure 2.9: Comparison between IFT's of Experimental, Parachor and Mechanistic Parachor Models for Schrader Bluff Crude Oil with (PBG + NGL) Solvents at 1300 psi and 82^{o}F

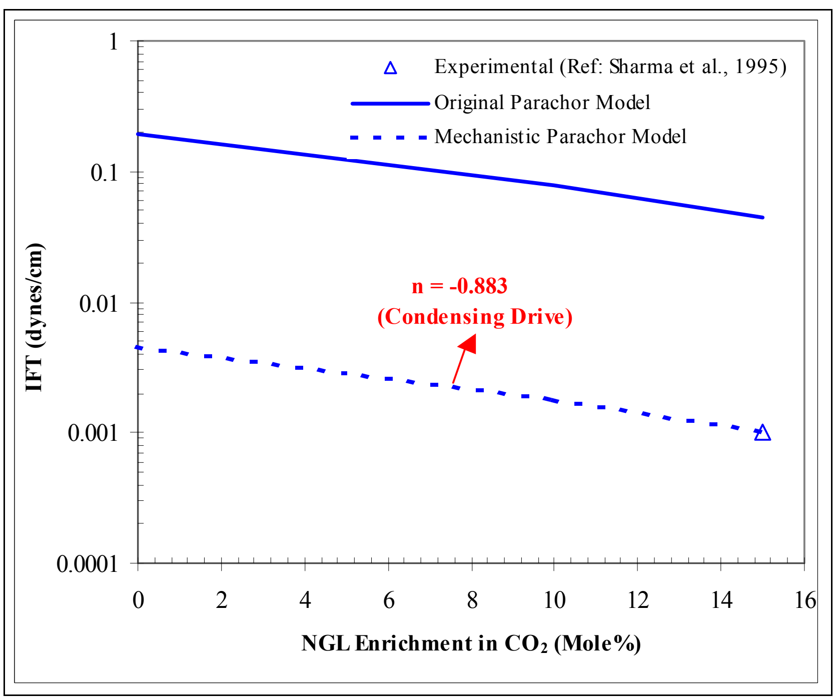

Figure 2.10: Comparison between IFT's of Experimental, Parachor and Mechanistic Parachor Models for Schrader Bluff Crude Oil with (CO_2 + NGL) Solvents at 1300 psi and 82^{o}F

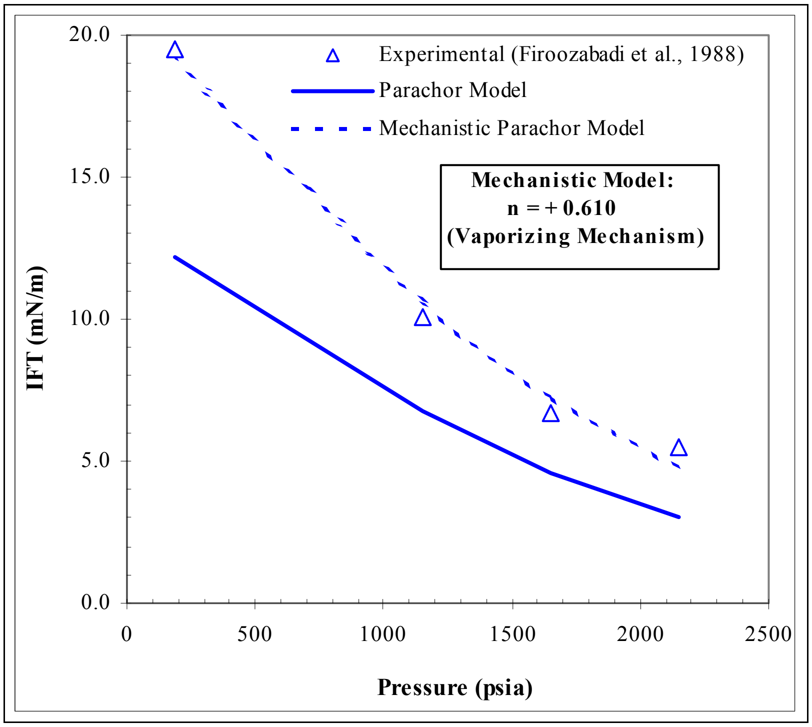

Figure 2.11: Comparison of IFT Measurements with Parachor and Mechanistic Parachor Model Predictions for Crude Oil A

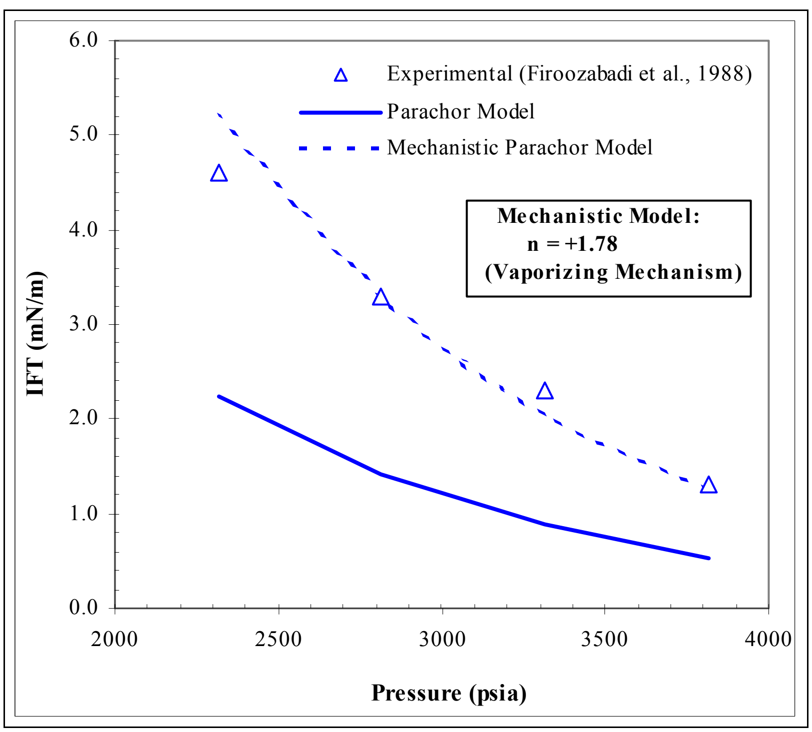

Figure 2.12: Comparison of IFT Measurements with Parachor and Mechanistic Parachor Model Predictions for Crude Oil C

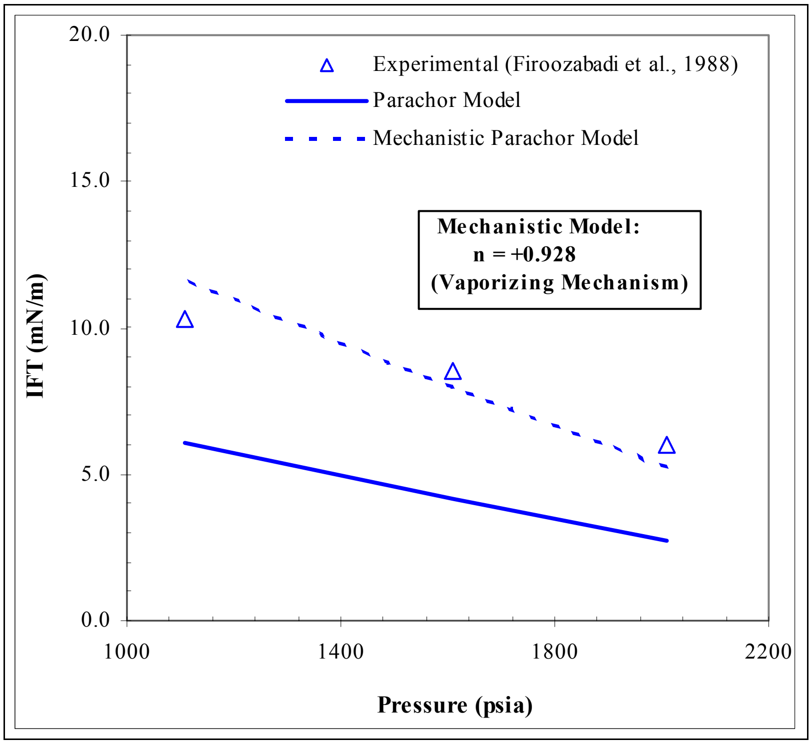

Figure 2.13: Comparison of IFT Measurements with Parachor and Mechanistic Parachor Model Predictions for Crude Oil D

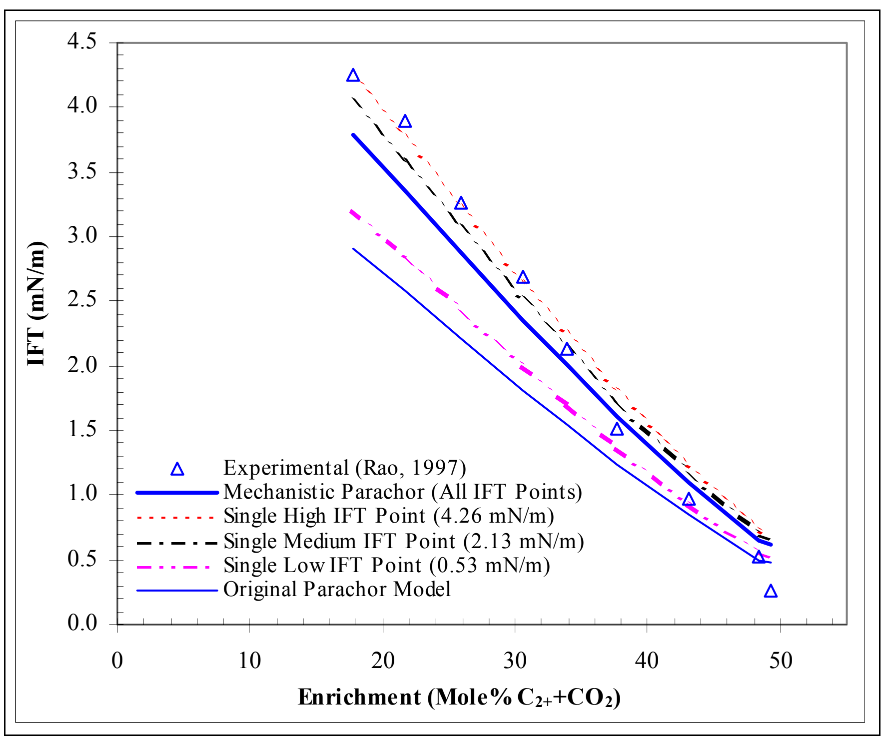

Figure 2.14: Sensitivity Studies for the Effect of Number of Experimental Data Points on Mechanistic Model Results for RKR Fluids at 14.8 MPa and 87° C

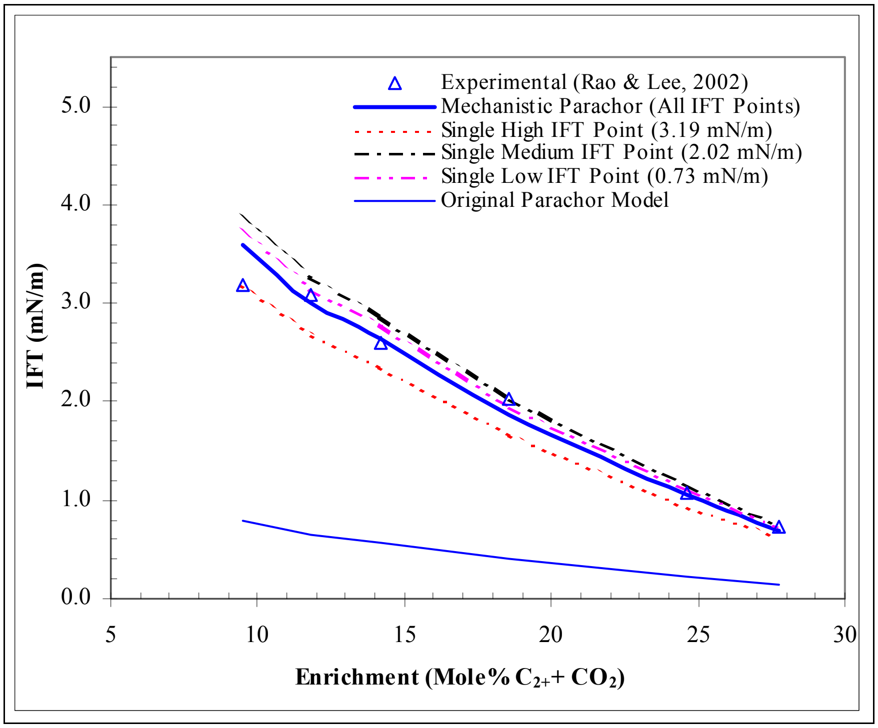

Figure 2.15: Sensitivity Studies for the Effect of Number of Experimental Data Points on Mechanistic Model Results for Terra Nova Fluids at 30.0 MPa and 96° C

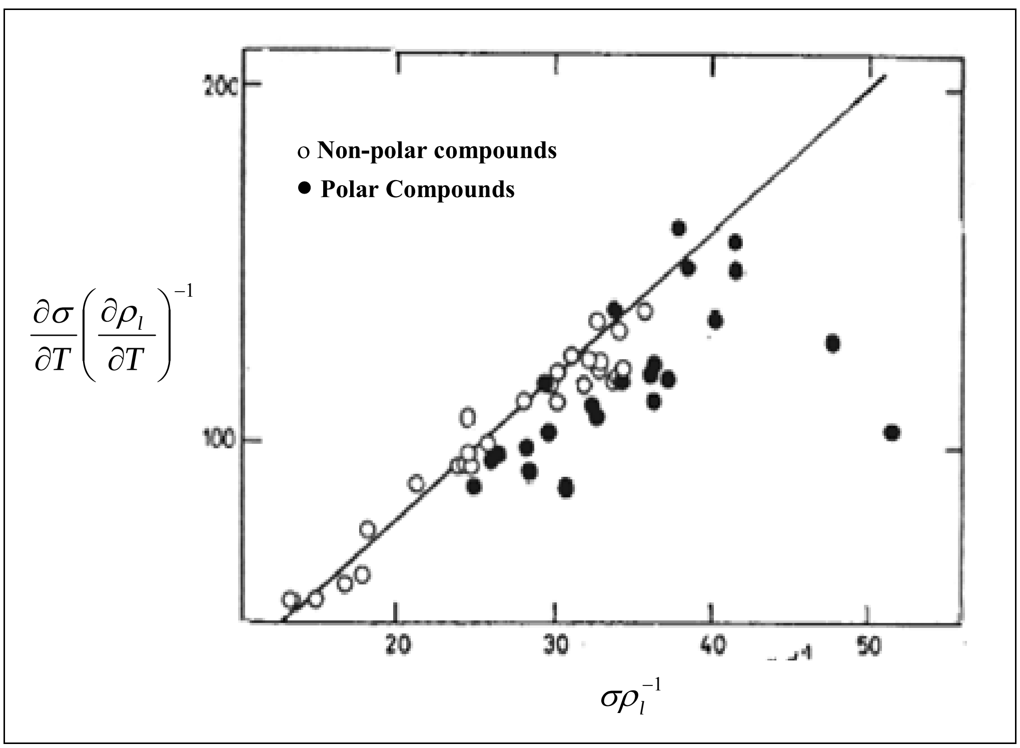

Figure 2.16: Effect of Temperature on Parachors (Exner, 1967)

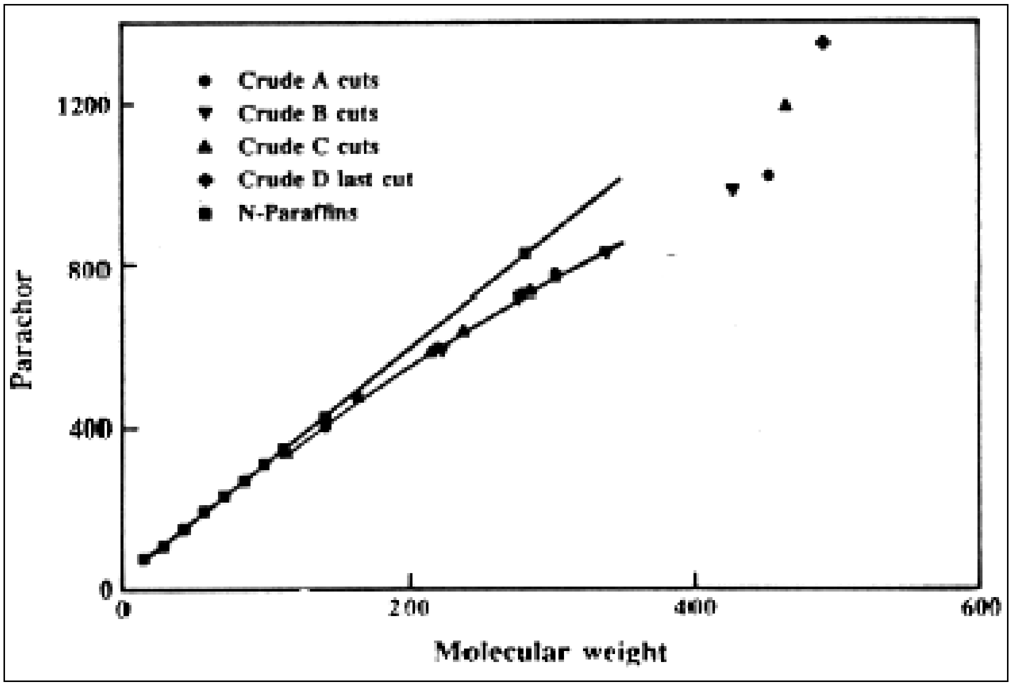

Figure 2.17: Parachors vs. Molecular Weight for Crude Cuts and n-Paraffins (Firoozabadi et al., 1988)

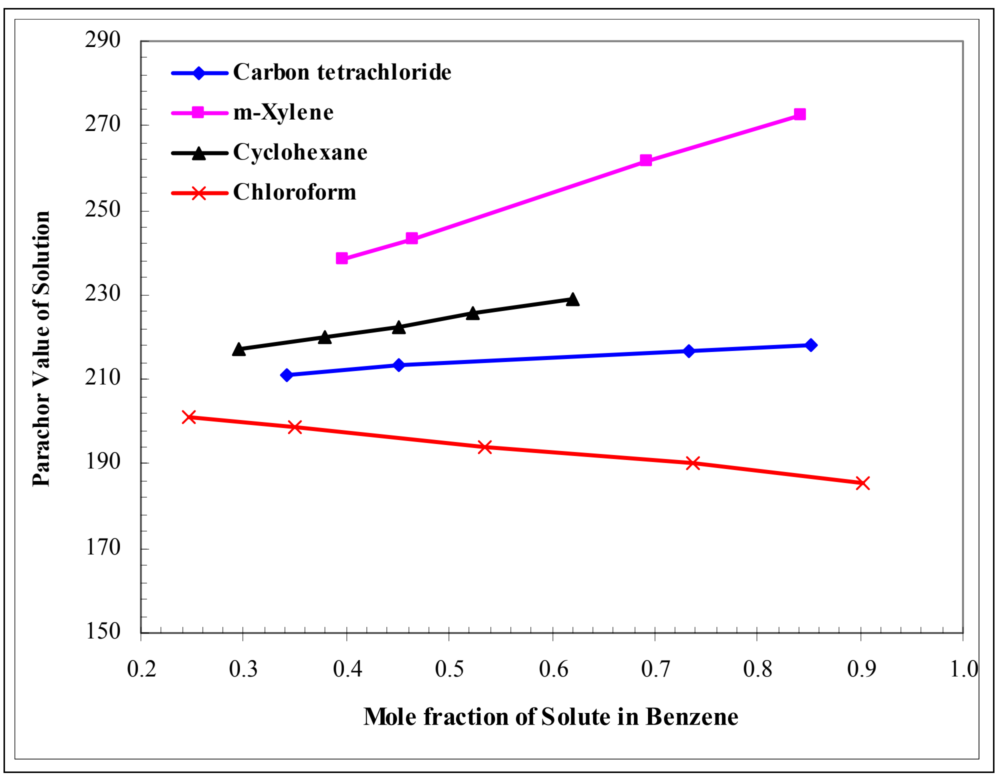

Figure 2.18: Effect of Solute Composition on Parachor Value of Solution (Hammick and Andrew, 1929)

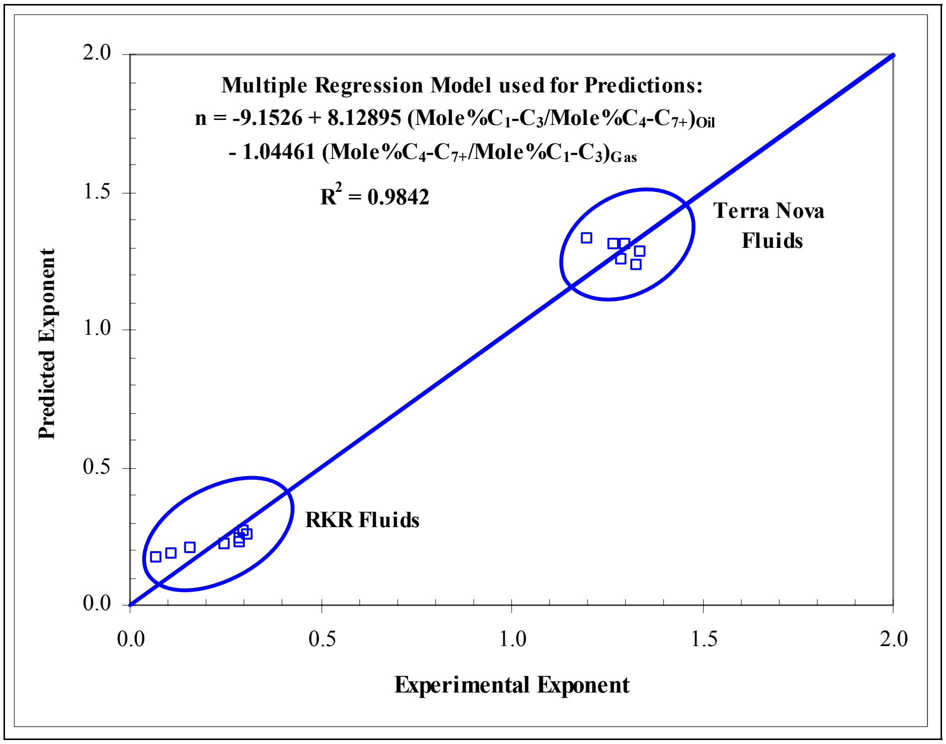

Figure 2.19: Multiple Linear Regression Model for the Mechanistic Model Exponent Prediction in Crude Oil-Solvent Systems

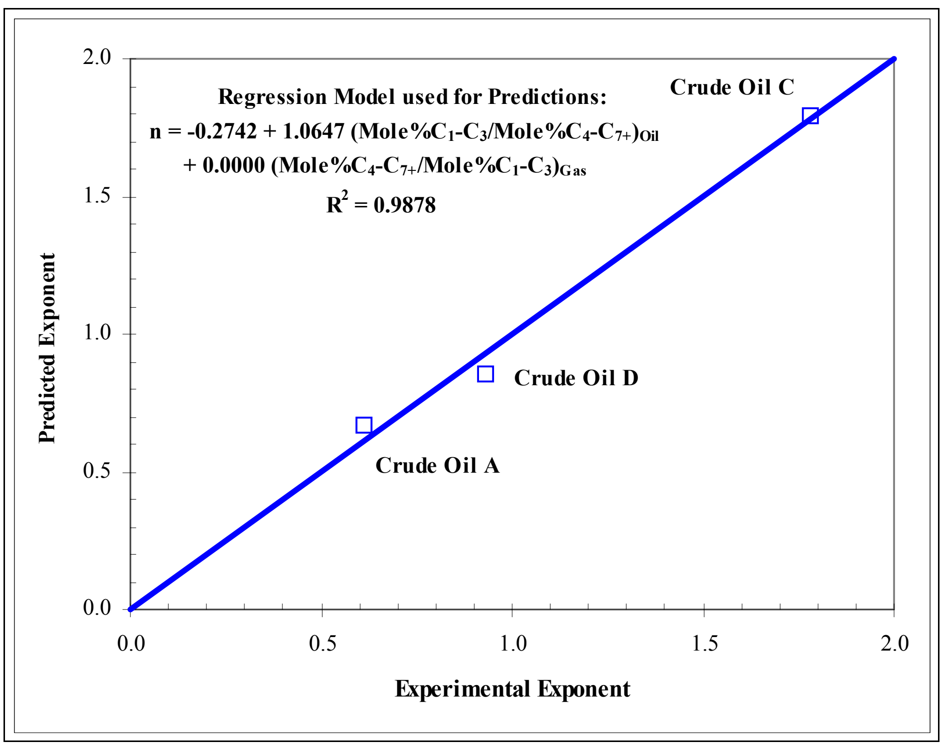

Figure 2.20: Simple Linear Regression Model for the Mechanistic Model Exponent Prediction in Crude Oil Systems

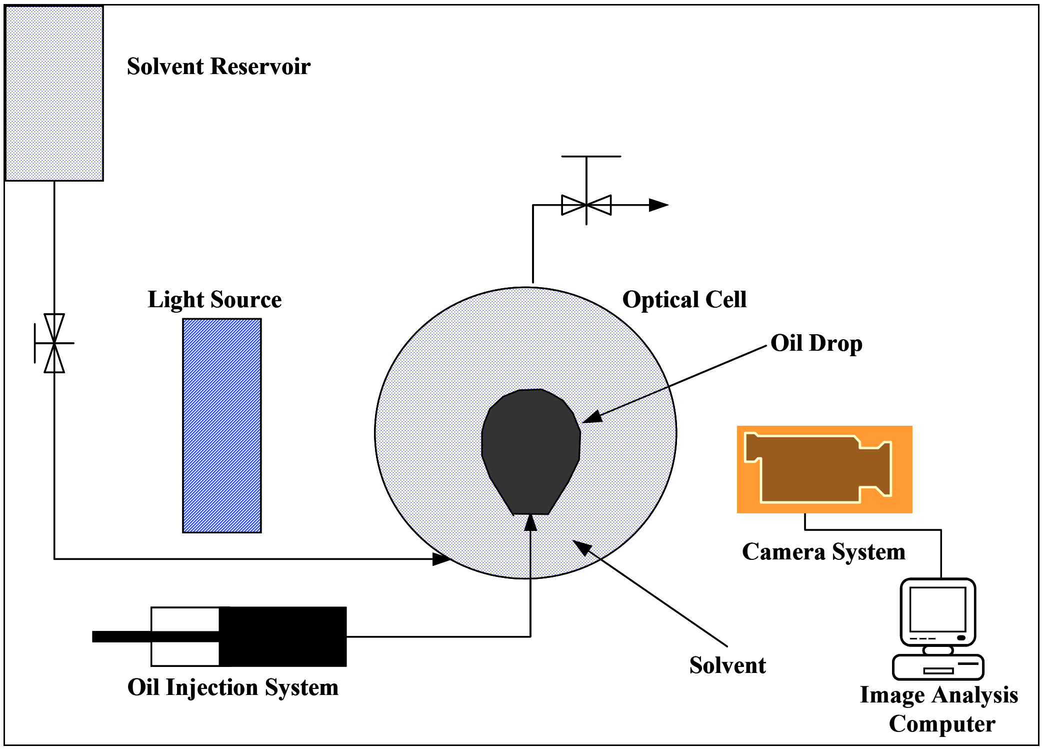

Figure 2.21: Schematic of the Experimental Setup used for IFT Measurements in Pendent Drop Technique

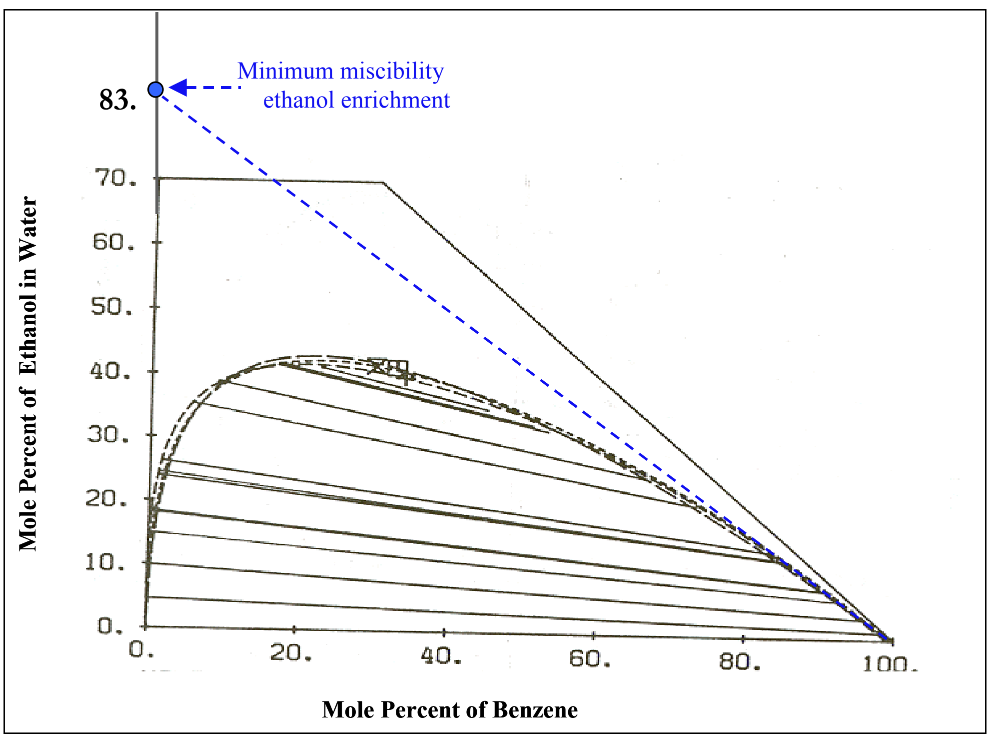

Figure 2.22: Phase Diagram of Benzene, Ethanol and Water Ternary System (Chang and Moulton, 1953)

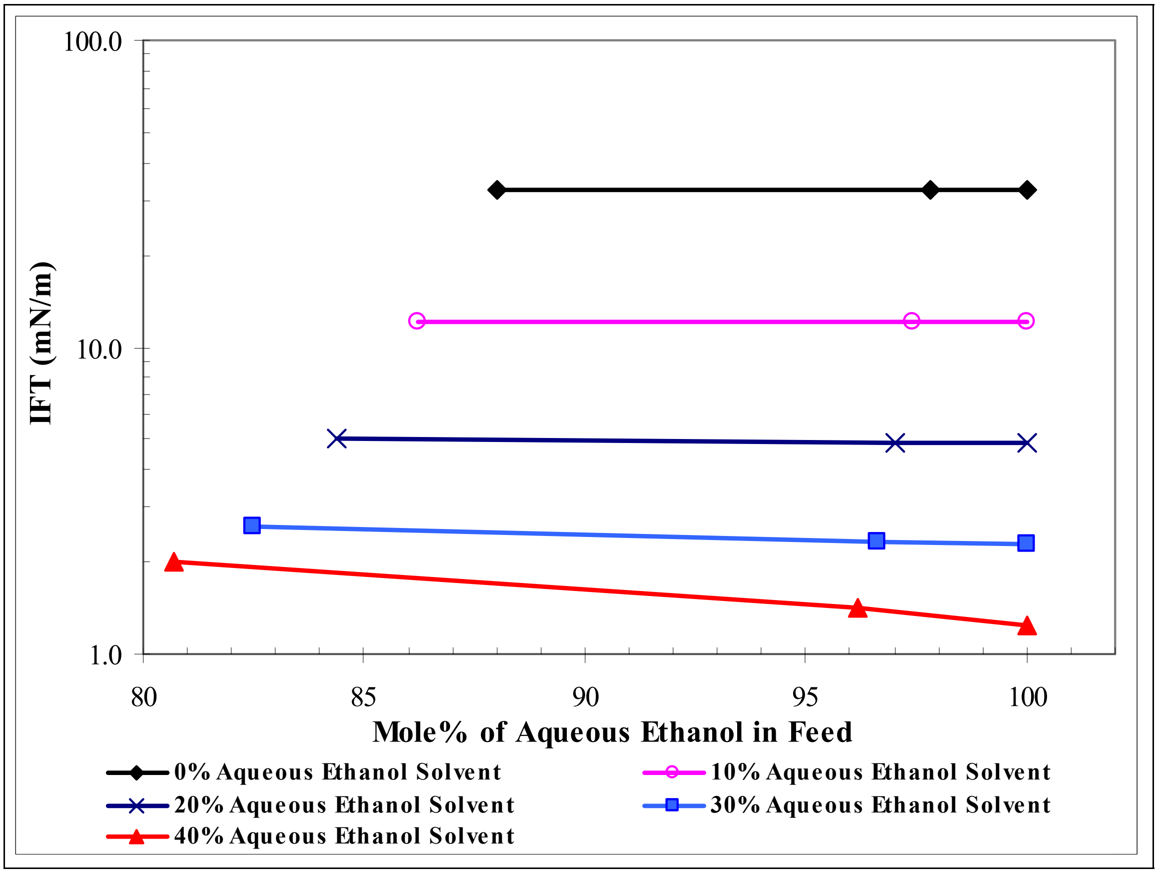

Figure 2.23: Effect of Solvent-oil Ratio on IFT in Feed Mixtures of Non-equilibrated Benzene and Aqueous Ethanol Solvents

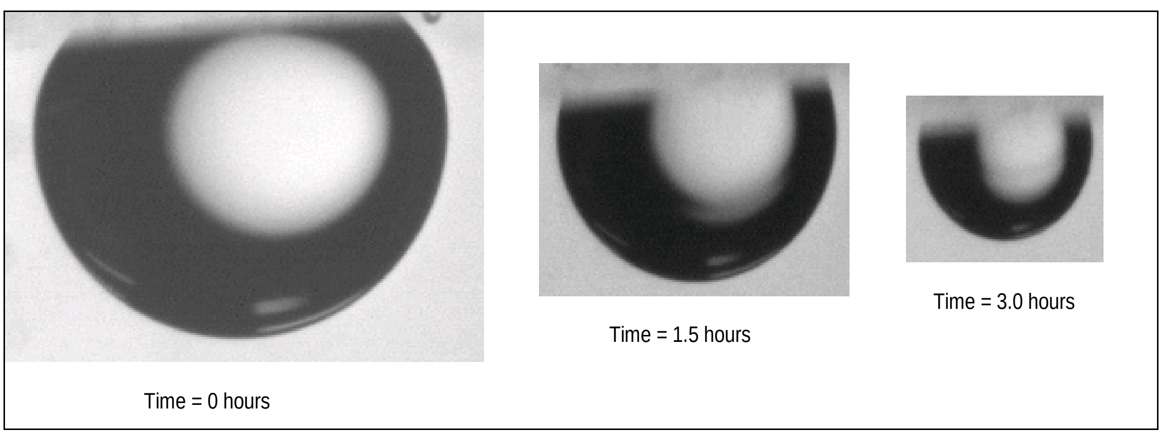

Figure 2.24: Photographs Showing the Effect of Benzene Dissolution on Benzene Drop Size with Time in Non-equilibrated Aqueous Ethanol Solvent at 30% Ethanol Enrichment

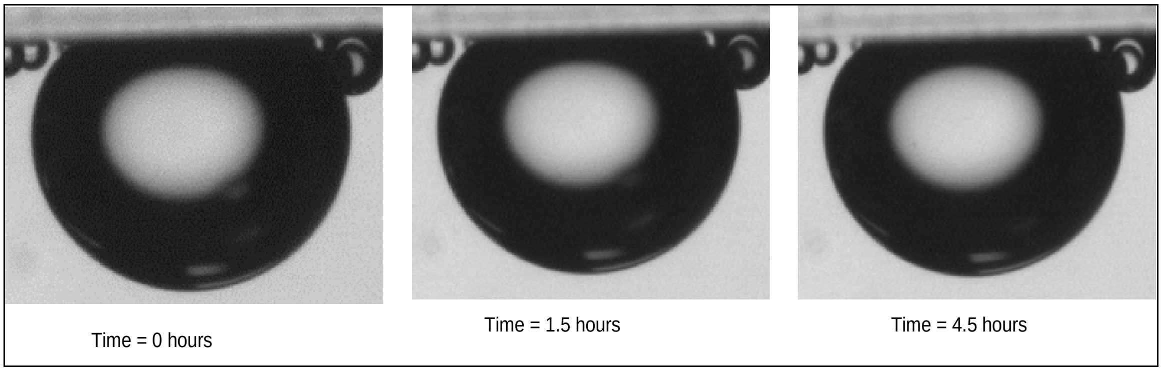

Figure 2.25: Photographs Showing the Absence of Benzene Dissolution on Benzene Drop Size with Time in Pre-equilibrated Aqueous Ethanol Solvent at 30% Ethanol Enrichment

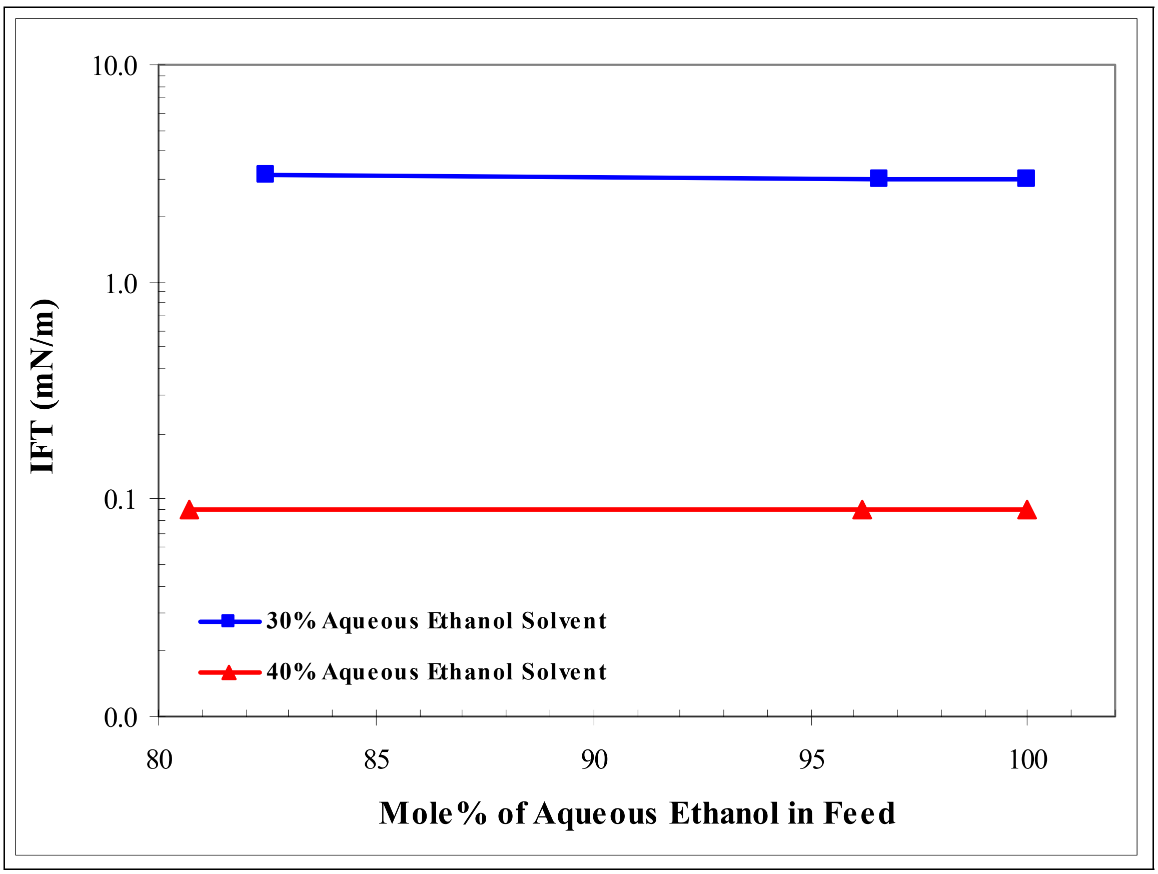

Figure 2.26: Effect of Feed Solvent-oil Ratio on IFT in Pre-equilibrated Aqueous Ethanol Solvents

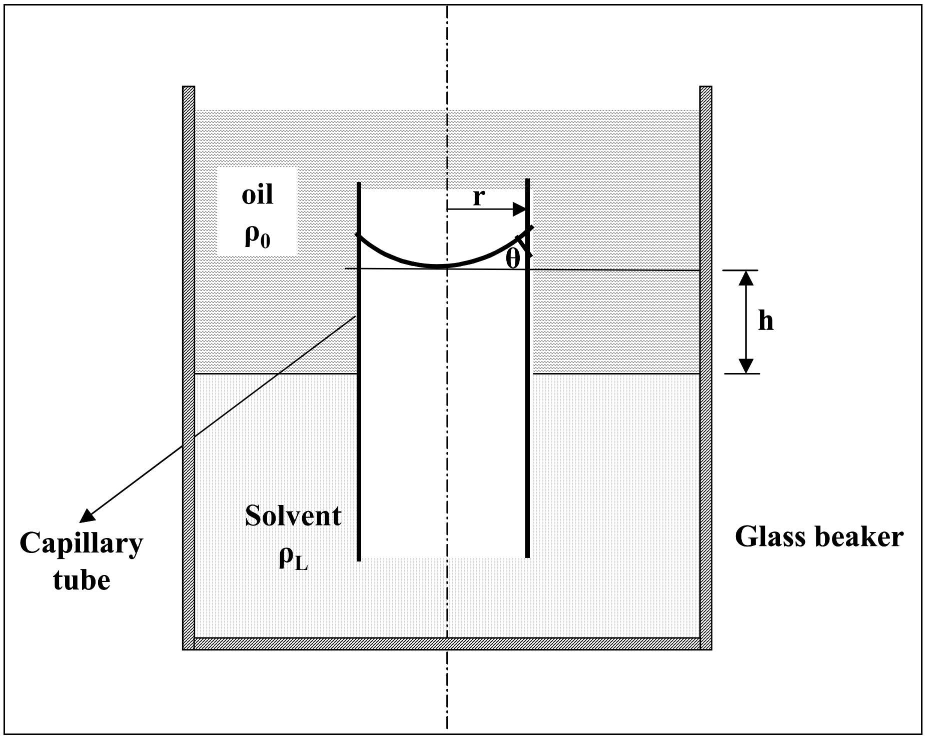

Figure 2.27: Schematic of Capillary Rise Technique

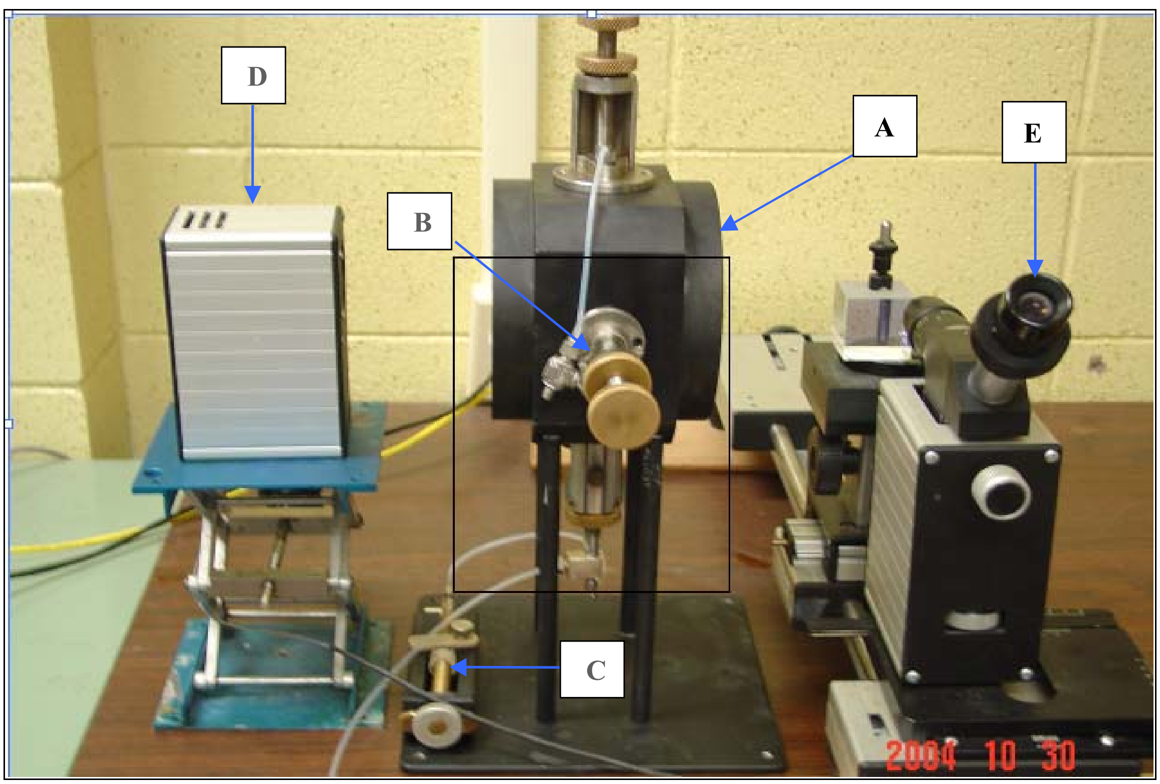

Figure 2.28: Photograph of the Equipment Used for Contact Angle Measurements (A: Optical cell; B: Crystal holder; C: Injection system, D: Light source; E: Goniometer)

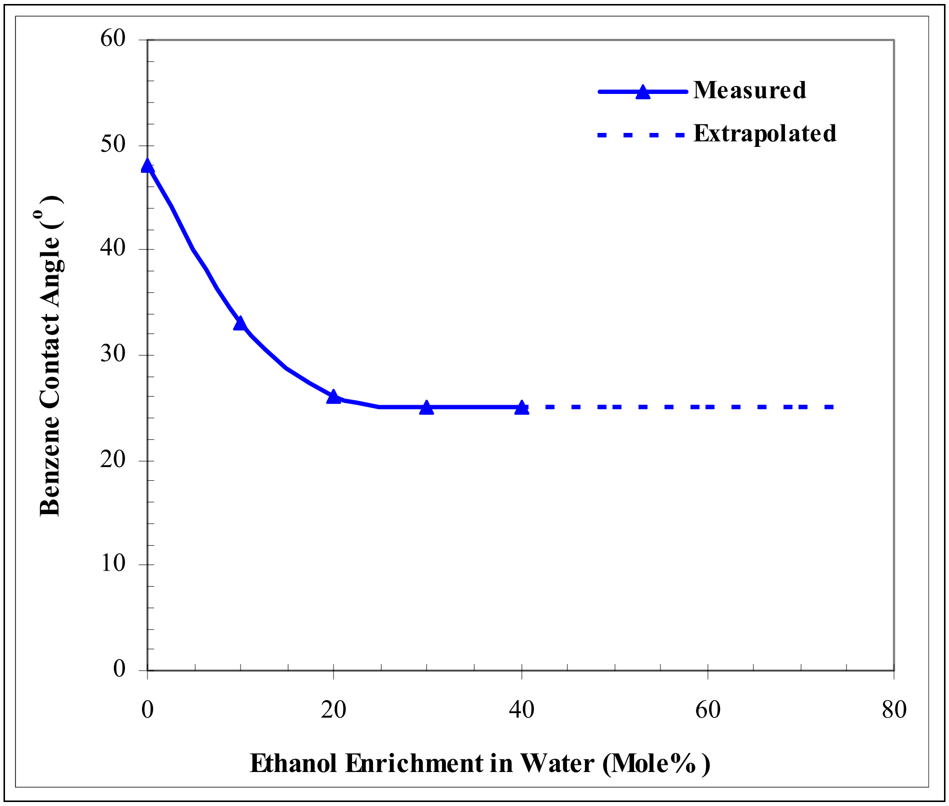

Figure 2.29: Equilibrium Contact Angles against Ethanol Enrichment in Aqueous Phase

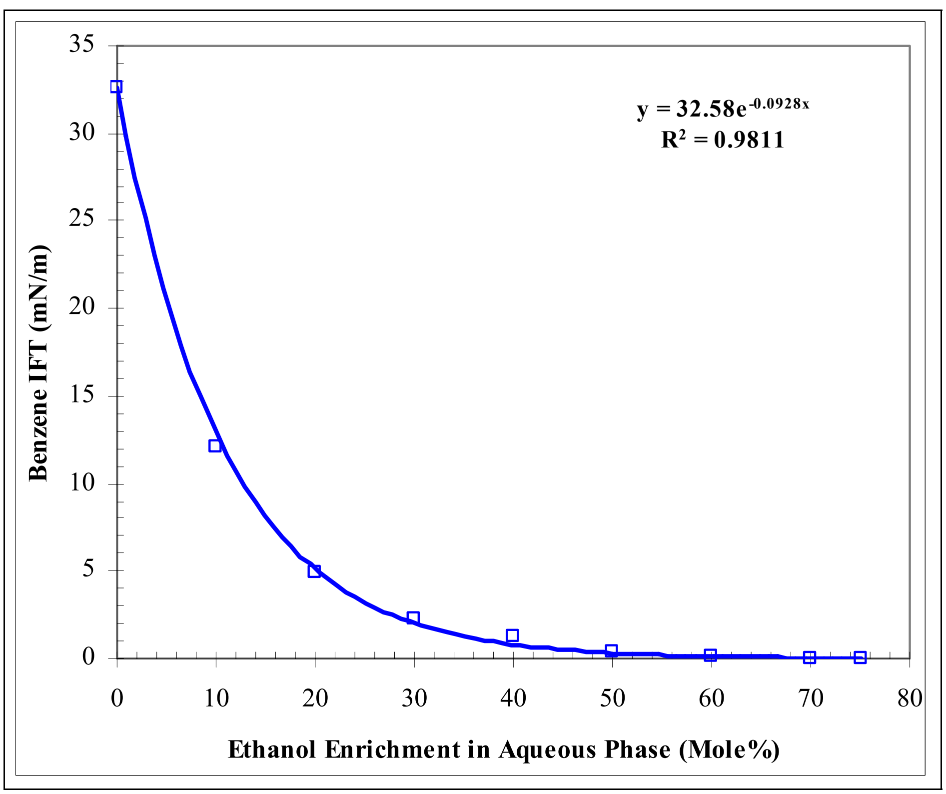

Figure 2.30: IFT of Benzene in Water at different Ethanol Enrichments

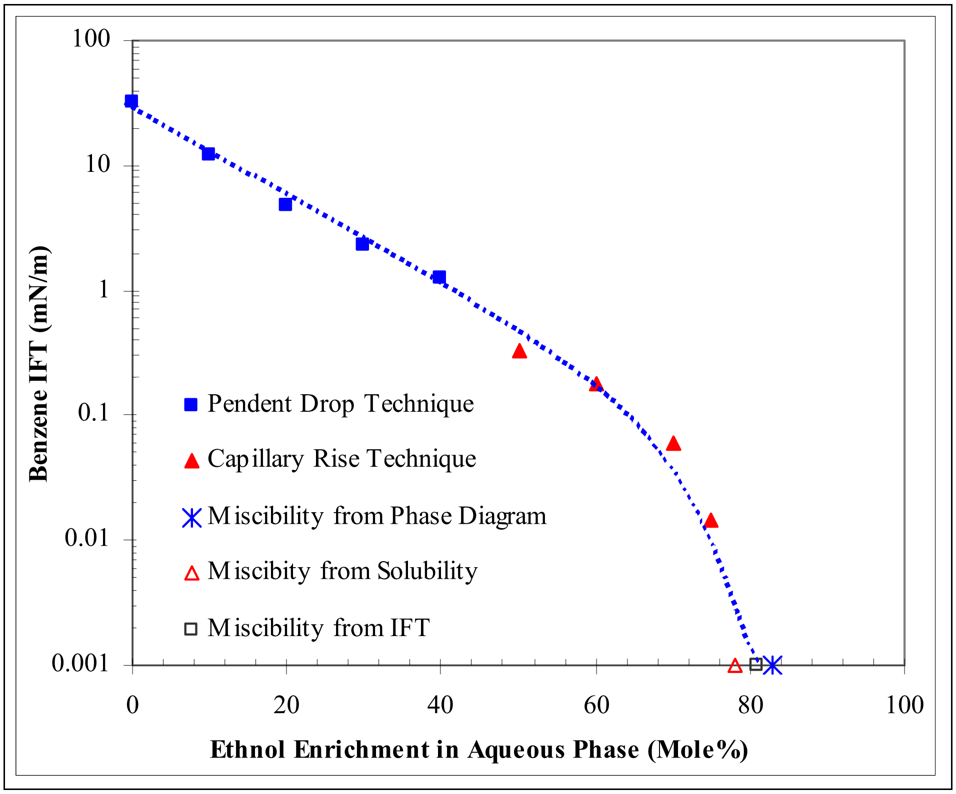

Figure 2.31: Semi-log Plot of IFT vs. Ethanol Enrichment for Miscibility Determination

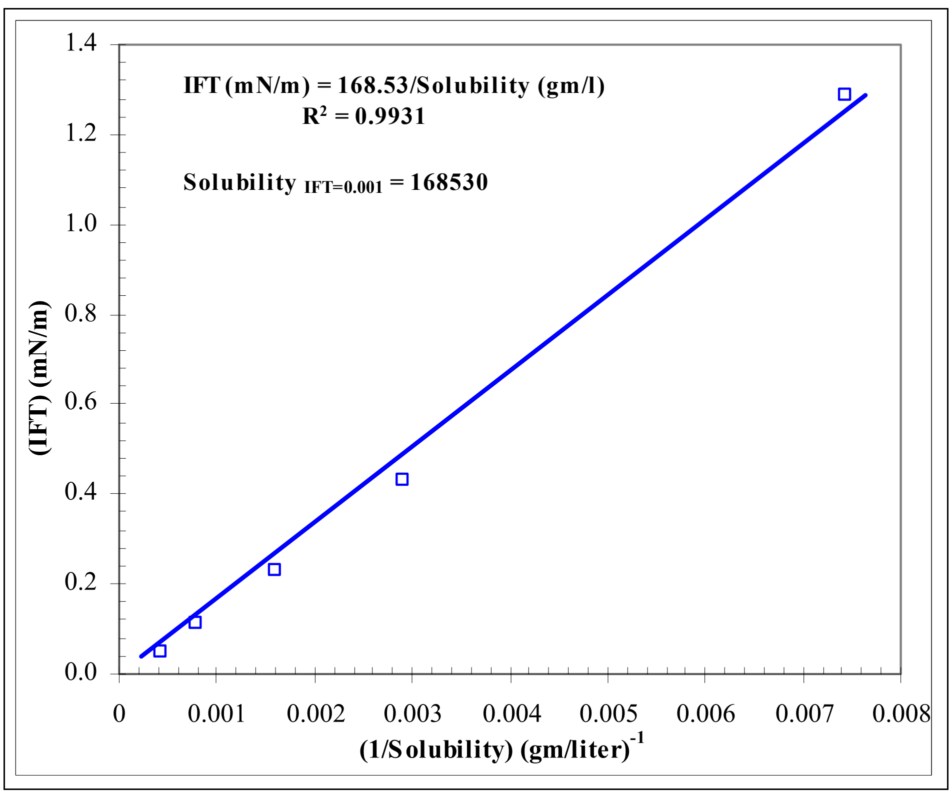

Figure 2.32: Relationship between IFT and Solubility

Figure 2.33: Frontal View of the Assembled Experimental Setup for IFT Measurements at Reservoir Conditions

III. Determination of Multiphase Displacement Characteristics In Reservoir Rocks

In the last reporting year (October 1, 2002 to September 30, 2003), experimental evaluation of the multiphase displacement characteristics in horizontal mode gas injection enhanced oil recovery processes was completed. This work concentrated on the most popular modes of horizontal gas injection, namely Continuous Gas Injection (CGI) and Water-Alternating-Gas (WAG) processes. The results of these experiments and their recommendations were utilized to further refine the experimental research protocol of the current reporting year. The major findings / recommendations from previous CGI and WAG coreflooding experiments were: (i) secondary CGI and WAG coreflood experimentation was essential, (ii) the optimal mode of horizontal injection was a combination of CGI and WAG modes of injection – the 'Hybrid-WAG' type floods, and (iii) the dimensional similarity approach was best suited for laboratory coreflood experimental design.

This report covers the work completed in the second year of the project (October 1, 2003 to September 30, 2004) and includes: (i) Detailed literature review on gravity drainage concepts and factors influencing gravity stable gas injection processes, (ii) Identification of various multiphase mechanisms and fluid dynamics operative in the GAGD process, (iii) detailed dimensional analysis of the gravity stable GAGD process, (iv) calculations of various dimensionless groups identified for the field projects studied, (v) 'scaling / correlation' of the laboratory experiments conducted to various gravity stable gas injection field projects studied, (vi) Updated experimental protocol based on the dimensional similarity approach, (vii) experimental work update(s), and (viii) future work.

3.1 Literature Review on EOR by Gas Injection

Gas Injection Enhanced Oil Recovery (EOR) has become the most popular process to recover large amounts of oil left behind in the reservoir by the primary and secondary processes. The world EOR production shows a steep rise in the last two years, with a significant increase of 0.25 MMm^3/d (1.6 MMBbl/d).

Gas injection processes, second largest EOR process next to steam processes used in heavy oil reservoirs, produced almost 42% of US-EOR oil in 2002 with the major share of the production from CO_2 injection. The EOR surveys of the Oil and Gas Journal show that the gas injection processes are versatile and were successful in almost all types of reservoirs containing very low to very high waterflood residual saturations.

3.1.1 Gas Injection EOR

The gas processes have high microscopic sweep efficiency under miscible conditions; however, the volumetric sweep of the flood has always been a cause of concern (Hinderaker et al., 1996). The mobility ratio, which controls the volumetric sweep, between the injected gas and displaced oil bank in gas processes, is typically highly unfavorable due to the relatively low viscosity of the injected phase. This difference results in severe gravity segregation of fluids in the reservoir.

Gas injection can be considered for four types of applications: WAG, Downdip Injection, Crestal (gas cap) injection, and Gas Recycle mode injection. WAG injection is practiced in normal horizontal reservoirs, where downdip injection is difficult; and the beneficial gravity effects are difficult to obtain. In WAG injection water is alternatively injected with gas to 'offset' or 'mitigate' the gravity segregation phenomenon and achieve a stable flood front (Christensen, 1998). The downdip injection is favored in sloping reservoirs targeting waterflood residual and attic oil (Jayasekera & Goodyear, 2002). Even in cases miscibility is cannot be achieved there may be benefits from three phase relative permeability effects. WAG type injection can also be practiced for downdip gas injection. Crestal injection is generally useful in saturated reservoirs with gas cap, and gravity stable displacements using miscible or immiscible gas help to increase reservoir sweeps. Crestal type gas injection has been employed on some continental shelves (such as U.K. Offshore), but this has usually been driven by the need for gas storage or to manage the position of oil rims under gas caps (Jayasekera & Goodyear, 2002). Also gas recycle mode process has been proved useful for improved liquid recovery from rich gas condensate reservoirs (Jayasekera & Goodyear, 2002).

Of the above applications of gas injection, the WAG injection is most popular. The WAG process attempts to combine the good microscopic displacement arising from gas injection with improved macroscopic efficiency by injection water to reduce mobility ratio. Hence for improved mobility and flood profile control, water and gas (CO_2 / HC) are alternately injected into the reservoir. The Water-alternating-gas (WAG) process, first proposed by Caudle and Dyes in 1958, is commonly employed to improve the gas injection process performance in the field and today is applied to nearly 83% (49 out of 59 field reviews reported (Christensen, 1998)) of the miscible gas injection field projects. The application of WAG process has yielded better EOR performance than continuous gas injection (CGI) field projects (Kulkarni, 2003).

The best WAG effect is obtained when gravity effects are insignificant, i.e. in reservoirs that are thin or have low permeability (Jayasekera & Goodyear, 2002). However, this expectation may not always be correct, resulting in lower than expected WAG efficiencies. Nevertheless, the attempt to resolve one problem of adverse mobility, the WAG process gives rise to other problems associated with increased water saturation in the reservoir including diminished gas injectivity and increased competition to the flow of oil. This results in severe injectivity problems and difficulties in establishing gas-oil contact and miscibility in the reservoir. The disappointing field performance of WAG floods with oil recoveries in the range of 5 - 10% (Christensen et al., 1998) is a clear indication of these limitations.

Although less popular as an EOR method, the gravity stable crestal or downward displacement type injection, either through gas cap expansion or by gas injection at the crest of the reservoir is an attractive method of oil recovery. The drainage of oil under gravity forces is an efficient method as it can reduce the remaining oil saturation to below that obtained after secondary recovery techniques. The detailed WAG literature review has been reported previously (Kulkarni, 2003). This report focuses on gravity stable gas floods only.

3.1.2 Gas Gravity Drainage

Gravity drainage is a recovery process in which gravity acts as the main driving force and where gas replaces the voidage volume (Hagoort, 1980). Gravity drainage can occur in primary phase of oil production through gas cap expansion as well as in the latter stages wherein gas is injected from an external source. Muskat (1949) provided a detailed review on the effects of gravity forces in controlling oil and gas segregation during the primary-production phase of gas drive reservoirs. It was suggested that the most efficient type of gravity-drainage production would be an idealized case wherein no free gas is allowed to evolve in the oil zone by maintaining the reservoir pressure above its bubble point, or by pressure maintenance at current GOR levels (Muskat, 1949).

The original description (Hagoort, 1980) of gravity-drainage suggests it to be a displacement process wherein gas displaces oil, and that the classical theories of Darcy and Buckley-Leverett are relevant. Inspite, the material balance equation, applicable to most displacements, does not in itself provide any information regarding the gravity drainage phenomenon (Muskat, 1949). The material balance method refers only to the thermodynamic equilibrium between the net liquid / gas phases in the reservoir and hence cannot characterize the mechanistic and fluid-dynamic aspects of the gravity drainage process.

Muskat (1949) presented the equations for down-dip free fall oil velocity (Equation 3.1) and drainage per unit projected GOC surface area (Equation 3.2).

$$V_S = \frac{k_o \, \Delta\gamma \, g \, Sin\theta}{\mu_o} \quad \text{…(3.1)}$$

Where V_S is the down-dip free fall oil velocity, k_o is oil permeability, μ_o is oil viscosity, θ is the dip angle, and $\Delta\gamma$ is the density difference between the oil and gas. It is important to note that if the gas phase is immobile (especially under primary production conditions), there is no buoyancy reaction on the oil due to gas, and the term $\Delta\gamma$ needs to be replaced by the oil density (γ).

$$Q = \frac{k_o\, \Delta\gamma\; g\; Sin^2\theta}{\mu_o\; \beta_o} = 21.29 \frac{k_o\, \Delta\gamma\; g\; Sin^2\theta}{\mu_o\; \beta_o} . \frac{bbl / D}{acre} \qquad (3.2)$$

Where k_o is expressed as millidarcy oil and $\Delta\gamma$ as specific gravity. The direct driving force ($\Delta\gamma$) for gravity drainage is determined (Muskat, 1949) by crude density and reservoir pressure. This driving force decreases with increasing API gravity (since the oil – gas gravities approach each other), but increases with decreasing pressure (due to increased segregation). In addition to the density difference, the mobility ratio (k_o/μ_o) directly influences the voidage replacement rate, under fixed production rates, and that unless the mobility ratio is inherently very small, it may be possible to utilize the beneficial effects of gravity drainage attributable to the high natural segregation tendencies of the fluids.

Analytical analysis of gravity drainage (Hagoort, 1980), show that the fractional flow of oil under gravity drainage is a function of the gravity number, capillary number and oil relative permeability (Corey exponent). Furthermore, in the absence of capillary forces (i.e. miscible displacement) the fractional flow of oil is only a function of the displaceable oil saturation and the displacement is purely piston-like (Buckley-Leverett type).

Centrifuge gravity drainage experiments (Hagoort, 1980) also substantiate that gravity drainage is an effective oil-recovery process in water-wet, connate water bearing reservoirs. However, duplication of these laboratory recovery factors to the field is a function of (Hagoort, 1980, Muskat, 1949): (i) the magnitude of the gravitational forces relative to the viscous forces, (ii) the shape of the oil relative permeability (Corey exponents) and (iii) the reservoir characteristics.

3.1.3 Displacement Instabilities for Gravity Stable Gas Flow through Porous Media

Unfavorable mobility contrast is the main reason for the development of instability 'fingers' during gas displacements in porous media. Macroscopic / microscopic heterogeneities result in unequal displacement rates between the displaced and displacing fluids, magnifying the 'fingering' phenomenon. Fingers result in poor aerial sweep efficiencies and early breakthrough thus decreasing recovery considerably.

'Buckley-Leverett' type displacements are normally difficult to attain mainly due to capillary pressure (immiscible displacements), dispersion effects and poor mobility ratio (M > 1) between the displacing and displaced fluids. The instability development is a function of many parameters such as rock and fluid properties, saturation distributions in the porous medium, viscous forces and rock fluid interaction parameters such as wettability, surface tension, development of miscibility etc.

For miscible fluids, Hill (1952) derived a critical velocity expression to predict the rates above which viscous instabilities can occur due to lower gravity forces compared to viscous forces. This equation (Equation 3.3) assumed a single interface contact between the injected and displaced phase with no mixing of solvent and oil behind the front.

$$V_C = \frac{2.741.\Delta\rho.k.Sin\theta}{\phi.\Delta\mu} \quad \text{……………………………………………...…….……...…(3.3)}$$

Where:

V_C = Critical rate (ft/d)

$\Delta\rho$ = Density difference (gm/cc)

k = Permeability (D)

θ = Dip angle (degrees – measured from horizontal)

ϕ = Porosity (fraction)

$\Delta\mu$ = Viscosity difference (cP)

Dietz (1953) proposed a method of analysis of stability of a system with the following assumptions: homogeneous porous medium, vertical equilibrium of oil and water, piston displacement of oil by water, no oil-water capillary pressures, and that the compressibility effects of rock and fluid may be neglected. The Dietz equation is given by Equation 3.4 below.

$$\tan\beta = \frac{1-M_e}{M_e.N_{ge}Cos\alpha} + \tan\alpha \quad \text{…with } \beta > 0 \text{ being the stability criterion………....…...(3.4)}$$

Where,

M = Mobility Ratio

α = Dip angle (degrees – measured from horizontal)

N_{ge} = Gravitational force

Dumore (1964) derived a stability equation, avoiding the limitation of the Hill equation that solvent and oil do not mix. The Dumore equation is given by Equation 3.5. The Dumore stability criterion is more stringent than the Hill criterion, and for all rates lower than V_{st}; each infinitesimal layer of the mixing zone is stable with respect to each successive layer.

$$V_{st} = \frac{2.741.k.Sin\theta}{\phi}\left(\frac{\partial\rho}{\partial\mu}\right)_{\min} \quad \text{…………………………….……………...………………...(3.5)}$$

Where
V_{st} = Critical velocity for stable flow (ft/D)
k = Permeability (Darcy)
θ = Dip angle (degrees – measured from horizontal)
ϕ = porosity (fraction)
$\Delta\rho$ = Density difference (lbm/ft^3)
$\Delta\mu$ = Viscosity difference (cP)

Brigham (1974) observed that the estimate of stability of a coreflood front could be obtained by measuring mixing zone length. The mixing zone length could then be used to calculate the effective mixing coefficient (α_e) an important reservoir simulation parameter. Perkins (1963) and Brigham (1974) solved the diffusion-convection equation and concluded that by measuring the mixing zone between 10% and 90% injected fluid concentrations at the core exit; the effective mixing coefficient (α_e) can be easily determined. Brigham (1974) suggest that in absence of viscous mixing, the effective mixing coefficient (α_e) is a function of the porous medium only and typical values for Berea are 0.001524 m (0.005 ft) in laboratory scale systems.

Rutherford (Used by PRI-ARC) developed a stability criterion for miscible vertically oriented corefloods in laboratory. The equation is given as Equation 3.6 below.

$$(q/A)_{CRITICAL} = 0.0439\frac{k*(\rho_O - \rho_S)}{\mu_O - \mu_S}Sin(\alpha) \quad \ldots\ldots\ldots\ldots\ldots\ldots(3.6)$$

Where,
(q/A) = Critical velocity for stable flow (ft/D)
k = Permeability (Darcy)
($\Delta\rho$) = Density difference (lbm/ft^3)
($\Delta\mu$) = Viscosity difference (cP)
α = Dip angle (degrees – measured from horizontal)

Moissis et al. (1987) used numerical simulation techniques to study effects of several parameters on miscible viscous fingering. The important variables considered were the effects of local permeability, overall heterogeneity and mobility ratio. It was found that the local permeability distribution near the entrance of the porous medium plays an important role in finger formation, where as the downstream permeability variations do not significantly affect fingering. The number and growth rates of viscous fingers strongly depend on mobility ratio. The favorable mobility ratios do not generate significant fingers and displacement is uniform in homogeneous porous medium.

Ekrann (1992) generalized the Dietz's correlation to establish a stability criterion in stratified reservoirs. Virnovsky et al. (1996) used analytical and numerical techniques to study the stability oil-gas-water displacements in two spatial dimensions. It was concluded that stable oil-gas-water displacement fronts, if at all occur, they do so only for a limited number of injection gas-water ratios. The authors argue that this stability analysis is applicable to more practical applications like WAG, and suggest the optimization of the WAG ratio based on this stability analysis.

Coning is another serious production problem in gas injection projects. Coning and displacement stabilities are considered different production issues (Supraniowicz & Butler, 1989). However, coning problems are attributed to the mobility contrasts in displacements, and can occur in both water-drive and gas-drive type displacements. The stability criterion applicable, discussed in the previous section, to viscous instabilities is not necessarily applicable to coning problems and critical velocity constraints to mitigate coning are generally stricter. With the use of horizontal wells in gravity drainage applications becoming popular, most of the analysis available in this field deals with the production from horizontal wells with vertical injectors.

3.1.4 Critical Rates for Gravity Drainage

Slobod and Howlett (1964) derived a critical rate equation for frontal stability in homogeneous sand packs and is given by Equation 3.7.

$$q_{oc} = \frac{k_o}{\Delta\mu_o}(\Delta\rho g) \qquad (3.7)$$

Barkve and Firoozabadi (1992) derived the initial (also maximum) gravity drainage rate (q_o) for an immiscible process in a homogeneous rock matrix, given by Equation 3.8.

$$q_o = \frac{k_o}{\mu_o}(\Delta\rho g - P_c^{(TH)} / L) \qquad (3.8)$$

Where:

k_o = Single phase oil permeability

μ_o = Oil viscosity

$\Delta\rho$ = Density difference between injected / displaced fluids

g = gravitational acceleration

$P_c^{(TH)}$ = Threshold capillary pressure

L = Height

The assumptions in the derivation included infinite gas mobility during displacement. The authors also comment that in the initial phase, the gravity drainage rate in fractured media does not exceed the un-fractured media, provided the fractures have negligible storage. In developed flow conditions, the capillary pressure contrast between the matrix and fracture, results in lower gravity drainage rates in case of fractured media.

For miscible displacements (capillary pressure = 0), the initial (also maximum) gravity drainage rate (q_o) in a homogeneous rock matrix is given by Equation 3.9.

$$q_o = \frac{k_o}{\mu_o}(\Delta\rho g) \quad \text{...(3.9)}$$

Comparison of the two equations (3.7 & 3.9) shows that the maximum drainage rate (q_o) is less than critical rate (q_{oc}) when the displacing fluid has a negligible viscosity (e.g. gas displacement).

Supranowicz and Butler (1989) examined the vertically confined waterflood to horizontal wells assuming equal water / oil densities. The authors define a critical production rate equation beyond which fingering would occur. This critical rate is different than for coning / cresting and authors considered it 'a serious limitation' in horizontal wells. It is suggested that this analysis be used to constitute production rate guidelines in the horizontal producers to prevent fingering and coning problems.

Meszaros et al. (1990) examine the potential use of inert gas injection using horizontal wells using scaled model studies and numerical simulation. Johnson scaling criterion was used for the physical models. The authors suggest that for high recovery factors the stability of the displacing front is important, and that a slant / horizontal front propagation results in severe reduction in recoveries.

Butler (1992) presents the theoretical analysis for production from heavy oil reservoirs via gravity drainage with a gas cap advancing downward a horizontal well. It was assumed that the reservoir pressure is maintained by crestal gas injection and production rate is controlled to just below the critical rate for gas coning. It was assumed that there is vertical fluid flow in the vicinity of the horizontal well. The potential gradient extending along vertical plane extending through the horizontal well located at the base of the reservoir.

The straight line corresponds to simple radial flow from an unbound reservoir and is given by –

$$\Phi = \frac{2q\mu}{\pi kL}\ln(y) \quad \text{.........One Side...(3.10)}$$

Where

q = Oil production rate to vertical well from one side of horizontal well

k = permeability

L = Length of horizontal well

μ = Viscosity
y = Height of interface
Φ = Potential

Whereas the curved line depicts the reservoir confined by two vertical boundaries as derived by Maxwell as well as Muskat. The potential equation is given by –

$$\Phi = \frac{2q\mu}{\pi kL}\ln\left[\cosh(\frac{\pi y}{W}) - \cos(\frac{\pi x}{W})\right] \text{……………………………..……......…...………..(3.11)}$$

$$\Phi_{(x=0)} = \frac{2q\mu}{\pi kL}\ln\left[\cosh(\frac{\pi y}{W}) - 1\right] \text{………One Side………………………………...…..……(3.12)}$$

Where
q = Oil production rate to vertical well from one side of horizontal well
k = permeability
L = Length of horizontal well
μ = Viscosity
y = Height of interface
Φ = Potential
W = Horizontal distance from horizontal well

Thus, in the near well-bore region (of a horizontal producer), the two equations result in the same potential gradient, while far above the well, the potential gradient becomes constant and results in linear flow between parallel boundaries. It was also assumed that for critical flow, the potential gradient in the liquid interface above the well, at height h_W, can be calculated using the above equation, and it must equal ($\Delta\rho.g$) for critical flow.

Butler (1992) notes that for very small well spacing, the critical flow is determined by the tendency for interfacial instability in a simple flat interface moving downward (drained horizontal fracture). On the other hand, for large well spacing, the critical production rate is dictated by the need for horizontal displacement of oils as against the vertical limitation for very small well spacing, which is intuitive. The authors explain that for most practical cases, the ‘conventional’ well spacing is larger than the maximum limit set by this theory, and considerable improvements in well productivity can be achieved by decreasing the well spacing.

3.1.5 Laboratory Studies for Gravity Drainage

Green and Willhite (1998) suggest that the same density difference that causes problems like poor sweep efficiencies and gravity override in these types of processes can be used as an advantage in dipping reservoirs. The beneficial results of flooding in gravity stable mode have been demonstrated by many laboratory and field studies.

Gravity-assisted displacements offer the advantages of eliminating gravity tongues and stabilizing viscous fingers. Tiffin and Kremesec (1986) conducted a series of gravity-assisted vertical core displacements of both first contact miscible and multiple contact miscible type, with CO_2 – recombined crude oil systems at various pressures and temperatures. Significant improvements of the vertical flood performance over similar horizontal core displacements were observed. In an attempt to elucidate the mechanisms of the process, the authors that while miscibility development in vertical core displacements was at similar pressures as their horizontal counterparts, miscibility was achieved in the vertical downward displacement at a considerably shorter core length. The paper also demonstrates that component mass transfer, similar to those in multiple contact miscible processes, strongly affect flood front stability and that displacement efficiency increases at lower fluid cross flow and mixing conditions.

Kantzas et al. (1988) analyzed the mechanisms in gravity drainage processes by measuring capillary pressure curves for capillaries of regular pore geometry. The analysis was done for immiscible fluid and water-wet rock systems, and a pore co-existence criterion for three immiscible phases was defined to determine water and oil saturation distributions at pore level.

Chatzis et al. (1988) carried out downward displacements of oil by injection of inert gas at initial and waterflood residual oil saturations. Very high recovery efficiencies under strongly water-wet systems in consolidated or unconsolidated porous media were observed. Further experimentation with CT scans and regular capillary tubes for immiscible gravity stable inert gas displacements conclude that very high recoveries under these conditions are only possible when oil spreads over water, the reservoir is strongly water wet and a continuous film of oil over the water in the corners of the pores invaded by gas exists. The spontaneous spreading of oil at the water gas interface is limited in the case of water wet rock samples and positive spreading coefficients.

CO_2 cyclic 'huff and puff' injection in Berea cores using live oil samples for gravity stable (vertical) displacements and dead oil samples with horizontal cores were studied by Thomas et al. (1990). It was found that gas cap, gravity segregation as well as higher residual oil saturations help to increase the overall oil recovery in gravity-stable floods. Moreover, it was observed that gravity segregation (beneficial in gravity-stable floods) helps deeper penetration of CO_2 (hence better recovery), and accidental injection of CO_2 in gas cap do not have detrimental effects on recovery.

Mungan (1991) conducted miscible and immiscible coreflood experiments using heavy and light oils with CO_2. It was concluded that CO_2 could increase heavy oil recovery even without miscibility development. Furthermore breakthrough recovery increase from 30% to 54% was observed when CO_2 was used instead of CH_4 as a displacing fluid.

Karim et al. (1992), similar to Thomas et al. (1990), conducted CO_2 cyclic 'huff and puff' coreflooding experiments using 6-ft long Berea cores and Timbalier Bay light crude. The core-inclination was found to substantially influence the oil recovery efficiencies and gas utilization factors of the coreflood and the 'best' performance was observed when CO_2 was injected into the lower end of a core tilted at a 45 or 90 degree angle.

Oren et al. (1992) attempted to characterize the pore-scale displacement mechanisms responsible for mobilization and production of waterflood residual oil accountable to immiscible gas flooding. A numerical three-phase invasion-percolation type network model was built incorporating these pore-scale displacement mechanisms, and used to predict the recoveries due to tertiary mode gas floods for 3-phase water-wet type systems with varying spreading coefficients. The model concluded that spreading oil films (i.e. positive spreading coefficients) are important to increase tertiary waterflood residual oil recovery by gas injection.

Kalaydjian et al. (1993) conducted sand-pack experiments in both horizontal and gravity stable modes. These results were similar to the previous experimental findings that the gravity stable floods had higher incremental recoveries over horizontal floods.

Longeron et al. (1994) studied the influence of capillary pressure on oil recovery. It was shown that the gas-oil capillary pressures were always higher in presence of connate water than the capillary pressures without connate water saturation. Further investigation using numerical simulation showed that recovery was very sensitive to capillary pressure input data, and the authors suggest "using scaled capillary pressures from mercury-air data, the recovery is underestimated by about 6% PV".

Chalier et al. (1995) used the gamma-ray absorption technique to visualize the fluid saturation distribution in the core as a function of the volume of gas injected. The three-phase oil relative permeability curve was analytically deduced from the oil saturation profiles and used for development of a numerical triphasic relative permeability model. The authors emphasize "three-phase oil relative permeability was the key for the evaluation of tertiary gas-gravity drainage project".

The above laboratory studies show that residual oil saturation, oil relative permeability and three-phase flow conditions not only are dependant on wettability of the porous medium but also are strongly influenced by the spreading coefficient. A positive spreading coefficient is desirable for continuous oil films on water and result in higher oil recovery factors in strongly water-wet systems.

3.1.6 Field Studies of Gravity Drainage

The gravity drainage process has been applied and has been successfully implemented in many field applications and pilots. Coreflood as well as field studies (Lepski and Bassiouni, 1998) have confirmed that incremental oil could be recovered from dipping water-drive reservoirs using gravity assisted gas injection processes such as Double Displacement Process (DDP), and Second Contact Water Displacement (SCWD). Empirical screening criteria for gravity assisted gas injection are available in the literature (Lepski and Bassiouni, 1998) and are summarized below as Table 3.1.

Table 3.1: Screening Criteria for Gravity Assisted Gas Injection.

Parameter	Value
WF Residual Oil Saturation	Substantial
Reservoir Permeability	> 300 mD
Bed Dip Angle	> 10^o
Oil Viscosity	Free flow
Spreading Coefficient	Positive

King and Lee (1976) developed modeling techniques to study the Hawkins (Woodbine) field in east Texas. Reservoir characterization was done using 10942.32 m (35,900 ft) of conventional cores obtained from 193 wells in the field. The field oil gravity was 12-30 API with viscosity varying from 2-80 cP. The reservoir characteristics include 40468730 m^2 (10,000 acres) of area with > 304.8 m (1000 ft) of hydrocarbon column. The reservoir is highly faulted with 6^o dip with strong aquifer support. Detailed phase behavior and modeling studies suggested gas injection to prevent oil encroachment in the gas cap and prevent further shrinking. Predictive simulation studies indicated that ~ 30.05 million m^3 (189 million bbl) of additional oil could be produced of which 18.44 million m^3 (116 million bbl) would be produced by converting the water-drive areas into gas-drive/gravity drainage, and 10.65 million m^3 (67 million bbl) from prevention of the oil loss caused by gas cap shrinkage. The authors conclude that the gas-drive/gravity drainage process would help produce nearly 1/3rd more oil than possible through water drive mechanisms.

DesBrisay et al. (1981) reviewed the vertical gravity stable miscible flood performance in the Intisar 'D' reservoir in the Libyan Sirte basin. Geological studies show the reservoir as upper Paleocene pinnacle reef, roughly circular (diameter 4828.03 m ~ 3 miles) in plan with original hydrocarbon column of 289.56 m (950 ft). The reservoir oil was highly under saturated, very light (40^o API) with 0.46 cP viscosity. The calculated MMP of this oil with gas in nearby fields (27.58 MPa (4000 psi)) was lower than the original reservoir pressure of 29.35 MPa (4257 psi). Modeling studies showed that the volumetric nature of the reservoir would result in extremely low primary recoveries, and pressure maintenance program by both water injection and crestal gas injection was initiated. "Extensive reservoir engineering studies indicated that miscible gas injection would almost double the waterflood oil recovery and would also conserve large amounts of solutions gas being produced from this and other fields". The authors predict that almost 0.25 billion m^3 (1.6 billion bbl) of OOIP (of which 78.86 million m^3 (496 million bbl) recovered till date) would be recovered yielding a recovery factor of ~ 70%, and most of which is attributable to miscible gas gravity drainage.

Cardenas et al. (1981) presented a laboratory design for a gravity stable miscible CO_2 flood for the Texaco's Bay St. Elaine field, Terrebonne parish, LA. The reservoir oil characteristics include light (36 ^oAPI) oil and viscosity 0.667 cP, with 20% residual waterflood oil saturation, with an MMP of 22.99 MPa (3334 psi) with CO_2 gas which was the current reservoir pressure. The reservoir had a 36^o dip and is well confined with natural sealing faults. For gravity stable and miscible displacement the density of CO_2 slug was reduced using CH_4 gas. The paper describes the following studies that were conducted:

- **PVT studies**
- **Empirical design of CO_2 solvent slug**

The critical velocity for gravity stable flooding was calculated using a modified Dumore equation shown below,

$$V_C = 8.473E-04 \frac{K_m Sin\alpha_d (\rho_2 - \rho_1)}{\phi_m (\mu_2 - \mu_1)} (m/d) \qquad \text{(3.13)}$$

Where,

V_C = Critical front velocity (m/day),

K_m = Mobile fluid permeability (μm^2)

α_d = Angle of dip (degrees)

ρ = Fluid density (kg/m^3). 1 = displacing, 2 = displaced

ϕ_m = Mobile fluid porosity

μ = Fluid viscosity (m-Pa-s). 1 = displacing, 2 = displaced

- **Slim tube tests**

Based on the results of PVT analysis, four CO_2-solvent mixtures were prepared using pure components. Displacement tests using these four solvent mixtures were conducted using 12.19 m (40 ft) & 0.0062 m (¼”) ID SS slim tube packed with clean silica sand.

- **Sand Pack floods**

Two 1.83 m (6 ft) & 0.064 m (2.5”) ID sand packs filled with clean silica sands (2400 mD and 36% porosity) were used to study two types of displacements: Continuous slug injection and CO_2 slug followed by N_2 chase gas. The slug flood exhibited a residual oil saturation of 5.8% while the continuous flood had a residual oil saturation of 4.1%.

The analysis indicated a 0.24 PV CO_2 slug would be required for the field project, however to provide an adequate safety factor, and ensure better oil recovery a 0.33 PV slug was selected for the Bay St. Elaine CO_2 project. However, field performance was not reported.

Nute (1983) evaluated the miscible Bay St. Elaine Field flood performance using pulse pressure tests, and measurements of oil saturations in situ to improve reservoir definition. The author describes the flood as 'successful' however production data are not available.

Backmeyer et al. (1984) report the tertiary extension of the Wizard lake D3A pool, Alberta, HC miscible flood and update the secondary flood data till date. The reservoir is dolomitized bioherm reef of Devonian age with oil zone of 197.51 m (648 ft) with a bottom water drive (Cooking Lake Aquifer). The reservoir characteristics include vuggular and matrix porosities with average horizontal permeability of 1375 mD and average vertical permeability of 107 mD with original reservoir pressure of 15.65 MPa (2270 psi). Reservoir oil is paraffin based 38 ^{o}API crude with saturation pressure of 14.69 MPa (2131 psi) at 71.11 ^{o}C (160 ^{o}F). The secondary HC miscible slug injection was 7.5% HCPV, and with the tertiary extension of the HC miscible flood, the projected recovery increase was 4.53 MMm^3 (28.5 MMSTB) thus raising the overall recovery from the reservoir to 59.26 MMm^3 (372.7 MMSTB) or 95.5% overall recovery factor.

Johnston (1988) summarized the Weeks Island S sand reservoir B (S RB) gravity stable field test. The S RB reservoir was chosen due to the small, well confined nature and exceptional sand quality and continuity. Reservoir characteristics include permeability of 1200 mD and a bed dip of 26^{o}.The reservoir oil properties are not specified, however residual oil saturation before the pilot was 22% based on SCAL. Low oil rates, water cuts and increasing GOR made tertiary recovery (CO_2 injection) necessary in the field. A 25.5% PV gravity stable miscible CO_2 – HC slug (24% PV & 1.5% PV) was injected resulting in additional 32.5924 Mm^3 (205 MBbl) or 60% waterflood unrecoverable oil. The displacement efficiencies were found > 90% (sidewall cores) and a CO_2 usage rate of 1407.05 m^3/m^3 (7.90 MCF/bbl) considering the recycled gas.

Howes (1988) summarized the EOR projects in Canada till date. There were 51 commercial scale projects (all hydrocarbon (HC) miscible) operational in Canada for recovery of light – to- medium crude (Density < 900 kg/m^3) and the gravity stable 'vertical' floods conducted in Canada till 1986/12/31 are compiled in Table 3.2 below. Detailed description and analysis of the projects are un-available and out of scope of the study.

The comparisons of the projects showed that oil recoveries were much higher, in the range of 15 – 40 % OOIP, for gravity stable gas floods in the pinnacle reefs of Alberta, compared to WAG recoveries of 5 – 10 % (Christensen et al., 1998). The miscible flood average ultimate recovery factors in Alberta were 59% OOIP, whereas the Alberta waterflood ultimate recoveries were only 32%.

Table 3.2: Summary of Canadian 'Vertical' HC Miscible Field Applications

Year	Project	Operator	Area (ha)	OOIP MMm^3	Ult. Recovery %OOIP	Dated Prodn %OOIP
1964	Golden Spike D3A Pool	Esso	590	49.60	58.0	56.1
1968	Rainbow Keg River A Pool	Canterra	253	14.30	88.1	61.5
1969	Wizard Lake D3A Unit	Texaco	1075	62.00	95.2	79.9
1969	Rainbow Keg River T Pool	Esso	87	3.18	81.8	55.7
1970	Rainbow Keg River O Pool	Canterra	281	6.21	79.9	61.0
1970	Rainbow Keg River EEE Pool	Canterra	24	1.91	70.2	36.6
1972	Rainbow Keg River E Pool	Canterra	69	3.97	85.4	44.3
1972	Rainbow Keg River G Pool	Canterra	65	2.38	77.3	56.3
1972	Rainbow Keg River AA Pool	Mobil	259	15.90	78.0	40.9
1972	Rainbow Keg River B Pool	Amoco	223	6.52	79.9	50.9
1973	Rainbow Keg River H Pool	Canterra	19	2.35	74.9	59.1
1973	Rainbow Keg River Z Pool	Esso	181	1.49	65.8	44.3
1973	Rainbow Keg River FF Pool	Esso	92	2.50	66.0	41.2
1976	Rainbow Keg River D Pool	Canterra	34	1.13	82.3	53.1
1980	Bigoray Nisku B Pool	Amoco	67	1.50	60.0	28.7
1980	Brazeau River Nisku A Pool	Petro-Canada	108	5.30	75.1	45.5
1980	Brazeau River Nisku E Pool	Petro-Canada	142	2.30	65.1	38.7
1981	Brazeau River Nisku D Pool	Petro-Canada	157	2.70	65.2	28.9
1981	Pembina Nisku G Pool	Texaco	133	3.00	70.0	32.0
1981	Pembina Nisku K Pool	Texaco	58	2.43	70.0	31.7
1981	Westpem Nisku A Pool	Chevron	62	2.65	75.1	34.0
1981	Westpem Nisku D Pool	Chevron	74	2.20	70.0	34.1
1982	Rainbow Keg River B Pool	Canterra	1090	43.00	71.6	43.5
1983	Pembina Nisku M Pool	Canadian Reserve	78	2.85	75.1	27.0
1983	Pembina Nisku O Pool	Texaco	85	1.70	70.0	20.6
1983	Pembina Nisku P Pool	Texaco	170	4.25	75.1	22.4
1983	Rainbow Keg River II Pool	Mobil	73	3.49	75.1	48.7
1984	Rainbow Keg River I Pool	Esso	146	1.88	70.2	N/A
1984	Westpem Nisku C Pool	Chevron	60	4.00	80.0	31.5
1984	Brazeau River Nisku B Pool	Chevron	90	2.30	80.0	29.1
1985	Pembina Nisku A Pool	Chevron	124	2.80	70.0	30.0

1985	Pembina Nisku D Pool	Chevron	143	4.80	72.1	31.7
1985	Pembina Nisku F Pool	Chevron	170	2.10	61.9	3.8
1985	Pembina Nisku L Pool	Texaco	253	5.00	82.0	25.4
1985	Pembina Nisku Q Pool	Texaco	122	2.80	83.9	12.5
1986	Bigoray Nisku F Pool	Chevron	52	2.80	76.1	32.5
1987	Acheson D3 A	Chevron	N/A	3.70	83.8	N/A

Texaco's Wizard Lake D-3A pool reservoir, Alberta was under primary production since 1951, history of which 19 years had primary production and nearly 20 years of gravity stable HC miscible injection. Hsu (1988) developed a 3-D (11 x 14 x 53), 4-ϕ (gas, solvent, oil & water) simulation model to predict reservoir behavior so as to help plan better injection-production strategy for the reservoir. The central theme of the paper was the good history match for ~ 40 years of reservoir production and model features developed specifically for this reservoir case.

Laboratory studies for the performance evaluation of the Hawkins field, under gas drive – pressure maintenance, were studied by Carlson (1988). It was concluded that the gas gravity drainage process had a recovery efficiency of > 80% compared to the water drive efficiency of only 60%. It was concluded that even under immiscible conditions, the gas could recover additional oil from the water invaded portions of the reservoir and thereby reducing the residual oil saturation in water invaded oil column from 35% to about 12%. The above conclusion helped the development of the 'Double Displacement Process' (DDP) and initiation of a field DDP pilot in the east fault block of the reservoir. The pilot test results are not included.

Da Sle and Guo (1990) analyzed the vertical hydrocarbon miscible flood in Westpem Nisku D pool, 160934.4 m (100 mi) southwest of Edmonton, Canada. The reservoir was of pinnacle reef type and the miscible flood implemented in May 1981 with a miscible slug of 80% Methane and rest of C_{2+} fraction, which was later changed to 85% C1, and 15% C_{2+} fraction with 33.10 MPa (4800 psi) working pressure to assure miscibility development. The reservoir oil was light (45 API) with 0.19 cP viscosity. Flood analysis for solvent/oil interface behavior showed that the interface was consistently flat across the reef, as predicted by the Dumore stability criterion. Further the core-analysis results indicated very low residual oil saturation to the order of 5% making the flood a success.

Bangla et al. (1991) studied the field performance of the gravity stable vertical CO_2 flood in Wellman unit of the Wolfcamp reef reservoir, which is a limestone reef reservoir in western Midland basin of Terry county, Texas. Reservoir oil was light (43.5 API) with 0.43 cP viscosity. A tertiary CO_2 miscible flood was planned after a successful waterflood with a ROS of 35%. CO_2 was injected into crest of reservoir with water injection continued in the water zone to maintain the MMP of 13.10 MPa (1900 psi).

Numerical model was constructed previously to predict the performance of the CO_2 injection under gravity stable modes. The model predicted the CO_2 ultimate sweep efficiency to be 78%. The actual sweep efficiency was found better than expected at 84% and the critical residual oil saturation was only 10.5% compared to the waterflood residual of 35%. The net utilization ratio of the flood was 1157.7 m^3/m^3 (6.5 MSCF/STB) and the ultimate recovery was 68.8% of the OOIP of the field with CO_2 incremental recovery of 27% excluding 'sandwich losses'.

Further developments suggested may push the ultimate recovery up to 74.8% of the OOIP. The wettability of the reservoir rock is not mentioned; nevertheless, the CO_2 miscible project was highly successful.

Huge reservoirs such as the Prudhoe Bay may have many oil recovery mechanisms operational in the field. For proper field management, understanding of the interaction / interdependence of these recovery mechanisms is critical. One of the common mechanisms operational, not only in Prudhoe Bay but many reservoirs where gravity drainage is the dominant production mechanism, are gravity drainage and bottom water drive or waterflood. Espie et al. (1994) tried to quantify these mechanisms via core studies and numerical simulation techniques. Espie et al. (1994) conducted series of corefloods using Prudhoe Bay cores and Prudhoe Bay analogue fluids at ambient conditions with the intention of mechanistic investigation of three phase flow. The flood sequence was:

- **Waterflood**
- **Tertiary displacement I**

  Gas / Oil gravity drainage from initial water saturations followed by waterflood.
- **Tertiary displacement II**

  Gas / Oil gravity drainage experiment from initial water saturations followed by an injected oil slug then followed by waterflood.

It was found that the initial oil saturation, oil mobility, and trapped gas saturation were critical to determine the velocity of the oil bank and that either the Stone I and Cheshire 3-ϕ permeability models could predict the 1D experiment efficiently.

Durandeau et al. (1995) studied the application and integration of the new sponge coring technology to obtain the fluid distributions and efficiency of the gas gravity drainage floods in one of the Arab D sub-reservoirs of a major oil field in offshore Abu Dhabi. SCAL and centrifuge tests were conducted on the cores to determine effective oil saturations.

The authors quote: "The effective oil saturation results showed that the gravity segregation mechanism has been very active and efficient to recover the oil in the reservoir". However detailed data to support this statement is not available in the paper.

Langenberg et al. (1995) documented initial 6 years of the double displacement process (DDP) in the East fault block 'Dexter' sands of the Hawkins Field, Wood

County, Texas. Field histories showed that the field, producing under strong bottom water drive, resulted in the invasion of the oil columns into the gas cap. To reduce further gas cap shrinkage; inert gas (N_2) shrinkage was started in March 1977. Studies showed that the gravity drainage rate was lower than expected and hence the injection rates were revised using Richardson-Blackwell gravity drainage rate calculations. The authors suggest that the DDP process has been successful in EFB and can reduce the residual oil saturations substantially thus improving recovery considerably.

Fong et al. (1999) compile the design factors and operational strategies for a successful tertiary 'vertical' miscible flood scheme and present their application to a tertiary hydrocarbon miscible flood in the NW lobe of the Rainbow Keg River F Pool reservoir. The authors suggest that the successful design factors are:

- Operating pressure selection
- Optimal solvent composition to ensure first contact miscible (FCM) displacement, there by reducing technical risks associated with miscibility, dispersion, diffusion and gravity stabilization.
- Optimum solvent size to maintain miscibility throughout the life of flood as well as prevent loss of miscibility by accidental mixing and dispersion with chase gas.
- Critical frontal advancement rate should be greater than vertical advancement rate (Dumore stability criterion applied).
- Good pattern design to ensure proper placement of solvent slug.

Field performance monitoring showed significant oil production improvement in the early life of the flood, attributable to the high reservoir quality, proper design criteria and sound operational strategy.

Gunawan and Caie (1999) analyzed the Handil reservoir performance for three years of lean gas injection in the Mahakam delta of Borneo, Indonesia. Reservoir and economic studies showed that the crestal injection of lean HC gas into the water flooded Handil field would yield additional oil from this near abandonment reservoir. Predictive simulation studies predict that the reservoir would yield additional 4.769619 MMm^3 (30 MMSTB) EOR oil.

Ren et al. (2003) used IMEX® black oil simulator to study the macroscopic level mechanisms of the DDP process. The 3D model was populated using reservoir properties from successful tertiary gas gravity drainage field tests. The important conclusions are:

- Injection/production rates strongly affect oil bank formation and recovery.
- Highly dipping reservoirs are good candidates for gravity assisted tertiary gas injection.
- Accurate modeling of 3-ϕ relative permeability and capillary pressures is necessary for accurate representation of the process.

- The secondary contact water displacement process (SCWD) fares better than DDP since higher oil drainage rates are obtained.

The incremental oil obtained in the gravity assisted tertiary gas injection processes is twofold –

- **Recovery of the bypassed oil**

Recovery of continuous oil phase that was unrecoverable in previous processes on account of reservoir heterogeneity and well placement.

- **Recovery of residual oil in water swept zones**

Discontinuous oil phase trapped due to capillary and viscous forces.

The positive spreading coefficient helps the formation of oil films in the pores when it comes in contact of the gas. These films can connect to all the residual oil in the gas swept zone to the oil bank in front of the gas front. Thus incremental oil recovery is due to oil film flow, and hence the rate of oil recovery is a strong function of the rate of oil drainage through these oil films.

The summary of the above cited field applications are included as Table 3.3 below.

Table 3.3: Summary of above cited Gravity Drainage Field Applications

Property	**West Hackberry**	**Hawkins Dexter Sand**	**Weeks Island S RB - Pilot**	**Bay St. Elaine**	**Wizard Lake D3A**	**West Pembina Nisku D**	**Wolfcamp Reef**	**Intisar D**	**Handil Main Zone**
State / Country	LA	Texas	LA	LA	Alta	Alta	TX	Libya	Borneo
Rock Type	Sand-Stone	Sand-Stone	Sand-Stone	Shaly-Sand	Dol-omite	Carbonate	Lime-Stone	Biomicrite / Dolomite	Sand-Stone
Application Type	Field	Field	Pilot	Lab	Field	Field	Field	Field	Field
Injection Mode	Secondary	N/A	Tertiary	Secondary	Secondary	Secondary	Tertiary	Secondary	Tertiary
Injection Type	Immsc	Immsc	Immsc	Immsc	Misc	Misc	Misc	Misc	Immsc
Start Date	11/1994	8/1987	1/1979	1/1981	1/1969	5/1981	7/1983	1/1969	1/1994
Project Area (Acre)	N/A	2,800	8	9	2,725	320	1,400	3,325	1,500
Enhanced Production (b/d)	150-400	1000	160	7	1,300	2,300	1,400	40,000	2,383
Status (Date)	C ('02)	NC ('02)	NC ('86)	NC ('86)	NC ('02)	HF ('92)	HF ('98)	NC ('02)	N/A
Porosity (%)	23.9 – 27.6	27	26	32.9	10.94	12	8.5	22	25
Permeability (mD)	300 – 1000	3400	1200	1480	1375	1050	110	200	10 – 2000
Connate Water Sat. (%)	19 – 23	13	10	15	5.64	11	20	N/A	22
WF Residual Oil Sat. (%)	26	35	22	20	35	N/A	35	N/A	27
GI Residual Oil Sat. (%)	8	12	1.9	N/A	24.5	5	10	N/A	3
Oil Saturation at Start (%)	N/A	N/A	22	20	93	90	35	80	28
Oil Saturation at End (%)	N/A	N/A	2	5	12	5	10	18	N/A
Reservoir Temperature (°F)	205 – 195	168	225	164	167	218	151	226	197.6
Bed Dip Angle (Degrees)	23 – 35	8	26	36	Reef	Reef	Reef	Reef	5 – 12
Pay Thickness (ft)	31 – 30	230	186	35	648	292	824	950	15 – 25 (m)
Oil API Gravity	33	25	32.7	36	38	45	43.5	40	31 – 34
Oil Viscosity (cP)	0.9	3.7	0.45	0.667	0.535 (BP)	0.19	0.43	0.46	0.6 – 1.0
Bubble Pt Pressure (psi)	2920.304	1985	6013	N/A	2154	3966	1375	2224	2800– 3200
GOR (SCF/STB)	500	900	1386	584	567	1800	450	509	2000
Oil FVF at Bubble Pt	1.285	1.225	1.62	1.283	1.313	2.45	1.284	1.315	1.1 – 1.4
Injection Gas	Air	N_2	CO_2/HC	CO_2	HC	HC	CO_2	HC	HC
Minimum Miscibility Pressure (psi)	--	--	N/A	3334	2131	4640	1900	4257	--
Displacement Velocity (ft/D)	.095 – .198	N/A	.04 – 1.2	N/A	.021 – .084	.020 – .203	.116	.06	N/A

WF recovery (% OOIP)	60	60	60 - 70	N/A	N/A	N/A	N/A	N/A	58
Ultimate Oil Recovery (%OOIP)	90.0	> 80.0	64.1	N/A	95.5	84.0	74.8	67.5	N/A
Project Results	Successful	Successful	Successful	Discouraging	Successful	Successful	Successful	Successful	Successful
Profit (?)	Profit	Profit	No Profit	No Profit	Profit	Profit	Profit	Profit	Profit

3.1.7 Literature Review Summary

This section summarizes the extensive literature review, which focused on the displacement characteristics (instabilities and critical rates), and laboratory studies and field applications for gas gravity drainage.

- **Gravity Drainage Laboratory Studies**
    1. Gravity drainage displacement instabilities (such as viscous gas fingering) are a function of rock-fluid properties, fluid saturation distributions, the viscous forces and rock-fluid interaction parameters like rock wettability, interfacial tension and miscibility.
    2. Cross flow and mixing (between miscible slug and chase gas) in the reservoir results in displacement instabilities consequently decreased displacement efficiencies.
    3. The well spacing as well as the injection rate dictates the stability of the growing interface as well as coning / cresting phenomenon. Injection rates above the critical results in ‘short-circuiting’ of the injected gas to the production well, drastically reducing sweep.
    4. Characterization and quantification of conditions of displacement instabilities and critical injection rates are important for flood profile control and need to be evaluated using 3D physical models and / or reservoir simulation.
    5. Miscibility between the injected gas and reservoir fluid helps the reduction of viscous displacement instabilities by reducing the fingering. Furthermore miscibility development lengths are shorter in gravity-assisted floods than horizontal floods helping better gas-oil contacts in the reservoir.
    6. Very high recoveries to the order of 90 – 95% OOIP in gravity drainage reservoirs are possible only if oil spreads on water film (that is under positive spreading coefficient conditions). Micromodel studies show that positive spreading coefficients are obtainable under strongly water-wet conditions, where continuous oil films over water are obtainable in gas swept zones.
    7. Vertical coreflood displacement studies suggest the use of CO_2 over hydrocarbon gases due to the higher recovery efficiency and injectivity characteristics of CO_2; although economical and assured supply of CO_2 for EOR applications could be an issue in some cases.
- **Gravity Drainage Field Studies**
    1. Up dip / crestal gas injection into oil reservoirs is one of the most efficient methods to recover residual oil.

2. Gas gravity drainage process has been applied as secondary as well as tertiary recovery processes with encouraging results.
3. Gas gravity drainage process has been applied to all reservoir types, from extremely geo-complex reservoirs like Biomicrite / Dolomite to high quality turbidite (sandstone) reservoirs.
4. All types of common field injectant gases like Air, Nitrogen (N_2), Hydrocarbon (HC) and Carbon Dioxide (CO_2) have been successfully employed for the gas gravity drainage process.
5. Gas gravity drainage process is applicable to low permeability – low porosity reservoirs as well as high permeability - high porosity formations, and is not greatly affected by the variation of common reservoir – fluid parameters like reservoir heterogeneity, bubble point pressure, Gas Oil Ratio (GOR), reservoir temperature & oil formation volume factor (FVF).
6. Gas gravity drainage process is best applicable to light oil reservoirs, low connate water saturations, mixed wettability (to promote film flow), thicker formations, moderate-high vertical permeability, highly dipping or reef structured reservoirs, and minimal reservoir re-pressurization requirements.
7. Corefloods and field investigations confirm that a large amount of incremental tertiary oil can be recovered using gravity assisted gas injection.
8. Recoveries as high as 85 – 95% OOIP have been reported in field tests, with the calculated average ultimate recoveries for all the fields referred in this study being 76.62 %OOIP, and laboratory gas gravity drainage floods yielding nearly 100% recovery efficiencies.

The field reviews show that gas gravity drainage is applicable to all reservoir types and reservoir characteristics using common injectant gases in both secondary as well as tertiary recovery modes. Gravity drainage is seen ‘best applicable’ to low connate water, thick, highly dipping or reef type, light oil reservoirs with moderate to high vertical permeability and low re-pressurization requirements. Field applications show oil recoveries as high as 85 – 95% OOIP with calculated average ultimate recoveries for all the fields studied in this review being 76.62% OOIP.

3.2 Operating Multiphase Mechanisms during Gas Gravity Drainage

Literature review clearly shows that CO_2 and hydrocarbon gases are the most common injectants in the commercial gas injection projects. The important mechanisms operative in any gas injection project are influences of (i) gravity segregation, (ii) reservoir wettability, (iii) spreading coefficient, (iv) miscibility development, (v) mobile water saturation, (vi) connate water saturation, and (vii) reservoir heterogeneity. A brief literature review on these mechanisms is included below.

3.2.1 Gravity Segregation

As discussed earlier, the mechanism of gravity segregation is dominant in horizontal type gas injection projects. Although the WAG process is employed to minimize this effect, significant differences in viscosities / densities between the injected water, gas and reservoir fluid results in water 'under-ride' and gas 'over-ride'. In reservoirs with high K_V/K_H ratio there exist higher cross-flow and convective mixing tendencies that may increase the vertical sweep; however, this phenomenon is detrimental to oil recovery attributable to increased gravity segregation and decreased flow velocity. Contrary to the horizontal floods, gravity stable (vertical) gas injections demonstrate marked benefits due to this phenomenon of gravity segregation.

3.2.2 Effect of Wettability

Limited studies on the effects of wettability on gas injection EOR are available in the literature. Rao et al. (1992) studied the water and miscible gas flood performance in four different rock-fluid systems with different wettabilities. It was concluded that the mixed wet system was the best from both waterflooding as well as gas flooding point of view. Recoveries from the intermediate wet, oil wet and water wet systems were the second, third and fourth in performance respectively. This data indicate that confident characterization of reservoir wettability aid the formulation of a proper exploitation strategy for the reservoir and help maximize recovery (Rao, 2001).

3.2.3 Effect of Spreading Coefficient

The spreading coefficient affects the gas-oil-water distributions, consequently recoveries during a gas injection program. Equation 1 below defines the spreading coefficient.

$$S = \sigma_{G/W} - \sigma_{G/O} - \sigma_{W/O} \quad \text{………………………………………..……………...……(3.14)}$$

Lower residual oil saturations in gas floods are obtainable if continuous oil films in the reservoir exist. The continuity of this oil film is an interfacial phenomenon and depends on the ability of the oil phase to spread onto the water phase in presence of gas that establishes a film on rock surfaces. The spreading coefficient can be positive or negative depending on the fluids under consideration. The positive value of the spreading coefficient helps ensure development and maintenance of continuous oil films between injected gas and reservoir water resulting in minimal losses of the injected gas to the reservoir water. Laboratory and theoretical studies (Section 3.1) suggest that a positive spreading coefficient under strongly water-wet systems may result in significantly high gravity drainage recoveries. On the other hand a negative value signifies a lense-type discontinuous distribution of oil between water and gas, thereby enabling gas-water contact and lower oil recoveries. However, negative spreading coefficients in real reservoir cases are rare and seldom found.

3.2.4 Effect of Miscibility

The miscibility issue is generally based on gas availability, but is mainly reported as an economic consideration and the extent of reservoir repressurization required for field applications. However, almost all of the commercial CO_2 / hydrocarbon gas injection projects conducted in the United States and Canada today are miscible. Oil and Gas Journal – EOR survey of 2002, shows that the commercial immiscible projects have significantly decreased over the last decade and that no immiscible floods have been planned in the immediate future.

The miscible gas floods yield higher oil recoveries by raising the capillary number (discussed later) due to the relatively low interfacial tension values between the oil and injected gas. The CO_2 flood design criteria (for both miscible and immiscible floods) (Green and Willhite, 1998) suggest a minimum depth limitation as well as dictate the density and viscosity of the oil to be produced from the concerned reservoir. Hence in shallow and medium gravity (22 to 31 API) oil reservoirs, the flood is by default immiscible. However, the immiscible type injection may not be always due to reservoir limitations: operational, economic and design factors may sometimes call for immiscible floods. Although the recoveries for immiscible floods are lower than those of miscible floods, the costs of reservoir repressurization may be prohibitive in certain cases for miscible flooding. It is important to note that although horizontal immiscible floods fare significantly lower than horizontal miscible floods (WAG as well as CGI) (Christensen et al., 1998); the miscible and immiscible flood performances have been comparable for gravity stable (vertical) gas injection projects (Section 3.1.6).

In miscible flooding, the incremental oil recovery is obtained by one of the three mechanisms: oil displacement by solvent through the generation of miscibility (i.e. zero interfacial tension between oil and solvent – hence infinite capillary number), oil swelling and reduction in oil viscosity (Schramm et al., 2000). Miscible flooding in horizontal floods has been used with or without WAG for the control of viscous fingering and reduction in gas-oil interfacial tension of the system by conducting the flood above the minimum miscibility pressure (MMP).

Although both immiscible and miscible floods have their own merits and demerits, there seems to be no consensus in the literature for the need for development of miscibility in gas floods (Thomas et al., 1995, Schramm et al., 2000, Rao 2001, Jakupsstovu et al., 2001). This debate could be partially due to the ‘industry-definition’ of the capillary number, which leaves out the contact angle (Cos θ) term (Rao, 2001), which eliminates the reservoir wettability from consideration. The general belief is that the IFT is the most easily modifiable term in the capillary number definition (Rogers and Grigg, 2000), which resulted in increased research efforts for the development of new and better surfactants for IFT reduction. However, overlapping values of interfacial tension for immiscible, near-miscible and miscible floods for similar fluid system have been reported

(Taber et al., 1996, Christensen et al., 1998, Rao, 2001). If the ultimate goal is to make the value of capillary number large, gas injection in a neutral-wet reservoir (or made neutral wet using surfactants), where the condition of $\theta = 90$ or $\cos\theta = 0$ makes capillary number infinity (Rao, 2001). Inspite of these different schools of thought on miscible gas injection, the inclination of the industry towards miscible flooding is very evident (EOR survey, 2002).

3.2.5 Effect of Mobile Water Saturation

Presence of mobile water saturation in the reservoir strongly influences gas-oil displacement process. Farouq Ali (2003) suggests that one of the main reasons for failures of miscible gas injection flood is its application in tertiary mode, wherein significant quantities of water need to be displaced and also the injected solvent (especially CO_2) is lost into the reservoir brine.

The mobile water 'shields' the oil from the injected gas resulting in delayed oil productions, decreased gas injectivity and lower oil relative permeabilities. The water-shielding phenomenon is a strong function of wettability and is more strongly exhibited in water-wet media than oil-wet media (Rao et al., 1992, Wylie and Mohanty, 1999). This phenomenon leads to decreased oil recoveries in water-wet media (Wylie and Mohanty, 1999) and similar oil trapping effects are seen for HC and CO_2 injectants in both multiple contact miscibility (MCM) and first contact miscibility (FCM) displacements (Tiffin et al., 1991).

3.2.6 Effect of Connate Water Saturation

In gravity-drainage processes (especially secondary displacements), three phases usually exist, even though the connate water is regarded as immobile. Micromodel studies (Sajadian and Tehrani, 1998) have shown that this may not be always the case. Changes in the gravity – capillary force balances may result in saturation redistributions and / or mobilization of the connate water in the actual displacements. However, studies on the effects of connate water saturation are sparse (Dumore and Schols, 1974; Katzas et al., 1988; Skauge et al., 1994; Nahara et al., 1990; Sajadian and Tehrani, 1998).

Literature review on the influence of effects connate water saturation on gas gravity drainage provided conflicting conclusions. Nahara et al. (1990) based on centrifugal gas-oil displacements, reported that gas-oil relative permeabilities are unaffected by the presence of water, as long as the water is immobile. Dumore and Schols (1974) reported that the presence of immobile connate water in Bentheim sandstones resulted in extremely low residual oil saturations, for both low and high gas/oil interfacial tensions, during gravity drainage. Pavone et al. (1989) conducted free gravity drainage experiments at low interfacial tensions in fractured reservoir cores and concluded that the presence of immobile water reduces the oil relative permeability, and thereby reducing the oil production. These findings contradict the observations of Hagoort (1980) that presence of connate water helps increase oil relative permeability. Skauge et al. (1994) carried out gravity drainage experiments at various connate water saturations using radioactive brine, Marcol 172 and n-Decane and reported that presence of connate water increases oil production and that the maximum HCPV oil recovery is possible at a connate water saturation of about 30%, in gravity drainage processes.

3.2.7 Effect of Reservoir Heterogeneity

Stratification and heterogeneities strongly influence the oil recovery process since they control the injection and sweep patterns in the flood. Heterogeneity has played havoc with horizontal gas floods leading to early breakthroughs and poor reservoir sweeps (Rao, 2001). On the contrary, in gravity stable (vertical) gas floods heterogeneous stratification can delay breakthrough due to physical dispersion, and reduced gas channeling through the high permeability layer.

The vertical-to-horizontal permeability (K_V/K_H) ratio is a major factor that represented the reservoir heterogeneity effects. Higher K_V/K_H ratio leads to increased cross flow perpendicular to the bulk flow direction, in horizontal floods, which is mainly influenced by viscous, capillary, gravity and dispersive forces (Rogers and Grigg, 2000). Although, cross-flow may increase the vertical sweep, it generally has detrimental effects on oil recovery – mainly due to increased gravity segregation and decreased flow velocity – leading to reduced frontal advancement in lower permeability layer(s) in horizontal (CGI/WAG) displacements. Higher K_V/K_H and higher reservoir permeability contrasts not only adversely affect oil recovery in WAG process (Jackson et al., 1985) but also cause severe injection and conformance control problems (Gorell, 1990). Reservoir simulation studies for various K_V/K_H ratios suggest that higher ratios adversely affect oil recovery in WAG process (Jackson et al., 1985).

As against the horizontal gas floods, the gravity stable gas injection seems largely immune to heterogeneity effects – instead the heterogeneity could be beneficial in improving injectivity and reservoir sweeps. The above statement is supported by successful gravity stable injections demonstrated in sand-packs (Cardenas et al., 1981), laboratory corefloods (Soroush and Saidi, 1999), and commercial field injections in heterogeneous or fractured onshore / offshore reservoirs (Henriquez and Jourdan, 1996, Rao, 2001, Krijn et al., 2002, Section 3.1).

3.3 Operating Fluid Dynamics during Gas Gravity Drainage

Multiphase flow behavior (fluid dynamics) strongly affects performance of the gas injection processes including CGI, WAG and GAGD. The fluid dynamic effects are mainly displayed through relative permeability, oil recovery, injectivity patterns and water-to-oil ratios (in WAG processes). These factors are influenced mainly by the relative magnitude of gravity versus capillary versus viscous forces. This section summarizes the literature reviews for: (i) effect of injection mode (ii) gravity / capillary / viscous force effects, (iii) effect of dispersion / flow regime characterization (iv) relative permeability and (v) oil recovery characteristics.

3.3.1 Effect of Injection Mode

Literature review (Kulkarni and Rao, 2004; Rao et al., 2004; Section 3.1), discussed below, clearly shows that the gas gravity drainage processes have been applied in both secondary as well as tertiary injection modes.

- **Secondary Mode Gas Gravity Drainage**

Gas injection under secondary conditions, generally assumes that the connate water is immobile. Injection under secondary conditions, especially in an unsaturated reservoir (without gas cap), results in an initial single-phase oil displacement, followed by gas-oil gravity drainage in the gas-invaded zone (Saidi and Sakthikumar, 1993). The secondary gravity drainage is controlled by the spreading coefficient and that oil film flow (under positive spreading coefficients) is critical for high recoveries. If the displacement is immiscible, then the threshold capillary pressure of the pore controls the gas invasion. This capillary retention traps oil in the reservoir, which can be remobilized by lowering of the interfacial tension and / or increasing the viscous forces.

Secondary drainage micromodel studies (Sajadian and Tehrani, 1998) conducted for visualization of gravity drainage phenomena resulted in conflicting inferences with the previous assumptions. These studies show that the connate water does not necessarily remain immobile during gravity drainage and saturation mobilization and redistributions can occur due to changing the balance between gravity and capillary forces. The micromodel studies also suggest that horizontal movement of the gas-oil contacts is not possible, and that initially the buoyancy forces overshadow the viscous forces. However, in the latter stages of gas injection, liquid film flow is critical both before and after the breakthrough of gas.

- **Tertiary Mode Gas Gravity Drainage**

Carson (1988) introduced the concept of updip gas injection during the analysis of a tertiary gravity-stable gas injection flood in the Hawkins field. Carson named this process ‘Double Displacement Process’ (DDP) defined as ‘the use of gas to displace a previously water displaced oil column’. The ‘Gravity Assisted Tertiary Gas Injection Process’ as defined by Kantzas et al. (1988), experimentally demonstrated that gravity drainage plays a very important role in gas injection processes and showed that the reservoir wettability (Kantzas et al., 1988, Chatzis et al., 1988), and spreading coefficient (Kantzas et al., 1988, Chatzis et al., 1988) strongly influenced this process. Kantzas et al. (1988; and Chatzis et al., 1988) further suggested that a positive spreading coefficient and strongly water-wet conditions are beneficial for this process and that the process efficiency is a function of the 'spreading phenomenon'. Network model studies (Oren and Pinczewski, 1994), confirmed the observations of Kantzas et al. (1988; and Chatzis et al., 1988) by recovering higher oil in positive spreading systems than in negative spreading systems.

The incremental oil recovery by tertiary gravity drainage consists of two-parts (Ren et al., 2003); namely, the bypassed oil, existing as a continuous oil phase in unswept areas (by secondary waterflood) and the residual oil existing at the microscopic scale as isolated oil ganglia. The injected gas improves the reservoir sweep by reestablishing the hydraulic continuity of the residual oil, under positive spreading conditions, resulting in positive flow into the oil bank. The connectivity of the oil bank with both the bypassed oil as well as the isolated oil ganglia helps their drainage once the oil bank reaches the production well.

In gravity assisted tertiary gas injection processes, the carrying capacity of the oil films (transmissibility) is critical (Ren et al., 2003). In watered-out reservoirs, the oil distribution could be continuous (oil-wet rocks) or as disconnected ganglia (other wetting states). In the presence of a third phase (namely injected gas), the oil can spread between the gas and water films under positive spreading conditions. However under negative spreading conditions, continuous oil films may not develop substantially decreasing recoveries. Micromodel studies (Kantzas et al., 1988; Dawe, 1990, Oren et al., 1992) on water-wet media provided visual proof for this phenomenon.

Other pore-level experiments (Ren, 2002) of the gravity assisted tertiary gas injection process showed that the oil flow rates through oil films are dependent on both, weight of the oil ganglia as well as the incremental volume of gas injected till gas breakthrough. After gas breakthrough, the gas flows out of the model intermittently (Sajadian and Tehrani, 1998), and the film flow rates are mainly gravity driven and hence consequently low. Another process 'Second Contact Water Displacement' (SCWD) process has been suggested (Lepski et al., 1996; and 1998) to increase the oil rates after gas breakthroughs. Micromodel studies (Ren, 2002) have shown some incremental recoveries, and saturation redistributions attributable to the SCWD process. However, increased water saturations, decreased oil relative permeabilities, increased water shielding effects and higher surface water-handling costs are not addressed, which might be the controlling economic parameters.

3.3.2 Gravity versus Capillary versus Viscous Force Effects

The gravity forces tend to reduce volumetric sweep by gravity segregation of fluids (for horizontal injections). As against this, the capillary forces may improve sweep by allowing water to imbibe (in water-wet matrix) into low permeability zones that would otherwise be bypassed; whereas the viscous force influences tend to displace the water through the path of least resistance in the reservoir, bypassing low permeability regions.

In gravity stable injections, the beneficial gravity segregation effects aid the gravity forces to increase reservoir sweep and oil recoveries. Furthermore, the capillary imbibitions into low permeability zones (in water-wet reservoirs) and miscibility development would be beneficial to oil recovery. The effect of the viscous forces, which result in bypassing of the low permeability regions in the reservoir, would be minimized due to the countercurrent gas-liquid and concurrent oil-water displacement tendencies in gravity stable gas injections.

Performance prediction in highly heterogeneous reservoirs is extremely difficult since different forces may be active in different parts and length scales within the same reservoir. The best quantification of the relative importance of gravity / capillary / viscous forces is through rigorous experimentation designed using various dimensionless numbers to describe the relative importance of the different forces in a given displacement process. The latter method is desirable since it incorporates both: relative importance of the different forces in different parts of the reservoir as well as length scale. This helps scale up (or down) of laboratory scale results to field scale and vice versa. However, it is important to note that almost all the dimensionless numbers involving gas-oil IFT and gravity-viscosity differences ($\Delta\sigma, \Delta\mu$) are applicable to immiscible floods only. Further work is underway to identify the parameters governing miscible flood performance.

3.3.3 Effect of Dispersion and Flow Regime Characterization

Effects of dispersion and flow regime characterization are significant fluid mechanisms for flow through porous media, and are discussed below.

- **Dispersion**

Fluid-fluid dispersion during miscible displacement is an important parameter for scaling the experimental data. Pozzi and Blackwell (1963) added a basic dispersion-scaling group to those developed by Geertsma et al. (Kulkarni, 2004). Use of the Pecklet's number (ratio of the convective to dispersive transport) is recommended (Novakovic, 2002) for dispersion scaling of both miscible as well as immiscible displacements.

$$N_{Pe} = \frac{uL}{\phi D} \qquad \text{...}(3.15)$$

However, under ideal gravity drainage conditions, the dispersion would be minimal, since the dispersion is localized and influenced only by local permeability variations, rather than fluid mechanics.

- **Flow Regime Characterization**

General fluid mechanics literature (Johnson, 1998) characterizes the prevailing flow regimes as a function of the gravity number (N_G), since it focuses on small-scale gas-liquid systems. Figure 3.1 shows the four flow regimes based on visual observations from different sand-pack experiments.

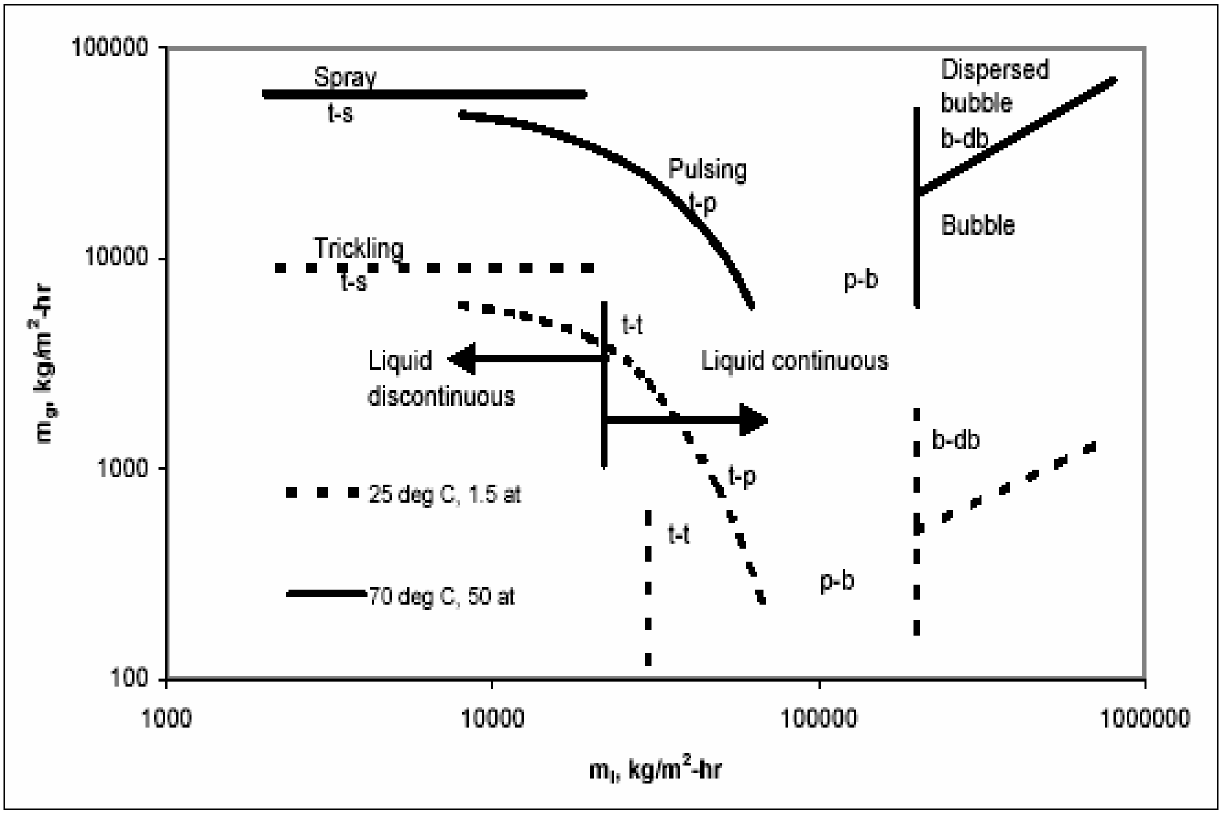

Figure 3.1: Liquid-Gas Flow Regimes at Small-Scale as a Function of a Fluid Mass Flux (Johnson, 1998)

The tricking flow regime (t) occurs when the particles and gas flows in remaining pore space. Pulsing flow regime (p) prevails when gas-liquid slugs traverse the columns alternately. The flow channels could be plugged by liquid slugs, which are blown off intermittently by gas plugs. During the spray flow regime (s), the liquid travels down the column in the form of entrained droplets in the continuous turbulent gas phase. In the bubble dispersed-bubble (b/db) regimes, the gas phase flows as slightly elongated bubbles, and these bubbles become highly irregular with increasing gas flow rates.

Lenormand et al. (1988) introduced the concept of ‘phase-diagram’ for small-scale drainage experiments as a plot of capillary number versus the viscosity ratio. They suggested that the use of gravity numbers to depict the flow regimes is just a ‘snapshot’ of that particular rock type, and it does not characterize either the capillarity scaling or the global effect on oil recoveries. Figure 3.2 shows the major flow regimes, and their range of applicability.

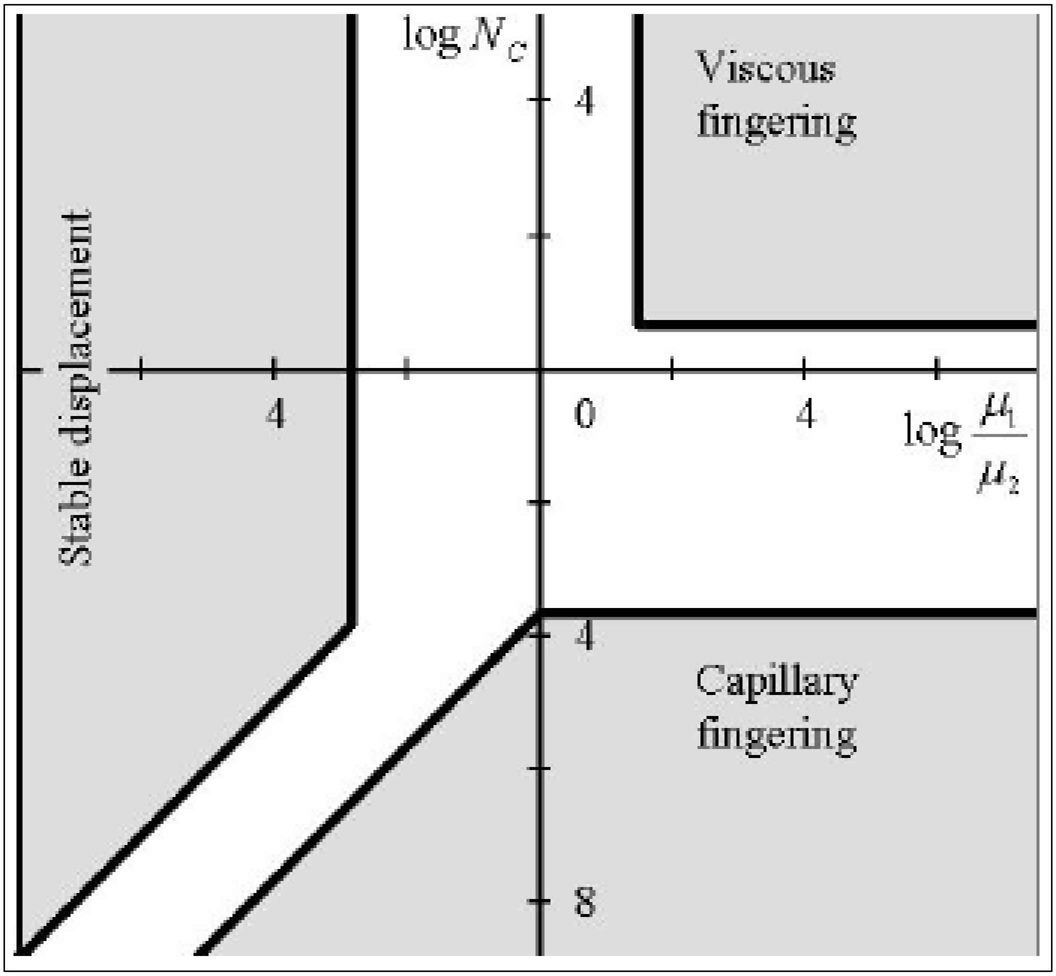

Figure 3.2: Flow Regime Map as a Function of Capillary Number and Viscosity Ratio (Lenormand et al., 1988)

Lenormand et al. (1988) also reported that the drainage displacements are fully characterized by capillary number and viscosity ratio. However, this conclusion is seriously flawed as the pore size distribution in not accounted for. This limitation can be taken care of by the incorporation of the Bond number in the analysis, which contains the term 'characteristic length' relating to the pore size distribution of the porous medium.

Li and Lake (1993) used dimensional analysis approach based on statistically generated numerical reservoir. The flow regime description was based only on the effect of heterogeneity, neglecting the conventional viscous-capillary-gravity-dispersive force balances (Figure 3.3).

Coll et al. (2000) tried to overcome this limitation by using the fractional flow equation and the dimensionless scaling numbers from Shook et al. (1992). They defined the flow regimes based on the dominant force governing the flow. The ranges are presented in Table 3.4. The details of this technique are available elsewhere (Novakovic, 2002; Coll et al. 2000).

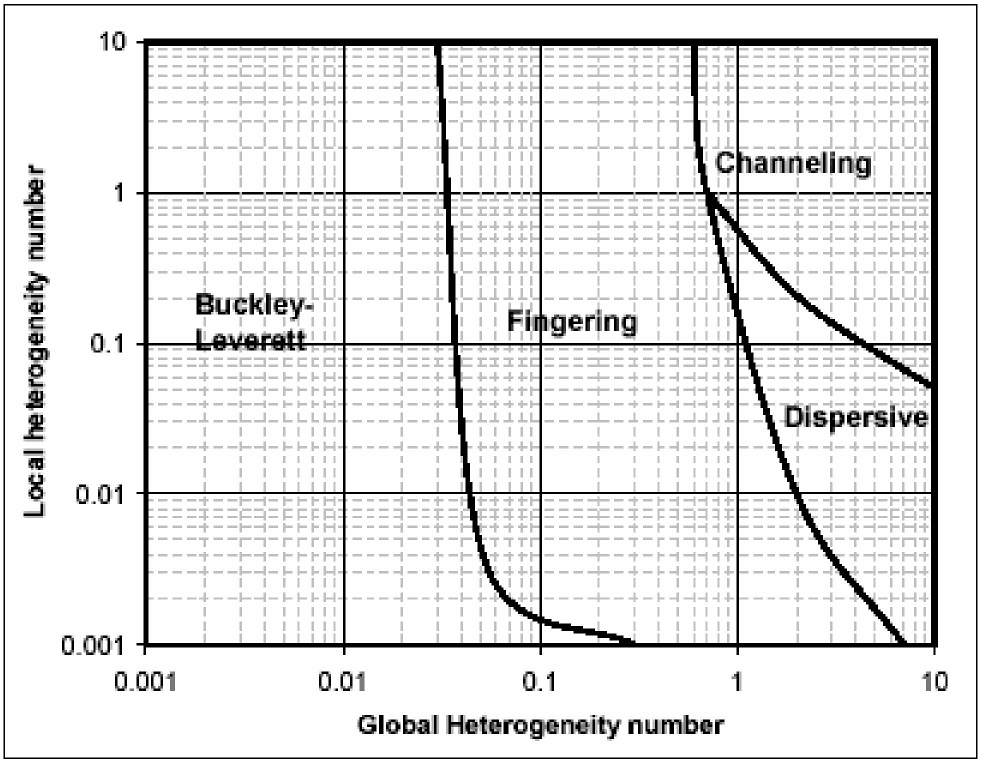

Figure 3.3: Flow Regimes as a Function of Local and Global Heterogeneity (Li and Lake, 1993)

Table 3.4: Gravity and Capillary Dominated Flow Regimes (Novakovic, 2002; Coll et al., 2000)

Flow	Boundaries	Condition	Regime
Longitudinal	$N_{gcutoff} = \frac{\varepsilon_1}{L \cdot \sin\alpha} \cdot \lambda_{ro}^{o} \cdot \left(\frac{\lambda_{ro}+\lambda_{rw}}{\lambda_{ro}\cdot\lambda_{rw}}\right) \cdot H \cdot \cos\alpha$ $N_{Pccutoff} = \frac{\eta_1 \cdot \lambda_{rw}^{o}}{\frac{\partial S_w}{\partial x}} \cdot \left(\frac{\lambda_{ro}+\lambda_{rw}}{\lambda_{ro}\cdot\lambda_{rw}}\right)$	$N_g > N_{gcutoff}$ $f_w << 1$ $N_{Pc} < N_{Pccutoff}$	Gravity dominated
		$N_g < N_{gcutoff}$ $f_w << 1$ $N_{Pc} > N_{Pccutoff}$	Capillary dominated
Transverse	$N_{gcutoff} = \frac{\varepsilon_2 \cdot \left(\frac{v_t}{u_t}\right)}{\frac{L}{H} \cdot \left(\frac{k_z}{k_x}\right)} \cdot \lambda_{ro}^{o} \cdot \left(\frac{\lambda_{ro}+\lambda_{rw}}{\lambda_{ro}\cdot\lambda_{rw}}\right)$	$N_g < N_{gcutoff}$ $f_w << 1$ $N_{Pc} > N_{Pccutoff}$	Gravity dominated
	$N_{Pccutoff} = \frac{\eta_2 \cdot \left(\frac{v_t}{u_t}\right)}{\left(\frac{k_z}{k_x}\right)^{\frac{1}{2}} \cdot \frac{\partial S_w}{\partial z}} \cdot \lambda_{rw}^{o} \cdot \left(\frac{\lambda_{ro}+\lambda_{rw}}{\lambda_{ro}\cdot\lambda_{rw}}\right)$	$N_g < N_{gcutoff}$ $f_w << 1$ $N_{Pc} > N_{Pccutoff}$	Capillary dominated

3.3.4 Relative Permeability

The relative permeability, an important petrophysical parameter, is the connecting link between the phase behavioral and transport properties of the system. It is also a critical input parameter in predictive simulation of gas injection floods. The relative permeability influences the flow mechanics of the displacement process.

Capillary number influences the relative permeability via interfacial tension (IFT). In WAG processes, wherein water and gas are injected simultaneously, relative permeability becomes a complex parameter to quantify and predictive simulation / flow modeling requires the use of cycle dependant (three-phase) relative permeabilities. However, in GAGD process, the displacement could be modeled using 2-phase gas-liquid relative permeabilities, instead of the complex 3-phase relative permeabilities, attributable to countercurrent gas-liquid and concurrent oil-water displacement tendencies.

3.3.5 Oil Recovery Characteristics

The oil recovery characteristic of a process is the 'bottom-line' and the reason for all petroleum engineering studies. The performance evaluation(s) of the gas injection EOR processes is via the oil recovery characteristics demonstrated by that process. The gas injection processes considered for this study are: CGI, WAG, Hybrid-WAG and GAGD. All of the tertiary EOR processes display a finite delay in oil breakthrough (response time) and early production is characterized by 'mobile' water production. The key parameter for the success of any EOR process is to minimize the oil response time and maximize the recovery.

3.4 Dimensionless Reservoir Characterization

To properly 'scale' and characterize a representative experiment or numerical model, several aspects pertaining to the spatial and / or physical mechanisms need to be considered. Scaling is defined (Novakovic, 2002) as a procedure of extrapolation of results obtained at one scale to another, e.g. from a small-scale laboratory observation to a large-scale process and vice versa. Research efforts (Kulkarni, 2004) in the areas of multiphase mechanics and fluid dynamics, point towards dimensionless quantities as an effective scaling tool.

The various dimensionless groups used in the literature, can be classified as single-phase or two-phase groups. The single-phase numbers are not relevant to multiphase flow through porous media, but can sometimes be applicable to pressure-transient analysis (Novakovic, 2002) of under-saturated reservoirs. Unlike the single phase groups, the two-phase dimensionless groups focus on the balance of the four major forces that control gravity stable gas flow through porous media, namely viscous, gravity, capillary and dispersion, which ultimately control breakthrough time, recoveries and dispersion.

However, to facilitate accurate numerical / experimental modeling, the following five scaling issues must be addressed (Novakovic, 2002): (i) Scalability of physical effects, (ii) Scalability of boundary conditions, (iii) Scalability of reservoir shape, (iv) Compatibility with existing reservoir simulation tools, and (v) Numerical and physical dispersion. Of the previously referred scaling issues, only the first two are appropriate and relevant to our research aims, wherein duplication of the multiphase mechanisms and fluid dynamics operational in the actual reservoir displacements need be carried out in the laboratory. This section reinforces the relevance of dimensional analysis for development and optimization of the GAGD process, and also attempts to decipher the individual effects of these dimensionless quantities on multiphase mechanisms and fluid dynamics controlling gravity drainage.

3.4.1 Scalability of Physical Effects / Boundary Conditions

Scaling of the physical phenomenon as well as the imposed boundary conditions is critical in duplication of the multiphase mechanisms and fluid dynamics in the laboratory. Several dimensionless variables have been used in order to scale the flow behavior, with each variable representing a portion of reservoir fluid dynamics and multiphase mechanisms. Table 3.5 summarizes the basic dimensionless groups used for scaling of these phenomena from the laboratory to the field.

Table 3.5: Summary of Basic Multiphase Dimensionless Numbers (Novakovic, 2002)

Scaling Parameter	Variable	Formulation	Remarks
Boundary Conditions/ Response	Dimensionless Time	$t_D = \frac{V_{injected}}{V_{pore}}$	Imposed Injection Boundary Conditions
	Displacement Efficiency Factor	$E_D = \frac{V_{produced}}{V_{reference}}$	Dimensionless Production Response
Physical Effects Scaling	Mobility Ratio	$M = \frac{\lambda_{displaced}}{\lambda_{displacing}}$	Fluid-Fluid-Rock Interaction Effect on Flow Behavior
	Capillary Number	$N_C = \frac{F_{capillary}}{F_{viscous}}$	Fluid-Rock Interaction depicting entrapment at pore scale
	Gravity Number	$N_G = \frac{F_{gravity}}{F_{viscous}}$	Fluid-reservoir shape dependent, capturing the effect of buoyancy force

3.4.2 Dimensional Analysis of the Gravity Stable Gas Injection Process

Traditionally, the dimensional analysis has been an extremely utilitarian tool for scaling of the laboratory experiments to field scale and vice versa. The fluid flow literature shows two distinct possible procedures for obtaining different dimensionless numbers for a given system. Basic fluid mechanics literature (Johnson, 1998; Fox and McDonald, 1998) advocates the use of dimensional analysis (DA), while the porous media fluid mechanics studies (Shook et al., 1992) recommend the inspectional analysis (IA). The IA procedure was reported in previously, and this report focuses on dimensional analysis of the gravity stable gas injection processes.

Dimensional analysis is a powerful tool that can be used to reduce the number of experimental variables required for the adequate description of the relationship among these variables. In many applications of science and engineering, especially experimental work, the mathematical relationship between the variables of a system is unknown (Chandler, 2003). Experimental evaluation and verification of all the variables is not feasible or sometimes even impossible.

Studies for dimensional analysis and model studies of gravity drainage applications are sparse. Geertsma et al.'s (1955) derivation of dimensionless groups via inspectional analysis is important in that it not only generates dimensionless groups for solvent injection, but also helps generate a connecting link between dimensionless groups in other engineering sciences (such as Chemical and Mechanical engineering) and porous media flow. Further consideration of the Geertsma et al.'s correlation, from the gravity drainage perspective, suggests that six commonly used dimensionless groups could also play a role in gravity drainage flow characterization, namely Reynolds, Schmidt, Weber, Froude, Lewis and Grashoff groups.

Gravity drainage studies by Edwards et al. (1998) show that at least two dimensionless groups can be examined to help portray the importance of capillary forces on the gravity drainage process, namely the Dombrowski-Brownell number (Equation 3.16) and macroscopic bond number (defined as Equation 3.17). The D-B number can be interpreted as a microscopic Bond number.

$$N_{DB} = \frac{\Delta\rho g k}{\sigma} \qquad (3.16)$$

Where $\Delta\rho$ = fluid density difference, g is gravitational constant, k is permeability and σ is interfacial tension.

$$N_B = \frac{\Delta\rho g l^2}{\sigma\sqrt{\phi/k}} \qquad (3.17)$$

Where, Δρ is the difference between the displacing and displaced phase, g is the gravity, l is the characteristic length (represented by the grain diameter), σ is the interfacial tension, ϕ being the porosity and k the reservoir permeability.

Grattoni et al. (2001) studied the gas invasion under gravity-dominated conditions, to study the effects of wettability and water saturation on three-phase flow. Analysis of the results using dimensionless groups helped define a new dimensionless group by combination of the effects of gravity and viscous to capillary forces. This study shows that in addition to the Bond and Capillary numbers, the Gravity number plays a major role for the characterization of gravity drainage flow.

The capillary number (Grattoni et al., 2001) describes the balance between viscous and capillary forces and is defined as Equation 3.18, while the Bond number measures the relative strength of gravity (buoyancy) and capillary forces (Grattoni et al., 2000) as described by Equation 3.17. Equation 3.19 below defines the gravity number.

$$N_C = \frac{v\mu}{P_C R_A} 2Cos\theta \quad \text{(3.18)}$$

Where, v is the Darcy velocity, μ is the viscosity of the displacing phase, σ is the interfacial tension, θ being the contact angle and R_A the average pore throat radius.

$$N_G = \frac{\Delta\rho g k}{\Delta\mu u} \quad \text{(3.19)}$$

Where, Δρ is the difference between the displacing and displaced phase, g is the gravity, k is the reservoir permeability and u being the Darcy velocity.

There has been limited work done on characterization or dimensionless analysis for the gravity drainage fluid flow; hence, dimensional analysis was conducted using the Buckingham-Pi approach. Buckingham's Pi theorem states that 'physical laws are independent of the form of the units, hence quantification and generalization of most mathematical relationships used to describe a physical phenomenon is best expressed in a dimensionless form'. This analysis becomes especially necessary for better understanding and performance prediction of novel – newer processes like the GAGD. The procedure of analysis has been documented and available elsewhere (Lui, 2003). The dependant and independent variables used in this analysis are shown in Table 3.6 along with their fundamental dimensions.

The various dimensionless groups obtained after the analysis are included as Table 3.7. It is important to note that the Buckingham-Pi analysis does not rank the dimensionless groups obtained in order of relative importance as controlling variables of the process. Experimentation and inspectional analysis are required to further characterize the controlling groups of variable(s) in gravity stable gas injection processes.

Table 3.6: Dependant and Independent Variables used for Buckingham-Pi Analysis

Variable	Dimensions	Variable	Dimensions	Variable	Dimensions
Porosity (ϕ)	$[M^0.L^0.T^0]$	Length per Thickness (L/T) or Radius per Thickness (R/T)	$[M^0.L^0.T^0]$	Reservoir Absolute Permeability (k)	$[M^2.L^0.T^0]$
Reservoir Horizontal Permeability (k_h)	$[M^2.L^0.T^0]$	Ratio of Vertical to Horizontal Permeability (k_v/k_h)	$[M^0.L^0.T^0]$	Gas Injection Pressure (P_{IG})	$[M^1.L^{-1}.T^{-2}]$
Reservoir Pressure (P_R)	$[M^1.L^{-1}.T^{-2}]$	Minimum Miscibility Pressure (MMP)	$[M^1.L^{-1}.T^{-2}]$	Gravity Force (g)	$[M^1.L^0.T^{-2}]$
Velocity (V)	$[M^1.L^0.T^{-1}]$	Injector Flow Rate (Q_I)	$[M^3.L^0.T^{-1}]$	Producer Flow Rate (Q_P)	$[M^3.L^0.T^{-1}]$
Gas Viscosity (μ_g)	$[M^1.L^{-5}.T^1]$	Oil Viscosity (μ_o)	$[M^1.L^{-5}.T^1]$	Capillary Pressure (P_C)	$[M^1.L^{-1}.T^{-2}]$
Oil-Water Interfacial Tension (σ_{OW})	$[M^1.L^1.T^{-2}]$	Water-Gas Interfacial Tension (σ_{WG})	$[M^1.L^1.T^{-2}]$	Oil-Gas Interfacial Tension (σ_{OG})	$[M^1.L^1.T^{-2}]$
Waterflood Residual Oil Saturation (S_{OR})	$[M^0.L^0.T^0]$	Connate Water Saturation (S_{WC})	$[M^0.L^0.T^0]$	Time (T)	$[M^0.L^0.T^1]$

Table 3.7: Dimensionless Groups Obtained Using Buckingham-Pi Analysis

No.	D. L. Group	No.	D. L. Group	No.	D. L. Group
1	ϕ	8	Q_P/Q_I	15	S_{OR}
2	L/R	9	$\dfrac{\mu_g.g^{(0.6)}}{Q_I^{(0.2)}.P_R}$	16	S_{WC}
3	k_v/k_h	10	P_C/P_R	17	$\dfrac{T.g^{(0.6)}}{Q_I^{(0.2)}.P_R}$
4	$\dfrac{k_h.g^{(0.4)}}{Q_I^{(0.8)}}$	11	$\dfrac{\mu_o.g^{(0.6)}}{Q_I^{(0.2)}.P_R}$	18	$(MMP)/P_R$
5	$\dfrac{k.g^{(0.4)}}{Q_I^{(0.8)}}$	12	$\dfrac{\sigma_{OW}.g^{(0.2)}}{Q_I^{(0.4)}.P_R}$	19	$\dfrac{\Delta\rho.g^{(0.8)}.Q_I^{(0.4)}}{P_R}$
6	P_{IG}/P_R	13	$\dfrac{\sigma_{WG}.g^{(0.2)}}{Q_I^{(0.4)}.P_R}$		
7	$\dfrac{V}{g^{(0.4)}.Q_I^{(0.2)}}$	14	$\dfrac{\sigma_{OG}.g^{(0.2)}}{Q_I^{(0.4)}.P_R}$		

3.4.3 Dimensionless Number(s) Governing Gravity Stable Gas Injection

Dimensional analysis and literature review above suggests that the most important dimensionless groups governing the gravity stable gas injection are the Capillary number (N_C) and the Bond number (N_B). The microscopic Bond number, namely the Dombrowski – Brownell number (N_{DB}) could be a good parameter for displacement characterizations especially in gas injections where the microscopic sweeps are significantly high.

The N_C and N_B cover the major spectrum of the forces existing in the reservoir for oil recovery, namely the buoyancy forces, viscous forces and capillary forces. These along with the microscopic Bond number (N_{DB}) would help in definite characterization of the flow regimes and governing force(s) in field as well as laboratory displacements. The Gravity number (N_G) and the New Group (N) by Grattoni et al. (2001) are nothing but different combinations of the Capillary and Bond numbers incorporating a scaling parameter for better displacement characterizations and appear to be good augmentations for scale-up and finer characterizations.

3.5 Dimensional Similarity Approach for Experimental Design

This review shows that the five dimensionless numbers recommended for the characterization of the gravity drainage field projects (Kulkarni, 2004) provide adequate reservoir mechanics information. Literature review and dimensional analysis further advocate the dimensional similarity based experimental design. To facilitate this design, the five dimensionless groups were calculated for each of the gravity stable field projects studied (Table 3.3). The ranges of these dimensionless quantities were obtained and were attempted to be duplicated in the laboratory through proper fluids and operating conditions selection. This section summarizes the detailed calculation of the dimensionless numbers for the field cases and the resulting experimental design.

3.5.1 Calculation of Dimensionless Numbers for Field Projects

Nine commercial gas gravity drainage field applications were extensively studied and summarized for the identification and characterization of various multiphase mechanisms, fluid dynamics and calculation of the range of various dimensionless groups applicable to GAGD process. The detailed calculation protocol is included as Figure 3.4, while step-wise calculations for one commercial immiscible gravity drainage field project (West Hackberry Field, Louisiana) is included as Appendix A to this report.

Calculation of these dimensionless numbers for field projects involved the use of various well logs (for thickness, net-to-gross values, OWC, GOC and grain size), field maps (for Darcy velocity), use of grain size classification systems (for Bond number), production / injection data (for New Grattoni et al. (2001) group), bottom hole pressure survey plots (for PVT simulations), compositions of injected / produced fluids (for PVT simulations), and PVT compositional simulations (for fluid properties predictions).

It is important to note that all these five dimensionless groups are not applicable to miscible fluid injection mainly due to the absence of interfacial tension (IFT) and density / viscosity contrasts between displacing and displaced reservoir fluids. Definition of new dimensionless groups governing miscible flood behavior is necessary due to the increasing commercial trends toward miscible injections. Hence to facilitate the calculation of various dimensionless groups in miscible field cases, appropriate modifications to the definition of dimensionless numbers to reflect the reservoir physics using the following assumptions were employed:

1. Miscibility is achieved when the value of interfacial tension (IFT) between injected gas and reservoir oil reaches 0.001 dynes/cm.
2. There are no density / viscosity contrasts between injected gas and reservoir oil in the 'mixing-zone'.
3. Hence the $\Delta\rho$ and $\Delta\mu$ terms can be replaced by ρ_{avg} and μ_{avg} respectively.
4. The characteristic length term for the concerned reservoir can be expressed as a square root of the ratio of absolute permeability to porosity.

The complete ranges of dimensionless groups for all the commercial gravity drainage projects is included as Table 3.9 below, and plotted as Figure 3.5.

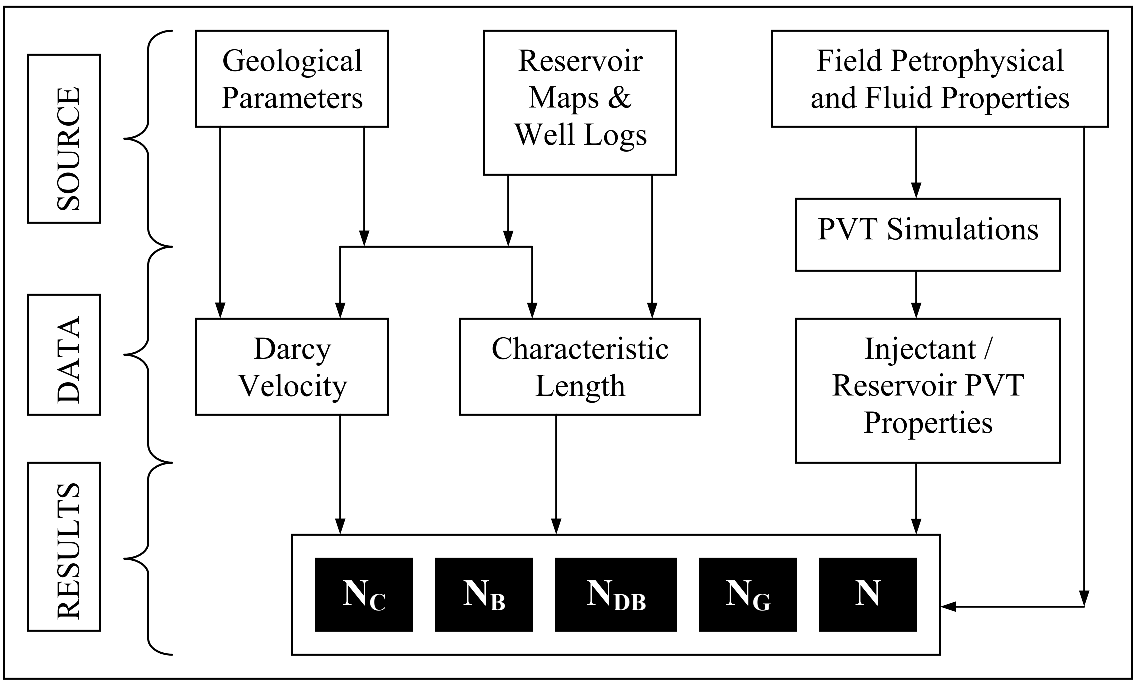

Figure 3.4: Protocol for Calculation of Dimensionless Groups for Field Cases

- **Calculation of Dimensionless Numbers for Field Projects – A Case Study**

Of the several field cases considered, calculation of dimensionless numbers for the West Hackberry tertiary air injection project is included here as an example case. The West Hackberry tertiary air injection project was a joint initiation by United States Department of Energy, Amoco Production Co. and Louisiana State University to demonstrate the feasibility of air injection in Gulf coast reservoirs with pronounced bed-dip via the Double Displacement Process (DDP) in 1993. The range of calculated dimensionless numbers for this project is included as Table 3.8. Calculation of these numbers involve the use of various well logs (for thickness, net-to-gross values, OWC, GOC and grain size), field maps (for Darcy velocity), use of grain size classification systems (for Bond number), production / injection data (for New Grattoni et al. (2001) group), bottom hole pressure survey plots (for PVT simulations), compositions of injected / produced fluids (for PVT simulations), and PVT simulations (for fluid properties predictions). Further detailed calculations and methodology are included as Appendix A of this report.

Table 3.8: Values of Dimensionless Groups Operating in West Hackberry Field

Number	Formula	Min. Value	Max. Value
Capillary Number	$N_C = \dfrac{V(m/s) * \mu(Pa.S)}{\sigma(N/m)}$	4.564E-09	4.1798E-08
Bond Number	$N_B = \dfrac{\Delta\rho(kg/m^3) * g(m/s^2) * l^2(m^2)}{\sigma(N/m)}$	0.03171	1.5932
Dombrowski-Brownell Number	$N_{DB} = \dfrac{\Delta\rho(kg/m^3).g(m/s^2).k(m^2)}{\sigma(N/m)}$	1.5024E-07	7.833E-07
Gravity Number	$N_G = \dfrac{\Delta\rho(kg/m^3).g(m/s^2).k(m^2)}{\Delta\mu(Pa.s).u(m/s)}$	0.3855	1.5932
New Group of Grattoni et al., (2001)	$N = N_B + A(\dfrac{\mu_D(Pa.s)}{\mu_G(Pa.s)}).N_C$	0.0361	1.627

- **Important Conclusions from these Calculations – Example Case Study**

The plots of operating Bond, Capillary, Dombrowski-Brownell, Gravity and N groups (by Grattoni et al. (2001)) for West Hackberry field are included in Appendix A. The ranges of operating bottom hole pressures (BHP) for West Hackberry field are 2400 psi – 3400 psi. For this range, the Capillary number is a weak function of the reservoir Darcy velocity but the Bond number shows a strong dependence of mean reservoir grain diameter. Hence, reservoir heterogeneity would become important parameter determining the overall displacement characteristics. The microscopic Bond number –Dombrowski – Brownell number and N group exhibit similar dependence on reservoir permeability and grain size distribution respectively. However, the Gravity number does not show significant dependence on grain size distribution and / or reservoir permeability. These groups are instead seen as strong functions of Darcy velocity.

The results indicate that these dimensionless numbers can be weakly characterized into two groups: (i) Petrophysical parameter(s) dependent groups – N_B, N and N_{DB} (which are characterized by reservoir permeability, porosity, grain size distribution and tortuosity) and (ii) Operational parameter(s) dependent groups – N_C, and N_G (which are characterized by injection pressures, rates, and other production parameters). It is anticipated that similar trends would be observed for other field studies, and the ranges of the dimensionless numbers shall be used for experimental design.

It is important to note that all these five dimensionless groups are not valid for miscible fluid injection mainly due to the absence of interfacial tension (IFT) and density / viscosity contrasts. Definition of new dimensionless groups governing miscible flood behavior was completed using various simplifying assumptions (elucidated above), due to this phenomenon and the increasing commercial trends toward miscible injections.

The dimensionless groups used to characterize field scale displacements and their laboratory extensions can be roughly divided into five types (Stalkup Jr., 1983): (i) Geometry (like L/H or L/W and Dip-angle), (ii) Viscous to gravity ratio (however these are not applicable to miscible displacements since the $\Delta\rho$ term is zero), (iii) Boundary and initial conditions, (iv) Fluid properties (μ_m/μ_s, dimensionless density (ρ_m-ρ_s/ρ_o-ρ_s), dimensionless diffusion coefficient (D_m-D_s/D_o-D_s)) and (v) Scale effects of mixing or microscopic dispersion (like transverse and longitudinal mixing groups).

The field project characterization(s) should be primarily based on the operating Bond, Capillary, Dombrowski-Brownell, Gravity and N groups (by Grattoni et al. (2001)). Furthermore, it is important to note that none of the dimensionless groups governing the gravity drainage process contain the macroscopic length term i.e. displacement characteristics are independent of the length of the porous medium. Hence, experimentation on 1-ft Berea cores would be as effective and comparable as 6-ft Berea; thus de-emphasizing the need to conduct all the experiments on 6-ft Berea cores.

3.5.2 Calculation of Dimensionless Numbers for Laboratory Core Displacements

The dimensionless groups Bond, Capillary, Dombrowski-Brownell, Gravity and N groups (by Grattoni et al. (2001)) were calculated for the GAGD corefloods (completed as well as planned) at the LSU – EOR Lab. The ranges of the dimensionless numbers for both laboratory and field projects are tabulated as Table 3.9 and plotted as Figure 3.5.

It is observed that values of the dimensionless numbers for laboratory corefloods as well as the unscaled physical model (Task 1 of the DOE Proposal) values lie within the field ranges. This clearly indicates that we are able to ‘mimic’ the various multiphase mechanisms and fluid dynamics operating in the field into the laboratory, and that the results of all the experiments planned (and completed) are ‘translatable’ to the field.

Therefore from a mechanistic point of view – the planned experiments are ‘scaled’. On the other hand, apart from scaling the laboratory corefloods, the important multiphase mechanisms and fluid dynamics need to be designed. The following section details on the mechanistic and fluid dynamic experimental design of the ‘scaled’ laboratory experiments.

Table 3.9: Comparison of Dimensionless Numbers for Field and Lab Applications

Dim. Groups		Field Range		Physical Model		Corefloods		
		IMM	*MIS*	*Para*	*nC10*	*Type*	*1-ft*	*6-ft*
N_C	*Min*	4.18E-08	1.84E-05			*IMM*	2.59E-06	2.59E-09
	Max	1.12E-09	1.83E-06	9.28E-09	6.92E-09	*MIS*	2.57E-04	2.57E-04
N_B	*Min*	1.21E-05	5.77E-02			*IMM*	1.64E-06	7.72E-07
	Max	2.84E-07	3.01E-03	1.48E-04	4.16E-05	*MIS*	1.70E-02	7.88E-03
N_{DB}	*Min*	3.14E-06	6.31E-03			*IMM*	3.09E-07	1.68E-07
	Max	1.50E-07	2.56E-04	1.23E+00	4.80E+01	*MIS*	3.15E-03	1.71E-03
N_G	*Min*	8.75E+02	2.96E+02			*IMM*	1.17E+01	6.38E+00
	Max	3.85E-01	1.62E+00	1.48E-04	3.90E-05	*MIS*	1.22E+01	6.66E+00
N	*Min*	-6.89E-05	-2.30E+00			*IMM*	-4.96E-04	-4.97E-04
	Max	-2.42E-03	-3.00E+00	6.17E-05	1.53E-05	*IMM*	-4.41E+00	-4.42E+00

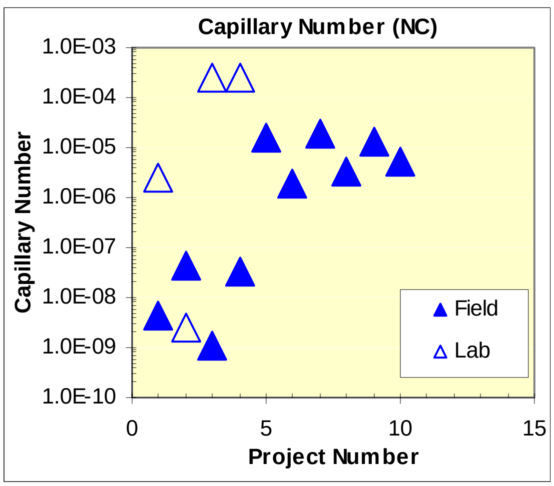

(a) Capillary Number Comparison

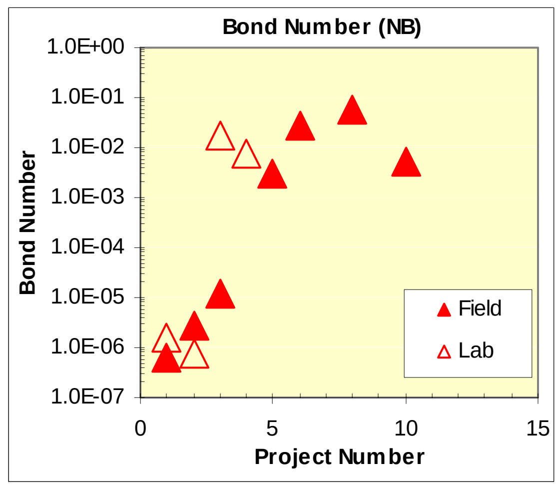

(b) Bond Number Comparison

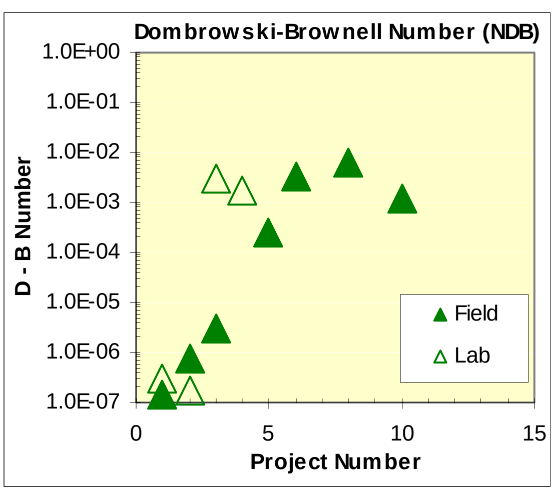

(c) D – B Number Comparison

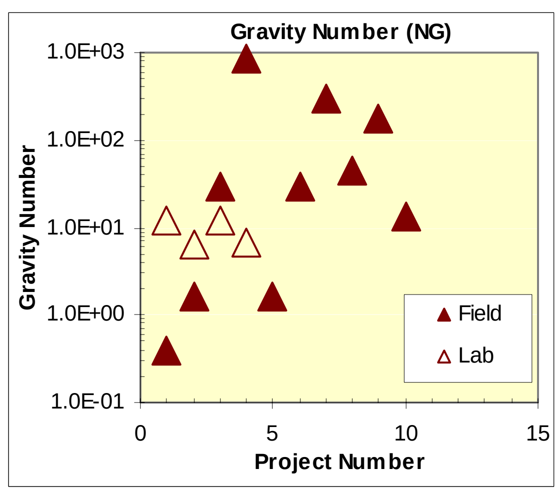

(d) Gravity Number Comparison

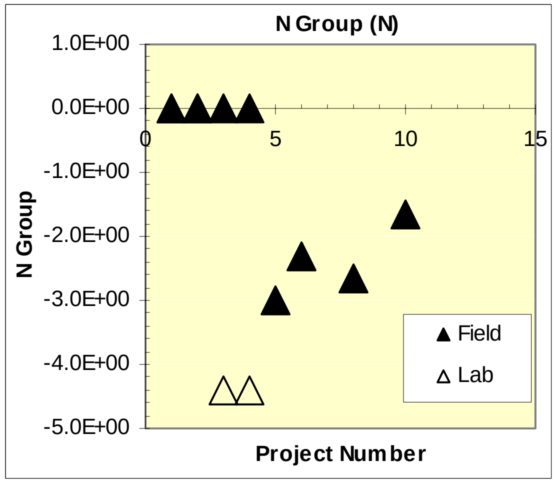

(e) N Group[30] Comparison

Figure 3.5: Graphical Comparison of Values of Dimensionless Groups Calculated for Field and Laboratory Cases

3.5.3 Flow Regime Characterization of Gas Assisted Gravity Drainage Applications

Flow regime characterization is important for the elucidation of operating fluid mechanics during gravity drainage, and is also helpful in designing efficient gas injection programs in commercial floods. Localized variations in the capillary forces, due to pore scale heterogeneities, result in non piston-like (Buckley-Leverett type) displacements, called 'capillary fingering' (Aker, 1996). On the other hand, the viscous forces act across the fluids at all length scales, and combined with mobility ratio, are responsible for the viscous fingering. The percolation model visual photographs depicting the various flow regimes (placed adjacent to the Lenormand et al.'s (1988) plot) are shown as Figure 3.6(a) below (Sukop and Or, 2003).

The Lenormand et al.'s (1988) for flow regime characterization diagram was used to determine the flow regimes dominant during gas-gravity drainage laboratory as well as field applications studied and planned in course of this study (Kulkarni, 2004). This diagram was chosen due to its relatively simple nature and minimal simulation requirements for flow regime determination. Dimensionless numbers for both planned miscible / immiscible GAGD laboratory (both 1-ft and 6-ft Berea) coreflood experiments as well as the field Gas assisted gravity drainage applications studied for determining experimental design, were calculated and superimposed on the digitized Lenormand et al.'s (1988) plot. This data is included as Figure 3.6(b).

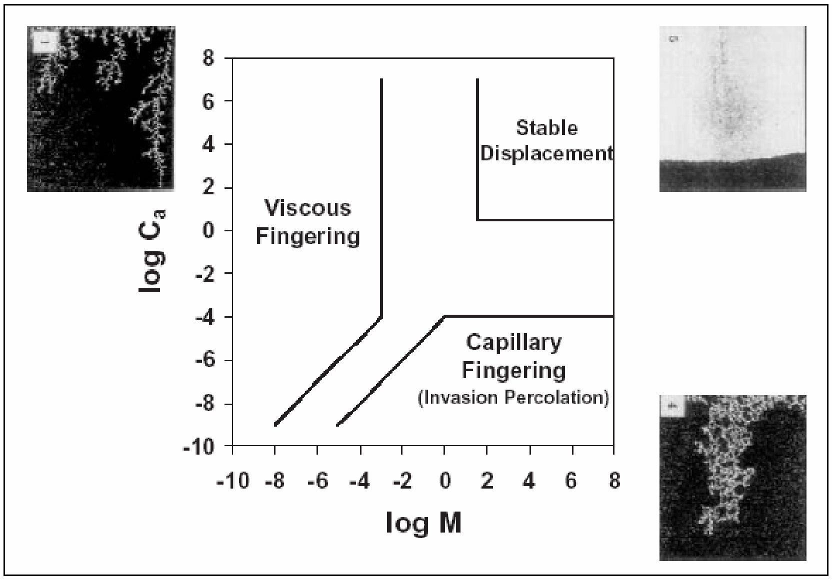

(a) Lenormand et al's Plot Superimposed with Lattice Boltzmann Percolation Model Photographs (Sukop and Or, 2003).

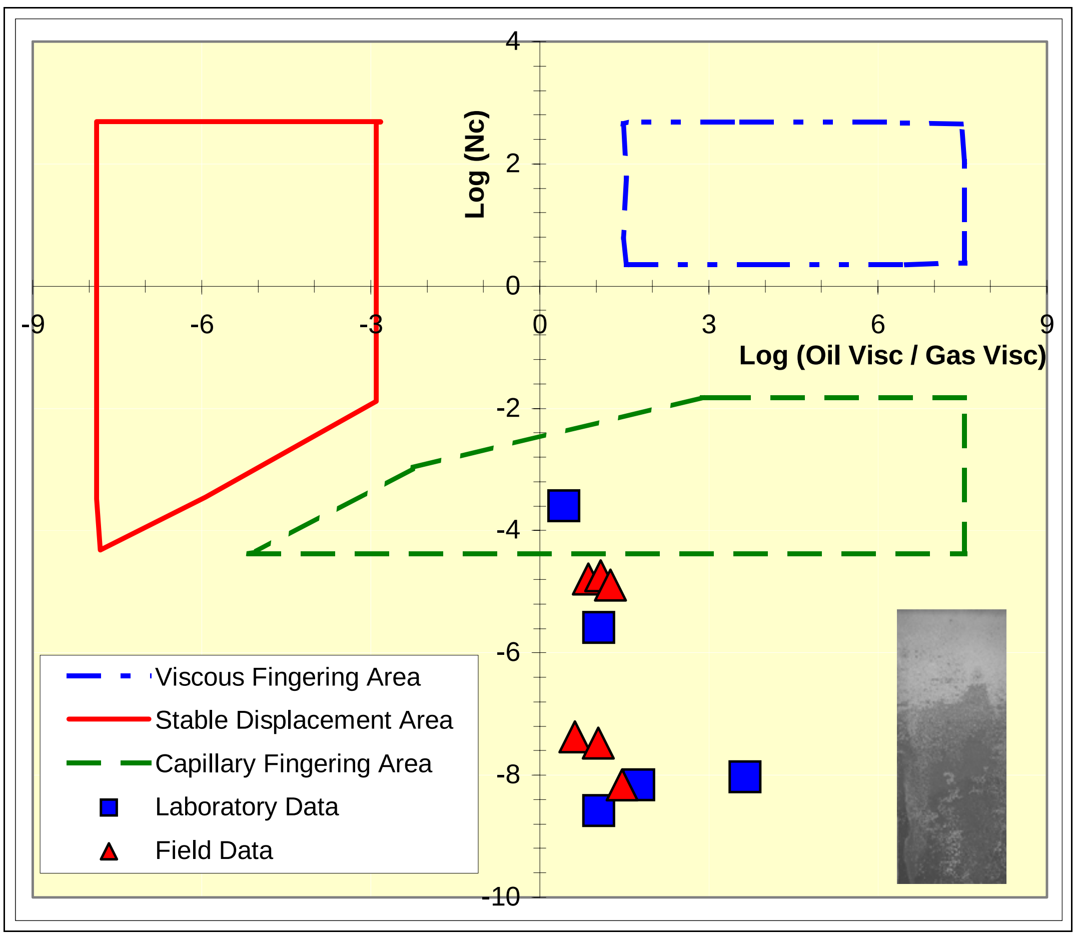

(b) Digitized Lenormand et al's (1988) Plot Superimposed with LSU Field and Lab Data (Photograph on the bottom right indicates similar observations to Sukop and Or, 2003)

Figure 3.6: Flow Regime Characterizations for Laboratory and Field Applications

Figure 3.6(b) shows that the flow regimes indicated by Lenormand et al.'s (1988) plot for the GAGD experiments, are relevant and that the capillary fingering type flow regime exists in these experiments as reported in report number 15323R04, Jan 2004 (Picture of capillary fingers observed in the physical model is shown on the bottom right of Figure 3.6(b)).

Figure 3.6 further reinforces the fact that the multiphase mechanisms and fluid dynamics operational in the field could be effectively duplicated in the laboratory by proper fluid and experimental condition selections. Although clear distinctions within the flow regimens that are operational during the various laboratory and field gravity drainage applications studied (Kulkarni, 2004) are not seen from Figure 3.6(b), the Lenormand et al.'s (1988) plot provides with some indicators toward the type of flow regimes that could be dominant during these applications.

Since the laboratory experiments are designed to be in the stable flow regimes (via the Leas and Rappaport, Dumore and Rutherford criteria); combination of these criteria with the Lenormand et al.'s (1988) plot suggests that although all the displacements considered are below the critical rates (hence stable), the capillary fingering phenomenon is also operational during these displacements.

The relation between the capillary number and the viscosity ratio for these applications was investigated by expanding the fourth quadrant of the Lenormand et al's (1988) plot (Figure 3.6(b)), as shown in Figure 3.7. It should be noted that all the field and laboratory data are obtained with widely varying reservoir, fluid and geographical characteristics. Even then, there appears to be a reasonable correlation between the laboratory data, and the field data lie close to this curve.

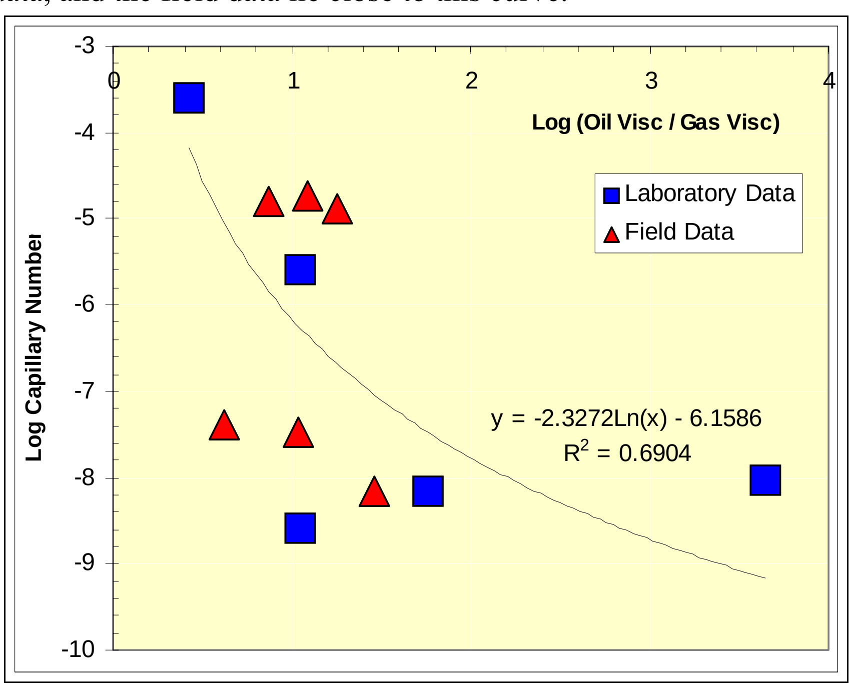

Figure 3.7: Plot Showing Relationship between N_C and Viscosity Ratio

3.5.4 Experimental Design Strategy

This section summarizes the isolation and characterization of various multiphase mechanisms and fluid dynamics duplicated from commercial gravity stable gas injection floods to the laboratory.

- **Experimental Design Considerations**

The important parameters to be considered in the experimental design are: miscibility development, effect of spreading coefficient, reservoir heterogeneity, reservoir wettability considerations, injectant type and mode(s) of injection.

➢ **Miscibility Considerations**

Important miscibility considerations while development of the new GAGD process shall be addressed by conducting miscible and immiscible GAGD floods on 1-ft Berea cores using Yates reservoir brine, n-Decane and CO_2.

➢ **Effect of Spreading Coefficient**

Laboratory and theoretical studies (Section 3.1) demonstrate that a positive spreading coefficient in strongly water-wet systems results in significantly high gravity drainage recoveries. Winprop simulations for the n-Decane, Water, and CO_2 fluid triplets show that a positive spreading coefficient results for the coreflood conditions being employed in the LSU-EOR laboratory. The values are summarized as Table 3.10.

Table 3.10: Spreading Coefficients for n-Decane, Water, and CO_2 fluid triplets

$nC_{10}/H_2O/CO_2$	$\sigma_{G/W}$ (dy/cm)	$\sigma_{G/O}$ (dy/cm)	$\sigma_{W/O}$ (dy/cm)	Spreading Coeff.
500 psia / 76 F	17.5074	8.7268	0.0044	**(+)** 8.78
2500 psia / 76 F	0.3279	0.0000	0.0031	**(+)** 0.3248

To study the effects of a negative spreading on oil recovery in water wet porous media, following three chemicals are being considered as the 'oleic' phase: Aniline, Carbon Tetrachloride and Isopropyl Acetate. The various properties for the three chemicals are included as Table 3.11 below.

Table 3.11: Aniline, Carbon Tetrachloride & Isopropyl Acetate Properties with CO_2 and Water

Property / Chemical	Aniline	Carbon Tetrachloride	Isopropyl Acetate
P & T Conditions	500 psi & 76 ^oF	500 psi & 76 ^oF	500 psi & 76 ^oF
Chemical Formula	C_6H_7N	CCl_4	$C_5H_{10}O_2$
Molecular Weight	93.1	153.8	102.1
Normal Boiling pt	363.2 ^oF	169.7 ^oF	192.2 ^oF
Specific Gravity	1.02	1.59	0.88
Water Solubility	3.4 gm / 100 ml	0.1 gm / 100 ml	4.3 gm / 100 ml
$\sigma_{G/W}$ (dynes/cm)	17.5074	17.5074	17.5074
$\sigma_{G/O}$ (dynes/cm)	91.4017	4018.3194	36.8204

$\sigma_{W/O}$ (dynes/cm)	2.8867	1627.9867	0.1899
$S = \sigma_{G/W} - \sigma_{G/O} - \sigma_{W/O}$ (dynes/cm)	(-) 76.78	(-) 5628.7987	(-) 19.5029

It is interesting to note that Isopropyl Acetate has moderate solubility in water and it exhibits negative spreading coefficient at 500 psia and 76 ^oF, however this first contact miscibility is achieved at 730+ psia system pressure and the spreading coefficient is positive at 2500 psia and 76 ^oF.

$S = \sigma_{G/W} - \sigma_{G/O} - \sigma_{W/O}$……@ 2500 psia & 76 F…………………………….……....(3.20)

$S = 0.3279 – 0.0 – 0.2377$

$\boxed{\mathbf{S = (+)\ 0.0902\ dynes/cm}}$.

Hence, coreflood experiments at these two conditions would help quantification of the spreading coefficient effects on GAGD process.

- **Effect of Reservoir Heterogeneity and Wettability**

Miscible and immiscible GAGD experiments would be conducted using Yates reservoir fluids on 1-ft Berea sandstone cores and Yates reservoir cores. Berea sandstone being homogeneous and strongly water wet would provide as a base case to compare GAGD performance against the GAGD floods in highly fractured, heterogeneous and oil wet to mixed wet Yates reservoir cores. Furthermore miscible and immiscible GAGD floods using n-Decane, Yates brine and CO_2 would help quantify the effects of miscibility relative to the spreading coefficient.

- **Injectant Fluid Type**

The recent spotlight on CO_2 sequestration makes CO_2 an ideal injectant in U.S. scenario (Kulkarni, 2003). Furthermore, the GAGD process could be highly appropriate for EOR applications offshore where limited facilities for processing / transport of produced natural gas exists. Hydrocarbon GAGD would be a boon in any producing oil field where ample and cheap natural gas is available. Both miscible and immiscible GAGD floods would be conducted using CO_2 injectant. However, only immiscible hydrocarbon GAGD floods would be conducted due to the complex mass-transfer effects involved in miscible HC slug design and displacement.

- **Injection Mode**

Farouq Ali (2003) suggests that one of the main reasons for failures of miscible gas injection flood is its application in tertiary mode, wherein significant quantities of water need to be displaced and also the injected solvent (e.g. CO_2) is lost into the reservoir brine. Furthermore, the horizontal well near the bottom of the pay zone in the GAGD process would most likely produce significant quantities of water initially due to gravity segregation and significant free water saturation. Hence application of the GAGD process in a secondary mode could also be of considerable importance.

- **Experimental Flow Chart**

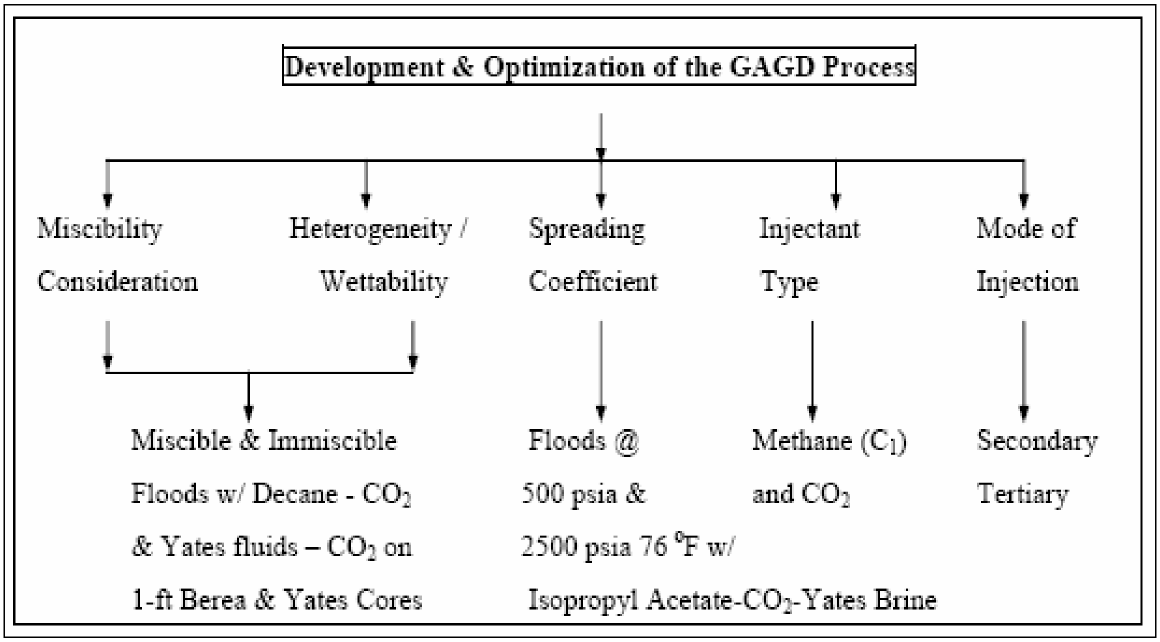

Figure 3.8: Experimental Flow Chart

3.5.5 Experimental Apparatus, Protocol, and Scope

- **Experimental Apparatus**

The vertical coreflooding system schematic that would be used for unsteady state GAGD experimentation is shown below as Figure 3.9.

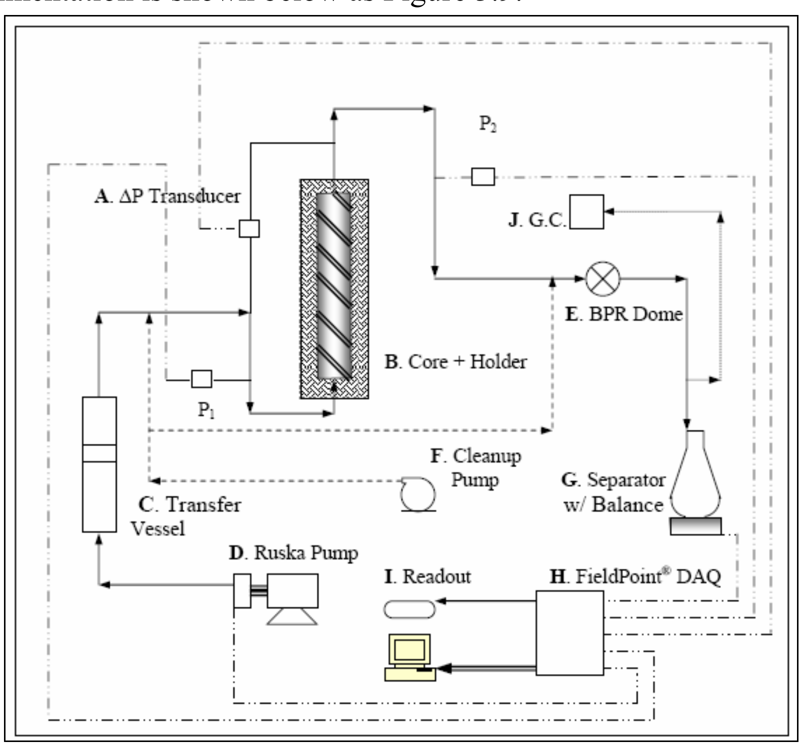

Figure 3.9: Vertical Core Flooding System Schematic

Legend for the above schematic:

- .... : Electrical Lines
- –··–··–··– : Instrumentation Lines
- ———————— : 1/8" High Pressure Piping
- - - - - - - - - - - - : Cleanup / Accessories Lines

Analytical grade chemicals (illustrated in the previous section) shall be used for the experimentation to conduct unsteady state gas injection coreflood experiments in Berea sandstone as well as Yates field cores. The tertiary mode experimental protocol consists of: absolute permeability determination, oil flooding to achieve connate water saturations, waterflooding as secondary recovery process and tertiary gas injection as EOR process. The secondary mode experimental protocol consists of all the above steps except the tertiary EOR process would replace the secondary waterflood. The detailed experimental protocol is available elsewhere (Kulkarni, 2003).

- **Research Scope**

The scope of this study shall be limited to the experimental flow chart depicted in Figure 3.8. Majority of the experimentation shall be conducted employing Yates reservoir fluids, n-Decane, in 1-ft Berea cores as the porous media. Since all the dimensionless numbers calculated are independent of the length of the porous medium, limited experimentation, if dictated by results from the future experimental results, on 6-ft Berea sandstone cores shall be completed. Reservoir condition scaled experiments using Yates reservoir fluid and Yates field cores shall be conducted to study the influence of parameters specified in the experimental design. Further, all the GAGD experiments shall be conducted using pure CO_2 as injectant; whereas pure Methane (CH_4) shall be employed as injected for the study of injectant type in immiscible mode only using 1-ft Berea cores.

3.6 Continued CGI / WAG Experimentation

The literature review completed on gas injection EOR processes coupled with the results of previous horizontal mode CGI / WAG experimentation (reported in the earlier reports to DOE, namely 15323R01, Apr 2003; 15323R02, Jul 2003; and 15323R03, Oct 2003) suggested further investigation of five specific parameters.

The additional experimentation required for confident characterization (as well as provide a fair comparison with the planned GAGD floods) of horizontal mode CGI / WAG corefloods were: (i) Effect of core length on horizontal mode tertiary oil recovery, (ii) Effect of CO_2-brine saturation (in secondary waterfloods as well as tertiary WAG (previously reported)) on horizontal mode oil recovery, (iii) Experimental investigation of the 'Happy-Medium' between CGI and WAG floods (in both secondary and tertiary injection modes), (iv) Effect of secondary mode gas injection on horizontal mode oil recovery and (v) Theoretical characterization of possible flow regimes dominant during gas injection EOR studies (both in the laboratory as well as commercial field applications).

To facilitate these investigations the following coreflood experiments ('scaled' to field scale commercial floods using dimensional similarity approach) were planned:

1. Effect of core length: Immiscible CGI and WAG coreflood experiments on 1-ft long Berea cores using 5% NaCl brine and n-Decane (experiments 1 and 2 reported in 15323R02, July 2003 report to DOE) are to be repeated at similar conditions (500 psia backpressure and 82 ^oF) on 6-ft long Berea cores.
2. Effect of secondary mode CO_2-brine saturation: Use of CO_2 saturated brine in secondary mode (for waterflooding) in immiscible CGI (n-Decane and Yates reservoir brine system) coreflood.
3. Effect of tertiary mode CO_2-brine saturation: Use of CO_2 saturated brine in tertiary mode in miscible WAG (n-Decane and Yates reservoir brine system) coreflood (previously reported in 15323R03, Oct 2003).
4. Experimental investigation of the 'Happy-Medium' between CGI and WAG: Conducting miscible 'Hybrid-WAG' type experiments – CGI up to 0.7 pore volume followed by 1:1 WAG.
5. Effect of secondary mode gas injection on horizontal mode oil recovery: Conducting two secondary mode miscible CGI and WAG coreflood experiments using Yates reservoir brine and n-Decane.

The characterization of possible flow regimes dominant during gas injection EOR studies (both in the laboratory as well as commercial field applications) is reported in Section 3.5.3 of this report, while this section summarizes the coreflood experiments completed in this reporting year.

3.6.1 WAG and CGI Experimentation on 6-ft Berea Core

Immiscible CGI and WAG experiments on 1-ft long Berea cores using 5% NaCl brine and n-Decane (experiments 1 and 2 reported in 15323R02, July 2003 report to DOE) were repeated at similar conditions (500 psia backpressure and 82 ^oF) on 6-ft long Berea cores to study the effects of length on tertiary recovery for n-Decane / 5% NaCl brine system.

Figure 3.10 (a, b) show almost identical tertiary recovery trends for CGI and WAG floods and comparable final oil recoveries for the short (1-ft) corefloods. Mitigation of gravity segregation, and the consequent improvements in flood profile control and recoveries due to WAG employment are not apparent from the short core (1-ft) recovery plots.

However, the CGI recoveries differ significantly from WAG for 6-ft Berea (33.5% and 54.4%, respectively) floods, suggesting the amplification of gravity segregation effects in the long cores. These results clearly indicate that long core tests are not only appropriate and useful but also essential to examine the effectiveness of the horizontal mode CGI and WAG processes.

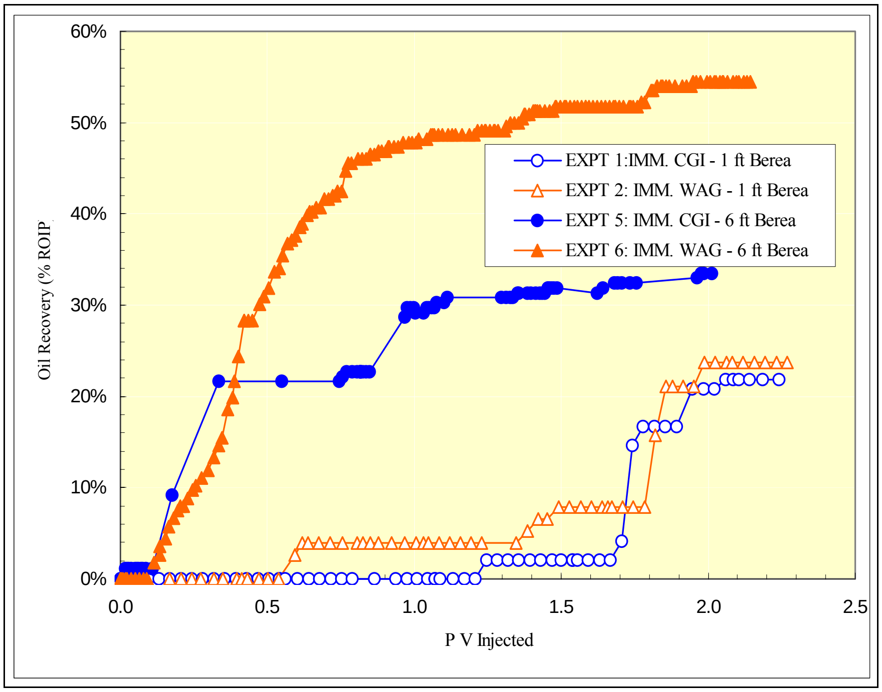

(a): Recovery in Percent of ROIP

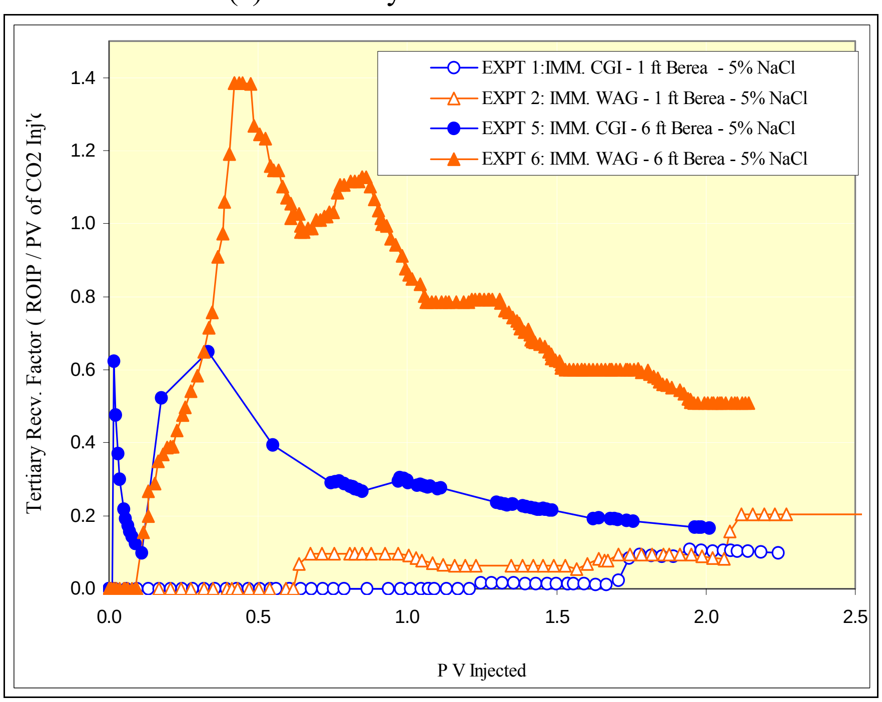

(b): Recovery As Fraction of Residual Oil In Place Per PV of CO_2 Injected

Figure 3.10: Effect of Core length on Tertiary Recovery: n-Decane - 5% NaCl Brine

3.6.2 Secondary WAG and CGI Corefloods

- **Secondary Miscible CGI Flood**

A secondary mode miscible CGI flood (using n-Decane, Yates reservoir brine and CO_2) has been completed and the results are summarized in Figure 3.11 below. As expected, the miscible CGI recoveries were excellent (94.4%) and the TRF plot shifted to the left indicating higher and quicker recoveries per unit volume of injectant, compared to those of tertiary floods, discussed below. No delays in oil breakthrough were observed, and no water was produced during the entire flood, indicating the connate water to be essentially immobile and the water shielding effect to be minimal.

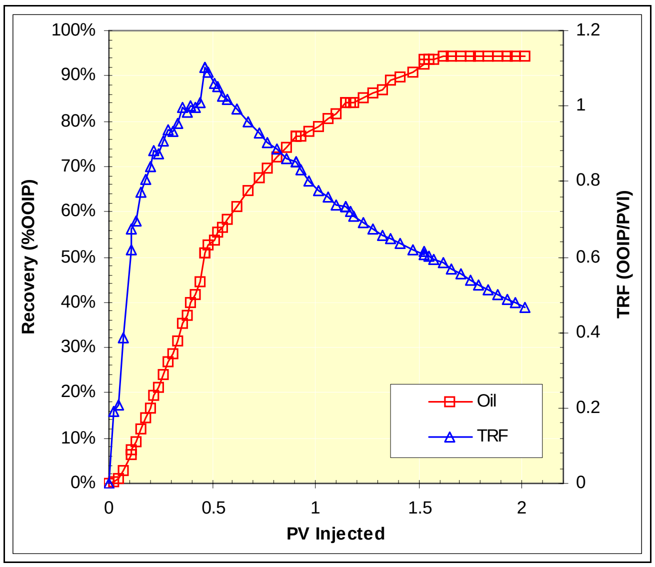

(a) Recovery and TRF Plot

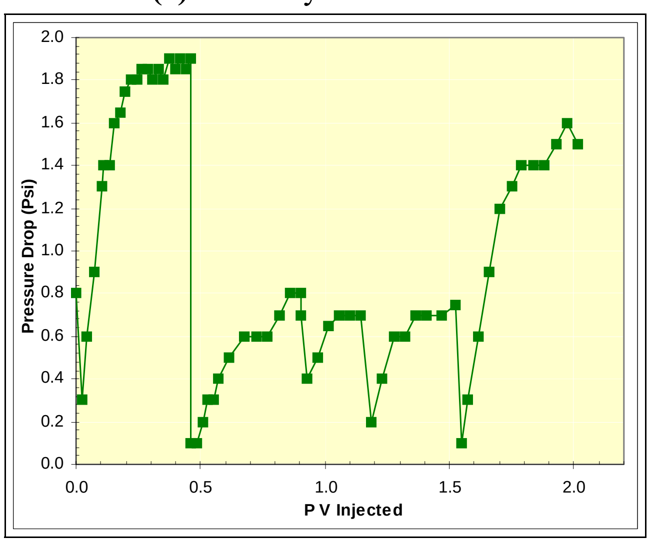

(b) Pressure Drop Behavior

Figure 3.11: Recovery, TRF and Pressure Drop Behavior in Secondary Miscible CO_2 CGI Flood in n-Decane, Yates Reservoir Brine, 1-ft Berea System at 2500 psi and 72 ^oF

- **Secondary Miscible WAG Flood**

To isolate and quantify the effects of water-shielding and three-phase relative permeability on oil recovery, a miscible secondary WAG coreflood was required. The miscible WAG flood was completed using n-Decane, Yates reservoir brine and CO_2 and the results are included as Figure 3.12. Note that each division on the X-axis in Figure 3.12(b) depicts one fluid slug, with the first slug being gas (CO_2).

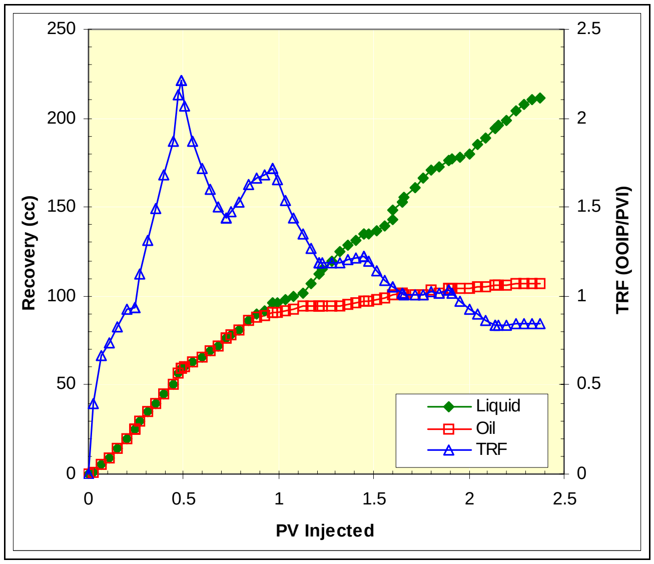

(a) Oil, Total Liquid Recovery and TRF Plot

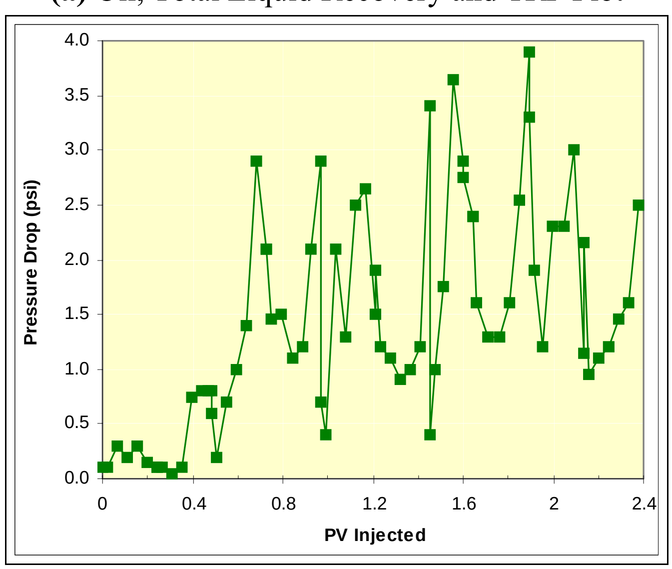

(b) Pressure Drop Behavior

Figure 3.12: Recovery, TRF and Pressure Drop Behavior in Secondary Miscible CO_2 WAG Flood in n-Decane, Yates Reservoir Brine, 1-ft Berea System at 2500 psi and 72 ^oF

- **Comparison between Secondary and Tertiary CGI / WAG Corefloods**

There are two main comparison parameters from the horizontal CGI/WAG floods completed that need to be analyzed: (i) Secondary floods – Injection Mode (CGI and WAG) and (ii) Effect of intermediate waterflood in gas flood oil recovery – Injection Type (Secondary and Tertiary). The individual comparisons are discussed below.

➢ **CGI and WAG Flood Comparisons in Secondary Mode**

Both of the miscible secondary floods (2500-psi backpressure) completed, show high oil recoveries (> 95% OOIP) in both CGI and WAG modes of injection. The oil recovery trends (both cc's of oil produced as well as %OOIP recovery) are almost identical in both injection modes (Figure 3.13 (a) and (b) respectively).

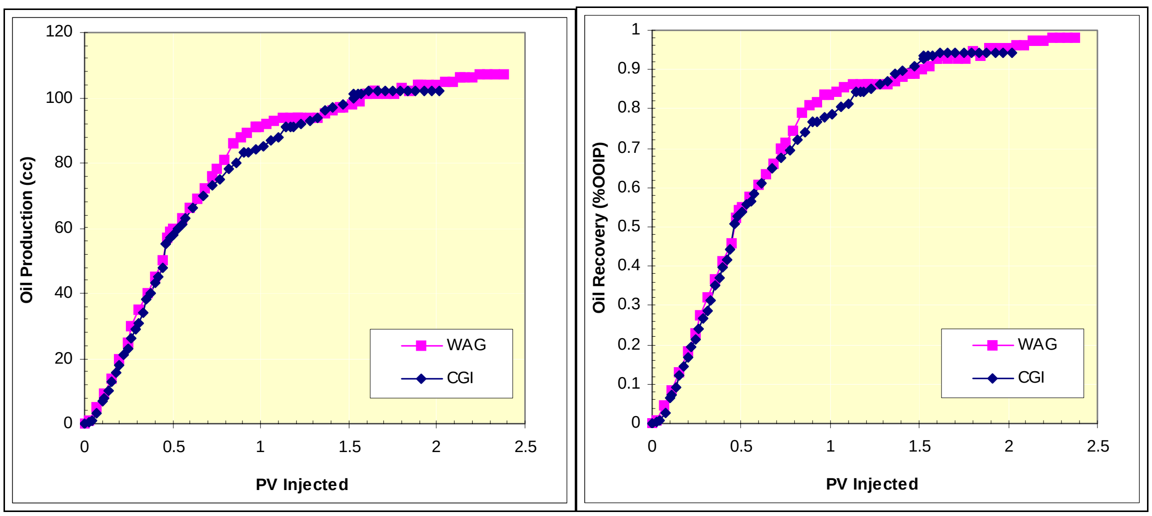

(a) Oil Recovery in cc **(b)** Oil Recovery as %OOIP

Figure 3.13: Oil Recovery Patterns in Secondary Miscible CGI and WAG Floods In n-Decane, Yates Reservoir Brine, 1-ft Berea System at 2500 psi and 72 ^{o}F

The secondary gas flood oil recoveries (> 95% OOIP) are significantly higher than the waterflood recoveries (~ 60% OOIP) obtained at similar flooding conditions, mainly attributable to the lower IFT values (miscibility development - consequently high capillary numbers) obtained in gas injection floods.

As expected, the TRF values for the secondary WAG floods are higher than those of the secondary CGI (Figure 3.14(a)). It is important to note that no free water production (Figure 3.14(b)) was observed during the secondary miscible CGI, affirming the assumption that the connate water saturation at the start of the experiment is essentially immobile, although saturation re-distributions are a possibility – as observed from the unstable pressure drops throughout the experimental run (Figure 3.11(b)).

➢ **Secondary and Tertiary Flood Comparisons of CGI and WAG Injection**

Since the differences between the tertiary CGI and WAG floods (completed and reported earlier) were apparent only under miscible mode(s) of injection – the secondary floods were conducted in the miscible mode using n-Decane, Yates reservoir brine and pure CO_2. This section summarizes the important observations from the comparisons between the secondary and tertiary mode miscible CGI and WAG floods. Figure(s) 3.15 to 3.18 are used in the discussion.

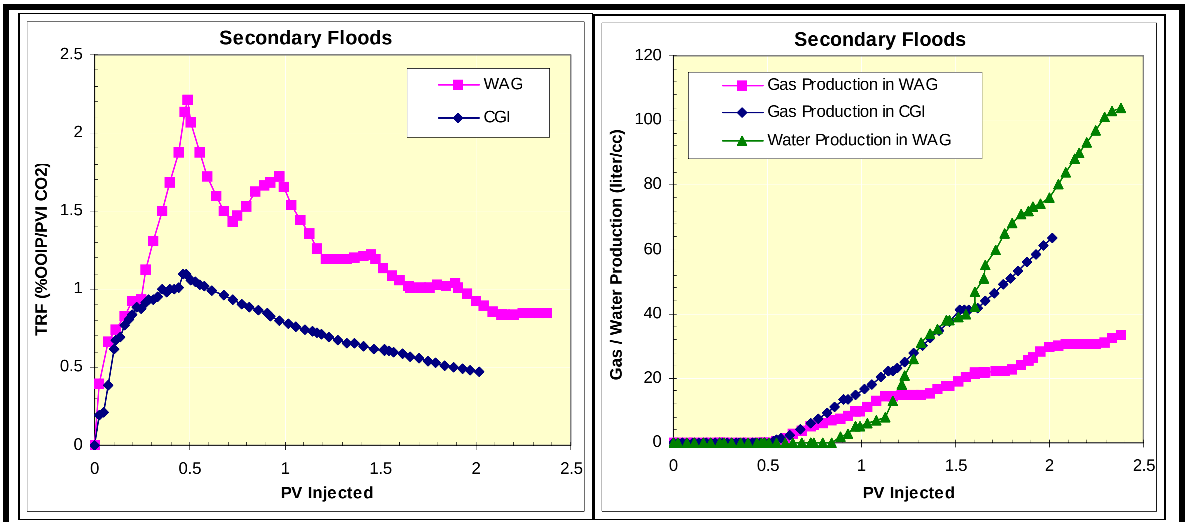

(a) TRF Plot **(b)** Gas / Water Production Plot

Figure 3.14: TRF and Gas / Water Production Plots for Secondary CGI / WAG Floods In n-Decane, Yates Reservoir Brine, 1-ft Berea System at 2500 psi and 72 ^oF

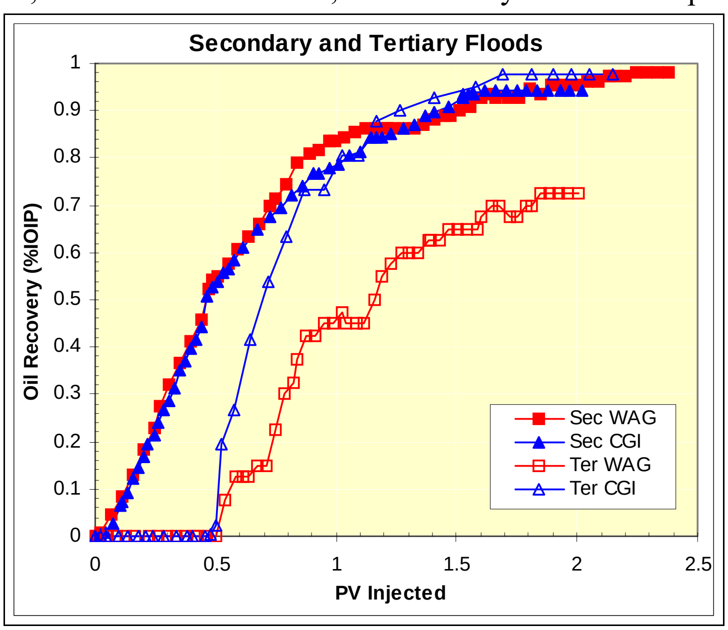

Figure 3.15: Oil Recovery Characteristics in Secondary and Tertiary Miscible Floods In n-Decane, Yates Reservoir Brine, 1-ft Berea System at 2500 psi and 72 ^oF

Figure 3.15 summarizes the oil recovery characteristics obtained in miscible secondary and tertiary CGI and WAG floods. It should be noted that the oil recovery is expressed as percent initial oil in place (%IOIP) in both secondary and tertiary floods. The initial oil corresponds to the oil saturation existing at the start of each gas flood. It is seen that the secondary floods and the tertiary CGI flood oil recoveries are high (> 95%). The tertiary CGI flood was extremely successful in recovering residual oil even after a secondary waterflood and in the presence of high free-water saturations. However, the tertiary WAG flood recoveries are only marginal, demonstrating that the free-water injection (to improve conformance) results in increased water shielding effects – consequently deteriorating WAG performance with time. The important feature of this plot is the immediate oil production in secondary mode, in contrast to the delayed oil production (after ~ 0.5 PV injection) observed in tertiary floods.

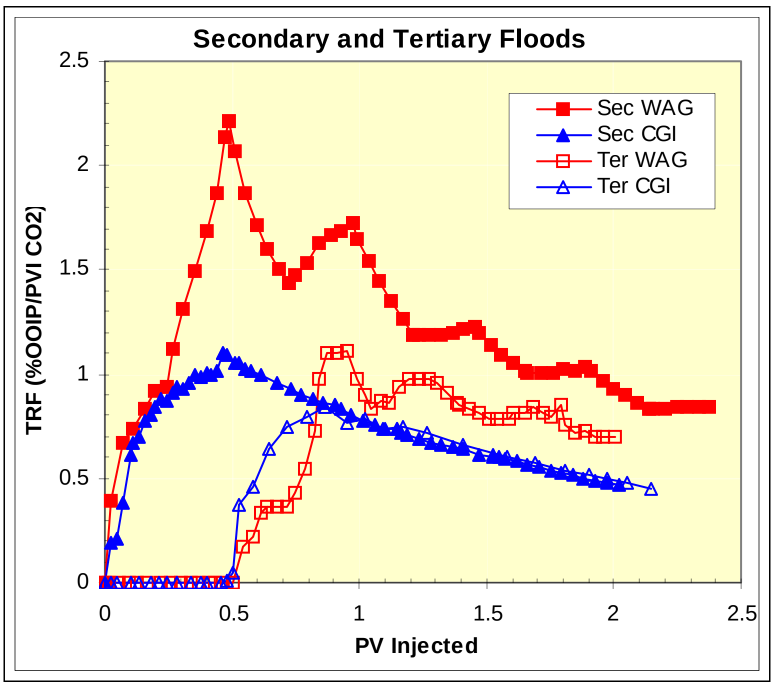

Figure 3.16: TRF Characteristics in Secondary and Tertiary Miscible Floods In n-Decane, Yates Reservoir Brine, 1-ft Berea System at 2500 psi and 72 ^{o}F

Figure 3.16 summarizes the TRF characteristics of the miscible secondary and tertiary CGI and WAG floods. The TRF plot clearly demonstrates the improved economics by virtue of secondary injection by hastened oil production and vastly improved CO_2 utilization factors. The striking feature(s) of Figure 3.16 are the first TRF peak obtained by WAG employment, shift of the CGI TRF line to the left (in secondary mode compared to tertiary) and the near perfect duplication of oil recovery mechanisms (as seen from the near similar re-traces of the TRF plots) in both secondary and tertiary mode CGI and WAG miscible floods.

Another interesting feature of Figure 3.16 is that the TRF trends of both secondary and tertiary floods are similar after ~ 0.8 (or 0.9) PV injections. The gas and water handling requirements in CGI and WAG secondary floods show that the CGI flood have higher cumulative gas recycling and handling requirements. On the other hand, in the WAG flood, water breakthroughs are observed at about ~ 0.84 PVI, and the gas productions are comparable to the CGI up to that extent. After about 0.8 PVI injection, the gas production in CGI increased rapidly, whereas the WAG employment controls gas breakthrough (Figure 3.18(b)).

Figure 3.17 summarizes the pressure drop behavior of the miscible secondary and tertiary CGI and WAG floods. The highest pressure-drops are observed under tertiary mode WAG injection, followed by secondary mode WAG injection, while the miscible CGI floods demonstrate comparable pressure-drop characteristics. Figure 3.17 exemplifies the importance of injectivity problems, common to most WAG commercial field applications, and suggests that injectivity problems in WAG can occur even under secondary mode injection. These injectivity problems can lead to pressure surges, and could also be partially responsible for the loss of miscibility at the flood displacement front, which can be exaggerated by reservoir heterogeneity. This plot also indicates that minimal operational problems, especially related to injectivity are associated with CGI mode injection (in both secondary as well as tertiary modes).

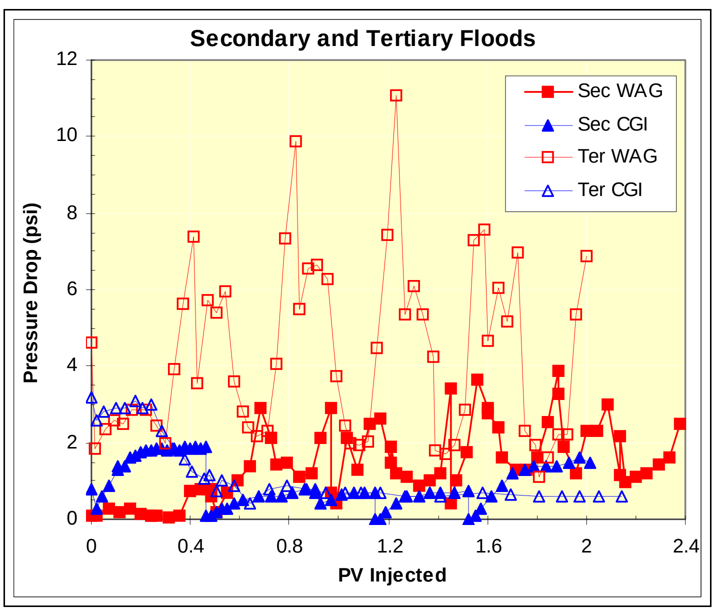

Figure 3.17: Pressure Drop Characteristics in Secondary and Tertiary Miscible Floods In n-Decane, Yates Reservoir Brine, 1-ft Berea System at 2500 psi and 72 ^{o}F

Figure 3.18 summarizes water and gas production characteristics in secondary as well as tertiary miscible floods. Figure 3.18(a) shows that tertiary floods start producing water right from the beginning of the flood whereas the water production and handling problems are almost non-existent in secondary floods until later life of the secondary CGI and WAG floods and that the secondary CGI flood does not produce any free-water.

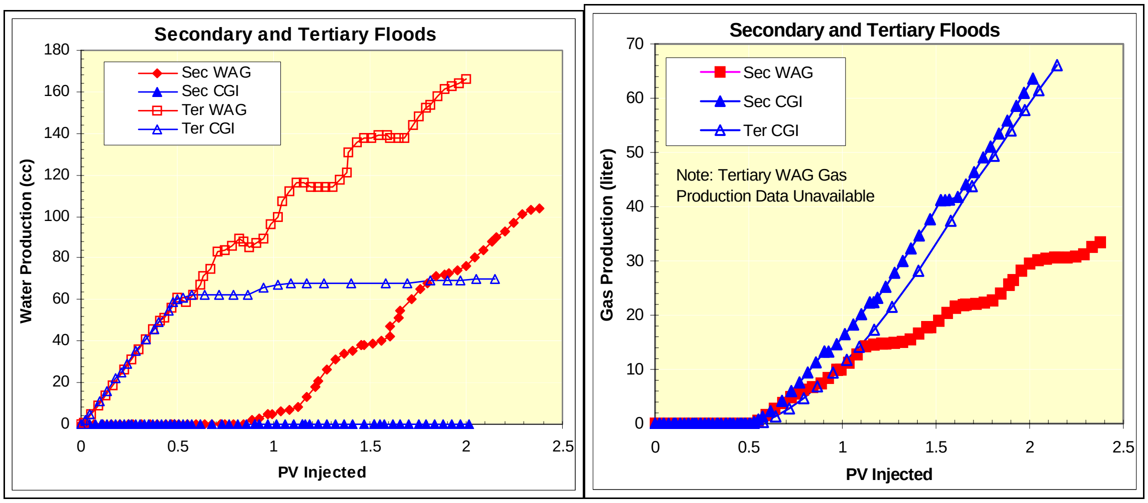

(a) Water Production **(b)** Gas Production

Figure 3.18: Water and Gas Production Plots for Secondary and Tertiary Miscible Floods In n-Decane, Yates Reservoir Brine, 1-ft Berea System at 2500 psi and 72 ^oF

3.6.3 Use of CO_2 Saturated Brine for WAG and CGI Corefloods

Higher oil recoveries observed in CGI/WAG experiments using 5% NaCl brine compared to Yates reservoir brine (reported in earlier reports to DOE) led to hypothesis that: lower CO_2 solubility in the brine results in relatively higher CO_2 volumes available for incremental oil recovery (by dissolution and swelling) in the 5% NaCl brine flood than Yates reservoir brine.

To test the validity of the above hypothesis, Experiments 7 (immiscible CGI) and 10 (miscible WAG) (Report 15323R02, Jul 2003) were repeated with CO_2-saturated brine. Since there is no water injection in CGI flood, the secondary waterflood was conducted using saturated brine, and the drainage (oil flood) and EOR (immiscible CGI) floods were conducted at conditions similar to Experiment 7. The miscible WAG experiment using CO_2-saturated brine was reported earlier (15323R03, Oct 2003).

In the case of the immiscible CGI flood (Experiment 11), the n-Decane drainage step was similar to those previously observed whereas the results of the secondary waterflood with saturated Yates reservoir brine showed significant pressure fluctuations up to breakthrough. However the pressure fluctuations were stabilized immediately after a sharp water breakthrough. Even after breakthrough, a significant delay (until 1.59 PVI) in the gas breakthrough (dissolved in brine) was observed along with increasing pressure-drops after breakthrough. These observations are attributable to the miscible displacement (consequently replacement) of the connate (unsaturated) brine by saturated injection brine. The replacement of the unsaturated connate brine with saturated brine, helped in significantly decreasing the oil and gas breakthrough time for the tertiary (EOR) CO_2 CGI injection with significantly improved TRF factors (Figure 3.19).

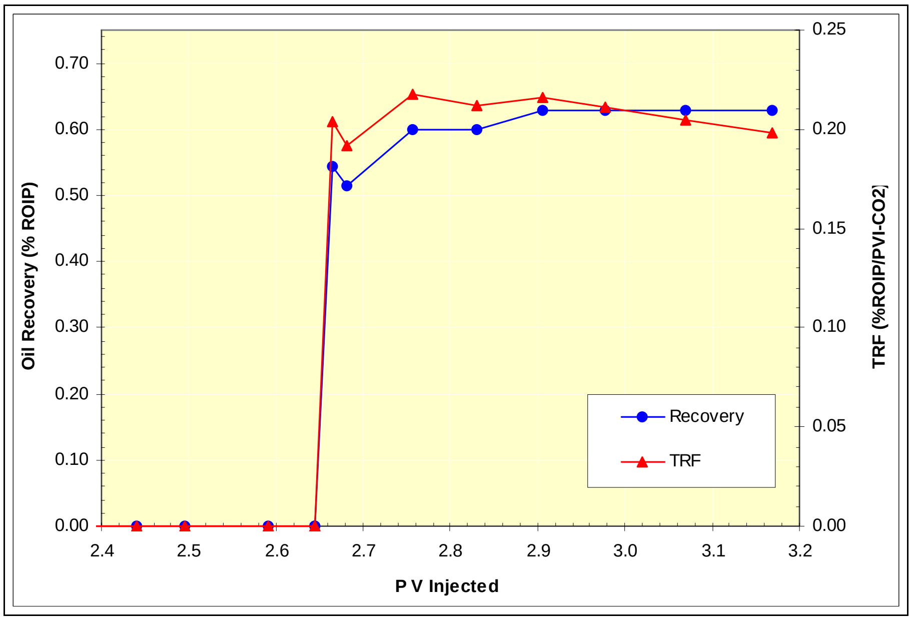

(a) Oil Recovery and TRF for CGI Flood with Unsaturated Brine Secondary Waterflood

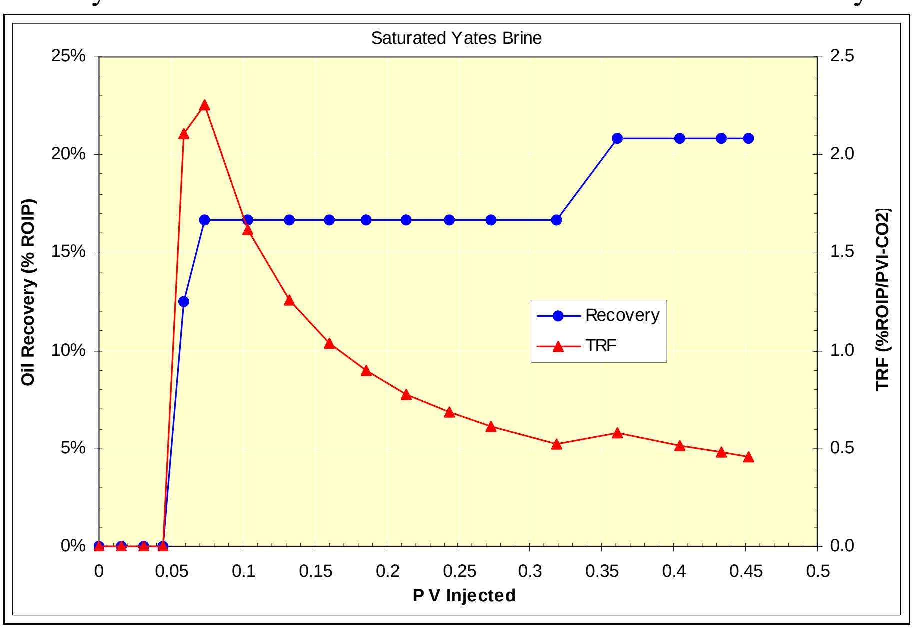

(b) Oil Recovery and TRF for CGI Flood with Saturated Brine Secondary Waterflood

Figure 3.19: Effect of Saturation of Brine with CO_2 on Immiscible CGI Recovery

3.6.4 'Happy-Medium' between WAG and CGI: Hybrid-WAG Coreflood

Hybrid-WAG type floods were conducted using Yates reservoir brine to asses the validity of the conclusions of the previous work that optimum performance may be obtained by the employment of the combination of CGI and WAG floods. Figure 3.20 shows the comparison of the miscible CGI, WAG and Hybrid-WAG corefloods.

The miscible 'Hybrid-WAG' experiment was conducted using Yates reservoir brine, n-Decane and pure CO_2. Figure 3.20(a) shows the conventional oil recovery (as % ROIP) plot for miscible CGI, WAG and Hybrid-WAG floods. As expected, the Hybrid-WAG type injection clearly out performs both the CGI as well as WAG floods from an oil recovery point of view. This data strengthens the initial speculation that optimum mode of injection is a 'combination' of CGI and WAG floods.

However, from a TRF factor point of view, the WAG process is still the 'best' mode of injection for maximum CO_2 utilization. However, the incremental benefits from CGI / Hybrid-WAG such as no free water injection, increased water relative permeability, water shielding effect and decreased gas injectivity cannot be inferred from the TRF plot. Furthermore, the need for lower CO_2 utilization to decrease overall project costs may become a passé with increasing importance for CO_2 sequestration.

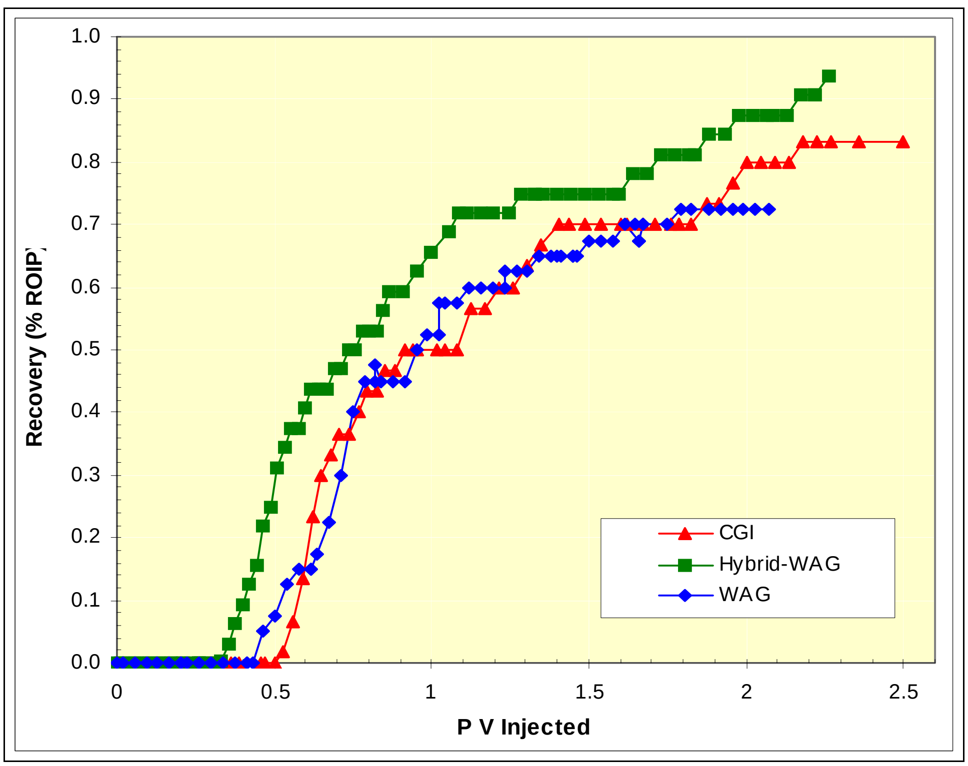

(a): Recovery as Percent Residual Oil in Place

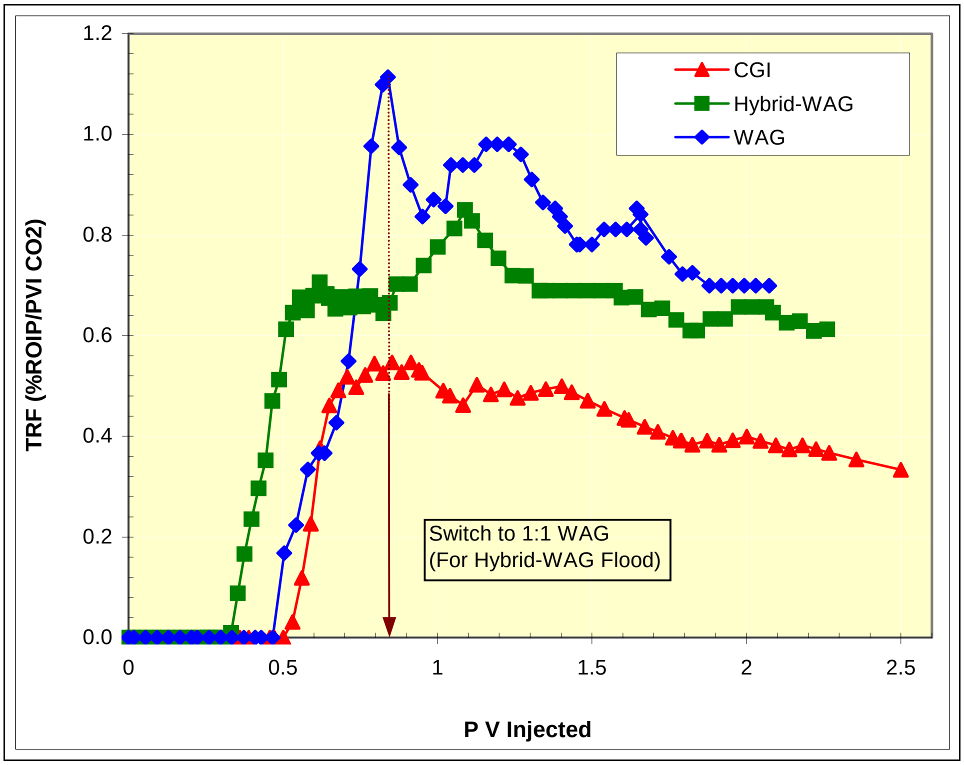

(b): Recovery as Fraction of Residual Oil in Place per PV of CO_2 Injected

Figure 3.20: Comparison of Miscible Hybrid-WAG, WAG and CGI Floods on 1-ft Berea

3.6.5 Preliminary Conclusions from Horizontal Mode Corefloods

The 6-ft Berea core tests demonstrated that long corefloods are appropriate and useful in accurate characterization of horizontal mode CGI and WAG floods.

Use of CO_2 saturated brine in CGI and WAG corefloods help explain the delayed oil breakthroughs observed during tertiary corefloods. This delay in oil breakthroughs observed are mainly attributable to the solubility effects between CO_2 and core-brine and is effectively explained by the saturated CGI and WAG experiments. These experiments clearly demonstrate that the replacement of the unsaturated core brine with saturated brine significantly helps in decreasing the oil and gas breakthrough times for the tertiary (EOR) CO_2 CGI injection with significantly improved TRF factors.

The miscible secondary floods (conducted at 2500 psi backpressure) demonstrate high oil recoveries (> 95%) in both CGI and WAG mode of injection. The oil recovery trends (both volumes of oil produced as well as %OOIP recovery) are almost identical in both injection modes. The secondary gas flood recoveries (> 95% OOIP) are significantly higher than the waterflood recoveries (~ 60% OOIP) obtained at similar flooding conditions, mainly attributable to the lower interfacial tension (IFT) values (miscibility development - consequently high capillary numbers) obtained during gas injection.

As expected, the TRF values for the WAG floods are higher than those of the CGI. The TRF values for CGI and WAG peak at nearly the same PV injections (0.46 and 0.49

PVI respectively), but are markedly lower than the TRF peaks in tertiary floods (0.7 – 0.8 PVI), thus demonstrating the beneficial effects of early gas injection (in secondary mode) by hastened oil recovery and improved CO_2 utilization factors. The water shielding effect, responsible for delayed oil production in tertiary floods, was almost non-existent in the secondary floods – even in WAG mode of injection.

The TRF trends (from secondary as well as tertiary corefloods) and the gas and water production trends indicate that it could be economical to inject in CGI mode up to about 0.7 to 0.9 pore volumes, and then switch over to 1:1 WAG for controlling gas and water productions, to improve efficiency. Therefore, the 'happy-medium' of Hybrid-WAG, which was demonstrated to be relevant to tertiary gas floods in previous reports, could also be applicable to the secondary floods, and may be employed for optimum flood economics.

3.7 Gravity Stable GAGD Experimentation

Five gravity stable GAGD experiments (three immiscible and two miscible) were completed during the reporting period. All the steps conducted during these experiments were in a gravity stable mode, i.e. the oil flood, water flood (secondary, if applicable) as well as the tertiary gas injection flood. The oil flood was completed by injecting n-Decane into a previously brine saturated core from the top, and the displacement was from top to bottom. The water flood was completed by injecting Yates reservoir brine from the bottom, and the final gas injection step was from the top. Although these experiments are not realistic, from a field perspective, they provide with an upper limit for the recovery characteristics of the GAGD process.

3.7.1 Immiscible Gravity Stable (GS) GAGD Floods

Three gravity stable GAGD immiscible coreflood experiments with n-Decane, Yates reservoir brine and pure CO_2 were conducted in this reporting period. The objectives of these experiments were: (i) to evaluate the effect of injection mode on GAGD recovery characteristics in an immiscible mode and (ii) to study the effect of injection rate on GAGD recovery characteristics in an immiscible mode.

Figures 3.21, 3.22 and 3.23 summarizes the data obtained from each gravity stable displacement step during GAGD immiscible floods on 1-ft Berea core and n-Decane, Yates reservoir brine and pure CO_2.

Part (a) provides the data for water recovery and pressure drop during the drainage cycle when n-Decane was injected into the brine saturated core. Part (b) provides the data for oil recovery and pressure drop when Yates reservoir brine was injected into the core at connate water saturations. Part (c) provides the data for water, and oil recoveries as well as pressure drop during the gravity stable GAGD tertiary recovery process, where in pure CO_2 was injected into the core at residual oil saturation.

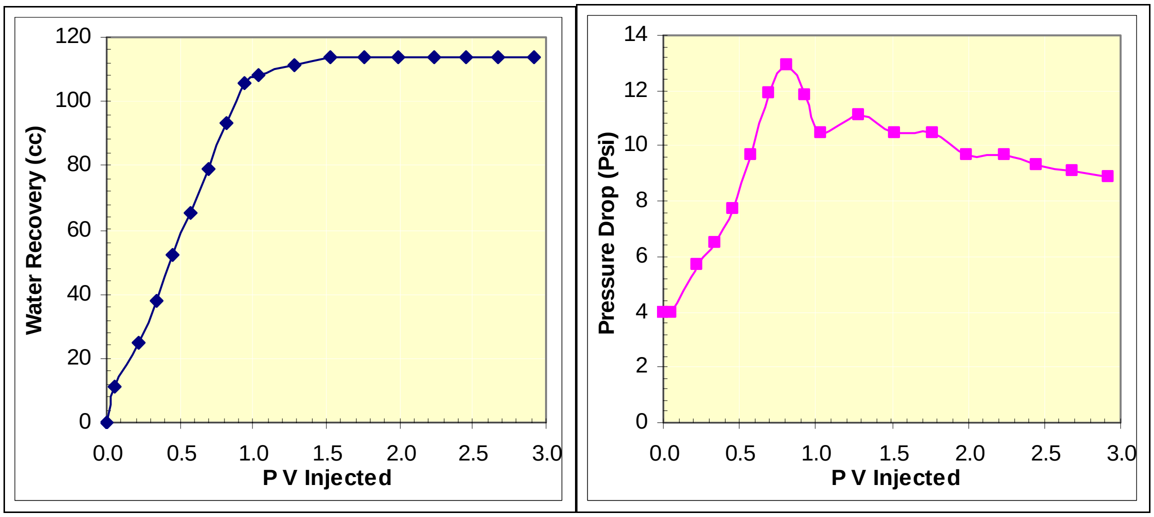

(a) Gravity Stable Drainage Cycle: Oil Flood with n-Decane

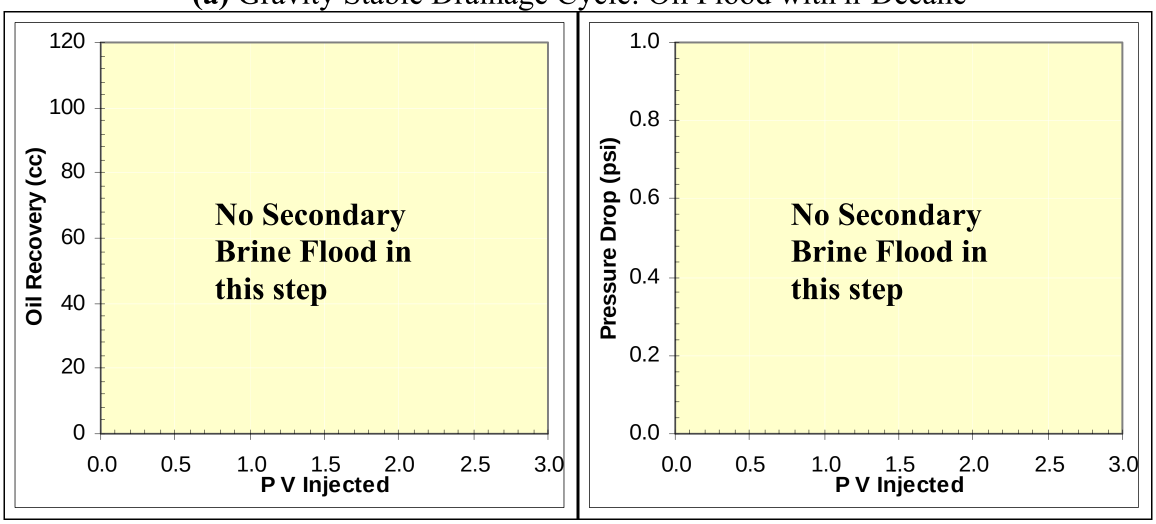

(b) Gravity Stable Imbibition Cycle: Brine Flood with Yates Reservoir Brine

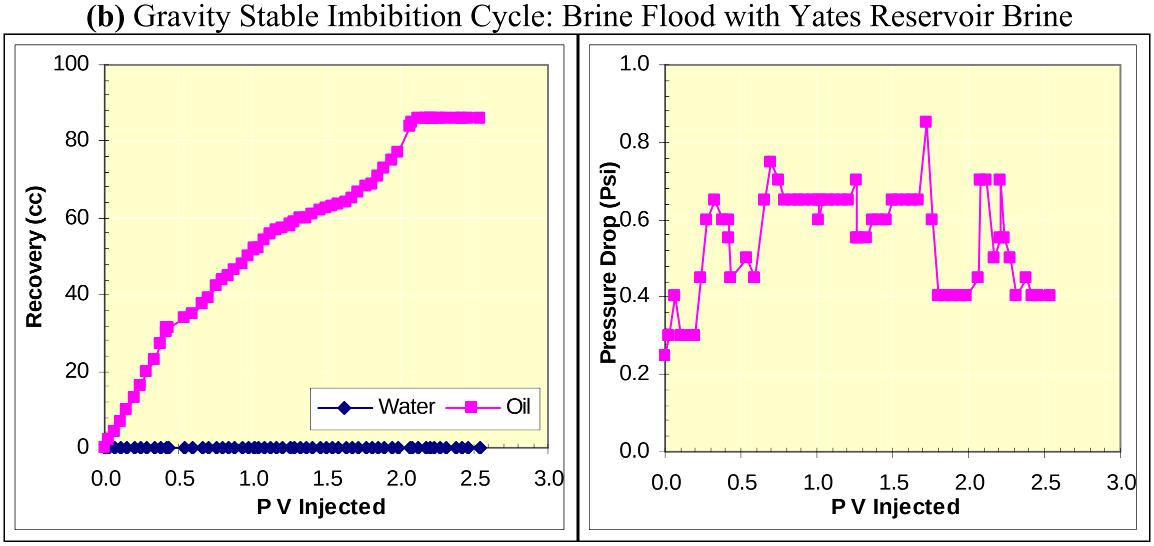

(c) Gravity Stable GAGD Cycle: Gas Flood with Pure CO_2

Figure 3.21: Data for Experiment GAGD GS # 1: 1-ft Berea Core + Yates Reservoir Brine with Gravity Stable Immiscible Secondary GAGD CO_2 Injection @ 10 cc/hr

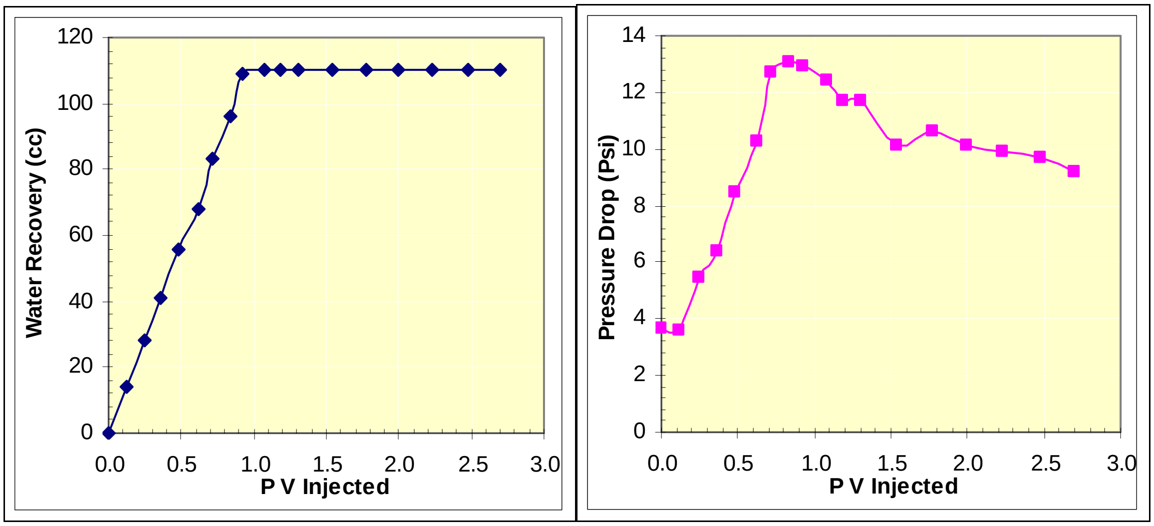

(a) Gravity Stable Drainage Cycle: Oil Flood with n-Decane

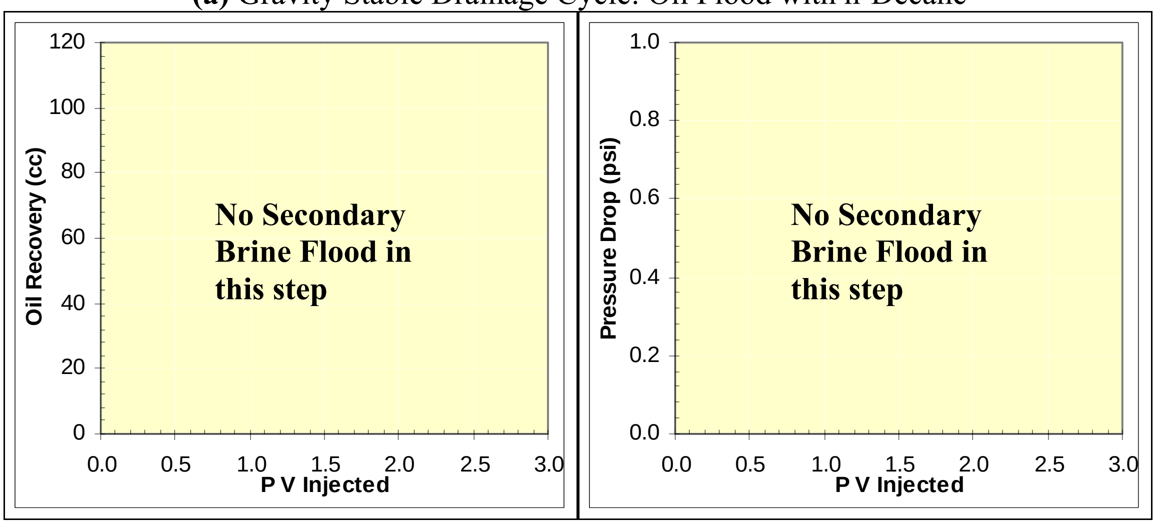

(b) Gravity Stable Imbibition Cycle: Brine Flood with Yates Reservoir Brine

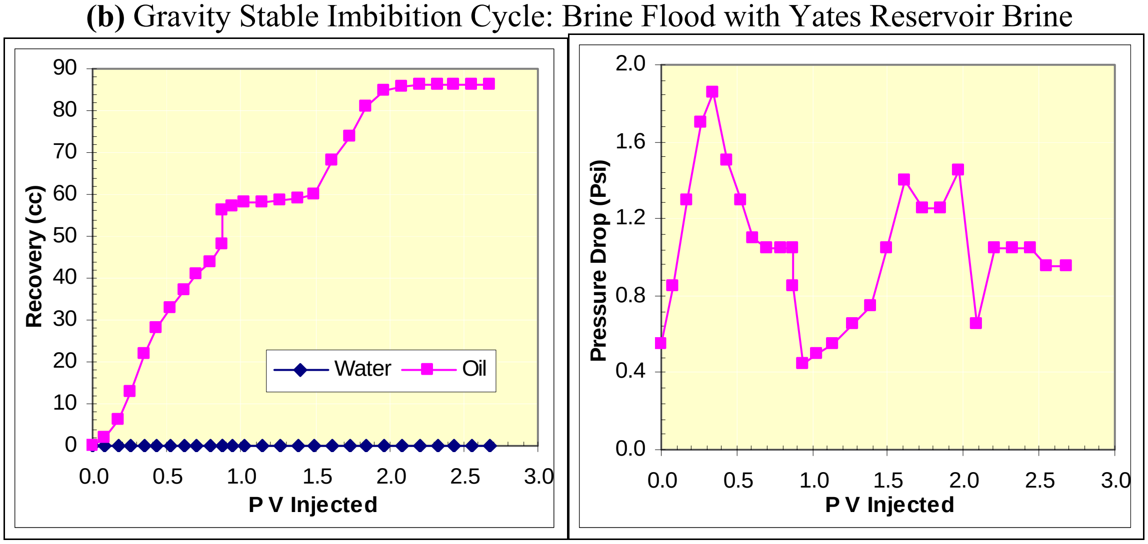

(c) Gravity Stable GAGD Cycle: Gas Flood with Pure CO_2

Figure 3.22: Data for Experiment GAGD GS # 1(A): 1-ft Berea Core + Yates Reservoir Brine with Gravity Stable Immiscible Secondary GAGD CO_2 Injection @ 40 cc/hr

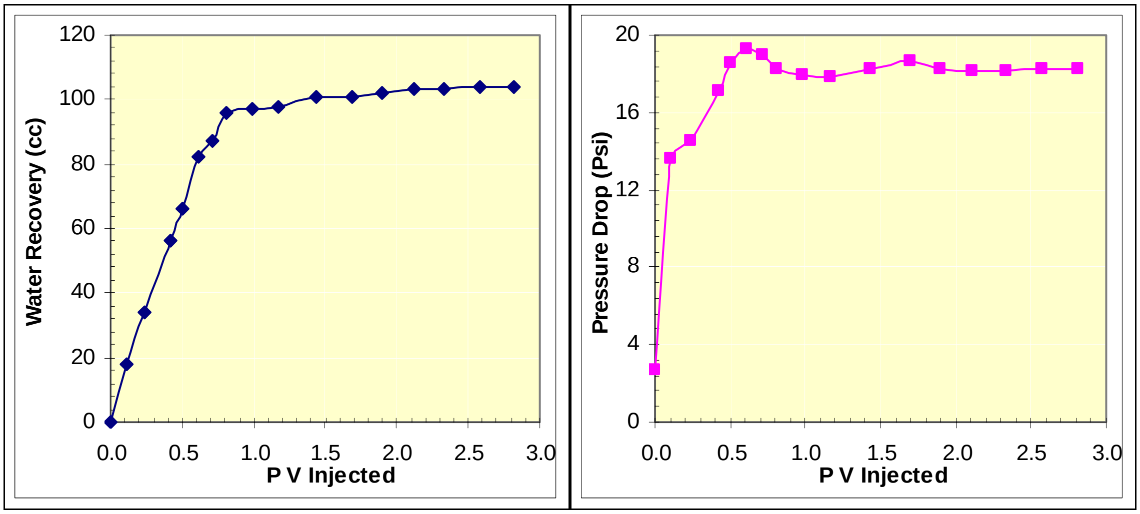

(a) Gravity Stable Drainage Cycle: Oil Flood with n-Decane

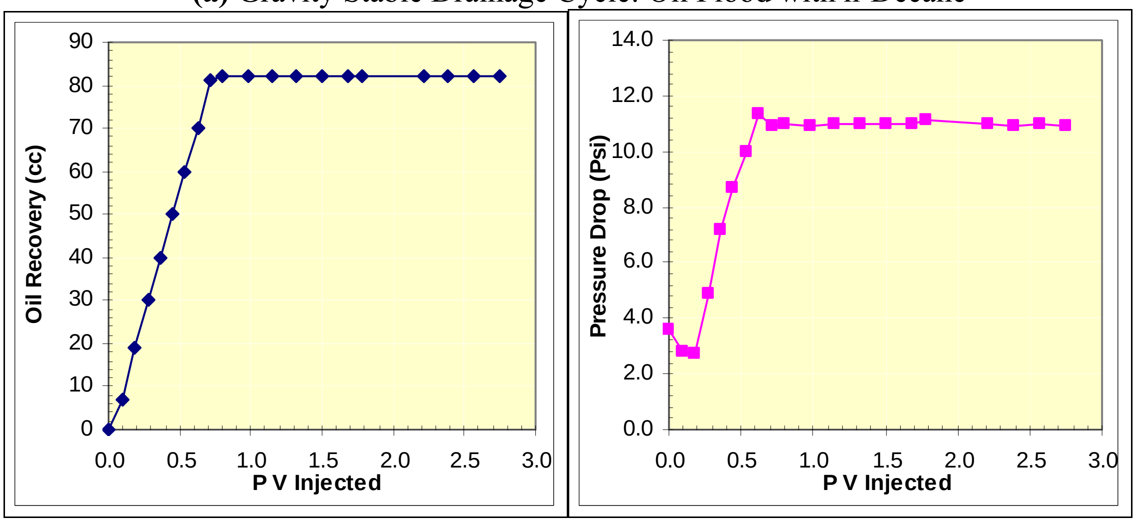

(b) Gravity Stable Imbibition Cycle: Brine Flood with Yates Reservoir Brine

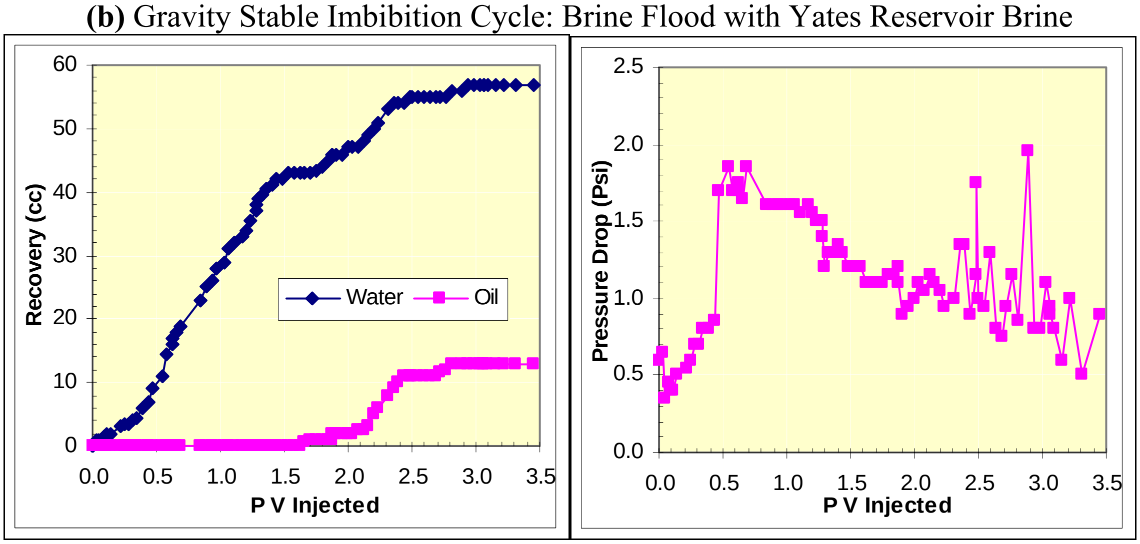

(c) Gravity Stable GAGD Cycle: Gas Flood with Pure CO_2

Figure 3.23: Data for Experiment GAGD GS # 2: 1-ft Berea Core + Yates Reservoir Brine with Gravity Stable Immiscible Tertiary GAGD CO_2 Injection @ 10 cc/hr

3.7.2 Miscible Gravity Stable (GS) GAGD Floods

Two gravity stable GAGD miscible coreflood experiments with n-Decane, Yates reservoir brine and pure CO_2 were also completed in this reporting period. The objectives of these experiments were: (i) to evaluate the effect of injection mode on GAGD recovery characteristics in a miscible mode and (ii) to study the effect of miscibility development on GAGD recovery characteristics.

Figures 3.24, and 3.25 summarizes the data obtained from each gravity stable displacement step during GAGD miscible floods on 1-ft Berea core and n-Decane, Yates reservoir brine and pure CO_2.

Part (a) provides the data for water recovery and pressure drop during the drainage cycle when n-Decane was injected into the brine saturated core. Part (b) provides the data for oil recovery and pressure drop when Yates reservoir brine was injected into the core at connate water saturations. Part (c) provides the data for water, and oil recoveries as well as pressure drop during the gravity stable GAGD tertiary recovery process, where in pure CO_2 was injected into the core at residual oil saturation.

3.7.3 Comparison of Immiscible and Miscible Gravity Stable GAGD Floods

There are five major comparisons that can be made from the gravity stable experiments completed till date: (i) effect of injection rate (10 cc/hr versus 40 cc/hr) on GAGD secondary immiscible floods, (ii) effect of injection mode (secondary versus tertiary) on GAGD immiscible floods, (iii) effect of injection mode (secondary versus tertiary) on GAGD miscible floods, (iv) effect of miscibility development (miscible versus immiscible) on GAGD floods, and (v) comparison of oil recovery characteristics of GAGD versus horizontal mode WAG floods.

- **Effect of Injection Rate on Secondary Immiscible GAGD Floods**

The effect of injection rate on secondary immiscible gravity stable GAGD floods is shown in Figure 3.26. During the dimensional analysis of the gravity stable field projects followed by the laboratory coreflood experimental design, various models were used to calculate the limiting ‘Critical Injection Rate’ (CIR) for the coreflood displacement to be gravity stable. In executing the corefloods, the lowest value of the CIR predicted (which was – 43 cc/hr) from model calculations were used as limiting injection rates. However, as the entire previous horizontal mode CGI / WAG corefloods were conducted at 10 cc/hr rates (as dictated by the Leas and Rappaport stability criterion); the GAGD corefloods were also completed at the same injection rates. This assured normalization of viscous / capillary / dispersive forces in all the corefloods to provide with an effective comparison based on buoyancy forces only.

However, to validate that the concept of CIR is applicable in these GAGD corefloods, two secondary immiscible gravity stable GAGD floods were conducted at different injection rates, namely 10 cc/hr and 40 cc/hr, using n-Decane and Yates reservoir brine.

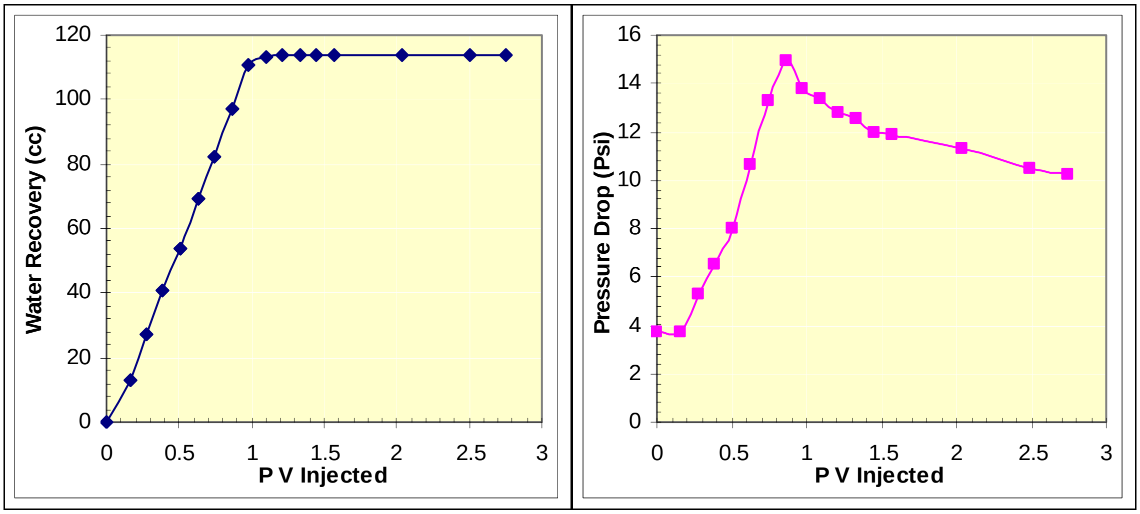

(a) Gravity Stable Drainage Cycle: Oil Flood with n-Decane

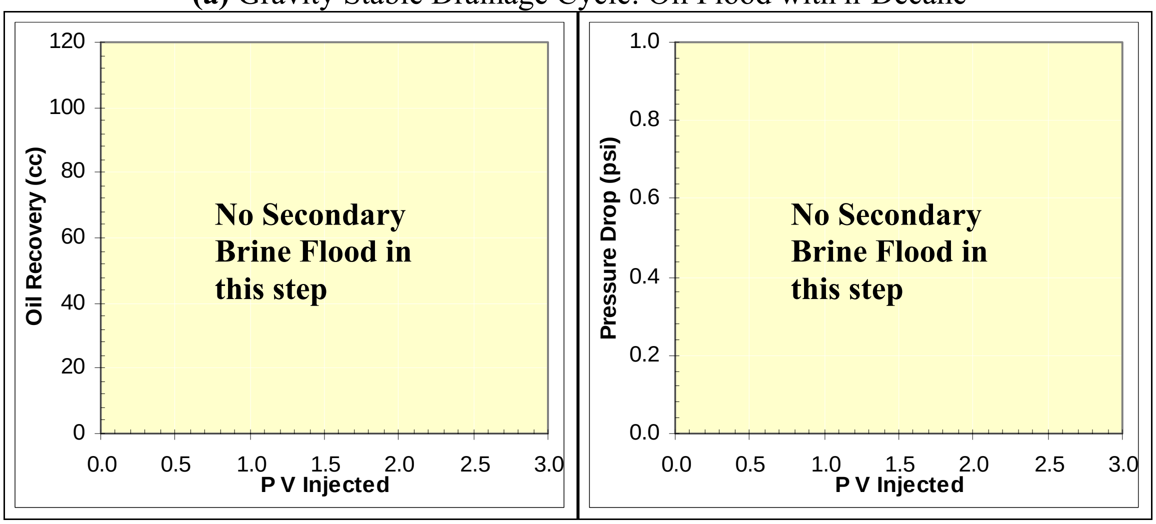

(b) Gravity Stable Imbibition Cycle: Brine Flood with Yates Reservoir Brine

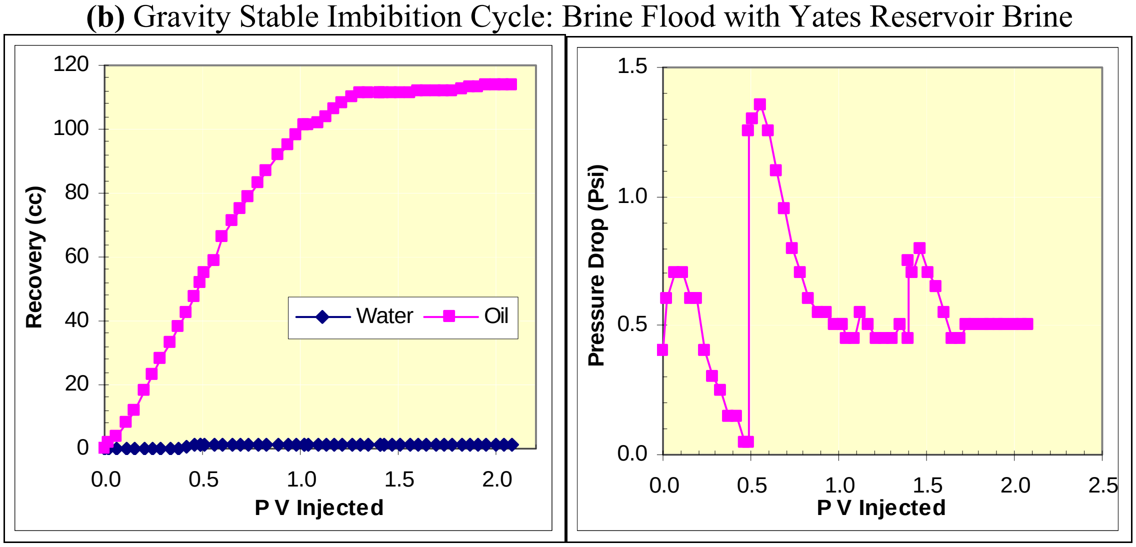

(c) Gravity Stable GAGD Cycle: Gas Flood with Pure CO_2

Figure 3.24: Data for Experiment GAGD GS # 3: 1-ft Berea Core + Yates Reservoir Brine with Gravity Stable Miscible Secondary GAGD CO_2 Injection @ 10 cc/hr

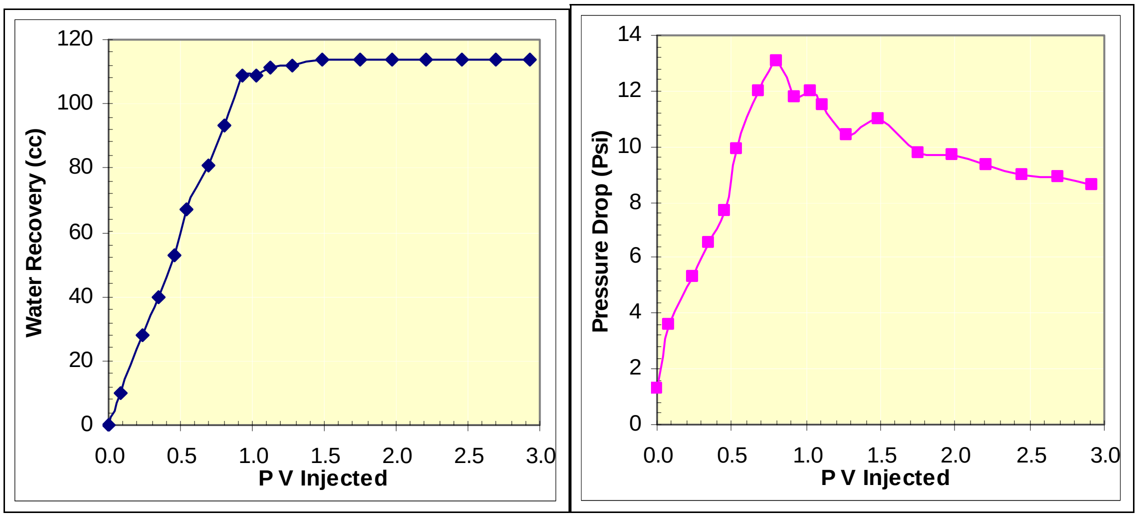

(a) Gravity Stable Drainage Cycle: Oil Flood with n-Decane

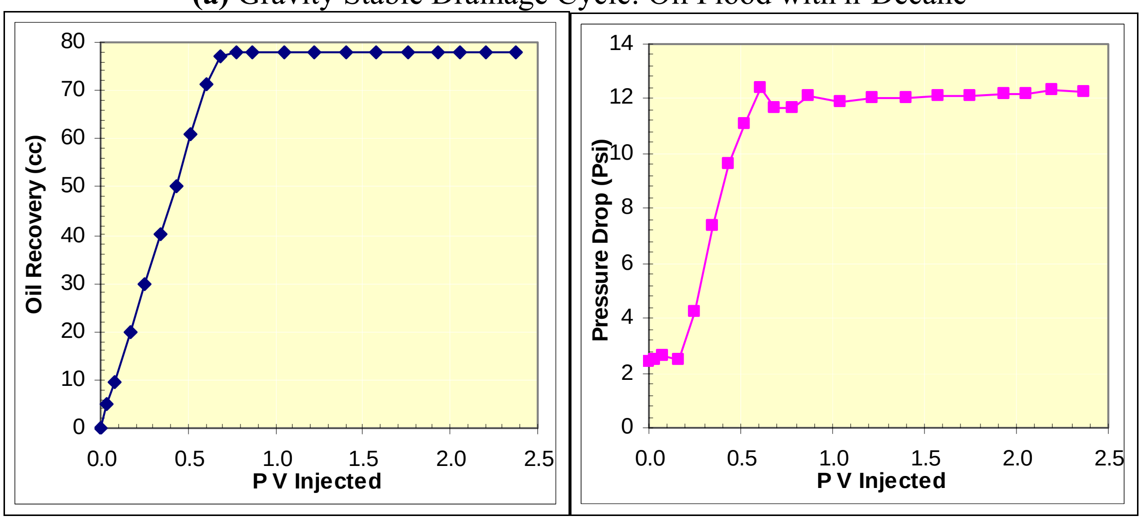

(b) Gravity Stable Imbibition Cycle: Brine Flood with Yates Reservoir Brine

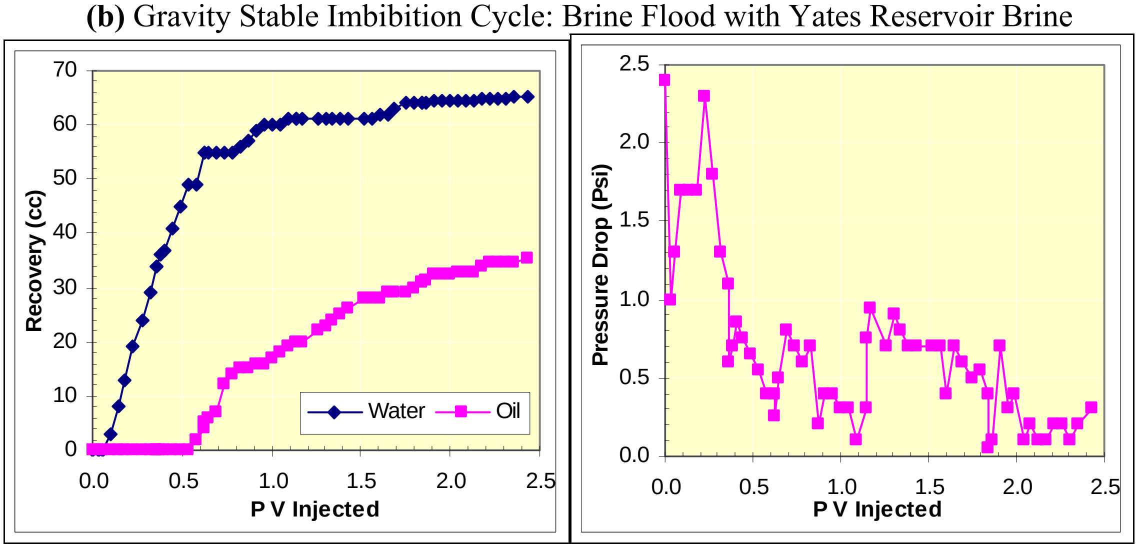

(c) Gravity Stable GAGD Cycle: Gas Flood with Pure CO_2

Figure 3.25: Data for Experiment GAGD GS # 4: 1-ft Berea Core + Yates Reservoir Brine with Gravity Stable Miscible Tertiary GAGD CO_2 Injection @ 10 cc/hr

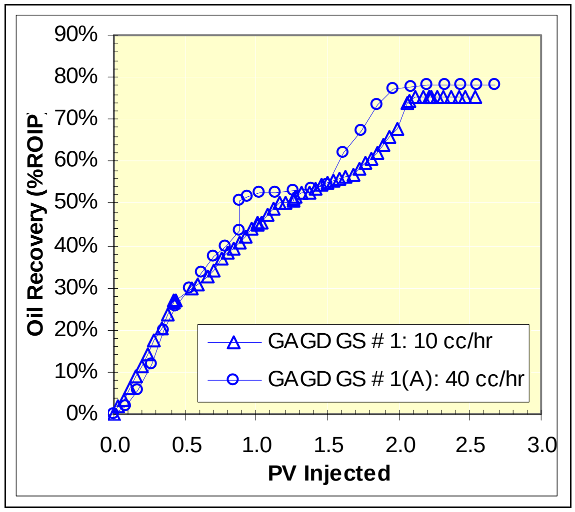

(a) Oil Recovery Characteristics versus PV CO_2 Injection

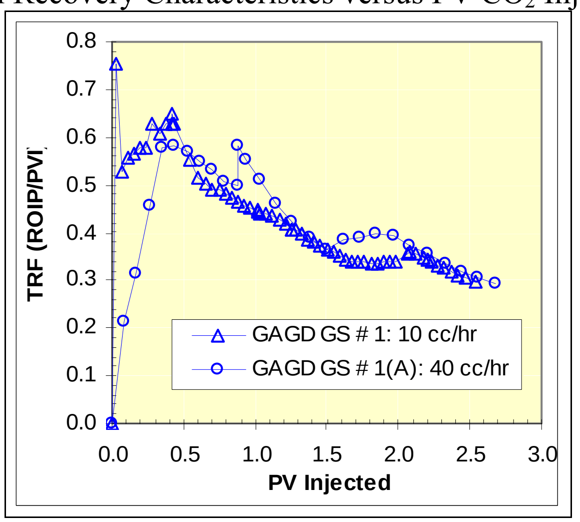

(b) TRF (%ROIP / PVI CO_2) Characteristics versus PV CO_2 Injection

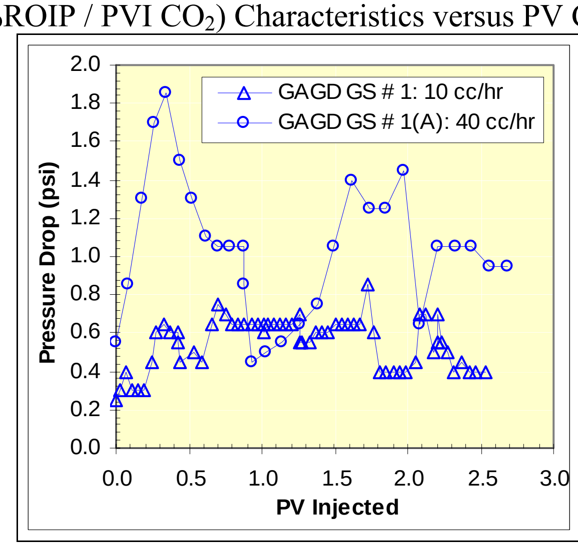

(c) Pressure Drop Characteristics versus PV CO_2 Injection

Figure 3.26: Effect of Injection Rate on Secondary Immiscible Gravity Stable GAGD Floods in n-Decane, Yates Reservoir Brine and Pure CO_2 System

Figure 3.26(a) clearly shows that the effects of injection rate on the gravity stable GAGD floods are minimal. On the other hand, near perfect duplication of the tertiary recovery factors (TRF) for the two corefloods (Figure 3.26(b)) suggest that the gas utilization efficiencies too are independent of the injection rates, provided the injection rates are below the CIR. The pressure drop behavior suggests that in secondary floods, the pressure drops tend to stabilize near the absolute permeability pressure drop value (Figure 3.26(c)), indicating very high sweep efficiencies.

- **Effect of Injection Mode on Immiscible GAGD Floods**

The effect of injection mode (secondary versus tertiary) on immiscible gravity stable GAGD floods is shown in Figure 3.27. The literature review suggests that the commercial gravity stable gas injection processes have be employed in both secondary as well as tertiary modes.

To provide with effective comparisons and performance review between horizontal WAG / CGI floods and GAGD, all these experiments were completed in both secondary and tertiary modes. The secondary mode CGI / WAG corefloods completed are reported in Section 3.6.2 of this report; while the tertiary mode CGI / WAG corefloods completed were reported in earlier reports to the DOE. During this reporting period, the secondary gravity stable GAGD floods were completed, while the non-gravity stable GAGD floods are planned for the next quarter.

To isolate the effects of injection mode on gravity stable immiscible GAGD floods, two immiscible gravity stable GAGD floods were conducted in secondary and tertiary modes of injection using n-Decane and Yates reservoir brine.

Figure 3.27(a) shows that the gravity stable GAGD recovery efficiencies (average incremental recovery: 67.27% ROIP) are significantly higher than horizontal CGI / WAG floods (average incremental recovery: 34.34% ROIP), even under immiscible modes of injection. These oil recovery numbers show that the GAGD mode of injection clearly outperforms the WAG floods. Also it is important to note that the mode of injection (secondary or tertiary) significantly affects the GAGD performance under immiscible mode. Tertiary immiscible GAGD flood recovery (59.09%) is significantly lower than the secondary immiscible GAGD flood recovery (75.44%), thus suggesting higher incremental benefits of GAGD application in secondary mode.

The utilization factors pertaining to secondary floods show high TRF values till 1.0 PVI, followed by a decline. However this decline is not exponential, as was observed in immiscible horizontal secondary CGI corefloods, suggesting sustained higher gas utilization factors for gravity stable GAGD corefloods.

As observed in Figure 3.26(c), the pressure drop behavior tends to reach a plateau, although the approach could be asymptotic in tertiary gravity stable GAGD floods, suggesting high sweep efficiencies during these corefloods.

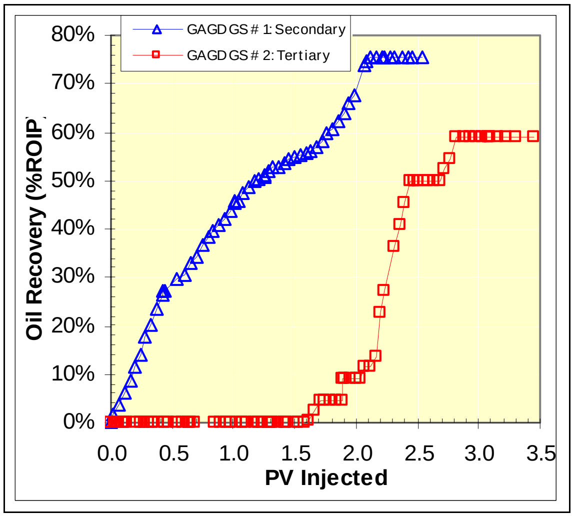

(a) Oil Recovery Characteristics versus PV CO_2 Injection

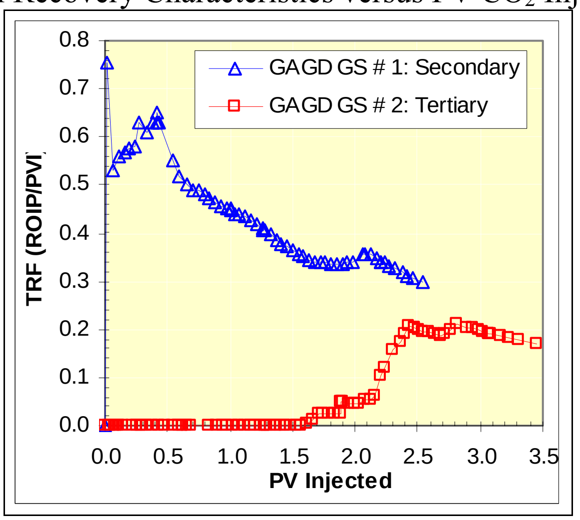

(b) TRF (%ROIP / PVI CO_2) Characteristics versus PV CO_2 Injection

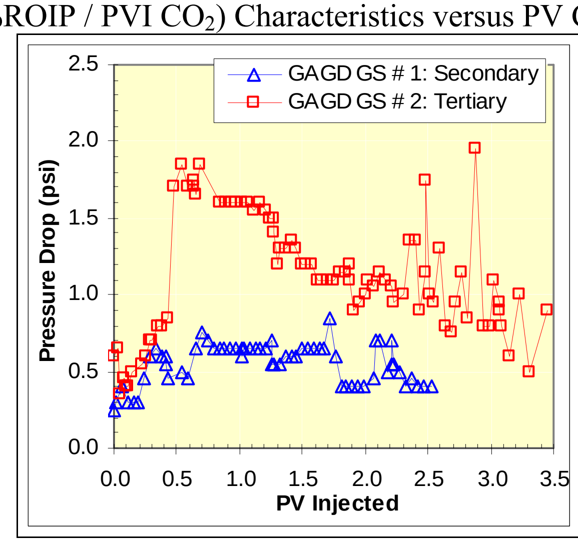

(c) Pressure Drop Characteristics versus PV CO_2 Injection

Figure 3.27: Effect of Injection Mode (Secondary versus Tertiary) on Immiscible Gravity Stable GAGD Floods in n-Decane, Yates Reservoir Brine and Pure CO_2 System

- **Effect of Injection Mode on Miscible GAGD Floods**

The effect of injection mode (secondary versus tertiary) on miscible gravity stable GAGD floods is shown in Figure 3.28. The literature review suggests that the commercial gravity stable gas injection processes have be employed in both secondary as well as tertiary modes, and that the miscible mode of injection is highly popular in commercial gas injection processes. As in immiscible gravity stable GAGD floods, the miscible gravity stable GAGD floods were also completed in both secondary and tertiary modes. To isolate the effects of injection mode on gravity stable miscible GAGD floods, two miscible gravity stable GAGD floods were conducted in secondary and tertiary modes of injection using n-Decane and Yates reservoir brine.

Figure 3.28(a) shows that in the miscible gravity stable GAGD floods, near perfect sweep efficiencies were observed, and are significantly higher than the CGI / WAG miscible flood recoveries. It is important to note that excepting the delay in oil production for tertiary floods, there are minimal effects of injection mode on miscible GAGD recovery. The average incremental recovery in gravity stable GAGD floods was 98.89% ROIP while the average incremental recoveries in horizontal mode CGI and WAG floods were 97.12% ROIP and 78.52% ROIP only. These oil recovery numbers show that the GAGD mode of injection far outperforms the WAG floods; while maintaining better gas utilization efficiencies as compared to the CGI floods (Figure 3.28(b)), by achieving hastened TRF peaks and asymptotic decreases in TRF values throughout the life of the flood. Furthermore, on a macroscopic scale, advantages of injecting in the GAGD mode far outweigh the CGI floods due to the favorable gravity forces during GAGD (Section 3.6.1). As observed in immiscible gravity stable GAGD floods, the pressure drop behavior, in miscible gravity stable GAGD floods, also tend to reach a plateau, although the approach could be asymptotic in tertiary gravity stable GAGD floods (Figure 3.28(c)), suggesting high sweep efficiencies during these corefloods.

- **Effect of Miscibility Development on GAGD Floods**

Comparison of Figures 3.27 and 3.28 clearly demonstrate the benefits of miscibility development. The average incremental oil recovery for miscible gravity stable GAGD floods is 98.89% ROIP while average incremental oil recovery for immiscible gravity stable GAGD floods is 67.27% ROIP, thus attributing a clear 31.63% ROIP incremental recovery to miscibility development. The trend to more efficient commercial miscible gas injection projects (EOR Survey, 2004) is comprehendible from the high recovery efficiencies observed in these vertical as well as horizontal gas injection coreflood experiments. However, it is important to note that the gravity stable GAGD floods fared well even in the immiscible mode of injection, in both secondary as well as tertiary applications. The high gas utilization efficiencies coupled with the good oil recovery characteristics could help make the GAGD process desirable in low pressure and depleted oil reservoirs.

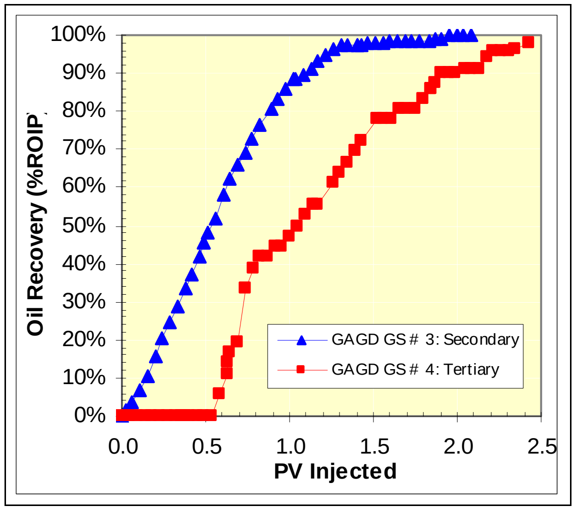

(a) Oil Recovery Characteristics versus PV CO_2 Injection

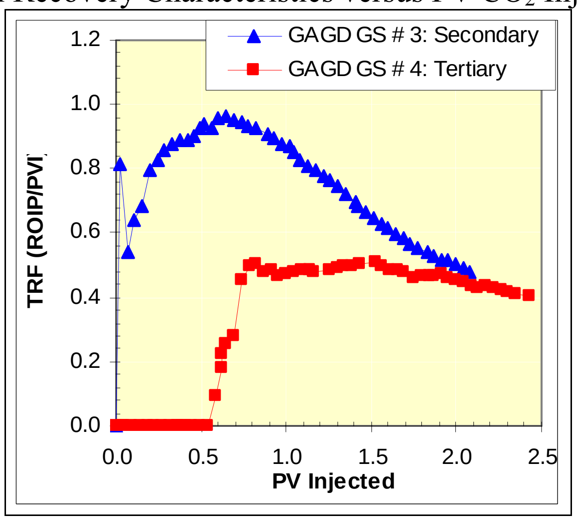

(b) TRF (%ROIP / PVI CO_2) Characteristics versus PV CO_2 Injection

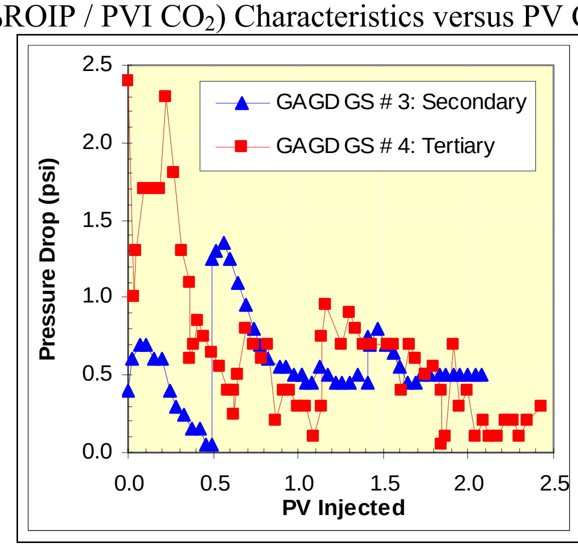

(c) Pressure Drop Characteristics versus PV CO_2 Injection

Figure 3.28: Effect of Injection Mode (Secondary versus Tertiary) on Miscible Gravity Stable GAGD Floods in n-Decane, Yates Reservoir Brine and Pure CO_2 System

- **Itemized Preliminary Conclusions from Gravity Stable GAGD Corefloods**

Some striking features of the GAGD corefloods completed in all gravity stable mode are included below:

Oil Recovery Characteristics:

1. Minimal effects of rate of gravity stable GAGD recovery.
2. Good oil recovery characteristics in immiscible gravity stable GAGD corefloods.
3. Perfect microscopic as well as microscopic sweep efficiencies in miscible gravity stable GAGD corefloods.

Tertiary Recovery Factor (TRF) Characteristics:

1. Early TRF peaks observed in all secondary floods with rapid decline after 1.0 pore volume injection.
2. Although TRF peaks are lower and occur later in tertiary mode injections, exponential decline in TRF values (as was observed in horizontal mode CGI / WAG injections), were not observed.
3. TRF plots clearly indicate the consistent GAGD performance as opposed to horizontal mode CGI / WAG injections.

Tertiary Recovery Factor (TRF) Characteristics:

1. Secondary GAGD floods (both immiscible and miscible) tend to stabilize at or near the absolute permeability pressure drop value, demonstrating excellent sweep efficiencies.
2. Tertiary GAGD floods demonstrate pressure drop characteristics similar to the secondary GAGD floods, although in tertiary floods, the approach to the absolute permeability pressure drop value is asymptotic.
3. Higher initial pressure drops are observed in tertiary GAGD floods, which can be attributable to the effects of CO2 solubility in brine and three-phase relative permeability effects.

3.8 Preliminary Conclusions

The literature review and experimental evidence collected so far clearly shows the benefit of working in tune with nature, more so in gas injection processes. The controlling mechanisms identified in gas injection processes are: gravity segregation (influenced by injected gas characteristics, reservoir fluid characteristics, injection mode and pattern, reservoir heterogeneity and stratification, etc.), water shielding (influenced by reservoir wettability, spreading coefficient, and mobile water saturation) and fluid dynamics (influences displacements on both microscopic and macroscopic scale).

The preliminary conclusions from the work till date are summarized below:

1. Gravity stable gas injection (consequently GAGD process) holds the promise of significant incremental recovery from ‘left-behind’ residual oil in both tertiary and secondary mode.

2. Preliminary GAGD experimentation (in an all gravity stable mode of injection) shows that the GAGD process can potentially outperform all the commercial modes of gas injection, namely CGI, WAG and Hybrid-WAG as demonstrated by laboratory corefloods completed and included in this report.
3. Minimal injectivity and operational problems would be encountered during the GAGD process applications.
4. The GAGD process is cost effective – utilizes existing infrastructure and vertical wells along with low cost horizontal wells for improving oil recovery.
5. Gravity segregation and water shielding effects are the controlling multiphase displacement mechanics in gas injection processes. Although these mechanisms have a negative impact in horizontal WAG displacements, the natural gravity segregation effects are beneficial for improving recovery in the GAGD process. The water shielding effects are also minimized in the GAGD process since the process does not require mobile water injection into the reservoir.
6. Lower CO_2 requirements for WAG employment may not be advantageous in the future due to increasing environmental and green-house-gas emission concerns.
7. Capillary and gravity forces appear to be the controlling forces in GAGD process – consequently the Bond number (the ratio of gravity and capillary forces).
8. Complex three-phase relative permeability modeling may not be required for the GAGD process due to countercurrent gas-liquid displacements.
9. Long coreflood scaled experimentation may not be required for the GAGD floods since all the dimensionless groups controlling the process do not contain the 'length' term.
10. Although miscibility development is beneficial in some cases, immiscible GAGD employment could generate comparable oil recovery characteristics. Consequently, miscibility development may not be a controlling economic decision for the application of the GAGD process.
11. The GAGD process appears to be less susceptible to the negative effects of reservoir heterogeneity, a dreaded concern for horizontal gas injections.

3.9 Project GAGD: Task III – Status and Future Work

- **Task III – 3 Status**

  The status report for Task III of the GAGD project is summarized below:

  1. Literature review for the dimensional analysis and identification of dimensionless groups completed.
  2. Dimensional analysis using Buckingham-Pi approach to determine the various dimensionless groups that may influence the GAGD process complete.
  3. Further extension of this dimensional analysis to both field and laboratory scale applications completed.

4. Experimental design based on dimensional similarity approach to elucidate operative multiphase mechanisms and fluid dynamics in the GAGD process completed.
5. Experimental design based on dimensional similarity approach further validated via flow regime characterizations.
6. All of the planned horizontal mode coreflood experiments have been completed.
7. Continued coreflood experimentation to identify individual parameter influences on GAGD experiments.
8. GAGD corefloods in all gravity stable mode completed.

- **Task III – Future Work**

  The future work queued for Task III of the GAGD project is summarized below:

  1. Continued literature update for light oil gravity drainage process.
  2. Experimental GAGD investigation of various multiphase mechanisms and fluid dynamics identified.
  3. Non-gravity stable mode GAGD experiments on 1-ft Berea core using Yates reservoir brine and n-Decane to complete that experimental set.

* * *

References

[1] Aker, E., "A Simulation Model for Two-Phase Flow in Porous Media", Thesis for the Degree of Candidatus Scientiarum, University of Physics, University of Oslo, Norway, December, 1996.

[2] Backmeyer, L A, Guise, D R, MacDonell, P E, Nute, A J, "The Tertiary Extension of the Wizard Lake D-3A Pool Miscible Flood" SPE 13721, presented at the 1984 SPE 59th Annual Technical Conference and Exhibition held in Houston, Texas, September 16-19, 1984.

[3] Bangla, V K, Yau, F, Hendricks, G R, "Reservoir performance of a Gravity stable vertical CO2 miscible flood: Wolfcamp reservoir, Wellman Unit", SPE 22898, presented at the 66th annual technical conference and exhibition of the Society of Petroleum Engineers, held in Dallas, TX, Oct 6-9, 1991.

[4] Barkve, T, Firoozabadi, A, "Analysis of reinfiltration in fractured porous media" SPE 24900, presented at SPE 67th Annual Technical Conference and Exhibition, held in Washington, DC, Oct 4-7, 1992

[5] Brigham, W E, "Mixing Equations in Short Laboratory Cores", SPE Journal, Feb 1974, pp. 91 – 99, Trans AMIE v. 257.

[6]Buckingham, E., "Model Experiments and The Forms of Empirical Equations" Trans. A.S.M.E. 37, 1915, pp. 263-296.

[7] Buckingham, E., "On Physically Similar Systems: Illustrations of The Use of Dimensional Equations", Phys. Review 4, 1914, pp. 345-376.

[8] Buckingham, E., "The Principle of Similitude", Nature 96, 1915, pp. 396-397.

[9] Butler, R M, "Gravity Drainage to Horizontal Wells", JCPT – 92 – 04 – 02, presented at the 42nd Annual Technical Meeting, of the petroleum society, Apr 1992, vol.31, No.4.

[10] Cardenas, R L, Alston, R B, Nute, A J, Kokolis, G P, "Laboratory Design of a Gravity Stable, Miscible CO2 Process," SPE 10270, presented at the 56th Annual Fall Technical Conference and Exhibition of the SPE of AIME, held in San Antonio, TX, October 5-7, 1981.

[11] Carson, L O, "Performance of Hawkins Field Unit Under Gas Drive-Pressure Maintenance Operations and Development of an Enhanced Oil Recovery Project," SPE 17324, presented at the SPE/DOE Enhanced Oil Recovery Symposium held in Tulsa, Oklahoma, April 17-20, 1988.

[12] Chalier, G, Giry, V, Madaoui, K, Sakthikumar, S, Maquignon, P H, "Three Phase Oil Relative Permeability Determination As A Key Point In The Evaluation Of A Tertiary Gas Gravity Drainage Project", SPE 30761, presented at the SPE Annual technical conference and exhibition of the Society of Petroleum Engineers, held in Dallas, TX, Oct 22-25, 1995.

[13] Chandler, M., "Linear Algebra", Course Notes, University of Missouri, Rolla, Fall 2003.

[14] Chang Y B, Coats B K, Nolen J S, "A Compositional Model for CO2 Floods Including CO2 Solubility in Water", SPE 35164, Presented at the 1996 Permian Basin Oil and Gas Recovery Conference, Midland, Texas, 27-29 Mar1996.

[15] Chatzis, I, Kantzas, A, Dullien, F A L, "On the investigation of gravity assisted inert gas injection using micromodels, long Berea cores and computer assisted tomography", SPE 18284, presented at the 63rd annual technical conference and exhibition of the Society of Petroleum Engineers, held in Houston, TX, Oct, 2-5, 1988.

[16] Christensen, J R, Stenby, E H, Skauge, A, "Review of the WAG field experience", SPE 39883, presented at the 1998 SPE International petroleum conference and exhibition of Mexico, Villhermosa, March 3-5, 1998.

[17] Coll, C., Muggeridge, A. H., and Jing, X. D., "Regional Upscaling: A New Method to Upscale Waterflooding in Heterogeneous Reservoirs for a Range of Capillary and Gravity Effects", SPE 59337, presented at 2000 SPE/DOE Improved Oil Recovery Symposium, Tulsa, OK, Apr 3 – 5, 2000

[18] Crawford H R, Neill G H, Bucy B J, Crawford P B, "Carbon Dioxide A Multipurpose Additive for Effective Well Stimulation", Journal of Petroleum Technology, Mar 1963, pp. 237.

[19] Da Sle, W J, Guo, D S, "Assessment of a Vertical Hydrocarbon Miscible Flood in the Westpem Nisku D Reef," SPE Reservoir Engineering, May 1990, pp. 147-154.

[20] Dawe, R. A., "Reservoir Physics at the Pore Scale", Commemoration volume of 75 years of oil field science at the Royal School of Mines, Imperial College of Science and Technology, University of London, 1990.

[21] DesBrisay, C L, Ghussein, F E, Holst, P H, "Review of Miscible Flood Performance, Intisar "D" field, Socialist People's Libyan Arab Jamahiriya," SPE 10245, presented at the 56th Annual Fall Technical Conference and Exhibition of the Society of Petroleum Engineers of AIME, held in San Antonio, TX, Oct 5 - 7, 1981.

[22] Dietz, D N "A Theoretical Approach to the Problem of Encroaching and Bypassing Edge Water," Proc., Koninklijke Nederlandsche Akad. Wetenschap, Vol.B56, 1953, p.83.

[23] Dumore, J M, "Stability Considerations In Downward Miscible Displacements", SPE Journal, Dec 1964, pp. 356 – 362, Trans AMIE 231.

[24] Dumore, J. M., and Schols, R. S., "Drainage Capillary Pressure Functions and the Influence of Connate Water", SPE Journal, Oct 1974

[25] Durandeau, M, El-Emam, M, Anis, A H, "Successful Field Evaluation Of The Efficiency Of A Gas Gravity Drainage Process By Applying Recent Developments In Sponge Coring Technique In A Major Oil Field", SPE 29809, presented at the SPE Middle East show held in Bahrain, Mar 11-14, 1995.
[26] Ekrann, S, "An Analysis of Gravity-Segregated Piston-Like Displacement in Stratified Reservoirs," SPE Reservoir Engineering, Feb 1992, pp. 143-148.
[27] Espie, A A, Brown, C E, Narayanan, K R, Wilcox, T C, "A Laboratory investigation of gravity drainage / waterflood interaction in Prudhoe bay", SPE 28614, presented at the 69th annual technical conference and exhibition of the Society of Petroleum Engineers, held in New Orleans, LA, Oct 6-9, 1994
[28] Fong, D K, Laflamme, A, Grenon, J P, Weaver, R, McIntyre, F, Stetski, S, "Design and Implementation of a Successful Vertical Tertiary Hydrocarbon Miscible Flood," presented at the 1999 CSPG and Petroleum Society Joint Convention, Digging Deeper, Finding a better bottom line, in Calgary, Alberta, Canada, June 14-18, 1999.
[29] Fox, R. W., and McDonald, T. A., "Introduction to Fluid Mechanics", J. Wiley, 1998
[30] Grattoni, C. A., Jing, X. D., Dawe, R. A., "Dimensionless Groups For Three Phase Gravity Drainage Flow In Porous Media", Journal of Petroleum Science and Engineering, 29 (2001), pp. 53 – 65.
[31] Green, D W, Willhite, G P, "Enhanced oil recovery", SPE Textbook series, Volume 6, 1998.
[32] Gunawan, S, Caie, D, "Handil Field: Three years of lean gas injection into water flooded reservoirs", SPE 57289, presented at the 1999 SPE Asia Pacific Improved Oil Recovery Conference held in Kuala Lumpur, Malaysia, Oct 25-26, 1999.
[33] Hagoort, J., "Oil Recovery by Gravity Drainage", SPE 7424, SPE Journal, Jun 1980.
[34] Hill, S, "Channeling in Packed Columns", Chemical Engineering Science, no. 6 - 1, 1952, pp. 247-253.
[35] Hinderaker, L, Utseth, R H, Hustad, OS, Kvanvik, B A, Paulsen, J E, "RUTH – A comprehensive Norwegian R&D program on IOR", SPE 36844, Presented at the SPE European Petroleum Conference held in Milan, Italy, Oct 22-24, 1996.
[36] Holm LW, "CO2 Slug and Carbonated Water Oil Recovery Processes", Producers Monthly, Sept 6, 1963.
[37] Howes, B J, "Enhanced oil recovery in Canada: Success in progress", Journal of Canadian Petroleum Technology, November – December 80-88, 1988.
[38] Hsu, H H, "Numerical Simulation of Gravity-Stable Hydrocarbon Solvent Flood, Wizard Lake D-3A Pool, Alberta, Canada," SPE 17620, presented at the SPE international Meeting on Petroleum Engineering, held in Tianjin, China, November 1-4, 1988.
[39] Jarrell P M, Fox C E, Stein M H, Webb S L, "Practical Aspects of CO2 Flooding", SPE Monograph, 2002 pp. 220.
[40] Jayasekera, A J, Goodyear, S G, "Improved hydrocarbon recovery in the United Kingdom continental shelf: past, present and future", SPE 75171, Presented at the SPE/DOE Thirteenth Symposium on Improved Oil Recovery held in Tulsa, OK, Apr 13–17, 2002.
[41] Johnson, R. W., "The Handbook of Fluid Dynamics", CRC Press, 1998
[42] Johnson W E, Macfarlane R M, Breston J N, "Changes in Physical Properties of Bradford Crude Oil When Contacted with CO2 and Carbonated Water", Producers Monthly, Nov 16, 1952.
[43] Johnston, J R, "Weeks Island Gravity Stable CO2 Pilot," SPE 17351 presented at the SPE/DOE Enhanced Oil Recovery Symposium held in Tulsa, Oklahoma, Aril 17-20, 1988.

[44] Kalaydjian, F, Vizika, O, Moulu, J C, "Role of wettability and spreading on gas injection processes under secondary conditions", presented at the 7th European IOR symposium, held in Moscow, Russia, Oct 27-29, 1993.
[45] Kantzas, A., Chatzis, I., and Dullien, F. A. L., "Enhanced Oil Recovery by Inert Gas Injection", SPE 17379, presented at the SPE/DOE Symposium on Enhanced Oil Recovery, Tulsa, OK, Apr 17 – 20, 1988.
[46] Kantzas A, Chatzis, I, Dullien, F A L, "Mechanisms of capillary displacement of residual oil by gravity assisted inert gas injection", SPE 17506, presented at presented at SPE rocky mountain regional meeting held in Casper, Wyoming, May 11-13, 1988.
[47] Karim, F, Berzins, T V, Schenewerk, P A, Bassiouni, Z A, Wolcott, J M, "Light oil recovery from cyclic injection: Influence of drive gas, injection rate and reservoir dip, SPE 24336, presented at SPE rocky mountain regional meeting held in Casper, Wyoming, May 18-21, 1992.
[48] King R L, Lee, W J, "An engineering study of the Hawkins (Woodbine) field", SPE 5528, SPE Journal of Petroleum Technology, Feb 1976, pp. 123 – 128.
[49] Kulkarni, Madhav M, "Immiscible and Miscible Gas-Oil Displacements In Porous Media", MS Thesis, The Craft and Hawkins Department Of Petroleum Engineering, Louisiana State University and A & M College, Baton Rouge, LA, Jul 2003. URL: http://etd.lsu.edu:8085/docs/available/etd-0709103-175151/
[50] Kulkarni, M. M., "Multiphase Mechanisms and Fluid Dynamics in Gas Injection Enhanced Oil Recovery Processes", Research Proposal for Ph.D. Qualifying Examination, The Craft and Hawkins Department of Petroleum Engineering, Louisiana State University and A & M College, Baton Rouge, LA 70803, April 2004.
[51] Kulkarni, M. M., "Multiphase Mechanisms and Fluid Dynamics in Gas Injection Enhanced Oil Recovery Processes", Ph.D. General Examination Report, The Craft and Hawkins Department of Petroleum Engineering, Louisiana State University and A & M College, Baton Rouge, LA 70803, July 2004.
[52] Kulkarni, M. M., and Rao, D. N., "Experimental Investigation of Various Methods of Tertiary Gas Injection, SPE 90589-PP, Presented at the 80th Society of Petroleum Engineers' Annual Technical Conference and Exhibition, Houston, TX, Sept 26 – 29, 2004.
[53] Langenberg, M A, Henry, D M, Chlebana, M R, "Performance and Expansion Plans for the Double-Displacement Process in the Hawkins Field Unit," SPE Reservoir Engineering, Nov 1995, pp. 301-308.
[54] Lenormand, R., Touboul, E., and Zarcone, C., "Numerical Models and Experiments of Immiscible Displacements in Porous Media", Journal of Fluid Mechanics, Vol. 189, 1988, pp. 165
[55] Lepski, B., Bassiouni, Z., and Wolcott, J., "Second-Contact Water Displacement Oil Recovery Process", SPE 35360, presented at the SPE/DOE Symposium on Enhanced Oil Recovery, Tulsa, OK, Apr 21 – 24, 1996.
[56] Lepski, B., Bassiouni, Z., and Wolcott, J., "Screening of Oil Reservoirs for Gravity Assisted Gas Injection", SPE 39659, presented at the SPE/DOE Symposium on Enhanced Oil Recovery, Tulsa, OK, Apr 19 – 22, 1998.
[57] Li, D., and Lake, L. W., "Scaling Fluid Flow Through Heterogeneous Permeable Media", SPE 26648, SPE Advanced Technology Series, Vol. 3. No. 1, 1993
[58] Longeron, D G, Kalaydjian, F, Bardon, C, Desremaux, L M, "Gas/oil capillary pressure: Measurements and reservoir conditions and effect on gas-gravity drainage", SPE 28612, presented at the

SPE Annual technical conference and exhibition of the Society of Petroleum Engineers, held in New Orleans, LA, Sept 25-28, 1994.
[59] Lui, C., "Dimensional Analysis", Course Notes ME503 Viscous Fluid Flow, Rose-Hulman Institute of Technology, Fall 2003.
[60] Martin J W, "Additional Oil Production Through Flooding with Carbonated Water", Producers Monthly, Jul 18, 1951.
[61] Meszaros, G, Chakma, A, Zha, K N, Islam, M R, "Scaled model studies and numerical simulation of inert gas injection with horizontal wells", SPE 20529, presented at the 65th SPE annual technical conference and exhibition, held in New Orleans, LA, Sept 23-26, 1990.
[62] Moissis, D E, Miller, C A, Wheeler, M F, "A parametric study of viscous fingering in miscible displacement by numerical simulation", Technical report 87-18, Rice University, Houston TX, June 1987, Available: Numerical Simulation in Oil Recovery, Minneapolis, Minn., 1986, pp. 227-247, Springer, New York, 1988.
[63] Moritis, G, "Impact of production and development RD&D ranked", Production Editor, Oil and Gas Journal, Oct 30, 1995.Vol 93, Issue 44.
[64] Mungan, N, "An evaluation of carbon dioxide flooding", SPE 21762, presented at the SPE Western regional meeting held in Long Beach, CA, March 20-22, 1991.
[65] Muskat, M., "Physical Principles of Oil Production", First Edition, McGraw Hill Book Company, TN 871 M85, 1949.
[66] Nahara, G. M., Pozzi, A. L., and Blackshear, T. H., "Effect of Connate Water on Gas / Oil Relative Permeabilities for Water-Wet and Mixed-Wet Berea Rock", SPE 20503, presented at the SPE Annual Technical Conference and Exhibition, New Orleans, LA, Sep 1990
[67] Novakovic, D., "Numerical Reservoir Characterization Using Dimensionless Scale Numbers with Application in Upscaling", Ph.D. Dissertation, The Craft and Hawkins Department of Petroleum Engineering, Louisiana State University and Agricultural & Mechanical College, Aug 2002
[68] Nute, A J, "Design and evaluation of a gravity stable, miscible CO2 solvent flood, Bay St. Elaine field", SPE 11506, presented at the Middle East Oil technical conference of the Society of Petroleum Engineers, held in Manama, Bahrain, March 14-17, 1983.
[69] Oil and Gas Journal, Biannual EOR surveys, 1992 - 2002.
[70] Oren, P E, Billiotte, J, Pinczewski, W V, "Mobilization of waterflood residual oil by gas injection for water wet conditions", SPE 20185, SPE Formation Evaluation, March 1992, pp. 70-78.
[71] Oren, P. E., and Pinczewski, W. V., "Effect of Wettability and Spreading on Recovery of Waterflood Residual Oil by Immiscible Gasflooding", SPE Formation Evaluation, 9 (2), 1994, pp. 149 – 156
[72] Pavone, D., Bruzzi, P., and Verre, R., "Gravity Drainage at Low Interfacial Tensions", Fifth European Symposium on Improved Oil Recovery, Apr 1989
[73] Perkins, T K, Johnston O C, "A Review Of Diffusion And Dispersion In Porous Media", SPE Journal, Mar 1963, pp. 70 – 84, Trans AMIE v. 228.
[74] Pozzi, A. L., and Blackwell, R. J., "Design of Laboratory Models for Study of Miscible Displacement", SPE 445, presented at the 37th Annual Fall Meeting, Los Angeles, CA, Oct 7-10, 1963
[75] Rao, D N, "Gas Injection EOR – A New Meaning in the New Millennium," JCPT (Feb. 2001) pp. 11-18.
[76] Rao, D N, "Rutherford Stability Criterion", Louisiana State University, Baton Rouge, LA.

[77] Rao, D N, Xu, Q, Ayirala, S, Kulkarni, M, "Development And Optimization Of Gas-Assisted Gravity Drainage (GAGD) Process For Improved Light Oil Recovery" Quarterly Technical Progress Report, Jul 2003

[78] Rao, D. N., Ayirala, S. C., Kulkarni, M. M., and Sharma, A. P., "Development of Gas Assisted Gravity Drainage (GAGD) Process for Improved Light Oil Recovery", SPE 89357, Presented at the 14th SPE/DOE Improved Oil Recovery Symposium, held in Tulsa, OK, Apr 17 – 21, 2004.

[79] Ren, W., "Application of the Gravity Assisted Tertiary Gas Injection Process", M.Sc. Thesis, University of Alberta, Edmonton, Canada, 2002

[80] Ren, W, Cunha, L B, Bentsen, R, "Numerical simulation and screening of oil reservoirs for gravity assisted tertiary gas injection processes", SPE 81006, presented at the SPE Latin American and Caribbean petroleum engineering conference held in Trinidad, West Indies, Apr 27-30, 2003.

[81] Saidi, A. M., and Sakthikumar, S., "Gas Gravity Drainage under Secondary and Tertiary Conditions in Fractured Reservoirs", SPE 25614, SPE Journal, 1993.

[82] Sajadian, V. A., and Tehrani, D. H., "Displacement Visualization of Gravity Drainage by Micromodel", SPE 49557, presented at the 8th Abu Dhabi International Petroleum Exhibition and Conference, Abu Dhabi, UAE, Oct 11-14, 1998.

[83] Shook, M., Li, D., and Lake, L. W., "Scaling Immiscible Flow through Permeable Media by Inspectional Analysis", In-Situ 4, 1992, pp. 311 – 349

[84] Skauge, A., Eleri, O. O., Graue, A., and Monstad, P., "Influence of Connate Water on Oil Recovery by Gravity Drainage", SPE/DOE 27817, presented at the SPE/DOE Ninth Symposium on Improved Oil Recovery, Tulsa, OK Apr 17 – 20, 1994

[85] Slobod, R L, Howlett, W E, "The effects of gravity segregation in studies of miscible displacement in vertical unconsolidated porous media", SPE Journal, March 1964, pp. 1-8.

[86] Supraniowicz, R, Butler, R M, "Vertical confined water drive to horizontal well: Part I: Water and oil of equal densities", Paper # 2, presented at the third technical meeting of the south Saskatchewan section, the petroleum society of CIM, held in Regina, Sept 25 – 27, 1989.

[87] Sukop, M. C., and Or, Dani, "Invasion Percolation of Single Component, Multi-phase Fluids with Lattice Boltzmann Models", Physica B 338, pp. 298 – 303.

[88] Thomas, J, Berzins, T V, Monger, T G, Bassiouni, Z A, "Light oil recovery from cyclic CO2 injection: Influence of gravity segregation and remaining oil", SPE 20531, presented at the 65th Annual technical conference and exhibition of the Society of Petroleum Engineers, held in New Orleans, LA, Sept 23-26, 1990.

[89] Tiffin, D L, Kremesec, V J, "A mechanistic study of gravity-assisted flooding", SPE/DOE 14895, presented at the SPE/DOE fifth symposium on Enhanced oil recovery of the Society of Petroleum Engineers and the Department of Energy, held in Tulsa, OK, April 20-23, 1986.

[90] Virnovsky, G A, Helset, H M, Skjaveland, S M, "Stability of Displacement Fronts in WAG Operations," SPE Journal, Dec 1996, pp. 383-394.

IV. Technology Transfer Efforts

Numerous technology transfer efforts were undertaken by the LSU-EOR Research Group during this reporting year 2003-04. The research efforts during this reporting period resulted in thirteen technical papers presented in National / International Symposiums, in addition to the four technical progress reports to the U.S. Department of Energy.

Two graduate students working on this project, Subhash C. Ayirala (Task II) and Madhav M. Kulkarni (Task III) successfully completed and defended two major Ph.D. requirements, namely the Ph.D. Qualifying Examination and the Ph.D. General Examination.

During this reporting period, oil-industry personnel showed considerable interest in the commercial implementation of the GAGD process. Discussions for a field test of the GAGD process in the depleted and abandoned oil fields of North Louisiana using CO_2 injectant are underway.

4.1 Technical Papers Prepared during this Reporting Period

1. Ayirala, S.C., Rao, D.N. and Casteel, J.: "Comparison of Minimum Miscibility Pressures Determined from Gas/Oil Interfacial Tension Measurements with Equations of State Calculations", SPE Paper 84187 presented at the 2003 SPE Annual Technical Conference and Exhibition, Denver, Colorado, October 5-8, 2003.

2. Ayirala, S.C. and Rao, D.N.: "Modified Parachor Model for Prediction of Interfacial Tension in Multi-Component Hydrocarbon Systems," Paper presented at the 227th National ACS Meeting, Anaheim, CA, March 28-April 1, 2004.

3. Ayirala, S.C. and Rao, D.N.: "Solubility, Miscibility and their Relation to Interfacial Tension for Ternary Fluid Systems," Paper presented at the 227th National ACS Meeting, Anaheim, CA, March 28-April 1, 2004.

4. Rao, D. N., Ayirala, S. C., Kulkarni, M. M., and Sharma, A. P., "Development of Gas Assisted Gravity Drainage (GAGD) Process for Improved Light Oil Recovery", SPE 89357, Presented at the 14th SPE/DOE Improved Oil Recovery Symposium, held in Tulsa, OK, Apr 17 – 21, 2004.

5. Kulkarni, M. M., "Is Gravity Drainage an Effective Alternative to WAG?", Presented at the SPE Gulf Coast Section Student Paper Contest (Doctoral Division), Lubbock, TX, Apr 21 – 22, 2004.

6. Rao, D.N. and Ayirala, S.C.: "Measurement and Modeling of Gas-Oil Interfacial Tension at Reservoir Conditions," Paper presented at the 2004 ATW-Gas Condensate Reservoir Development and Management, Houston, TX, May 19-20, 2004.

7. Rao, D.N. and Ayirala, S.C.: "The Multiple Roles of Interfacial Tension in Fluid Phase Equilibria and Fluid-Solid Interactions," Invited paper presented at Fourth International Symposium on Contact Angle, Wettability and Adhesion, Philadelphia, PA, June 14-16, 2004.

8. Kulkarni, M. M., and Rao, D. N., "Is there a 'Happy-Medium' between Single Slug and Water-Alternating-Gas (WAG) Processes?", 11th Annual India Oil and Gas Review Symposium and International Exhibition, Mumbai, India, Sept 6 – 7, 2004.

9. Kulkarni, M. M., and Rao, D. N., "Experimental Investigation of Various Methods of Tertiary Gas Injection", SPE 90589, Presented at the 80th Society of Petroleum Engineers' Annual Technical Conference and Exhibition, Houston, TX, Sept 26 – 29, 2004.

10. Ayirala, S.C. and Rao, D.N.: "Solubility, Miscibility and their Relation to Interfacial Tension for Application in Reservoir Gas-Oil Systems," SPE Paper 91918 presented at the SPE International Petroleum Conference, Puebla, Pue., Mexico, Nov. 7-9, 2004.

11. Ayirala, S.C. and Rao, D.N.: "Application of a New Mechanistic Parachor Model to Predict Dynamic Gas-Oil Miscibility in Reservoir Crude Oil-Solvent Systems," SPE Paper 91920 presented at the SPE International Petroleum Conference, Puebla, Pue., Mexico, Nov. 7-9, 2004.

12. Kulkarni, M. M., and Rao, D. N., "Is Gravity Drainage an Effective Alternative to WAG?", AIChE 2004 Annual Meeting, Austin, TX, Nov 7 –12, 2004.

13. Kulkarni, M. M., and Rao, D. N., "Characterization of Operative Mechanisms and Flow Dynamics in Gravity Drainage Field Projects through Dimensional Analysis", SPE 93770, 2005 Production Operations Symposium, held in Oklahoma City, OK, Apr 17 – 19, 2005.

Appendix A: Calculation of Dimensionless Numbers for Field Projects – A Case Study (West Hackberry Field – Louisiana)

The West Hackberry Field is located in the Cameron parish in Louisiana. The GIS field map (Source: Louisiana Department of Natural Resources – Strategic Online Natural Resources System) is included as Figure A1 below.

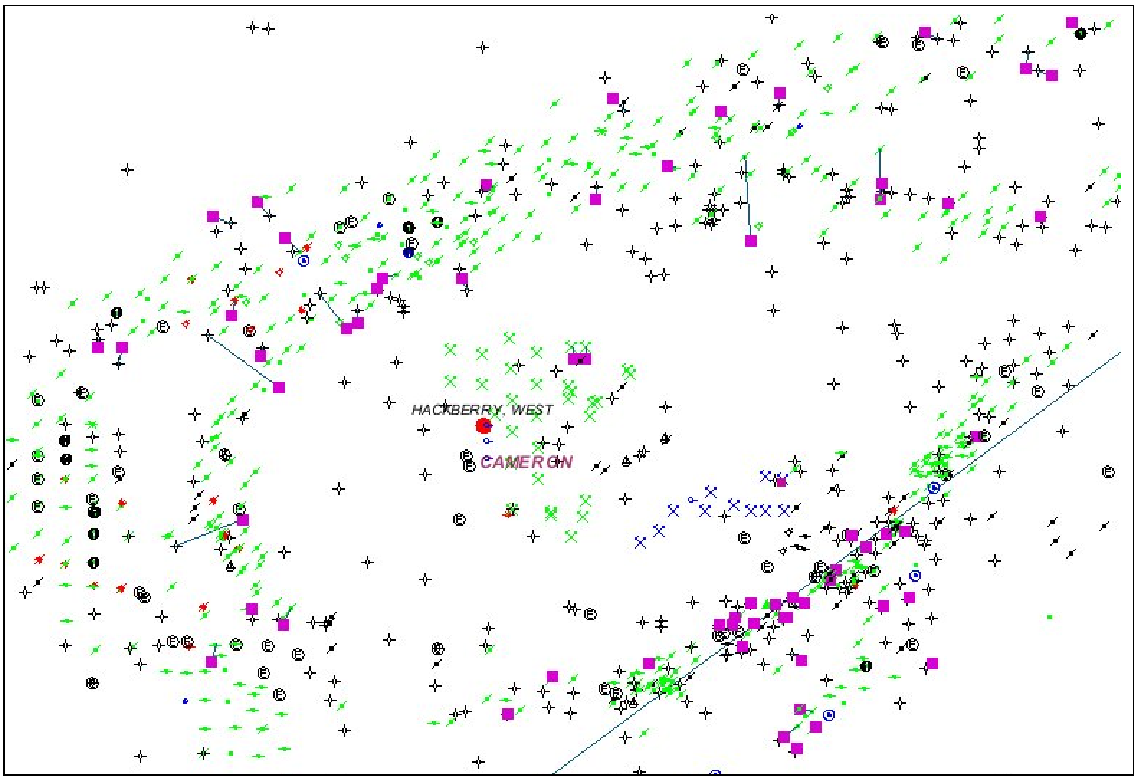

Figure A1: GIS Map of West Hackberry Field – Cameron Parish – Louisiana

The important dimensionless numbers that need to be considered for gravity drainage are: Capillary, Bond, Dombrowski-Brownell, Gravity and Grattoni et al.'s new group N. For the calculation of these numbers Darcy velocity, grain size distribution, injection air composition, reservoir fluid composition, reservoir petrophysical properties and injectant / reservoir oil PVT properties at reservoir conditions are required. The individual calculations for the above parameters are shown below.

A1 Calculation of Darcy Velocity

For the calculation of Darcy velocity displacement length, reservoir thickness, and average injection rates (surface and bottom hole) are required.

Figure A2 shows the Camerina sand C-1 plan (Gillham et al., 1996). There are mainly two air injectors in the field, Watkins # 16 and Gulf Land D # 51 as represented by solid triangles below.

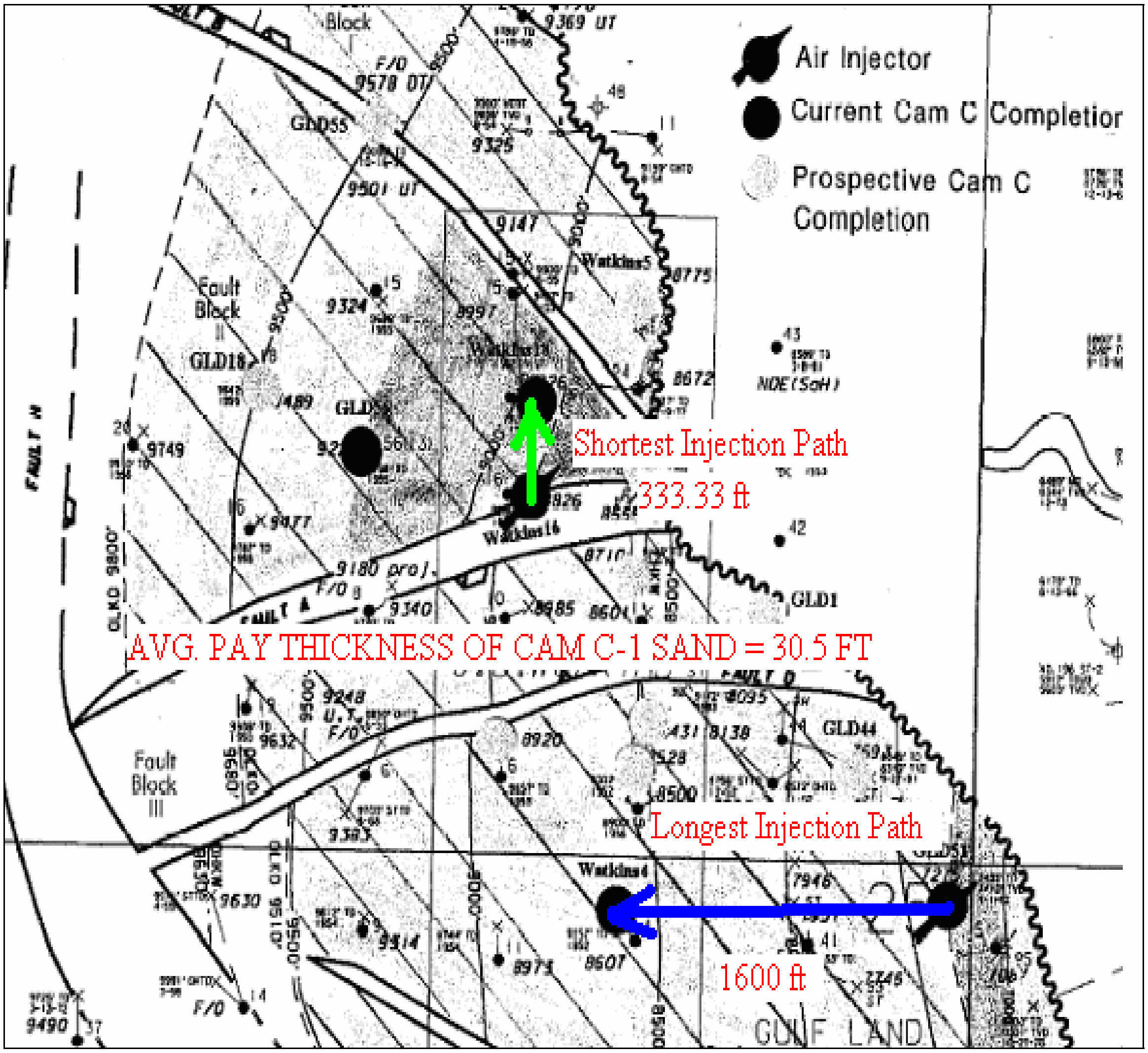

Figure A2: Cam C-1 Sand Map of West Hackberry Field – Cameron Parish – Louisiana

The shortest injection path is found to be 333.33 ft (from Watkins # 16 to Watkins # 18), whereas the longest injection path is 1600 ft (from Gulf Land D # 51 to Watkins # 4). The average air injection rates (Gillham et al., 1996) for the Watkins # 16 and Gulf Land D # 51 are shown in figure A3 below. It is seen that the average air injection rate for Watkins # 16 is 500 MSCFD while the average air injection rate for Gulf Land D # 51 ranges from 3250 MSCFD to 3800 MSCFD for the time interval of Nov 1994 - 1995.

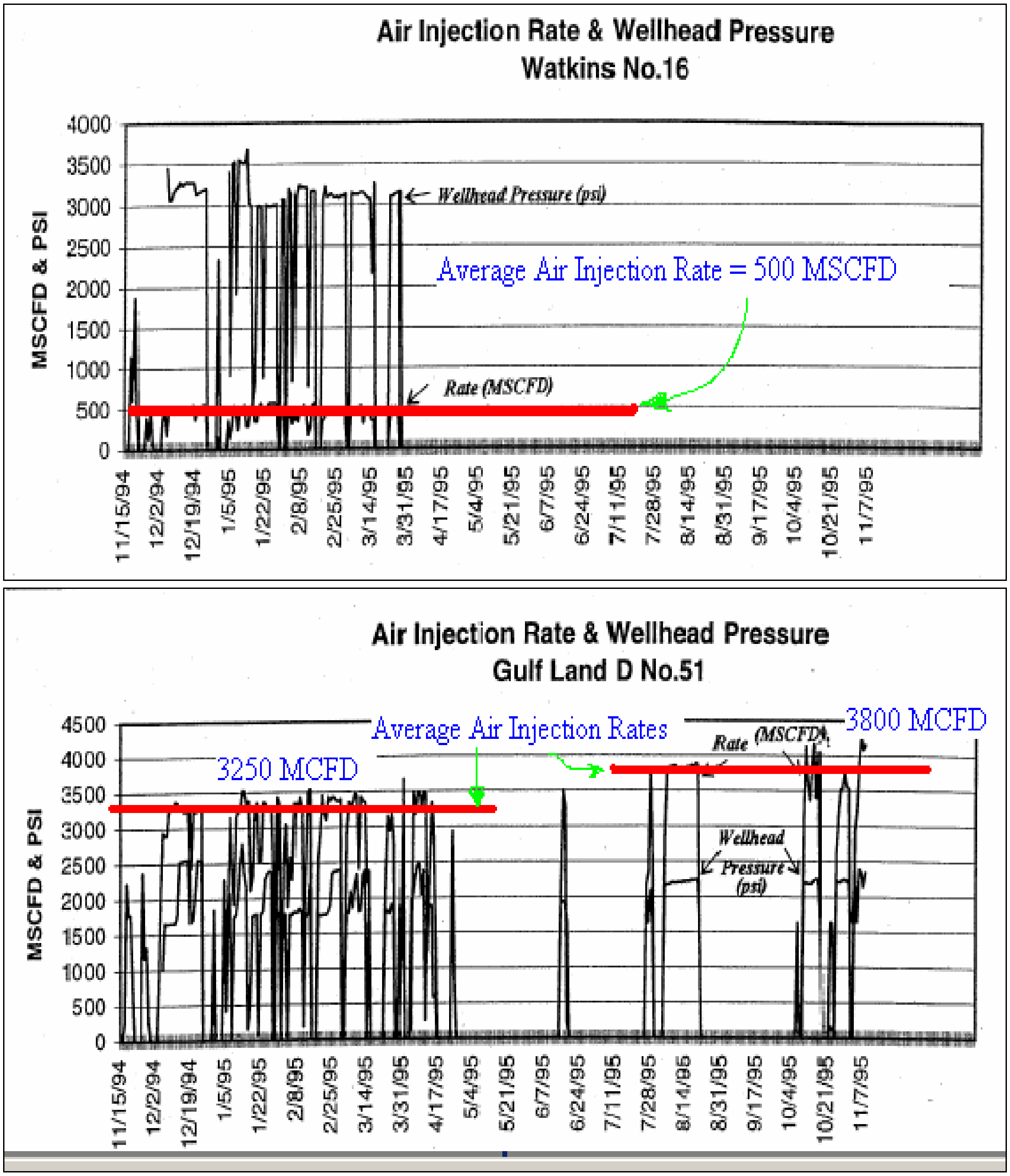

Figure A3: Average Air Injection Rates for Cam C-1 Sand Air Injectors

For the calculations for the bottom hole injection rates the bottom hole pressure are required. Figure A4 shows the BHP versus time for the West Hackberry Cam C-1 sand. The variations in the BHP are from 2300 psia to 3400 psia. These limiting vales are used for the calculation of the average bottom hole air injection rates by using gas law equations. The ranges of the bottom hole injection rates are 30.3 Mft^3/D to 21.3 Mft^3/D.

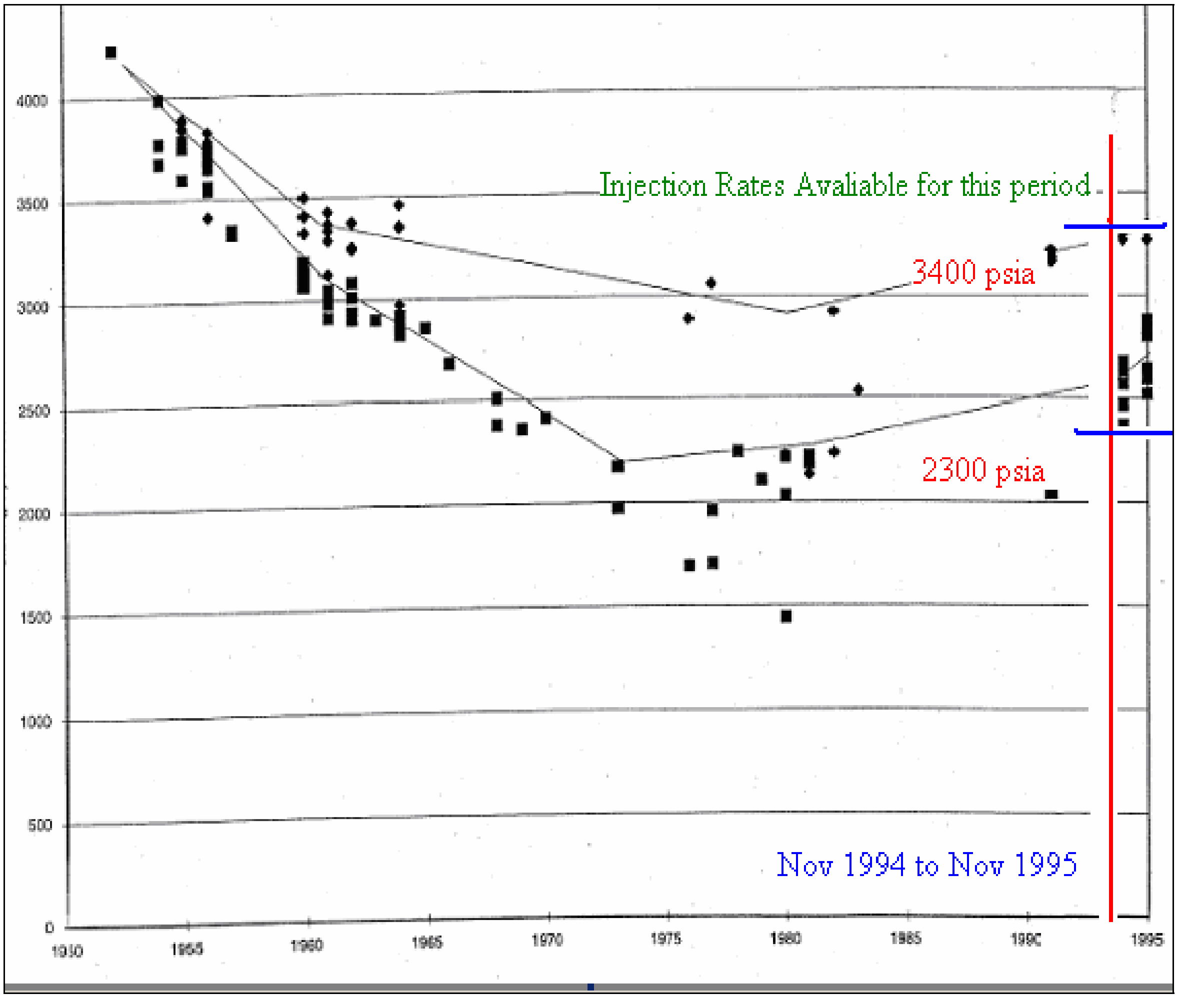

Figure A4: BHP @ 9000' (TD) Vs Time for Cam C-1 Sand

Shortest Displacement Path

Well # 8826 Injector (Watkins 16) to Well # Watkins 18 = 333.33 ft

Avg. Reservoir Thickness = 30.5 ft

Area = π*D*Thk = 3.14 * 333.33(ft) * 30.5 (ft) = 31939.5 ft^2

Average Injection Rate (Watkins 16) = 500 MSCFD

Bottom Hole Injection Rate (@ 2300 psi) = $V_{SC} * \frac{z*T}{P} * \frac{14.7(psia)}{520(R)}$

$$= 500 * \frac{1.072 * 661(R)}{2314.7(psia)} * \frac{14.7(psia)}{520(R)} = 4.33 \text{ Mft}^3/\text{D}$$

Bottom Hole Injection Rate (@ 3400 psi) = $V_{SC} * \frac{z*T}{P} * \frac{14.7(psia)}{520(R)}$

$$= 500 * \frac{1.112 * 661(R)}{3414.7(psia)} * \frac{14.7(psia)}{520(R)} = 3.04 \text{ Mft}^3/\text{D}$$

Min. Displacement Velocity = 3.04E+3 / 31939.5 = 0.095 ft/D
Max. Displacement Velocity = 4.33E+3 / 31939.5 = 0.136 ft/D
Darcy Velocity Range for Shortest Displacement Path: 0.095 – 0.136 ft/D.

Longest Displacement Path

Well # GLD 51 Injector to Well # Watkins 4 = 1600 ft
Avg. Reservoir Thickness = 30.5 ft
Area = π*D*Thk = 3.14 * 1600(ft) * 30.5 (ft) = 153309.7 ft^2
Average Injection Rate (Gulf Land # 51) = 3500 MSCFD (Avg. of 3250 & 3800)

Bottom Hole Injection Rate (@ 2300 psi) = $V_{SC} * \frac{z*T}{P} * \frac{14.7(psia)}{520(R)}$

$$= 3500 * \frac{1.072 * 661(R)}{2314.7(psia)} * \frac{14.7(psia)}{520(R)} = 30.3 \text{ Mft}^3\text{/D}$$

Bottom Hole Injection Rate (@ 3400 psi) = $V_{SC} * \frac{z*T}{P} * \frac{14.7(psia)}{520(R)}$

$$= 3500 * \frac{1.112 * 661(R)}{3414.7(psia)} * \frac{14.7(psia)}{520(R)} = 21.3 \text{ Mft}^3\text{/D}$$

Min. Displacement Velocity = 21.3E+3 / 153309.7 = 0.139 ft/D
Max. Displacement Velocity = 30.3E+3 / 153309.7 = 0.198 ft/D
Darcy Velocity Range for Longest Displacement Path: 0.139 – 0.198 ft/D.

A2 Grain Size Distribution Determination

The grain size distribution for the Camerina C-1 Sand is defined as ‘Medium’ to ‘Coarse’. The Spontaneous Potential (SP) logs for the Watkins # 16 and Gulf Land D # 51 air injectors are included as Figures A5 and A6. The SP clearly shows the well-developed sand bodies and the coarsening upward trend of the sand grains. Furthermore the increasing difference between the 9’ lateral and 18” normal resistivity traces clearly indicates the increasing permeability consequently the grain size. The folk grain size classification / Wentworth grade scale (Figure A7 Poppe et al., 2003) was employed for the further characterization of the grain sizes.

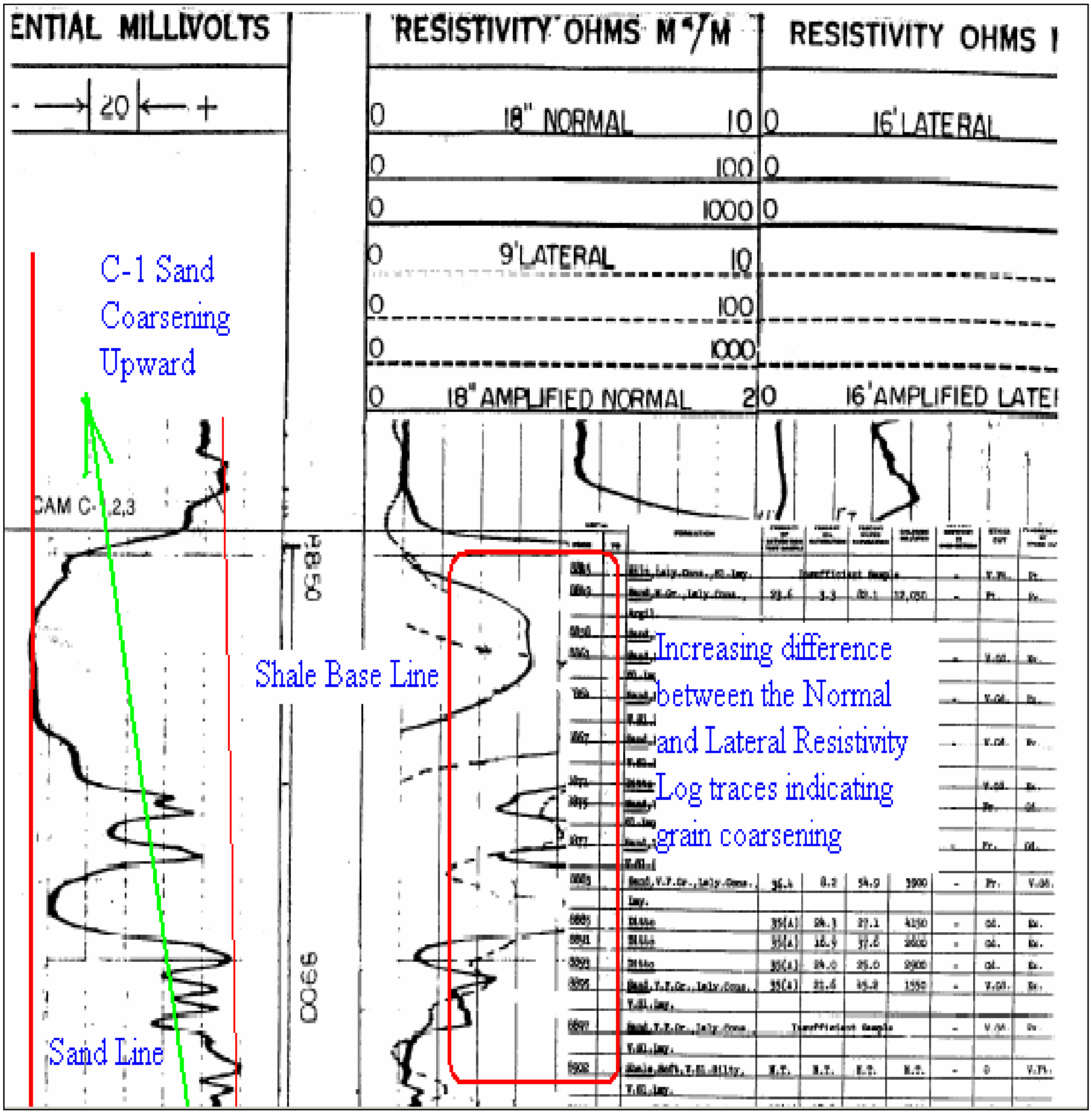

Figure A5: Electric Well Log for Watkins # 16 Air Injector

The grain size classification systems along with the electric logs suggest that the grain sizes for Camerina C-1 Sand ranges from 1 mm to ¼ mm. This range of values was used as the characteristic lengths for the calculation of Capillary, Bond, Dombrowski-Brownell, Gravity and Grattoni et al.'s new group N.

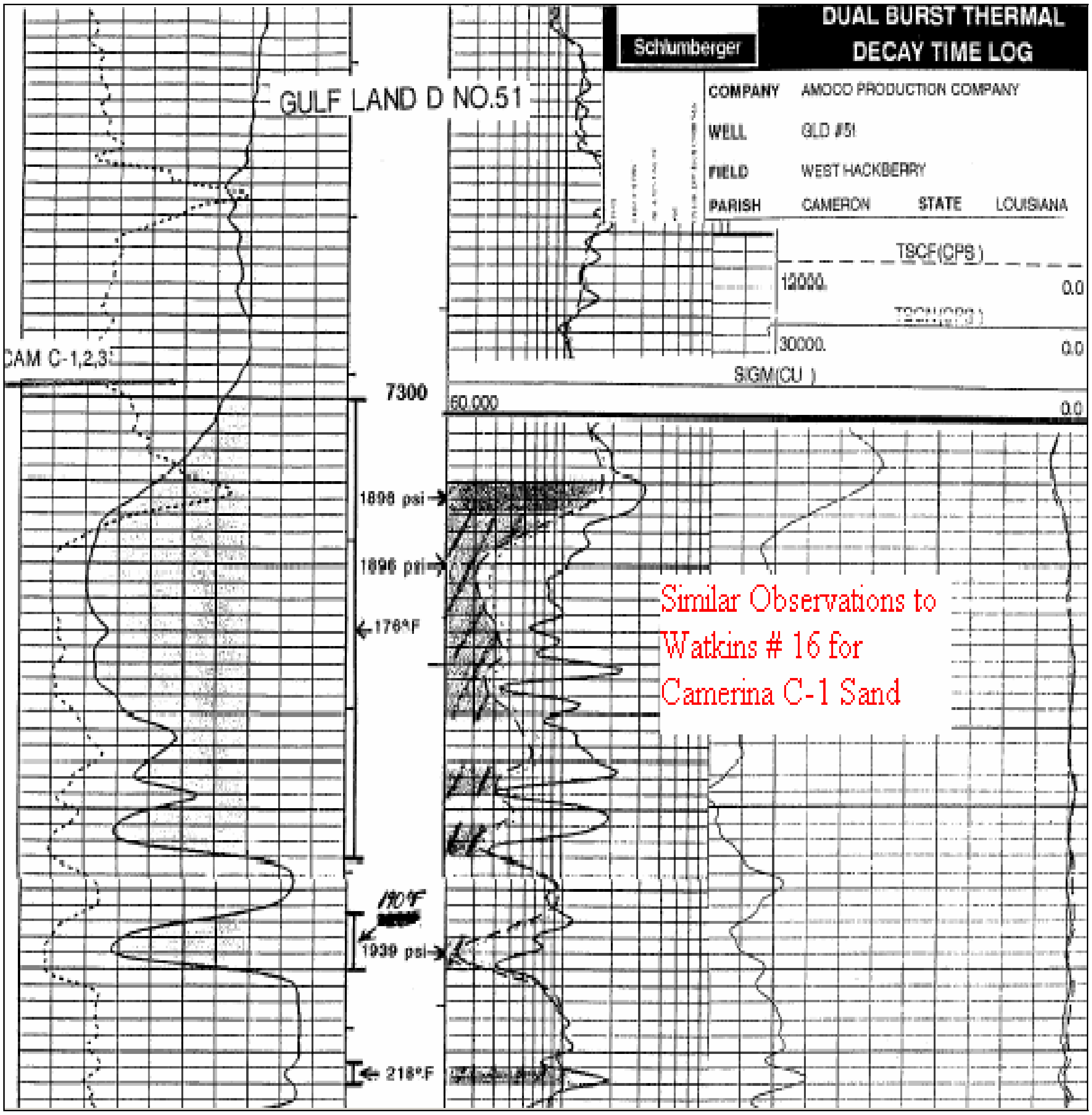

Figure A6: Electric Well Log for Gulf Land D # 51 Air Injector

A3 Injectant / Reservoir Fluid Compositions

The injection air composition is 21% Oxygen and 79% Nitrogen (Gillham et al., 1996). The reservoir fluid composition was obtained from Gillham et al. (1996). The representative sample compositions were obtained from producer Gulf Land D Well # 9, and the PVT properties reported (Gillham et al., 1996) were obtained by simulations using Amoco Redlich Kwong Equation of State and Hall Yarborough equations. However, PVT properties used for this work were obtained by using the Soave-Redlich-Kwong EOS model in WINPROP® PVT package and compositions reported (Gillham et al., 1996). The component properties of the feed stream are included as Figure A8. The simulated (using WINPROP®) properties of the injection / oil phase are summarized in Figure A9.

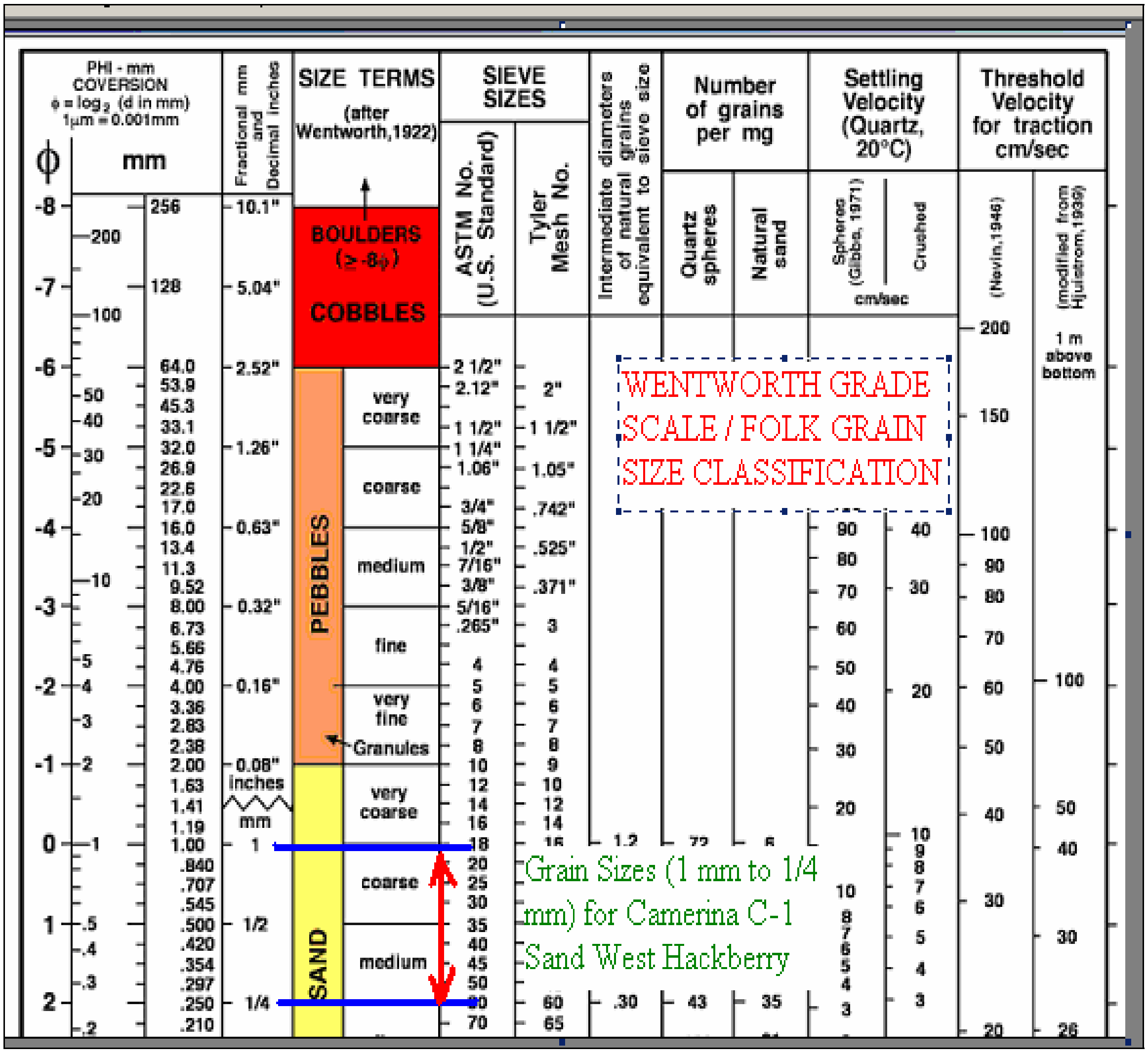

Figure A7: Wentworth Grade Scale / Folk Grain Size Classification

A4 Dimensionless Number Calculation for Cam C-1 Air Injection Project

Example calculations for the Capillary and Bond numbers for reservoir conditions (3500 psia and 201 ^{o}F) using 0.095 ft/D displacement velocity and 1 mm grain size are included below. A spreadsheet has been developed for these calculations and the results are included as graphs in Figures A10 and A11 below.

A M O C O P R O D U C T I O N C O M P A N Y

West Hackberry Field, Gulf Land "D" Well No. 9, (Camerina "C"), LA

DVA for 5 pseudos

Component Properties of Feed Stream
Table 1

Component	ID	Mole Weight	Critical Temp R	Critical Pressure psia	Acentric Factor
Nitrogen	1	28.01	227.2	493.1	0.0372
Methane	2	16.04	343.0	666.5	0.0105
Carbon dioxide	3	44.01	547.6	1070.7	0.2310
ps1	256	39.62	622.8	649.3	0.1331
ps2	257	79.99	875.2	460.3	0.2646
ps3	258	118.51	1080.4	440.2	0.3535
ps4	259	190.56	1399.4	287.9	0.5377
ps5	260	358.96	1633.0	156.1	0.8663

Heavy ends characterized by NTYPE characterization method using molecular weight of 228.0 and specific gravity of 0.8685.

A M O C O P R O D U C T I O N C O M P A N Y

West Hackberry Field, Gulf Land "D" Well No. 9, (Camerina "C"), LA

DVA for 5 pseudos

Component Properties of Feed Stream
Table 2

Component	Omega a	Omega b	Critical Volume cf/lb mol	Density @ 60F g/cc	Boiling Point F
Nitrogen	0.397549	0.094559	1.43	--	-320.5
Methane	0.446248	0.089117	1.58	--	-258.7
Carbon dioxide	0.399970	0.081033	1.51	--	-109.3
ps1	0.432528	0.087727	2.95	0.4465	-73.8
ps2	0.433754	0.079841	5.16	0.6481	122.1
ps3	0.453158	0.077436	6.90	0.7954	279.7
ps4	0.470217	0.069716	11.84	0.8563	482.3
ps5	0.473603	0.056612	23.71	0.8974	742.0

ARKES parameters via Yarborough-Morris-Turek correlation (1984). Omega a and omega b are ARKES parameters evaluated at 201.00 F.

Figure A8: Component Properties of Feed Stream

Capillary Number (3500 psia & 201 F) (Variation in Darcy Velocity)

$$N_C = \frac{V(m/s) * \mu(Pa.S)}{\sigma(N/m)}$$

$$\mathrm{N_C} = \frac{0.095(ft/D) * (0.0000035\ m/s/\mathrm{ft/D}) * 0.3791(\mathrm{cP}) * (0.001\,Pa.S/c\mathrm{P})}{4.4869(\mathrm{dyne/cm}) * (1E-3N/m/dyne/cm)}$$

$\boxed{\mathbf{N_C = 2.81E\text{-}08}}$.

Bond Number (3500 psia & 201 F) (Variation in Grain Size)

$$N_B = \frac{\Delta\rho(kg/m^3) * g(m/s^2) * l^2(m^2)}{\sigma(N/m)}$$

$$N_B = \frac{(51.0656 - 12.7301)(lbm/ft^3) * (16.01846\ \mathrm{kg/m^3/lbm/ft^3}) * (9.80665\ \mathrm{m/s^2}) * (0.001^2\ \mathrm{m^2})}{4.4869(\mathrm{dyne/cm}) * (1E-3N/m/dyne/cm)}$$

$\boxed{\mathbf{N_B = 1.3421}}$.

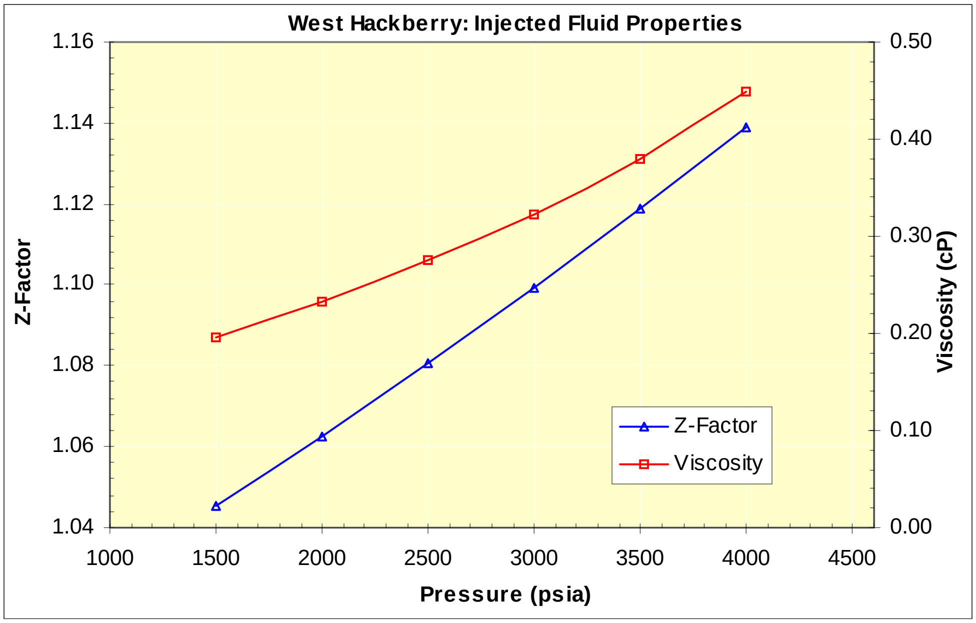

(a) Injectant Air Properties

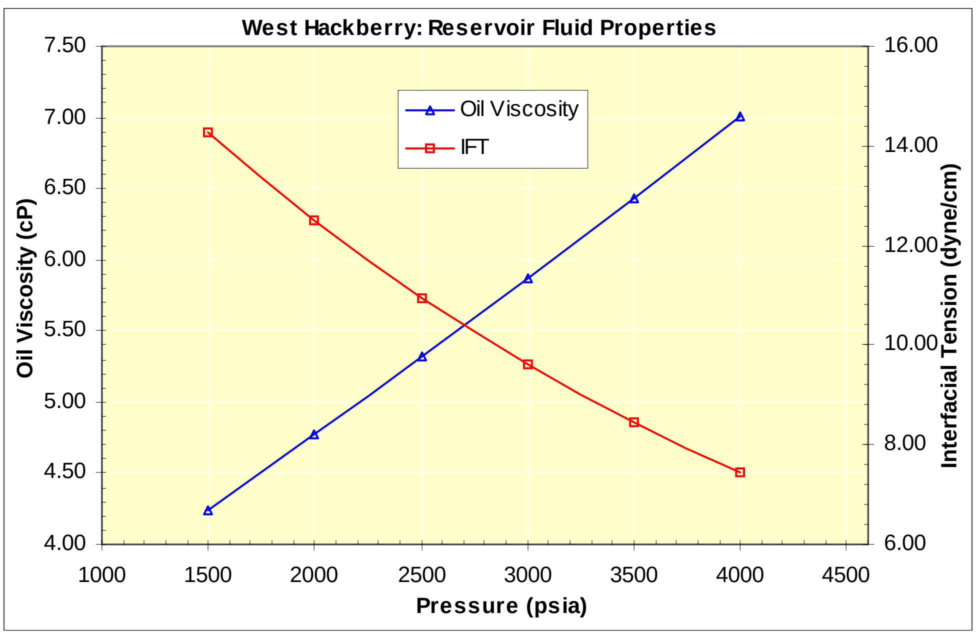

(b) Reservoir Fluid Properties

Figure A9: Injectant / Reservoir Oil Properties for West Hackberry Tertiary Project

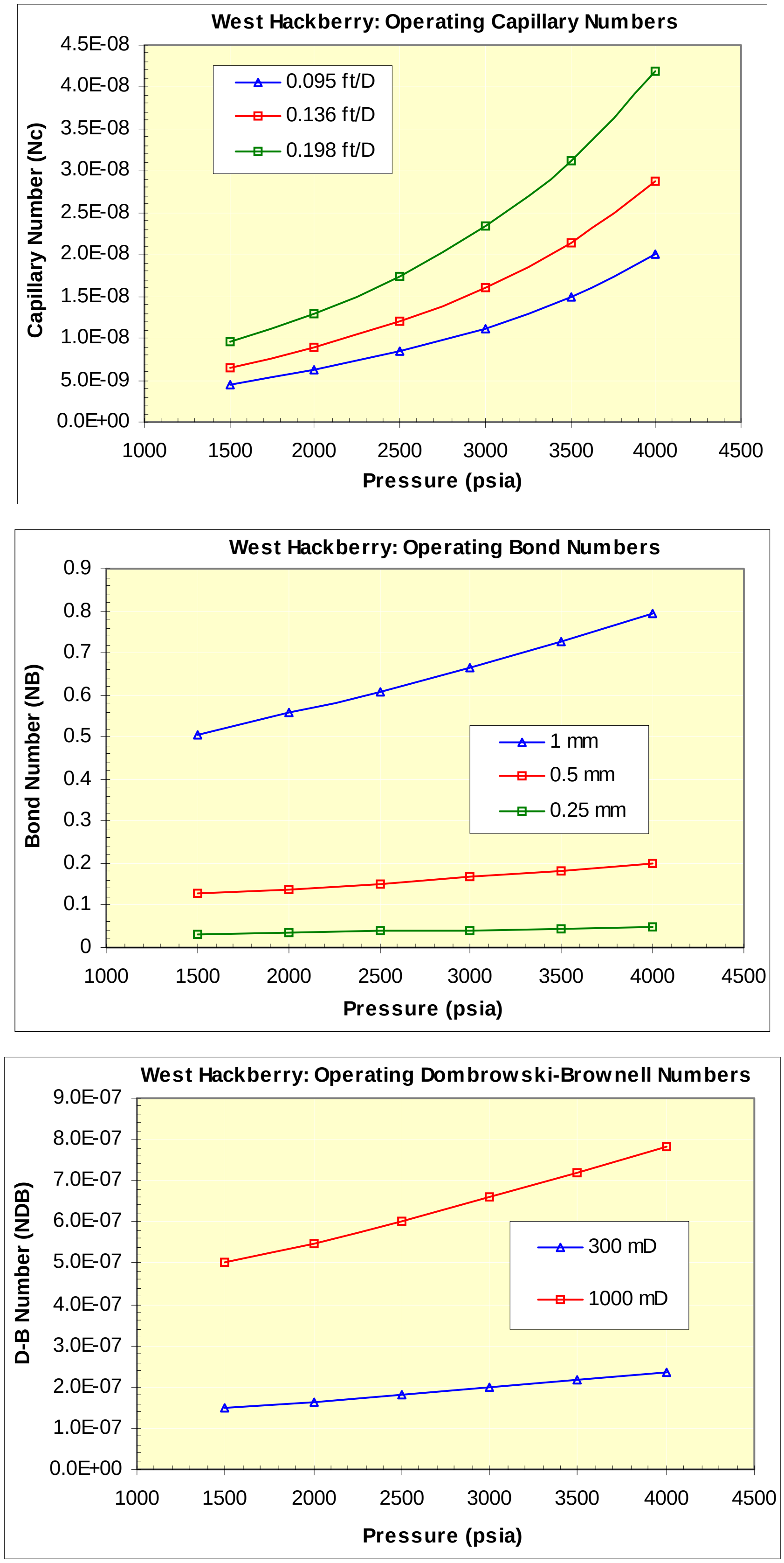

Figure A10: Calculated Operating Capillary, Bond and Dombrowski-Brownell Numbers

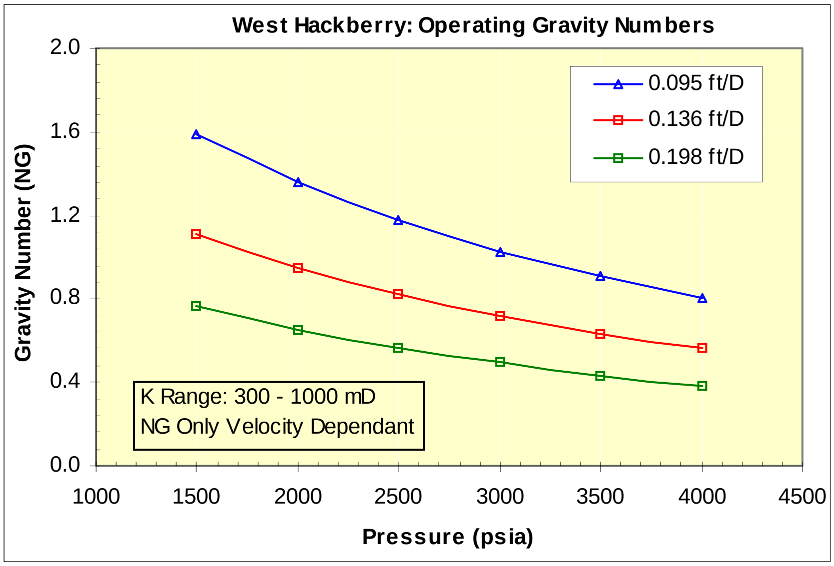

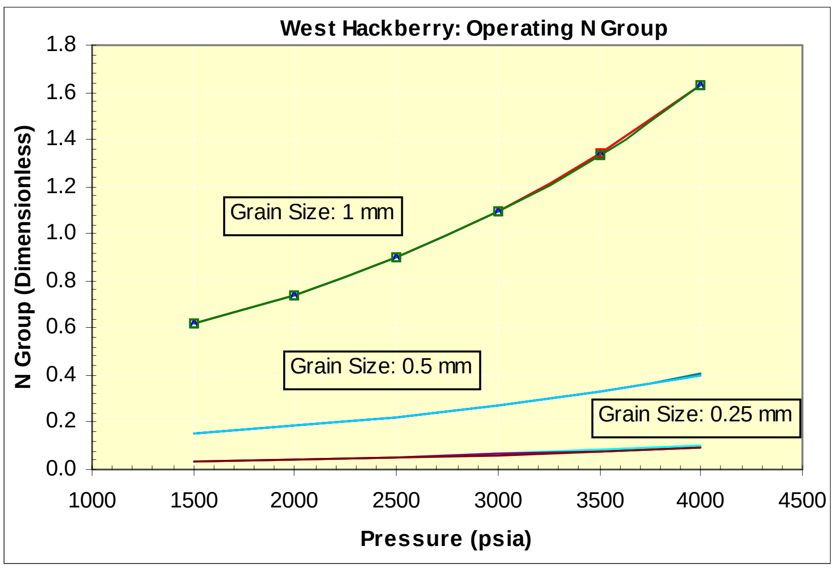

Figure A11: Calculated Operating Gravity and N Group Numbers

Table A1: Ranges of Values of above Calculated Dimensionless groups.

Number	Formula	Minimum Value	Maximum Value
Capillary Number	$N_C = \dfrac{V(m/s) * \mu(Pa.S)}{\sigma(N/m)}$	4.5639E-09	4.1798E-08
Bond Number	$N_B = \dfrac{\Delta\rho(kg/m^3) * g(m/s^2) * l^2(m^2)}{\sigma(N/m)}$	0.03171	0.79367
Gravity Number	$N_G = \dfrac{\Delta\rho.g.k}{\Delta\mu.u}$	0.38546	1.5932

Dombrowski-Brownell Number	$N_{DB} = \frac{\Delta\rho.g.k}{\sigma}$	1.50235E-07	7.83296E-07
New Group	$N = N_B + A(\frac{\mu_D}{\mu_G}).N_C$	0.0361	1.62736

References

[A1] Gillham, T, Cerveny, B, Turek, E, "West Hackberry Tertiary Project", Annual Report Sept 3, 1994 – Sept 2, 1995, DOE Contract # DE-FC22-93BC-14963, Report DOE/BC/14963-10, Amoco Production Co., Houston, TX, May 1996.

[A2] Poppe, L J, Paskevich, V F, Williams, S J, Hastings, M E, Kelly, J T, Belknap, D F, Ward, L G, FitzGerald, D M and Larsen, P F, "Surficial Sediment Data from the Gulf of Maine, Georges Bank, and Vicinity: A GIS Compilation", United States Geological Survey (USGS), Report 03-001, July 2003.